Contrails

NEW APPROACHES TO HUMAN-PILOT/VEHICLE DYNAMIC ANALYSIS

D. T. McRUER
L. G. HOFMANN
H. R. JEX
G. P. MOORE
A. V. PHATAK
D. H. WEIR
J. WOLKOVITCH

Distribution of this Report is Unlimited

Approved for Public Release

Contrails

FOREWORD

This report documents a study directed toward summarizing and evaluating new modeling approaches useful in human-pilot/vehicle analysis. It has been accomplished under Contract AF 33(615)-3652, BPSN: 6(638219-62405364), sponsored by the Flight Control Division of the Air Force Flight Dynamics Laboratory under Project 8219, "Stability and Control Investigations," Task 821904, "Flight Control Systems Analysis." The research has been performed by Systems Technology, Inc., at both its Hawthorne, Calif., and Princeton, N. J., offices. Work conducted under this program was performed between March 1966 and June 1967. The manuscript was initially released by the authors July 1967 for publication as an AFFDL technical report. The principal investigator has been Mr. D. T. McRuer, and the Flight Control Division project monitor has been Mr. F. L. George.

A number of STI staff members have participated in the study, because of the diversity of the included topics. Major contributors are listed as authors. Important contributions to several of the analytical activities have also been made by Mr. R. E. Magdaleno and Mr. G. L. Teper of STI. Gratitude is extended to Mr. F. L. George, Mr. R. O. Anderson, and Mr. P. E. Pietrzak of the Flight Control Division for their review and comments. Finally, the authors are indebted to the STI production staff for their careful work in preparing the manuscript.

This technical report has been reviewed and is approved.

Charles B. Westbrook

CHARLES B. WESTBROOK
Chief, Control Criteria Branch
Flight Control Division
Air Force Flight Dynamics Laboratory

Approved for Public Release

Contrails

ABSTRACT

New models for human pilot dynamics and new methods for pilot/vehicle dynamic analysis are investigated. The status of existing quasi-linear models is reviewed and deficiencies are noted as a basis for pinpointing areas needing the most effort. The pilot modeling topics explored include: low frequency lead generation using either velocity sensing at the periphery (eye) or difference computations accomplished at a more central level; mode-switching models for nonstationary or discrete inputs to the pilot/vehicle system; physiological aspects of pilot dynamics in tracking tasks; Successive Organization of Perception (SOP) theory for levels of pilot cognition higher than compensatory. For pilot/vehicle analysis, analytical approaches from control theory which appear to have promise are studied, including: time-optimal computing feedforward elements useful in the mode-switching models for response to nonstationary inputs; optimal control theory using the crossover model in the performance criterion to estimate pilot response characteristics in compensatory tasks; inverse optimal control theory using known experimental results and quasi-linear pilot response models in an effort to define the pilot's adjustment rules in terms of performance indices; optimal control theory to provide a simple test for optimality (to an elementary quadratic criterion) using only average performance measure data.

Distribution of this Abstract is Unlimited.

Approved for Public Release

Contrails

Approved for Public Release

Contrails

TABLE OF CONTENTS

Approved for Public Release

Contrails

Approved for Public Release

Contrails

LIST OF FIGURES

Approved for Public Release

Contrails

Approved for Public Release

Contrails

Approved for Public Release

Contrails

LIST OF TABLES

Approved for Public Release

Contrails

SYMBOLS

a, b, c, d	Equalization coefficients; a may also indicate lag to lead time-constant ratio
a_i	Local linear acceleration (see Fig. 10)
A	n × n matrix
A	Input height
$\underline{b}$	n × 1 vector
B_c	Manipulator damping
c	Pilot output, limb position
c_o	Optimal pilot output, limb position
c_1	Arbitrary control activity
C_p	Limb/muscle damping coefficient
d	Average distance between receptive fields
d_0, d_1, d_2	Controlled element parameters
db	Decibels; 20 $\log_{10}$ ( )
D(s)	Denominator polynomial
e	Base of the Napierian logarithm
e	Displayed error
$\underline{e}$	Error state vector
Δe	Error increment
$\dot{e}$	Sensed velocity signal
e*	Sampled and delayed error
$\overline{e^2}$	Mean-squared error
e_T	Error threshold of the operator
e_v	Visual stimulus
$E(j\omega)$	Display error Fourier transform

Approved for Public Release

Contrails

$f(\underline{e})$	Control logic
f_0, f_1, f_2	Coefficients of frequency weighting function
Δf_α	Spindle signal due to combined gamma motor neuron and alpha motor neuron
Δf_s	Spindle signal due to gamma motor neuron
F	Frequency weighting applied to the displayed error
FSW	Function switch
G	System transfer function
G_M	Muscle and manipulator dynamics
G_N	Neuromuscular system describing function
H	Wiener system transfer function
i	System forcing function
i_p	Internally generated pilot command
$I(j\omega)$	Forcing function Fourier transform
j	$\sqrt{-1}$
J	Performance index
J_c	Performance index component analytic in left half plane
J_d	Component of J containing the second variation with c_1
k	Constant
$\underline{k}$	Optimal vector of feedback gains (n x 1)
k_c	Manipulator spring constant
k_M	Limb/muscle spring constant
k_1, k_2	Controller gains
K	General symbol for gain
ΔK	Time-varying part of pilot gain
K_c	Controlled element gain
K_p	Pilot gain

Approved for Public Release

Contrails

K_{p_o}	Constant part of time-varying pilot gain
K_s	Spindle ensemble gain
K_1	Pilot gain in sampled-data feedforward
K_α	Muscle and manipulator gain
m	System output; lens/retina distance
m_d	Desired system output
m^*	Sampled and delayed output
M	Effective limb/manipulator mass; average absolute amplitude (for each Y_c) of the stick response assuming it to be bang-bang with equal positive and negative amplitudes
$M(j\omega)$	System output Fourier transform
n	Plant or controlled element order; noise, summation index
n_c	Remnant injected into pilot's output
n_i	Remnant referred to the input
N	Upper limit
N(s)	Numerator polynomial
$N_c(j\omega)$	Additive remnant Fourier transform
p	Probability
P	Unknown n x n symmetric matrix ("payoff matrix")
P_o	Steady-state isometric tension in muscles
q	(Unknown) coefficient in the performance index
q_i	Local angular velocity at canals (see Fig. 10)
Q	n x n symmetric matrix of performance index coefficients
r	(Unknown) coefficient in the performance index
r	Effective input to optimal pilot model
$\underline{r}$	Vector
$\mathcal{R}$	Real part

Approved for Public Release

Contrails

s	Laplace operator, $\sigma \pm j\omega$
t	Time
T	Sampling interval; first-order time constant
T_A	Neuromuscular actuation system time delay
T_c	Time to complete force response
T_d	Detection time
T_d'	Normalized detection time
T_g	Time constant of the ganglion cell's weighting function
T_I	Pilot lag equalization time constant
$T_{I,N}$	Combined pilot lag time constant
T_K	Low frequency neuromuscular lead time constant
T_K'	Low frequency neuromuscular lag time constant
T_L	Pilot lead equalization time constant
$T_{L_{hi}}$	High frequency pilot lead equalization time constant
T_{M_1}	Low frequency limb/manipulator time constant
T_{M_2}	High frequency limb/manipulator time constant
$T'_{M_1 p_1}$	Low frequency neuromuscular closed loop (CL) lag time constant for low value of average tension
$T'_{M_1 p_2}$	Low frequency neuromuscular CL lag time constant for high value of average tension
$T'_{M_2 p_1}$	High frequency limb/manipulator CL time constant for low value of average tension
$T'_{M_2 p_2}$	High frequency limb/manipulator CL time constant for high value of average tension
T_N	Lag time constant for first-order approximation to neuromuscular dynamics
T_{N_1}	Time constant in neuromuscular system
T_r	Recognition time
T_R	Vehicle roll subsidence time constant

Approved for Public Release

Contrails

u	Scalar control variable
u_0	Optimum control
v	Velocity of pilot stimulus across retina
$w(s)$	c to ϵ transfer function (from control to response error)
w_g	Effective weighting function of the ganglion cell to an individual action potential input
x	State variable
$\underline{x}$	State vector of plant (n x 1)
$x_g(t)$	Subthreshold electric potential in the ganglion cell due to the activity of its associated sensory and bipolar cells
x_r	Input to ganglion cell
Y_c	Controlled element dynamics
Y_{OL}	Open-loop dynamics
Y_p	General describing function form for pilot or operator for compensatory task
Y_pY_c	Open-loop dynamics of compensatory loop
Y_{p_e}	Pilot describing function operating on system error
Y_{p_i}	Pilot describing function operating on forcing function
Y_{p_m}	Pilot describing function operating on system output
Y_{p_p}	Pilot describing function operating on internal program
z	z transform variable, e^{Ts}
$z(s)$	Laplace transform of the coefficient of the first variation on the control
α	Low frequency neuromuscular phase lag
α_c	Alpha motor neuron command to limb/manipulator
α_c^*	Sampled limb command
α_v	Oculomotor command plus nystagmic crossfeeds
α_{vc}	Oculomotor command system output
γ	Limb position command from gamma motor neuron

Approved for Public Release

Contrails

γ_b	Spindle equalization and bias adjustment
γ_c	Gamma motor neuron command
δ	Control surface deflection (aileron)
ϵ	Frequency weighted error in frequency domain formulation
ϵ	Difference between desired output and actual output
ϵ_v	Eyeball position error
ζ	Damping ratio
ζ_{CL}	Closed-loop damping ratio
ζ_D	Damping ratio of Dutch roll second order
ζ_N	Neuromuscular system damping ratio
θ	Vehicle pitch attitude
θ_i	Attitude control input
λ	Weighting parameter for pilot control effort
λ_v	Eyeball position (see Fig. 10)
σ	Real part of complex variable, $s = \sigma \pm j\omega$
σ_c	rms value of pilot output
σ_v	rms value of error velocity
τ	Pure time delay
$\Delta\tau_e$	Pure time delay decrement due to forcing function
τ_e	Effective pure time delay
τ_o	Effective pure time delay for zero forcing function bandwidth
τ_α	Alpha motor neuron time delay
τ_γ	Gamma motor neuron time delay
φ	Vehicle roll or bank angle
φ_f	Final roll angle
φ_M	System phase margin

Approved for Public Release

Contrails

Φ_{ii}	Forcing function spectrum
Φ_{nn}	Pilot remnant spectrum
Φ_{nn_e}	This is special case of Φ_{nn_i} for compensatory display
Φ_{nn_i}	Pilot remnant spectrum when considered as a quantity injected at the system input
ω	Angular frequency (rad/sec)
ω_c	Crossover frequency, i.e., frequency at which $\lvert Y_p Y_c \rvert = 1$
ω_{c_o}	Basic crossover frequency for very low bandwidth inputs
ω_D	Undamped natural frequency of the Dutch roll second order
ω_i	Forcing function bandwidth
ω_M	Limb/manipulator undamped natural frequency
ω_n	Undamped natural frequency
ω_N	Neuromuscular system natural frequency
Ω	Rate of object motion
Ω_{eq}	Equivalent velocity of object
$( )'$	Prime denotes closed-loop time constant, or transpose of a vector or matrix
Σ	Summation
$\overline{( )}$	Complex conjugate
$\lvert \rvert_+$	Sum of terms in partial fraction expansion of enclosed quantity having left-half-plane roots
$(\dot{})$	Derivative with respect to time of quantity
$\tilde{\tilde{\tilde{( )}}}$	Denotes averaged values
$( )^+$	The ratio of the product of the left half plane zeros of ( ) to the product of the left half plane poles
$( )^-$	The ratio of the product of the left half plane zeros of ( ) to the product of the right half plane poles

Approved for Public Release

Contrails

Approved for Public Release

Contrails

SECTION I

INTRODUCTION

A. BACKGROUND

The current status of quasi-linear models for the description of human pilot dynamics is good enough to provide useful and effective tools for the solution of a variety of practical flight control problems. Nevertheless, a number of important and troublesome problems cannot be handled within the quasi-linear context and, as a consequence, a practical requirement exists for new approaches. Fortunately, there are a large number of methods available from automatic control theory which offer some promise as methods to be applied to manual control, and there are new views of old data which may also prove fruitful. From these well-springs it is hoped to evolve the new approaches needed. The purpose of this program is to match some of the methods to some of the problems, and to summarize and evaluate these new approaches to pilot/vehicle analysis.

B. CONTEXT OF DESIRED METHODS AND MODELS

The methods and models sought through the new approaches should have potential application to flight control tasks and control system design problems. A further qualification is that they be appropriate for use in some aspect of system prediction; for example, to predict

- System performance in a given situation
- Pilot activity in a given situation
- Pilot commentary and opinion rating trends across situations

The types of control situations for which the capability to predict becomes a requirement might include

- Closed-loop control and regulation of attitude or path about a fixed operating point or about time-variable operating points
- Open-loop response to external or internal commands and disturbances
- Control retention during abrupt changes in the controlled element, as during a stability augmenter failure

Approved for Public Release

Contrails

Ideally, the models should be able to describe behavioral differences in control situations which are due to changes in the informational input (or display) conditions. For the exemplary control situations noted above, this might be due to differences such as

- Complete VFR display plus all motion cues
- The more restrictive IFR display plus all motion cues
- Incomplete variants of the above, corresponding to various ground-simulator conditions

C. APPROACH

The inspiration and requirements for new methods or models can derive from two sources: (1) knowledge of analytical approaches which may conceivably be applied (solutions in search of problems); (2) deficiencies in existing models (problems in search of solutions). The basic approach adopted in this report is to use the status and deficiencies of extant quasi-linear models to structure a frame of reference for the pursuit of new methods and models. This does not imply a universality of application for quasi-linear techniques, but takes advantage of the accumulated knowledge of their shortcomings, and the realization that alternative approaches must be developed if a number of critical flight control problems are to be attacked at all. The new approaches derive, inductively, from consideration of what is deficient in the current state-of-the-art, followed by attempts to solve the particular problems exposed with whatever techniques are available; and, deductively, starting with a method or theory and looking for problems it can solve. Both kinds of initial points are represented here.

D. PREVIEW OF THE REPORT

The report really consists of two parts. The first comprises Sections II and III which summarize the status quo as evidenced by the quasi-linear pilot models. The remaining sections present the various new models/methods, each in a separate section for clarity.

Section II summarizes the current status of quasi-linear models for compensatory and pursuit tracking, multiloop tasks, and the neuromuscular

Approved for Public Release

Contrails

subsystem. This provides the prologue to Section III, where a comprehensive tabulation of the deficiencies of these models is given, thereby defining the problem areas.

The first new model/method topic (Section IV) is a preliminary examination of low frequency lead generation. Two possible and complementary schemes are proposed. In one the lead derives from velocity computation at the optic nerve level, whereas the other depends on computation of first-position differences at a more central location. Each model accounts for some of the observed differences in behavior between situations requiring low frequency lead and those which do not. Both models are refinements in detail to existing quasi-linear descriptions.

Section V examines the most elementary nonstationary situation, where the nonstationary feature is a transient, i.e., step forcing function. The most complete model available at the outset of this program is first reviewed and used as a basis for constructing an experimental program. The experimental data are then presented. In the event these contradict many of the features of the hypothetical model, a new dual-mode control model is presented as a replacement.

In Section VI the Successive Organization of Perception (SOP) hypothesis is reviewed and elaborated. The major purpose of this section is to present an efficient way of coding and selecting the most likely mode of behavior from those which have been identified and modeled as phases within the over-all Successive Organization of Perception context. It is, among other things, a description of an analysis procedure which enables one to select model forms appropriate to a specific situation.

Physiological aspects of human tracking behavior are described in Section VII. Signal flow and functional operations compatible with physiological knowledge are shown, and various substructures capable of exhibiting the "special case" behavioral patterns associated with compensatory, pursuit, and precognitive operations are discussed.

The last three sections are attempts to apply the powerful techniques of optimal control theory to alleviate some of the deficiencies in quasi-linear models summarized in Section III. The first question attacked (in Section VIII) is the optimality of manual control systems for elementary

Approved for Public Release

Contrails

performance criteria such as mean-squared error. This is accomplished using a simple test for optimality which involves only the mean-squared value of signals within the manual control system and requires no knowledge of the dynamic details. The experimental results are introduced to compare with the theoretical constructions.

In Section IX the inverse optimal control problem is used in an effort to formulate compensatory tracking performance indices for which the loop dynamics, $Y_p Y_c$, measured experimentally are optimal. This approach can provide a more quantitative basis for adjustment.

Finally, Section X considers the estimation of human pilot describing functions for novel situations by using optimal control theory. The procedures described permit much of the artistry in estimating describing functions for given controlled elements to be replaced by a concrete computational procedure.

Approved for Public Release

Contrails

SECTION II

STATUS OF QUASI-LINEAR MODELS

Quasi-linear models are the most extensively applied and best based empirically of all models for pilot behavior. They are totally satisfactory for many problems, while for others they either have some promise contingent on further development or are fundamentally deficient. To correct these latter shortcomings new model/method structures are needed, and one starting point for defining these new approaches is provided by the existing structure of quasi-linear pilot models.

The status of quasi-linear models is summarized in this section to provide this frame of reference. Single-loop compensatory situations are mentioned first, followed by the single-loop pursuit models. Then, a digression is made to consider the characteristics of the neuromuscular subsystem, a key element in any model of the pilot. Next, the structure of multiloop control is summarized. Finally, the more significant restrictions to be considered in the application of extant quasi-linear models are noted.

A. SINGLE-LOOP COMPENSATORY

The first problem in manual control system dynamics is to determine the pilot response in the single-axis compensatory tracking task defined by the block diagram of Fig. 1. A stationary random-appearing forcing function, i(t), is applied which results in a displayed error, e(t). The pilot output, c(t), acts on the fixed controlled element dynamics, Y_c, to produce the system output, m(t).

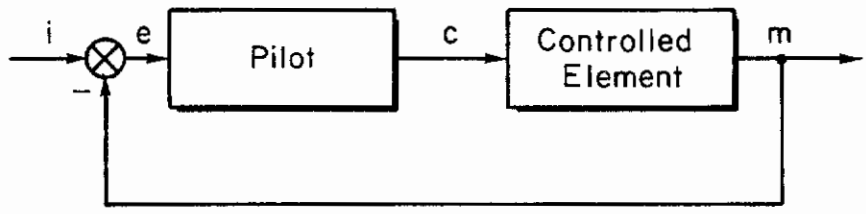

Figure 1. Single-Axis Compensatory Tracking

Approved for Public Release

Contrails

Measurements of pilot characteristics in this task have been made by a large number of investigators over the last twenty years (Refs. 1–15). A summary of results based on cross-spectral and spectral analysis is given in Table I.

At various times* throughout the period during which this now imposing data base was being accumulated, Analytical/Verbal Models were evolved which described or were compatible with all the then existing data. Besides serving as encapsulated descriptions of the data, these models were also intended to be used in new situations which are extrapolations of those for which the data were obtained. In fact, the primary emphasis in the entire model-building effort has been placed on models which can be used to predict pilot dynamic response characteristics in manual vehicular control systems.

Another cut has been taken recently at updating the Analytical/Verbal Quasi-linear Pilot Model. This was accomplished mainly in connection with Ref. 12, although it is not explicitly contained therein, and is summarized in Ref. 17 as the circa 1965 model. As with the other models mentioned above, the circa 1965 model consists of two parts — the describing function and the remnant — and contains two kinds of information: (1) analytical, giving the general form of the dynamics, and (2) verbal, providing the adjustment rules which tell how the parameters in the general form are to be adjusted so that the model is an estimate of pilot behavior for a specified situation. The describing function portion of the circa 1965 Analytical/Verbal Model is summarized below. It is generally applicable to fixed-base tracking or regulation problems where the system inputs are random-appearing, and where the pilot, vehicle, and inputs are reasonably time-stationary.

*For example: 1957, Ref. 6; 1959, Ref. 16; 1960, Ref. 11.

Approved for Public Release

Contrails

TABLE I

SUMMARY OF DESCRIBING FUNCTION PLUS REMNANT DATA

INVESTIGATOR (Ref.)	NO. OF RANDOM-APPEARING FORC. FUNC. TYPES INVEST.	NO. OF CONTROLLED ELEMENT TYPES INVESTIGATED	MANIPULATOR	NO. OF CROSSOVER REGION MEASUREMENTS	REMARKS
Tustin (1)	2	2	Spade grip, spring restraint	0	Simulated tank gun turret tracking. Single-dimensional input.
Russell (2)	2	11	Handwheel, no restraint	6	Single-dimensional input.
Goodyear (3,4)	2	2	Aircraft control stick	0	Simulated control of aircraft pitch axis in both stationary and pitching simulator. Single-dimensional input.
Krendel, et al (5,6)	3	3	Aircraft control stick	0	Simulated control of aircraft lateral and longitudinal axes in tail-chase, with and without airframe dynamics. Two-dimensional input.
Elkind (7)	20	1	Pencil-like stylus, no restraint	6	Single-dimensional input. Some remnant data.
Seckel, et al (8)	2	2	Aircraft control stick	2	Stabilization of aircraft lateral and longitudinal axes in both flight and fixed-base simulator. Two-dimensional input.
Hall (9,10,11)	1	20	Aircraft control wheel	19	Stabilization of various aircraft longitudinal dynamics while also controlling a fixed set of lateral characteristics. Two-dimensional input.
McRuer, et al (12)	3	22	Lateral side stick	230	Stabilization of a wide range of idealized dynamics contrived to evoke a complete range of operator transfer characteristics. Single-dimensional input. Good remnant data.
Stapleford, et al (13)	3	3	Lateral side stick and rudder pedals	37	True multiloop situation, lateral control in a tail-chase. Single-dimensional input, two-dimensional display.
Magdaleno, et al (14)	1	2	Longitudinal side stick, spring and inertia restraint	150	Extreme ranges of restraint and controlled element values. Single-dimensional input.
Smith (15)	1	3	Aircraft control stick	>24	Stabilization of aircraft lateral and longitudinal axes in both flight and fixed-base simulator. Single-dimensional input.

Approved for Public Release

Contrails

1. The Circa 1965 Analytical/Verbal Describing Function Model

a. General describing function form. For visual inputs in single-loop systems the general describing function form for the human pilot is that of the precision model:

$$Y_p = K_p e^{-j\omega\tau}\left(\frac{T_L j\omega + 1}{T_I j\omega + 1}\right)\left\{\underbrace{\left(\frac{T_K j\omega + 1}{T_K' j\omega + 1}\right)}_{e^{-j\alpha/\omega}}\underbrace{\frac{1}{(T_{N_1} j\omega + 1)\left[\left(\frac{j\omega}{\omega_N}\right)^2 + \frac{2\zeta_N}{\omega_N} j\omega + 1\right]}}_{\left[\frac{1}{T_N j\omega + 1}\right] \text{ or } e^{-j\omega T_N}}\right\} \quad (1)$$

For conditionally stable loops the low frequency phase can be an important feature of the manual control system and an appropriate simplified version of Eq. 1 is

$$Y_p \doteq K_p\left(\frac{T_L j\omega + 1}{T_I j\omega + 1}\right) e^{-j\left[\omega(\tau + T_N) + \alpha/\omega\right]} \quad (2)$$

This form is also adequate for most other systems as well. However, for loops wherein low frequency performance is essentially unaffected by the low frequency phase lag term, $e^{-j\alpha/\omega}$, Eq. 1 can be simplified to

$$Y_p \doteq K_p\left(\frac{T_L j\omega + 1}{T_I j\omega + 1}\right) e^{-j\omega(\tau + T_N)} \quad (3)$$

In either of Eqs. 2 and 3 the $e^{-j\omega T_N}$ is interchangeable with $(T_N j\omega + 1)^{-1}$ Furthermore, if $\omega T \leq 1$, $e^{-j\omega T} \doteq -\left[(T/2)s - 1\right]/\left[(T/2)s + 1\right]$.

b. Adjustment rules

(1) Equalization selection and adjustment. A particular equalization is selected from the general form $K_p(T_L j\omega + 1)/(T_I j\omega + 1)$ such that the following properties obtain:

(a) The system can be stabilized by proper selection of gain, preferably over a very broad region.

(b) Over a considerable frequency range in the crossover region (that frequency band centered on the crossover frequency, ω_c), $|Y_p Y_c|_{db}$ has approximately a −20 db/decade slope.

(c) $|Y_p Y_c| \gg 1$ at low frequencies to provide good low frequency closed-loop response to system forcing functions (commands).

Examples of form selection and basic adjustment are provided in Table II.

Approved for Public Release

TABLE II

PILOT EQUALIZATION CHARACTERISTICS

Controlled Element Approximate Transfer Function in Crossover Region	Pilot Equalizer Form	Equalizer Adjustments		
		Low Frequency ($\omega \ll \omega_c$)	Mid-Frequency (ω_c Region)	High Frequency ($\omega > \omega_c$)
K_c	Lag-lead	$\frac{1}{T_I}$	—	T_L to partially offset $\tau + T_N$
$\frac{K_c}{j\omega}$	High Frequency Lead	—	—	T_L to partially offset $\tau + T_N$ ($T_L\omega_c < 1$)
$\frac{K_c}{(j\omega)^2}$	Low Frequency Lead	$\frac{1}{T_L}$	—	T_L not available to offset $\tau + T_N$
$\frac{K_c}{j\omega(Tj\omega + 1)}$	Mid-Frequency Lead ($T > \tau$)	—	$T_L \doteq T$	—
	High Frequency Lead ($T < \tau$)	—	—	T_L to partially offset $\tau + T_N + T$
$\frac{K_c}{\left(\frac{j\omega}{\omega_n}\right)^2 + \frac{2\zeta}{\omega_n}j\omega + 1}$	Low Frequency Lead ($\omega_n \ll \frac{1}{\tau}$)	$\frac{1}{T_L}$	—	—
	Lag-Lead ($\omega_n \gg \frac{1}{\tau}$)	$\frac{1}{T_I}$	—	T_L to partially offset $\tau + T_N$

Approved for Public Release

Confidential

Contrails

(2) Effective time delay. After the appropriate equalization form has been adopted, the net effect in the region of crossover of high frequency (relative to crossover) leads and lags can be approximated by replacing these terms in Eqs. 1, 2, or 3 with a pure time delay term, $e^{-j\omega\tau_e}$. The effective time delay, τ_e, is the sum of all the human pilot's pure time delays and high frequency lags less the high frequency leads; i.e.,

$$\tau_e \doteq \tau + T_{N_1} + \frac{2\zeta_N}{\omega_N} - T_{L_{hi}} \quad \text{(for Eq. 1)} \tag{4}$$

$$\doteq \tau + T_N - T_{L_{hi}} \quad \text{(for Eqs. 2, 3)} \tag{5}$$

The notation $T_{L_{hi}}$ implies that only those T_L's used to partially compensate for high frequency phase lags (e.g., see Table II) are involved; otherwise $T_{L_{hi}} = 0$. In general τ_e depends on both the controlled element dynamics and the forcing function bandwidth. These dependencies are approximately serial; viz,

$$\tau_e(Y_c, \omega_i) = \tau_o(Y_c) - \Delta\tau_e(\omega_i) \quad \text{where} \quad \Delta\tau_e(0) = 0 \tag{6}$$

(a) Estimation of τ_o. τ_o can be estimated from the effective order of Y_c in the crossover region using the data of Table III.

TABLE III

EFFECT OF Y_c ON τ_o

Effective Y_c in Crossover Region	$\left[\frac{d\lvert Y_c\rvert_{db}}{d \ln \omega}\right]_{\omega \doteq \omega_c}$ (db/decade)	τ_o (sec)
K_c	0	0.33
$K_c/j\omega$	−20	0.36
$K_c/(j\omega)^2$	−40	0.52

(b) Incremental τ_e due to forcing function. The portion of τ_e given by τ_o is all there is to τ_e when the forcing function bandwidth, ω_i, is zero or very small. As ω_i is increased, however, the neuromuscular lag, T_N, and/or the equalizer lead, $T_{L_{hi}}$, are adjusted to reduce the net lag described by τ_e. A first-order approximation for this effect, good for all controlled elements, is

$$\Delta\tau_e \doteq 0.08\omega_i \tag{7}$$

where $\Delta\tau_e$ is in seconds and ω_i is in radians/second

Approved for Public Release

Contrails

(3) Crossover frequency, ω_c

(a) Basic crossover frequency, ω_{c_o}. The basic crossover frequency for tasks where ω_i is zero or very small, denoted as ω_{c_o}, is found by adding the phase angle, $-\omega\tau_o$, due to the high frequency phase lag, to that of the controlled element and the previously estimated Y_p equalizer characteristics. Estimates for the basic crossover frequency, ω_{c_o}, and the gain are then made from the conditions for neutral stability.

(b) ω_c invariance properties

1) ω_c — K_c independence. After initial adjustment, changes in controlled element gain, K_c, are offset by changes in pilot gain, K_p; i.e., system crossover frequency, ω_c, is invariant with K_c.

2) ω_c — ω_i independence. System crossover frequency depends only slightly on forcing function bandwidth with $\omega_i < 0.8\omega_{c_o}$.

3) ω_c regression. When ω_i nears or becomes greater than $0.8\omega_{c_o}$, the crossover frequency regresses to values much lower than ω_{c_o}.

4) Phase margin adjustment with ω_i. Since ω_c is essentially independent of ω_i, and $\Delta\tau_e$ is directly proportional to ω_i, the system phase margin, φ_M, is directly proportional to ω_i. This strong dependence of phase margin on the forcing function bandwidth is associated with the linear variation of $\Delta\tau_e$ with ω_i, and is essentially an alternate statement of Eq. 7.

B. SINGLE-LOOP PURSUIT

Pursuit behavior is formally distinguished from compensatory by the addition of the feedforward loop containing the block Y_{p_i} and/or the direct feedback of output via the block Y_{p_m} to describe the pilot's actions. These are shown in Fig. 2. The Y_{p_i} operation indicates that the pilot has full knowledge of the forcing function either directly or by implication and takes advantage of this knowledge to appropriately modify his response. The Y_{p_m} operation represents a similar kind of action on the output. Those functions which are typically internal to the pilot are enclosed by a dashed line in Fig. 2, including the differential which produces some error, e. In the alternative case where e and m are available, i may be inferred by the pilot.

Approved for Public Release

Contrails

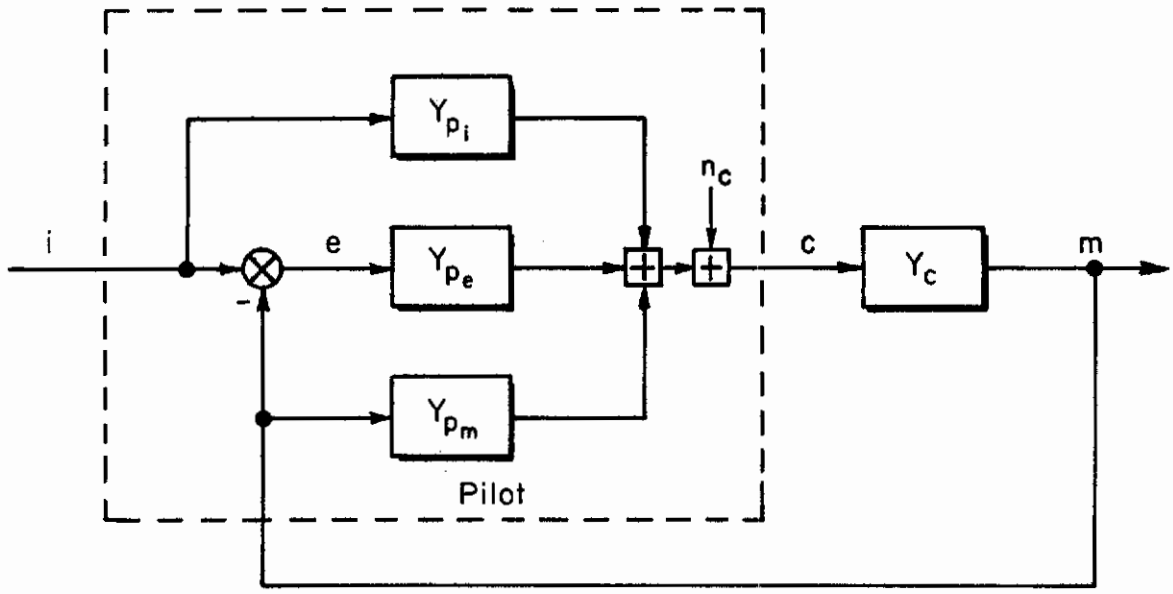

Figure 2. Single-Axis Pursuit Tracking

Recent experimental activities (Ref. 18) have resulted in a better understanding of pursuit behavior. One explanation of these results is that the block operating on the error, Y_{p_e}, is much the same as the quasi-linear describing function for compensatory tracking, and that the pilot does use his additional knowledge of the forcing function to improve his performance with Y_{p_i}. Operations in which Y_{p_m} are likely to be generated have not yet been demonstrated.

The adjustment of Y_{p_i} is nearly $|Y_{p_i}Y_c| \doteq 1$ over a fairly broad frequency range. The phase angle of $Y_{p_i}Y_c$ varies from zero somewhat, but otherwise the action of the feedforward is such as to reduce the error to zero, and to make the output follow the input closely. That the "proper" action by the pilot is to approximately invert the controlled element is apparent from the relationships between output, error, and forcing function, i.e.,

$$M(j\omega) = \frac{(Y_{p_i} + Y_{p_e})Y_c I(j\omega) + Y_c N_c(j\omega)}{1 + Y_{p_e}Y_c} \tag{8}$$

$$E(j\omega) = \frac{(1 - Y_{p_i}Y_c)I(j\omega) - Y_c N_c(j\omega)}{1 + Y_{p_e}Y_c} \tag{9}$$

If the remnant is neglected, the output, $M(j\omega)$, will equal the input and

Approved for Public Release

Contrails

the error will be zero when $Y_{p_i} = 1/Y_c$. In fact, the system becomes nearly open-loop through the feedforward, with the feedback acting as a vernier control and as a means of stabilizing the controlled element when needed.

An excellent example of pursuit activity is given in Fig. 3, which shows the Y_{p_i} generated in control of a second-order system with an unstable divergence. The degree to which the ideal $Y_{p_i}Y_c = 1$ can be approached in practice is remarkable for the amplitude ratio, although nowhere near as close in phase.

C. NEUROMUSCULAR SUBSYSTEM

Those aspects of the control force characteristics involving the pilot's neuromuscular system as a closed-loop actuation system are subtle and not generally understood. Yet they can be exceptionally important and critically limiting in such matters as

- Control precision where limited by the pilot's neuromuscular system
- Effects of control system nonlinearities, including their connections with control system sensitivity requirements

Fortunately, recent research on human pilot dynamics (e.g., Refs. 18–26) has revealed enough about the human pilot neuromuscular characteristics to allow a rational approach in considering such factors.

Although the details of the human's actuation system for even the simplest of motions are enormously complicated from a component standpoint, its behavior for random-appearing visual inputs and spring-restrained manipulators can be modeled quite well using the equivalent system of Fig. 4. The details of the "components" in this system, which amount to ensembles of neurological sensing, equalizing, and actuating apparatus, are beyond the present scope (see Ref. 28), although some features are discussed in Section VII-A. The net results of their actions can be treated, however. These are implicit in the component describing functions for the elements in Fig. 4. For the spindle ensemble, which provides in one entity the feedback, a bias adjustment, some adjustable series equalization, and the source of one command to the system, the describing function is a lead/lag, i.e.,

Approved for Public Release

Contrails

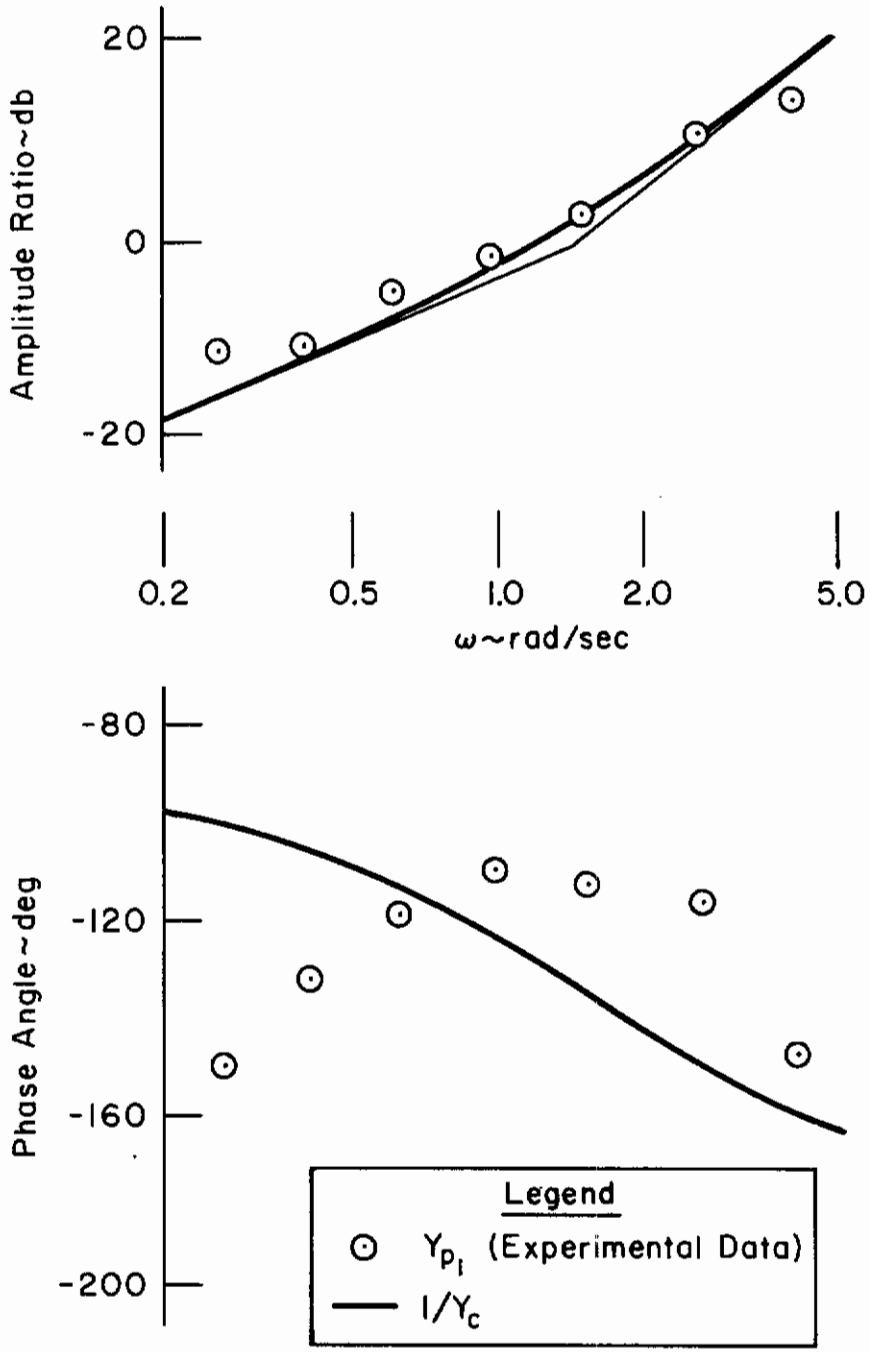

Figure 3. Feedforward, Y_{p_i}, for Pursuit System with $Y_c = 2.5/j\omega(j\omega-1.5)$

Approved for Public Release

Contrails

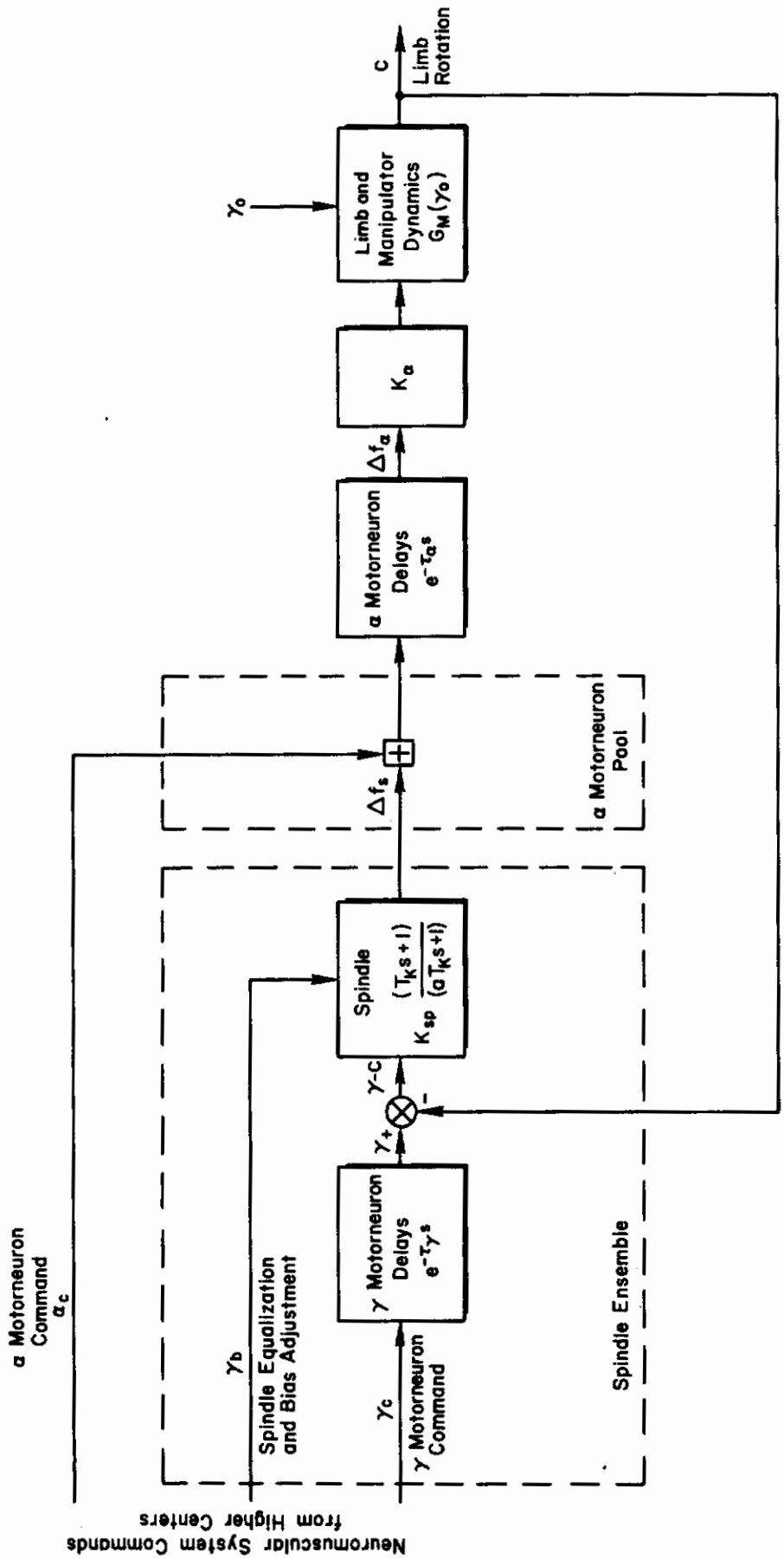

Figure 4. Elementary Neuromuscular System Model

Approved for Public Release

Contrails

$$\frac{\Delta f_s}{\gamma - c} \doteq \frac{K_s(T_K j\omega + 1)}{aT_K j\omega + 1} \tag{10}$$

The lag is a high frequency effect because $a \ll 1$, and the lead is the dominant part of the equalization. The γ motor neuron command provides one means of actuating the neuromuscular system.

For many inputs requiring faster signal processing, an α motor neuron command from higher centers provides the dominant signal to the neuromuscular system, as shown in Fig. 4. This is a second way to actuate the neuromuscular system.

The limb/muscle/manipulator dynamics, or actuation elements, are more complicated. An oversimplified equivalent circuit diagram of this subsystem is shown in Fig. 5, and a Bode diagram in Fig. 6. The effective damping and time constants in this subsystem can be changed by varying the average tension in the muscles. This can be done either consciously or subconsciously. The transfer characteristics are

$$K_\alpha G_M = \frac{c}{\Delta f_\alpha} = \frac{\frac{K_\alpha}{M}}{(j\omega)^2 + \left(\frac{C_P P_o + B_c}{M}\right) j\omega + \left(\frac{k_M + k_c}{M}\right)}$$

In tracking tasks the neuromuscular system average tension, P_o, is large, so the transfer characteristic is overdamped and has the form,

$$K_\alpha G_M = \frac{\frac{K_\alpha}{M}}{\left(j\omega + \frac{1}{T_{M_1}}\right)\left(j\omega + \frac{1}{T_{M_2}}\right)} \tag{11}$$

Approximate factors, which apply for $C_P P_o \gg B_c$, are

$$\begin{aligned} \frac{1}{T_{M_1}} &\doteq \left(\frac{k_M + k_c}{C_P}\right)\left(\frac{1}{P_o}\right) \\ \frac{1}{T_{M_2}} &\doteq \left(\frac{C_P}{M}\right) P_o \end{aligned} \tag{12}$$

Approved for Public Release

Contrails

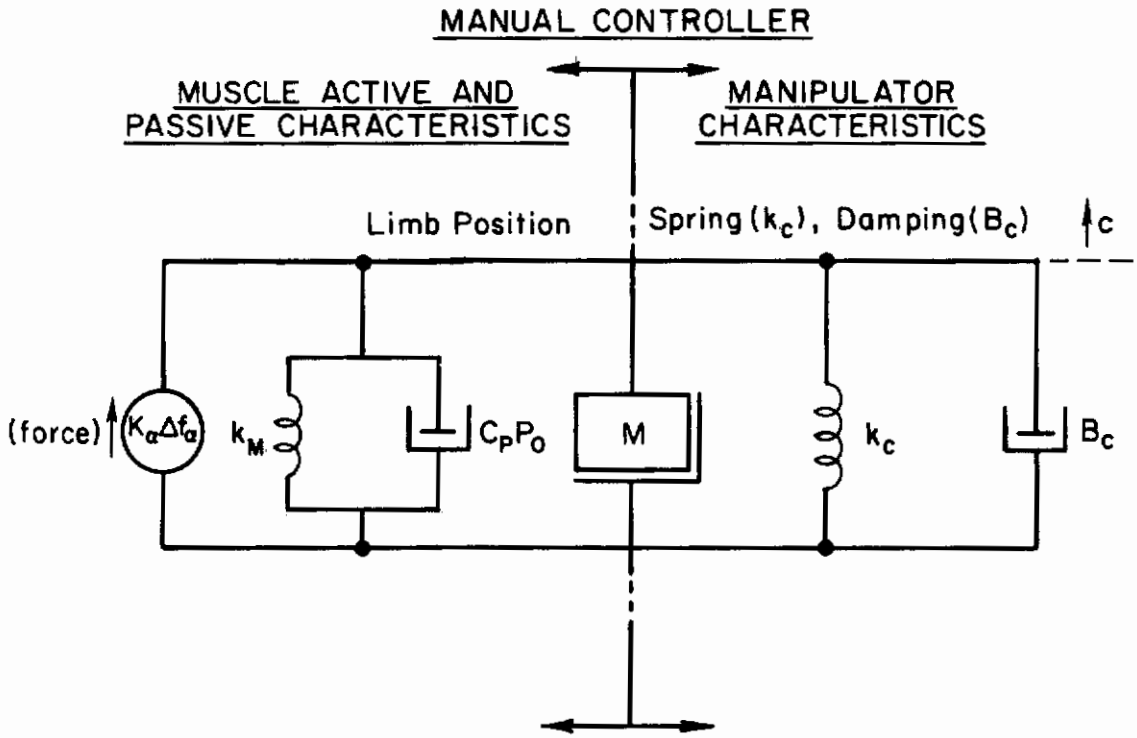

Figure 5. Limb/Manipulator Load Dynamics for Pilot's Neuromuscular (Actuation) System

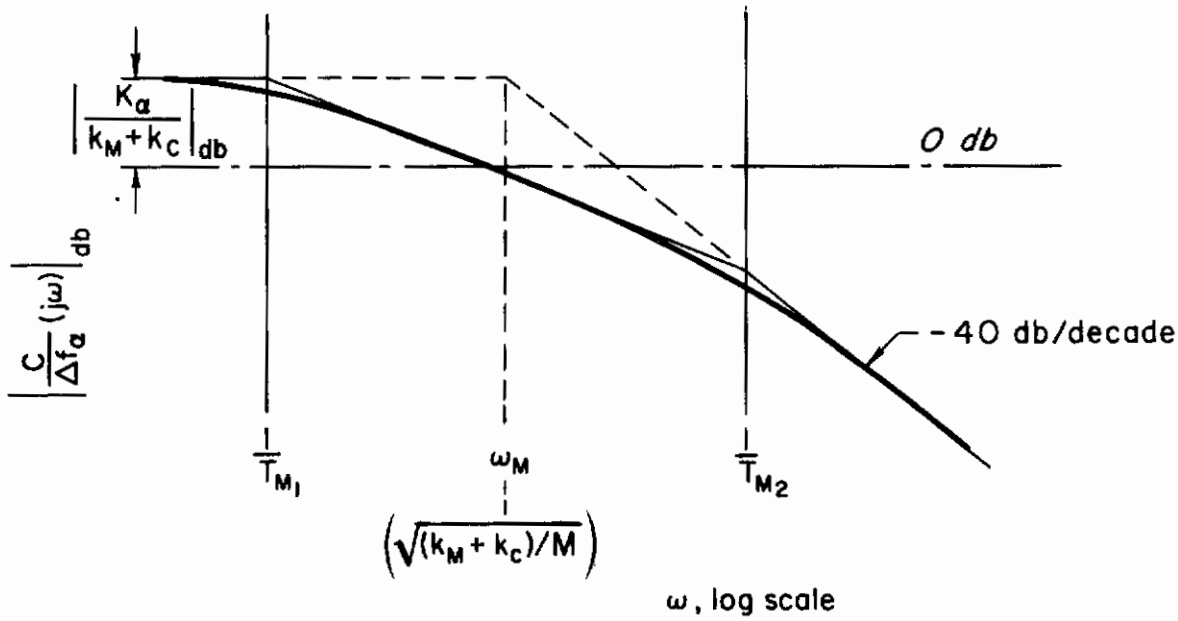

Figure 6. jω-Bode Diagram for Limb/Manipulator Dynamics

Approved for Public Release

Contrails

The relationships in Eq. 12 show the fundamental effects of changes in the steady-state isometric tension, P_o. If P_o is increased, the high frequency time constant, T_{M_2}, is decreased and the low frequency time constant, T_{M_1}, is increased. In the process, the width of the −20 db/decade portion of the limb/manipulator system Bode diagram is increased.

A variation in tension causes major changes in the neuromuscular subsystem dynamics and, therefore, in the over-all dynamic behavior of the human operator. The general nature of these changes is indicated for the γ motor neuron command input by the surveys given in Fig. 7. These surveys neglect the pure time delay, τ_α, within the loop. First, for a low value of average tension (which is still sufficient to make G_M over-damped) the closed-loop dynamics are given by

$$\frac{c}{\gamma_c} \propto \frac{(T_K s + 1)e^{-\tau_\gamma s}}{\left(T'_{M_1 P_1} s + 1\right)\left(T'_{M_2 P_1} s + 1\right)\left[(aT_K)'_{P_1} s + 1\right]} \qquad (13)$$

Then, with an increase in tension the open-loop plot changes to that shown for high tension. The closed-loop dynamics are similar in form, but the location of the poles has changed. The basic outcome of the steady-state tension increase is to decrease the effective time delay, T_N, which is approximately

$$T_N \doteq T'_{M_2} + (aT_K)'$$

Accompanying the effective time delay decrease is an increase in the very low frequency phase lag due to the shift in $1/T'_K$. Thus this extremely simple mechanism models the simultaneous variation of very low frequency phase lag and effective time delay observed experimentally (Refs. 12, 26).

A similar type of analysis follows for the neuromuscular system response to an α motor neuron command. The block diagram is that of Fig. 8a. The transfer characteristics are given approximately by

$$\frac{c}{\alpha_c} \propto \frac{(aT_K s + 1)e^{-\tau_\alpha s}}{\left(T'_{M_1} s + 1\right)\left(T'_{M_2} s + 1\right)\left[(aT_K)' s + 1\right]} \qquad (14)$$

where the P_1 or P_2 subscripts are left off as not needed in this context. The numerator time delay, $e^{-\tau_\alpha s}$, represents the effective delay in the stretch reflex loop. The Bode diagram for Eq. 14 is given in Fig. 8b.

Approved for Public Release

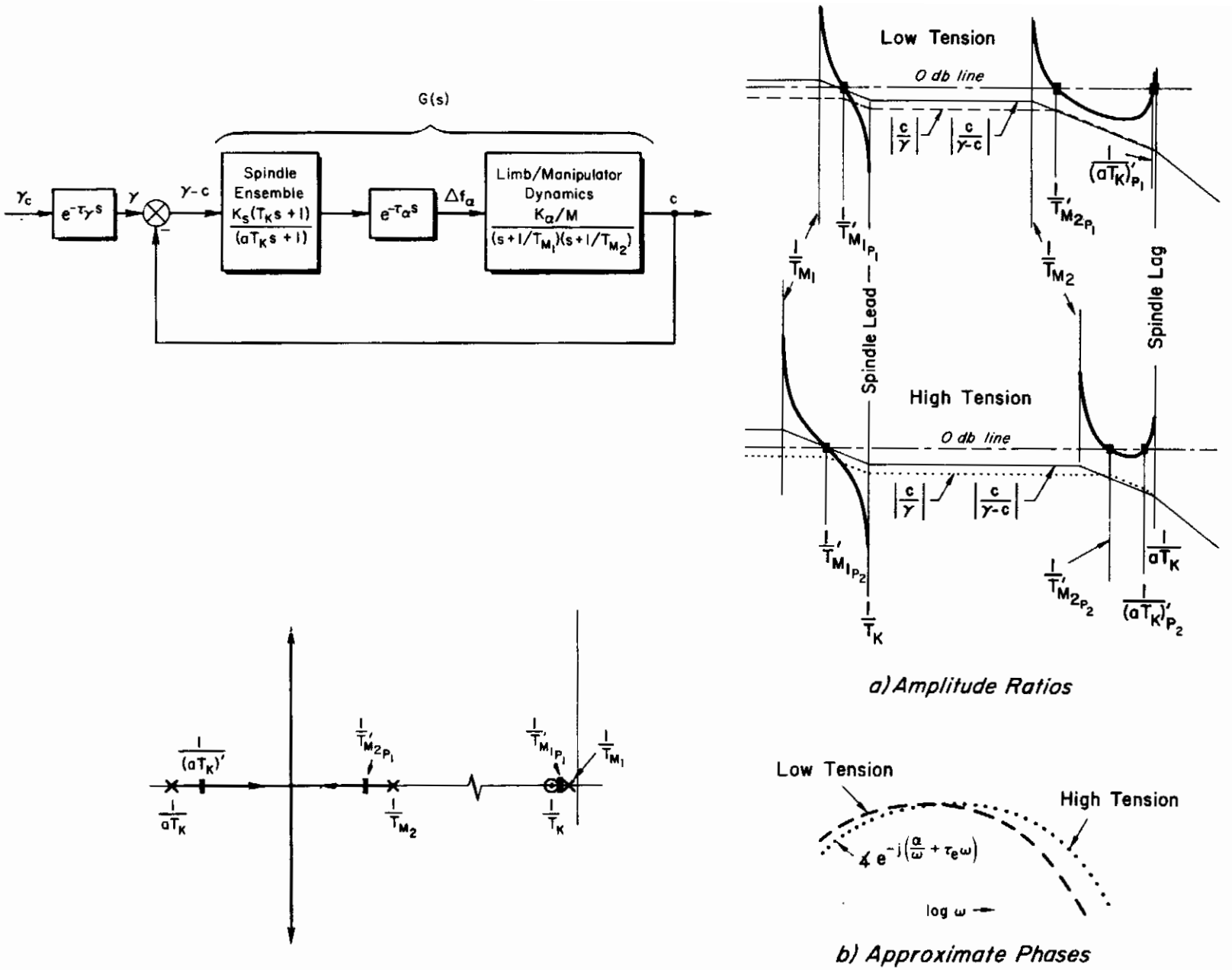

Figure 7. Root Loci of Neuromuscular Subsystem Dynamics with Two Levels of Tension

Approved for Public Release

Contrails

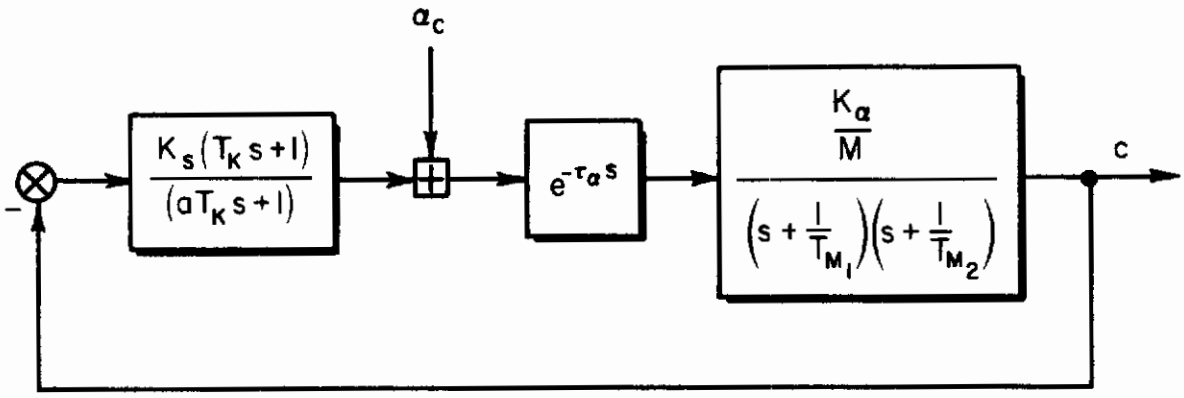

a) Block Diagram

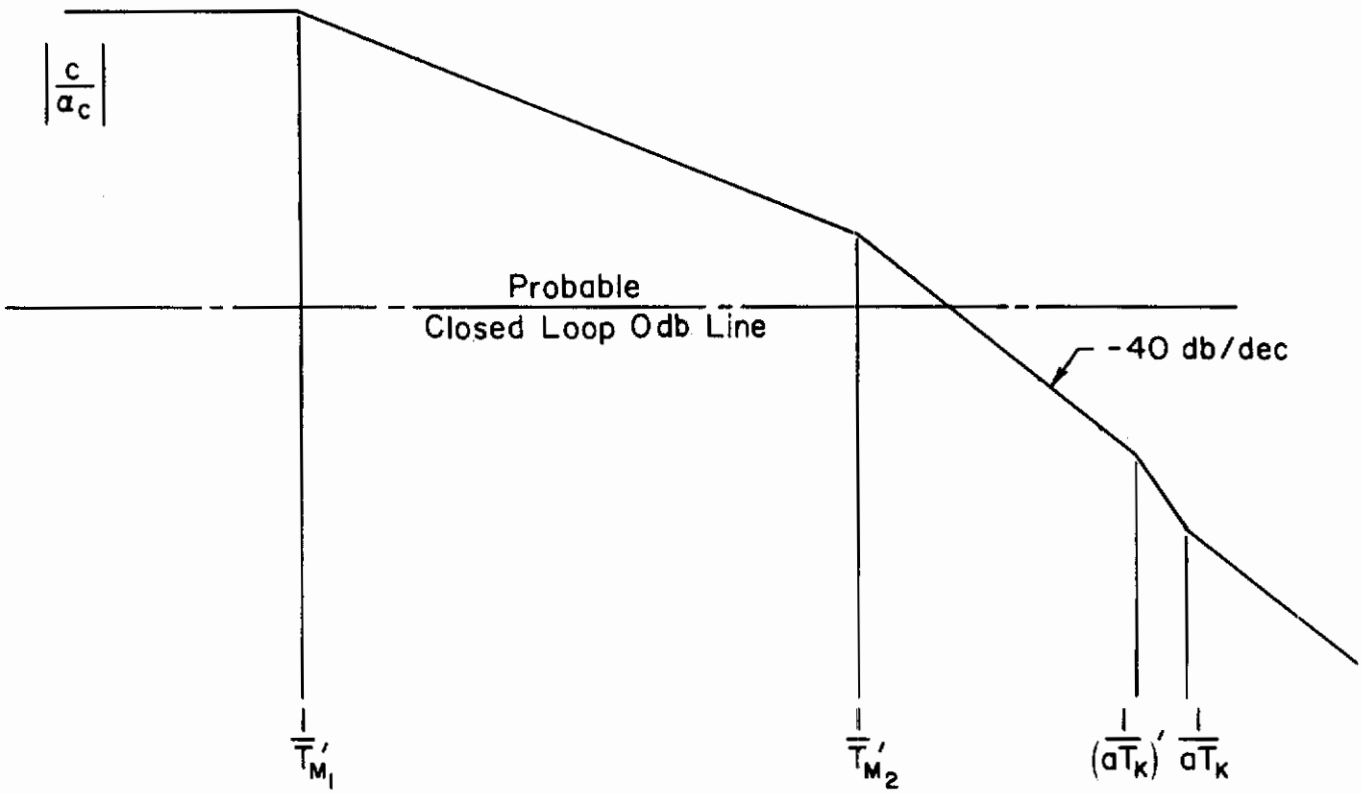

b) Bode Diagram

Figure 8. Alpha Motor Neuron Command System

Approved for Public Release

Contrails

For a closure with increased tension (higher gain) in the limb dynamics, the crossover for the over-all closed-loop system will occur in a frequency region with a slope of −40 db/decade as shown. Further, to the extent that

$$\frac{1}{(aT_K)'} \doteq \frac{1}{aT_K}$$

the α motor neuron command response becomes approximately

$$\frac{c}{\alpha_c} \propto \frac{e^{-\tau_\alpha s}}{\left(T'_{M_1} s + 1\right)\left(T'_{M_2} s + 1\right)} \qquad (15)$$

$$\propto \frac{1}{T'_{M_1} T'_{M_2}} \frac{1}{s^2} \quad ; \quad \frac{1}{T'_{M_2}} < |s| < \frac{1}{\tau_\alpha}$$

D. MULTILOOP PILOT MODEL

The pilot model for multiloop tasks is an extension to the quasi-linear describing function model for single-loop tasks summarized above. As used here the term "multiloop" refers to two or more interacting loops; control tasks involving noninteracting loops are referred to as "multiple-loop." For example, pitch and bank angle stabilization in straight and level flight is a multiple-loop task, while pitch attitude and altitude control is a multiloop task.

Multiloop tasks involve, in general, several sensed quantities (e.g., pitch attitude and altitude) as well as several different pilot outputs (e.g., elevator and throttle). The inputs to the pilot may be perceived by only one of the senses (single modality) or by several (multimodality). The single-modality case — visual cues only — is discussed in subsection 1 below. Some additional factors which must be considered in the multimodality situation — visual and motion cues — are outlined in subsection 2.

Multiloop tasks can also be classified according to the level of pilot activity or perceptive structure. As in single-loop cases, the pilot may operate at various limits, e.g., compensatory, pursuit, etc. In fact, it is possible for the pilot to have a combination of levels, e.g., compensatory in one loop and pursuit in another.

Approved for Public Release

Contrails

To avoid a lengthy and involved presentation, only compensatory behavior is discussed here. The ramifications of pursuit or precognitive pilot behavior can be inferred from the pertinent single-loop presentations.

1. Single Modality

The analysis procedure for a multiloop control task with only visual cues is illustrated in Fig. 9. The information required at initiation of the procedure is a description of the basic task or mission and the environment in which the task is to be performed. These provide the command/disturbance structure shown in Fig. 9 and result in the forcing function specification. Also needed initially is a detailed description of the vehicle dynamics with any associated stability augmentation.

Possible piloting techniques are determined by combining the command and vehicle data via the multiloop extension (Ref. 13) to the single-loop pilot model described above.

The application of the pilot model for multiloop compensatory systems then allows the analyst to estimate, for given command structures and a given set of controlled element dynamics:

- Possible competing sets of pilot loop closures.
- Pilot dynamics in terms of the pilot describing function for each of the loops closed.
- The closed-loop dynamics, such as the system output to command input describing function.
- That portion of the closed-loop average performance due to the pilot's linear operations on the forcing function. Less accurate estimates can be made for that portion of the system mean-squared error due to the pilot's remnant.
- Closed-loop error spectrum, including an estimate for the effective bandwidth.
- Ratios of crossover frequencies for the various loops closed by the pilot.
- Relative bandwidths for each of the loops closed.

In other words, for compensatory systems at least, a great deal of information about possible system structures, pilot and system dynamics, and average performance can be estimated.

Approved for Public Release

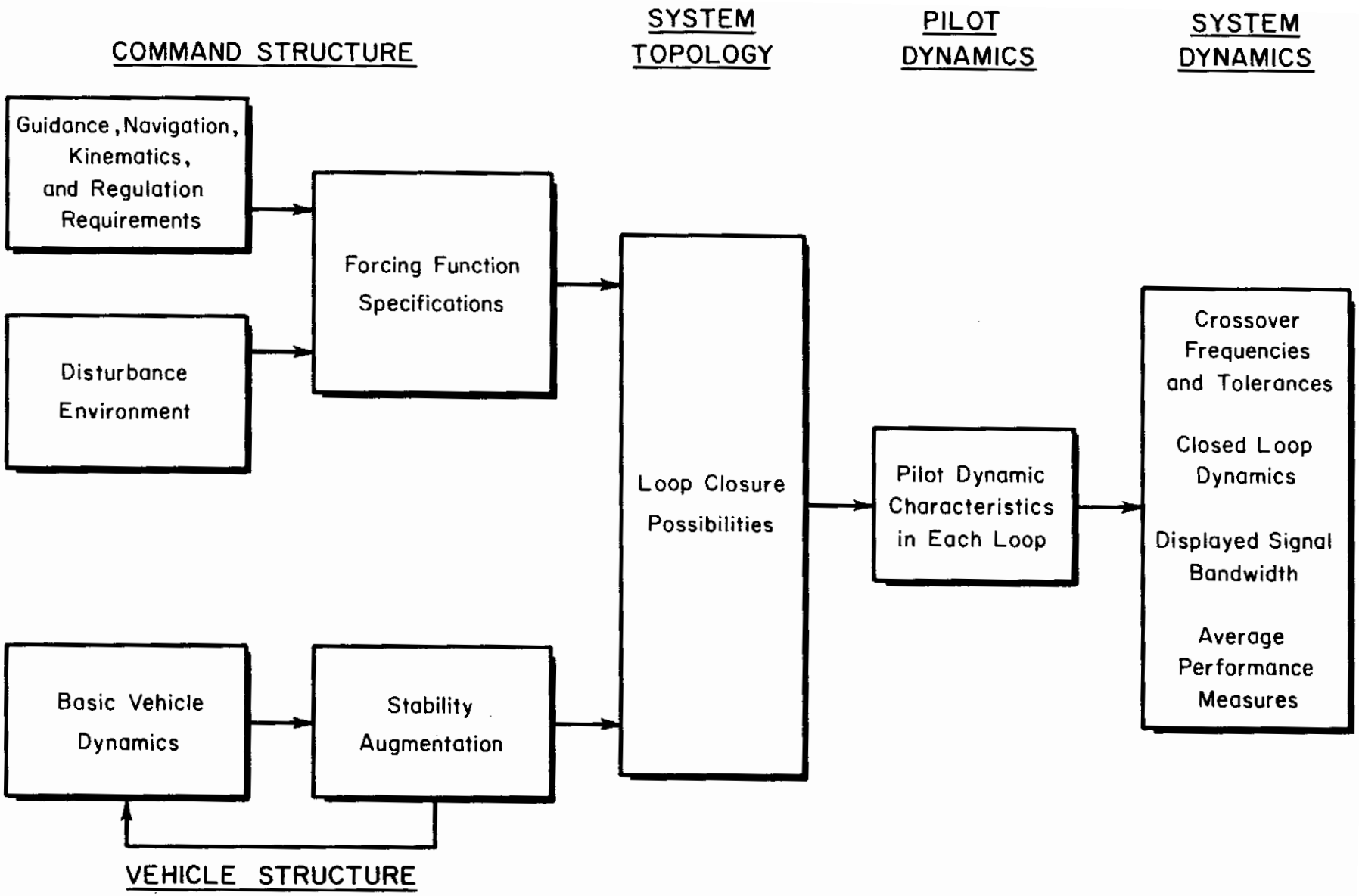

Figure 9. Multiloop Analysis Procedure

Approved for Public Release

Contrails

2. Multimodality

The vestibular apparatus comprising the semicircular canals and the utriculus is probably the most important primary motion response sensor. The canals have a basic second-order response to angular acceleration which is highly overdamped and effectively provides a signal proportional to turn rate over the frequency range from 0.1 to 10 rad/sec (Ref. 29). For prolonged turning the signal "washes out" so that spurious sensations occur when the turning motion stops. The utriculus provides signals proportional to linear accelerations and any washout characteristics it may have are not well documented.

The proprioceptive sensors in the neuromuscular system are of demonstrated importance to the dynamics of the actuator response characteristics. Also, the muscle spindles may be used to generate lead at the subcortical level. While such effects are important in characterizing pilot dynamics, they don't seem to be of particular significance in perception of motion. A possible exception is the extraocular neuromuscular system response in nystagmus.

The nystagmic crossfeeds produce involuntary eye motions as a function of the excitation of the vestibular apparatus. Such motions are known to be important in disorientations and illusions which result from the initiation or sudden cessation of large amplitude maneuvers (e.g., Ref. 30) and other flight operations which have no ordinary earthbound equivalent. Several important motion effects of this nature are summarized in Table IV.

Figure 10 shows a much simplified block diagram of the sensory feedback and crossfeed paths for visual and vestibular cues (see also Ref. 31). There are obviously many ways in which the various loops <u>can</u> be closed, but we will hypothesize that the functions are adjusted so that a "good" control system is obtained. This hypothesis is consistent with indications that a well-trained pilot seems always to achieve near-optimum adjustments of the <u>exterior</u> loops under his cognizance. That is, he picks the same feedbacks and roughly the same gains and (limited) equalization that a competent controls engineer would select. Such an approach to the block diagram of Fig. 10 is perhaps optimistic in that different

Approved for Public Release

TABLE IV

EXAMPLES OF KEY MOTION EFFECTS IN THE PILOT/VEHICLE SYSTEM

SITUATION	VESTIBULAR SENSORS PRIMARILY INVOLVED		
	Utricle	Semicircular Canals	
Attitude control in straight and level flight		X	Semicircular canals can aid total pilot equalization by providing a higher order lead.
Steady turn	X	X	Illusion of straight and level flight; G_{sc} and G_u terms are washed out.
Straight and level after steady turn		X	Sensation opposite of turning; visual sensation of tilt. G_{sc} and G_{vc} are dominant in creating these sensations.
Steady acceleration in horizontal flight, pushover from steady climb	X		Sensation of nose-up change in attitude.
Deceleration	X		Sensation of pitch-down change in attitude.
Straight and level after high angular path ($> 60^{o}$/sec) aerobatics		X	Sensation of turning.
Straight flight after long time high rate rolls.		X	Nystagmus, blurred vision, reversal of background.
High frequency pitching rotations, etc.		X	Blurred vision.

Approved for Public Release

Confidential

Contrails

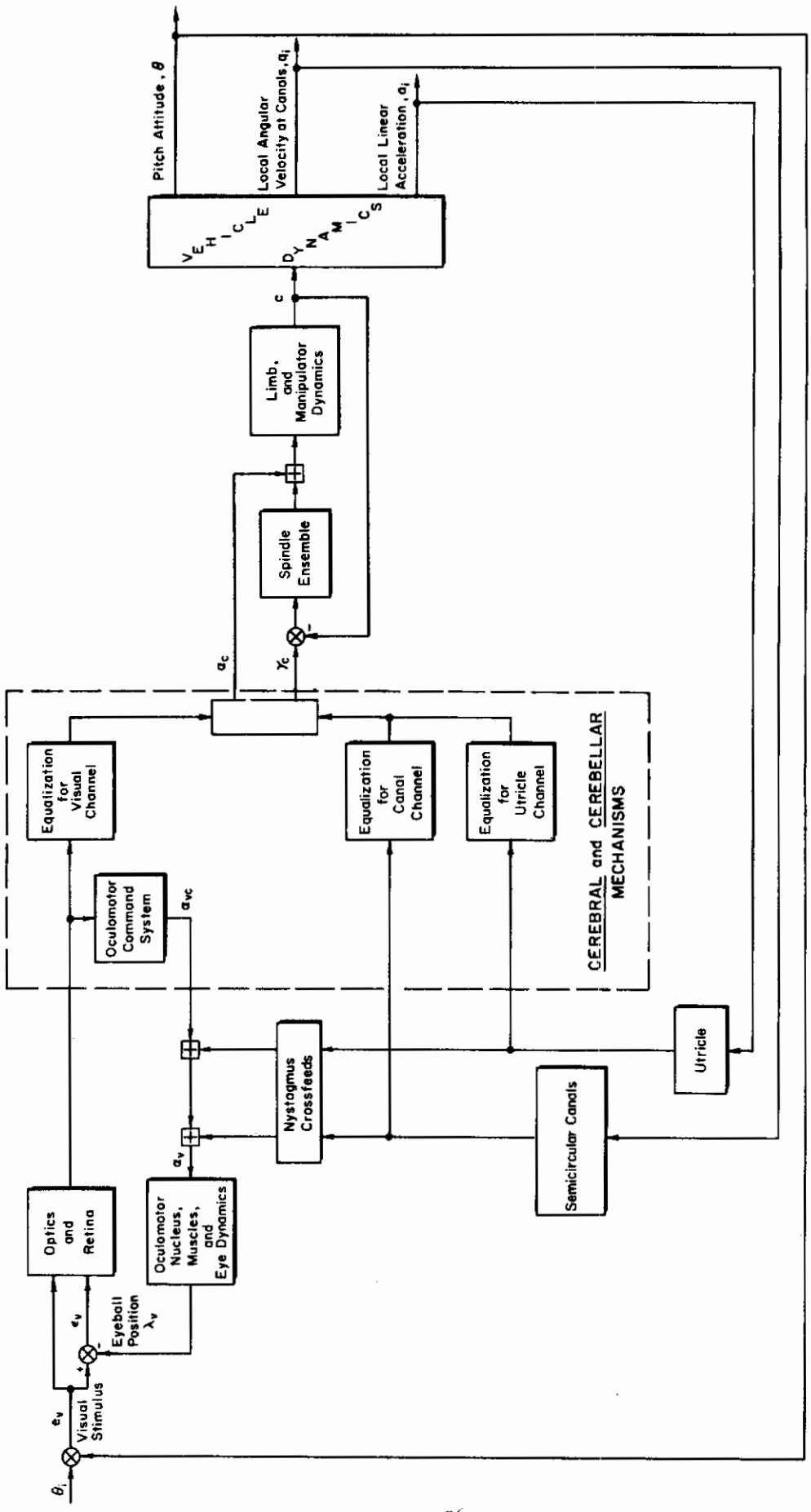

Figure 10. Pilot/Vehicle System for Head-Fixed, Pressure-Manipulator, Attitude Control Tasks

Approved for Public Release

Contrails

sensations are involved, the ways in which these "mix" are not quantitatively known, and relatively inflexible crossfeeds are present. Also, the transfer characteristics of some of the "blocks" may be highly nonlinear or otherwise poorly defined. Nevertheless, systems analyses which show the potential influence of motion effects while recognizing some of these uncertainties can at least serve as a useful guide.

E. RESTRICTIONS ON QUASI-LINEAR MODELS

The quasi-linear models have a number of important shortcomings. Those which restrict their usefulness and generality in situations to which they are normally and quite properly applied are discussed below. Those shortcomings which make them unsuitable at their current state of development for describing pilot response in other control situations are discussed in some detail in Section III, where they are called "deficiencies."

1. Stationarity

The control situation is assumed to be stationary. This implies that:

- The forcing function is a stationary, random-appearing process.
- The controlled element characteristics are time-invariant.

Only time-averaged or statistical properties of the pilot can be derived because of the random nature of the tracking process. As a result, the describing function data express his average behavior over periods greater than at least 5–10 sec duration. The short term variations in behavior are not represented in that portion of the pilot model which is linearly correlated with the forcing function.

Sophisticated subjects who have been trained to temporarily stable performance levels are used in order to enhance the repeatability of the measurements and to better represent skilled performance in flight control tasks. These subjects (frequently test pilots) are well adapted to the control situation, but are not necessarily at their limits of learning. The learning effect can be treated when necessary (e.g., Ref. 32) by considering frozen increments in a long term (days to years) learning process, with each increment a different quasi-linear situation.

Approved for Public Release

Contrails

2. Control Strategy or Criterion

Subjects in the behavioral measurement programs from which the quasi-linear models derive were instructed to reduce or maintain system errors within acceptable (near minimum) bounds. Instructions to the subject to minimize or constrain other state or control variables can result in significantly different control strategies and data (Refs. 33 and 34).

Approved for Public Release

Contrails

SECTION III

DEFICIENCIES IN EXISTING QUASI-LINEAR MODELS

Deficiencies in the quasi-linear models are examined here in some detail to define those areas where a new approach to pilot/vehicle dynamic analysis is needed. The quasi-linear context serves only as a convenient frame of reference, and it is not intended to suggest a short-sighted outlook toward alternative methodologies. On the contrary, an intimate familiarity with the many shortcomings of that model only serves to motivate more strongly the drive for new approaches and solutions to critical unsolved problems.

The summary of new approaches in the form of possible methods or models to relieve deficiencies is presented in Table V. The classification headings are assigned according to quasi-linear model deficiencies in

- Control situations
- Structural connections
- Application

The "control situation" refers to the combination of the system of which the pilot is a component and the external environment within which he is attempting to accomplish a control task. Some examples of manual control situations corresponding to the theoretical classifications used in Table V are given in Table VI. The "structural connection" classification refers to mechanisms and information flow internal to the pilot. Deficiencies classed according to "application" relate to known problems encountered in applying quasi-linear models to the study of handling qualities of manual control.

The nature of the deficiency, be it fundamental or resolvable, is given in Table V when known. Possible new approaches to modeling the phenomenon are given when the deficiency is fundamental. When the deficiency appears to be resolvable, possible extensions or improvements to the quasi-linear form are noted, as well as any applicable new methods or models. The "Remarks" column provides clarification of the deficiency and/or amplification of the possible new approaches to the problem.

Approved for Public Release

TABLE V

DEFICIENCIES IN EXISTING QUASI-LINEAR MODELS

DEFICIENCY	NATURE		POSSIBLE METHODS OR MODELS TO RELIEVE DEFICIENCY	REMARKS
	Fundamental	Resolvable		
IN CONTROL SITUATIONS:				
*Nonstationary forcing function or disturbances (e.g., steps, ramps) (Section V)	✓		Mode switching open-loop, closed-loop model Constant-rate sampled-data model	A feedforward and possibly internal command generation (patterned response, visual modality open-loop) are functional requirements to explain existing data. This may be the most appropriate single-loop application of constant-rate sampled-data model.
Sudden Y_c transitions (including changes in displayed quantities)	✓		Mode switching transition model	Fairly well developed; ties into quasi-linear model for pretransition and posttransition phases.
*Patterned response, progressions and regressions (Section VI)	✓		Successive Organization of Perception sequence with mode switching transitions	Successive increments in SOP are now fairly well understood for the effective compensatory, pursuit, and precognitive phases as individual entities. However, transitions between these phases and the criteria which govern the selection of a particular precognitive response from the set of alternatives are mysteries, and control situation limits are unknown.
Fine-grained behavior in stationary situation; remnant models		✓	Time-varying K_p and τ Random-rate sampled-data model	The short time (less than 5 – 10 sec) behavior of the pilot cannot be described adequately by constant-coefficient describing functions. Current indications from remnant and ρ data are that the pilot's characteristics are akin to those of a mathematical time-varying operator containing the terms $\left[K_{p_o} + \Delta K(t)\right] e^{-\left[\tau_o + \Delta\tau(t)\right]p}$ where ΔK and $\Delta\tau$ are random processes. A random-rate sampled-data system behaves similarly to some extent.
Other control strategies, (e.g., terminal control)		✓	Optimal control theory	Current quasi-linear model minimizes $\overline{e^2}$ approximately, per general instructions. If pilots are instructed to satisfy other criteria, they appear to adjust to minimize these (presuming all information is available) within the limits of fundamental capabilities. However, the multiloop aspects of combined performance criteria have not received much attention.
Gradual Y_c transitions		✓	Time-varying quasi-linear model	Vary the parameters of the quasi-linear model corresponding to a succession of "frozen system" Y_c dynamics.
Nonlinear Y_c, constant coefficient	✓		Nonlinear control theory	In some cases describing function techniques are applicable to Y_c, and quasi-linear models can be employed. In others a phase space description is needed. Time-optimal pilot response with nonlinear Y_c has been observed experimentally in several instances.
*Low frequency lead generation, pulsing behavior (Section IV)	?	?	Time-modulated, amplitude-limited model. Input velocity sensing — NMS pulsing. Input position 1st-diff. computation — NMS following.	To obtain low frequency leads needed to control K/s^2-like dynamics, pilots seem to use pulse rather than displacement inputs and exhibit larger effective time delays. A promising area for sampled-data models.

Approved for Public Release

TABLE V (Continued)

DEFICIENCY	NATURE		POSSIBLE METHODS OR MODELS TO RELIEVE DEFICIENCY	REMARKS
	Fundamental	Resolvable		
IN STRUCTURAL CONNECTIONS:				
*Coding, transmission, ensemble activation (Section VII)	✓		Σ pulse interval modulation	Pulse interval modulation with basic coding system underlying neural conduction, i.e., the links between generator potentials and graded outputs. What is currently applicable only to description of macroscopic behavior may be capable of expansion and summation into an adequate description of more complex behavior which is compatible with the small scale, short-time characteristics of human pilot response.
Sensory-equalization paradoxes	?	?		Whether the observed signal conditioning (equalization) is accomplished centrally or peripherally (in the basic sensors, i.e., retina, spindles, etc.) is not well understood. As a consequence, crucial modeling explanations and basic limitations on equalization are in a similar condition.
*Adaptation mechanism	✓		Learning servo analog with off-line monitor-adjuster	Currently the nature of the pilot adaptation is implied by its steady-state characteristics and its abrupt change for sudden Y_c transitions; and by what is known of anatomical connections. These lend some credence to a learning servo analog which, besides describing the adaptation mechanism, could also serve as a self-adjusting pilot analog for preliminary analysis.
IN APPLICATION:				
VFR inputs		✓		The inputs sensed for VFR conditions are currently estimated on the basis of control needs (i.e., what feedback paths are necessary or desirable for the closed-loop system). The actual quantities perceived are likely to be linear combinations of these, with the weightings between the independent inputs fixed by the geometry and perspective rather than being independently adjustable by the pilot. These aspects of perception can have profound effects on the closed-loop analysis of various hovering-like maneuvers (e.g., approach, landing, dive bombing, etc.).
Inner loop adjustment rules and modality intermix weightings		✓		These are not currently known as well as desired, but existing and future experimental and analysis programs are headed in this direction.
Eye movements for instruments driven by correlated quantities in manual control		✓		Most existing eye movement scan data suitable for predictive use are based on displays being fed uncorrelated signals, with the operator acting as a monitor.
Pilot rating connections with performance indices		✓	Fixed-form optimization	Correlations with pilot rating with forms like $\overline{e^2} + \lambda\overline{(\delta_s - \delta_{opt})^2}$ This is more a correlation effort than anything to do with optimal control per se. Could give a rationale and perhaps even a method to connect pilot ratings with pilot actions. However, the observed pilot rating degradation with high controlled element gain must also be strongly influenced by the minimum control input achievable, the probable magnitude of inadvertent inputs, etc.; and still other characteristics will affect the low controlled element gain cases. Such quantities will be strong functions of the manipulator force/displacement characteristics.
*Requirements for artistry in application (Sections VIII, IX, X)		✓	Inverse optimal control problem. Direct optimal control theory.	Find quadratic performance criteria underlying existing single-loop data. Problems solved may include: (1) basis for simpler applications of existing data using optimal control; (2) insight into internally generated criteria. As an alternative, use optimal control techniques to generate describing function estimates.

Approved for Public Release

Contrails

The entries in Table V are intended to make it comprehensive, and not all the deficiencies are capable of correction by new models or methods. Interest in this report is addressed primarily to models which hold some promise for alleviation of deficiencies noted by an asterisk in Table V.

TABLE VI. EXAMPLES OF CONTROL SITUATIONS

CONTROL SITUATION	EXAMPLES
Nonstationary forcing function or disturbances	Engine failure; discrete gust (shear or gradient); discrete terrain feature
Sudden Y_c transition	Stability augmenter failure; stage separation of space booster; transition to visual during ILS approach
Patterned responses	Procedural turns; sidestep maneuver; landing flare and decrab; VTOL transition; bank-and-stop; etc.
Other control strategies	Terminal control: landing; gunnery runs; dive bombing; orbital rendezvous and docking; satellite attitude changes
Nonlinear Y_c, constant coefficient	Satellite attitude stabilization with on-off controls

Certain of the Table V model/methods are under active investigation in other research programs, and these will not be included in this report. One example is the mode-switching model for step transitions in the controlled element dynamics, which is fairly well developed and has been documented (Ref. 35). Results of other studies of the effect of nonstationarity in the system's dynamics on the pilot's response are given in Refs. 36 through 47.

Approved for Public Release

Contrails

SECTION IV

MODELS FOR LOW FREQUENCY LEAD GENERATION

A. DATA TO BE EXPLAINED

The pilot response characteristics for systems which require low frequency pilot lead are fundamentally different from those characteristics exhibited in systems which do not need such lead equalization. When low frequency lead is not present, as, for example, with the controlled elements $Y_c = K_c$ and $Y_c = K_c/s$, the pilot responses are essentially smooth and uniform when the controlled element gain values, K_c, fall anywhere within a fairly broad range about the respective optimum gains. Inputs which have Gaussian amplitude distributions give rise to pilot output amplitudes which are also Gaussian; and the general character of the response is akin to that of a constant-coefficient linear system with occasional very short (about $1/4 - 1/3$ sec) horizontal flat stretches (see Figs. 11 and 12) which give a discrete appearance to those portions of the response. Not only does the pilot response qualitatively resemble that of a linear system, but the describing function portion alone of the quasi-linear model accounts for more than 80 percent of the total output power. Also, the adjustments rules are easily and accurately applied to the prediction of describing functions for specific controlled elements and sufficient remnant data exist to enable a first-order estimate of the output power due to that component. Consequently, for most engineering purposes we can be generally satisfied with extant quasi-linear models in situations not requiring low frequency pilot lead.

We cannot be so content, however, when low frequency lead is needed to stabilize the system, as with controlled elements which approximate $Y_c = K_c/s^2$ or K_c/s^3 in the frequency region about the pilot/vehicle system crossover. Associated with the lead generation is a marked difference in the character of the human's output from that exhibited when this lead is not present. For instance, the pilot's output is more discrete and pulse-like in nature (see Fig. 13), and the output amplitude distributions are not Gaussian. Quasi-linear models are still appropriate to describe the

Approved for Public Release

Contrails

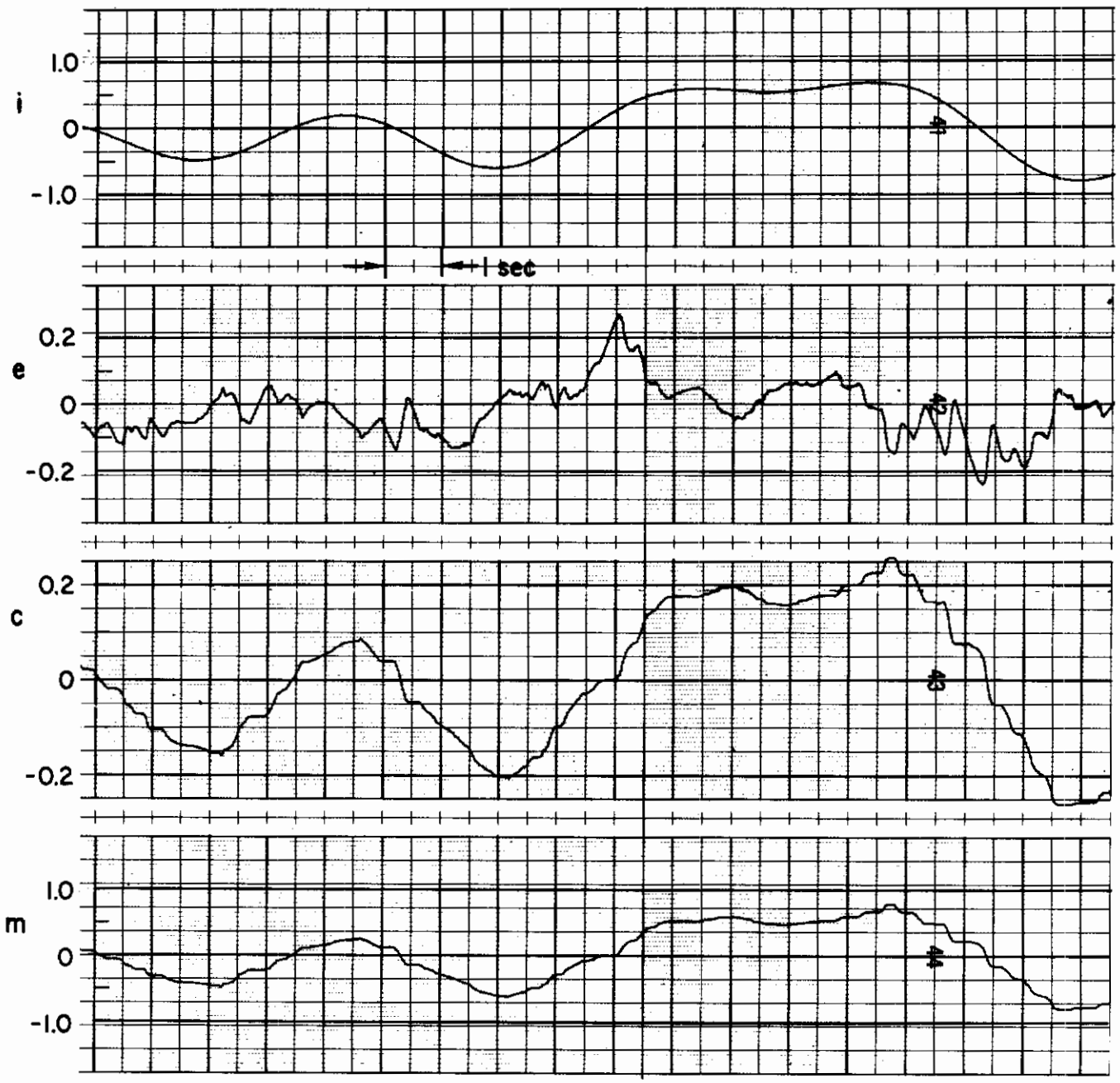

Figure 11. Examples of Tracking Responses for $Y_c = K_c$, $\omega_1 = 1.2$, Subject JDM

Approved for Public Release

Contrails

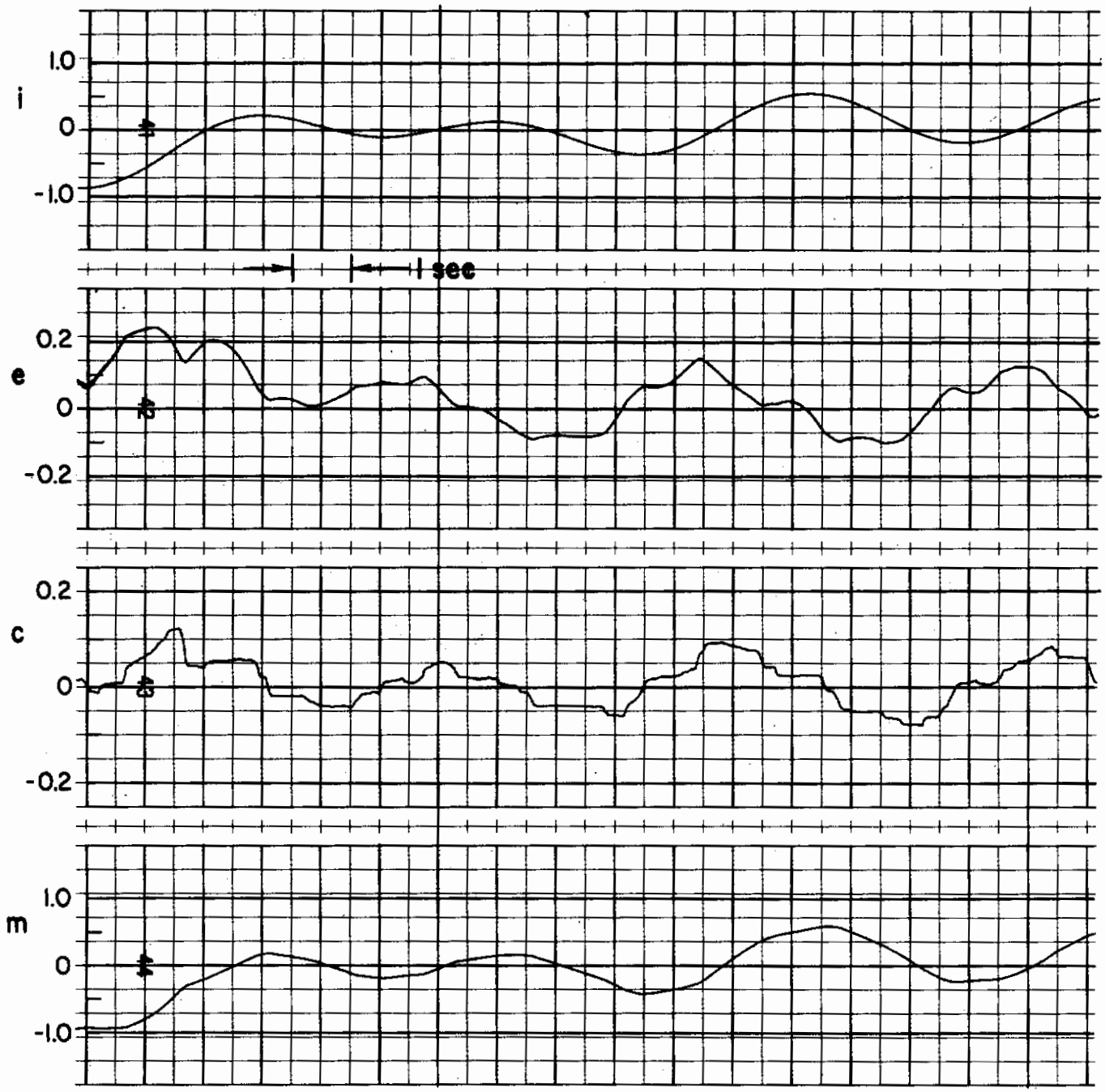

Figure 12. Examples of Tracking Response
for $Y_c = K_c/s$, ω_i = 1.2, Subject JDM

Approved for Public Release

Contrails

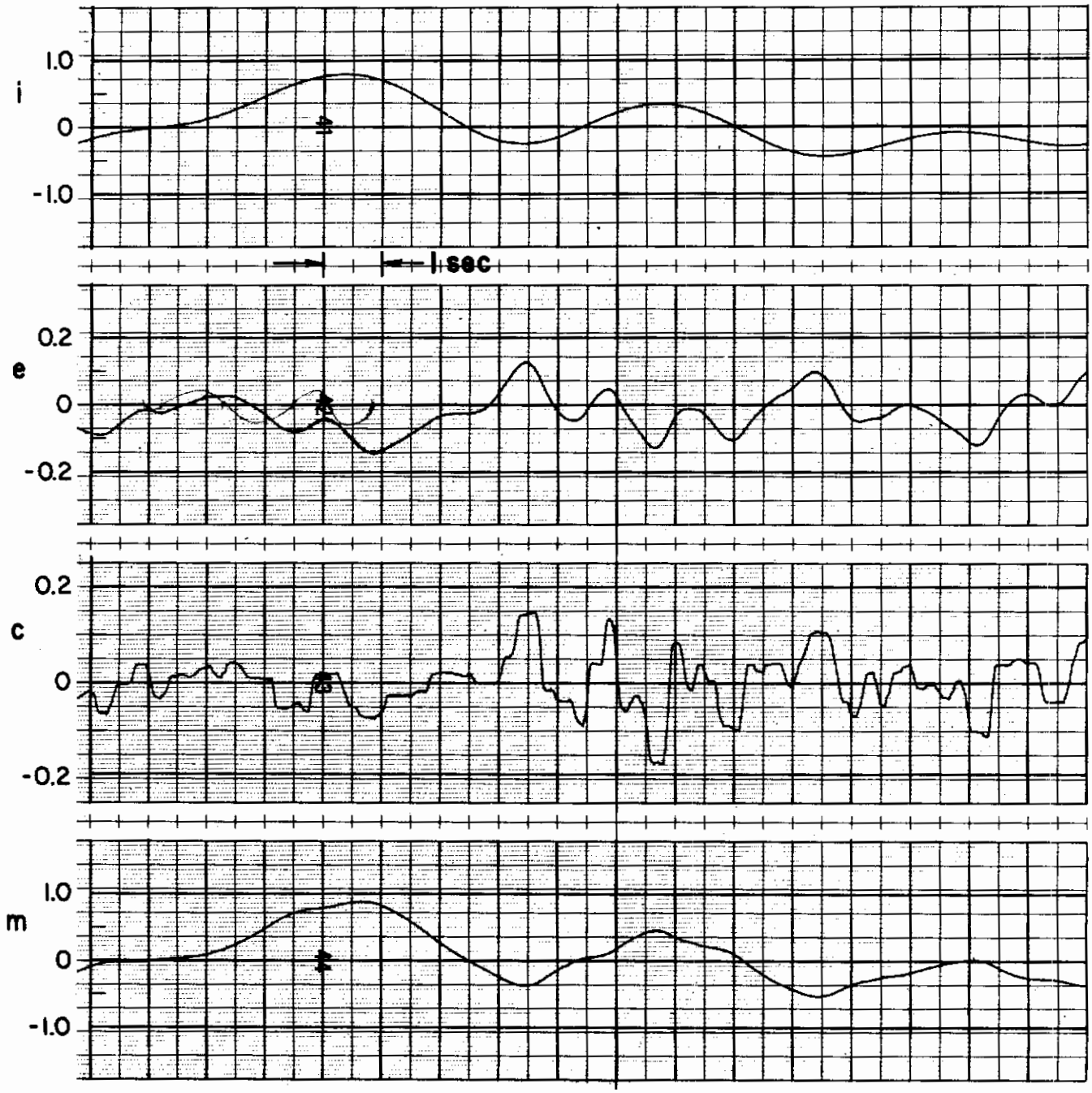

Figure 13. Examples of Tracking Response for $Y_c = K_c/s^2$, $\omega_i = 1.2$, Subject JDM

Approved for Public Release

Contrails

gross on-the-average behavior, but leave much to be desired for more detailed and fine-grained descriptions. The purpose of this section is to present models which are attempts to account for more of the fine-grained detail in the low frequency lead situation.

To be pertinent, the models to be constructed should be compatible with existing data (e.g., that of Ref. 12). These include:

Amount of low frequency lead. The low frequency lead is adjusted such that the open-loop amplitude ratio $|Y_pY_c|_{db}$ approximates a −20 db/decade slope over a very wide range of frequencies about crossover. For second-order controlled elements the lead is represented in the pilot describing function by the factor $T_Lj\omega+1$; the value of T_L is selected either to cancel approximately a controlled element lag [e.g., when $Y_c = K_c/s(T_Rs+1)$, $T_L \doteq T_R$] or to be very large [e.g., $T_L \geq 5$ sec for $Y_c = K_c/s^2$ or $K_c/s(s-a)$]. For the latter case, the frequency range available of measurements is insufficient to enable a pure lead, $T_Lj\omega$, to be distinguished from a lead factor, $T_Lj\omega+1$. Similar nearly pure second-order leads, $(T_Lj\omega)^2$, appear to be present for $Y_c = K_c/s^3$.

Increased effective time delay. The "crossover model" represents the dynamics of single-loop systems by the simplified open-loop describing function

$$Y_pY_c(j\omega) \doteq \frac{\omega_c e^{-j\omega\tau_e}}{j\omega} \doteq \frac{\pi}{2\tau_o(Y_c)} \frac{e^{-j\omega\left[\tau_o(Y_c)-\Delta\tau(\omega_i)\right]}}{j\omega} \qquad (16)$$

Here ω_c has been approximated by $\omega_{c_o} = \pi/2\tau_o(Y_c)$ as discussed at the top of page 11. That part, $\tau_o(Y_c)$, of the effective time delay, τ_e, which depends on the controlled element is larger for systems requiring low frequency lead. Nominally, $\tau_o \doteq 1/3$ sec without and 1/2 sec with (first-order) low frequency lead.

Amplitude distributions of pilot output. When maximum values of low frequency lead are present, the pilot's output amplitude distributions are non-Gaussian. Typically, these are bimodal distributions (Fig. 14) which reflect the pulsing nature of the output. The degree of bimodality depends primarily on the particular subject.

Approved for Public Release

Contrails

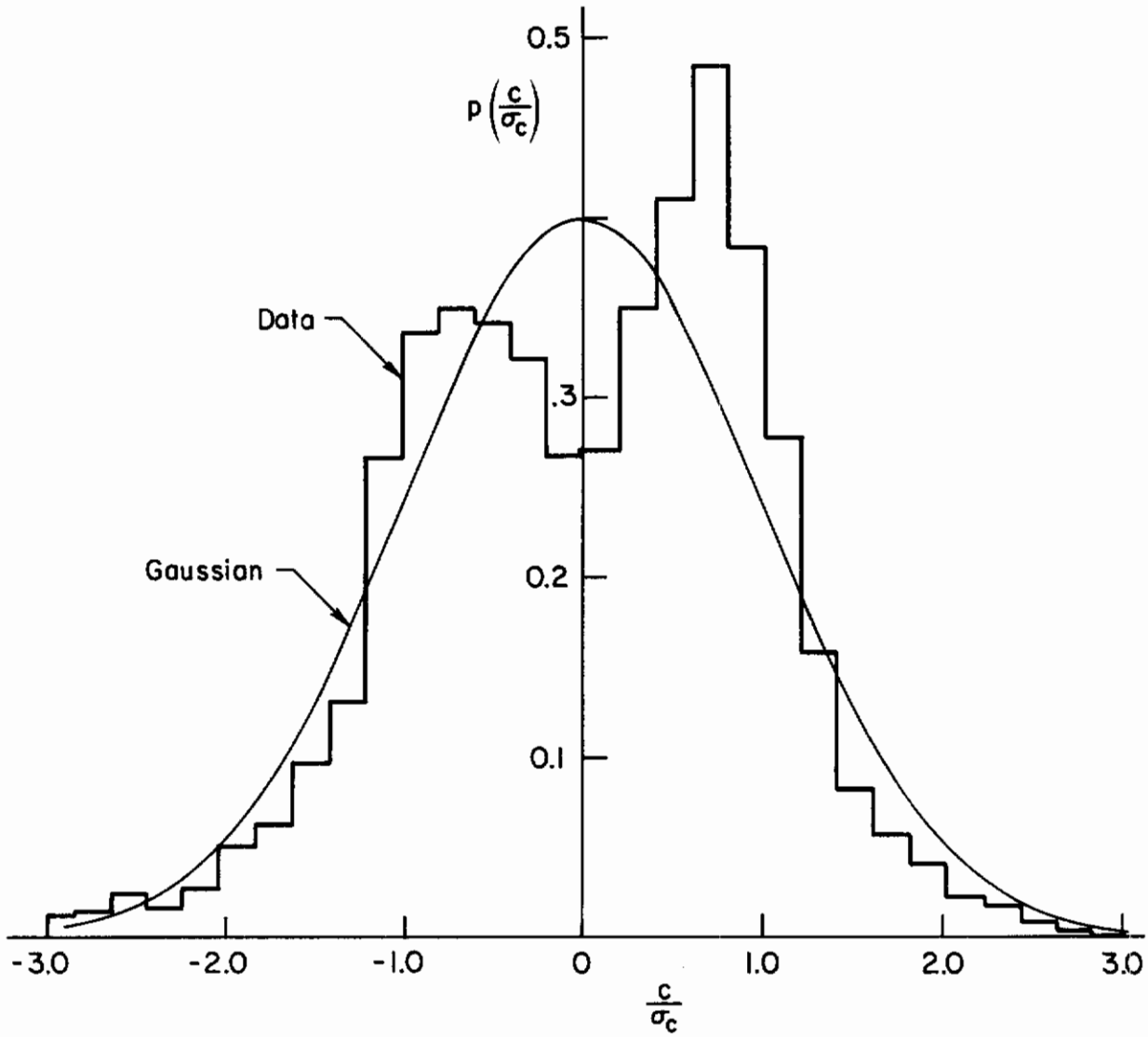

Figure 14. Example of Bimodal Amplitude Distribution for Pilot Output for $Y_c = K_c/s^2$, Subject BH

Approved for Public Release

Contrails

Increased remnant. Other things being equal, when the low frequency lead is present the amplitude of the remnant power spectral density is larger than otherwise.

Nature of the response. With near-optimum controlled element gains, the pilot's output motions appear more discrete and pulselike when large low frequency leads are present (cf. Figs. 13 and 15).

In the following sections two basically different models for lead generation are presented. The first starts with the development of a hypothetical model for the detection of stimulus velocity which is made plausible by comparison with velocity threshold data. Only the signs of the velocity so detected are then used as the basis for pulsing output motions of the pilot. The output motions are, accordingly, similar to the style shown in Fig. 15. For this model the primary remnant source is the high frequency output implicit in the pulses; secondary sources are gain variations which result in the distribution of pulse amplitude about idealized average values, and stimulus velocity detection time computation variations. The second model developed operates from stimulus position rather than rate, and uses a store of past stimulus values to create a differential signal. The differential position signal then triggers an output pulse which has an area proportional to the stimulus increment. The output motions here are similar to those shown in Fig. 13. For simplicity this model is idealized as a constant-rate sampled-data system, although some random variation in sampling rate is necessary to be compatible with actual remnant data which do not exhibit the periodicities expected from constant rate sampling. The remnant sources for this model are, again, implicit in the pulselike nature of the output, any gain variations throughout, and the random sampling variations. For both models it is convenient to think of lead generation as a separate channel within the human operator lying in parallel with the more proportional channels used in control of K_c and K_c/s-like controlled elements. The parallel channels join, of course, at or slightly before the final common path through the neuromuscular system.

Approved for Public Release

Contrails

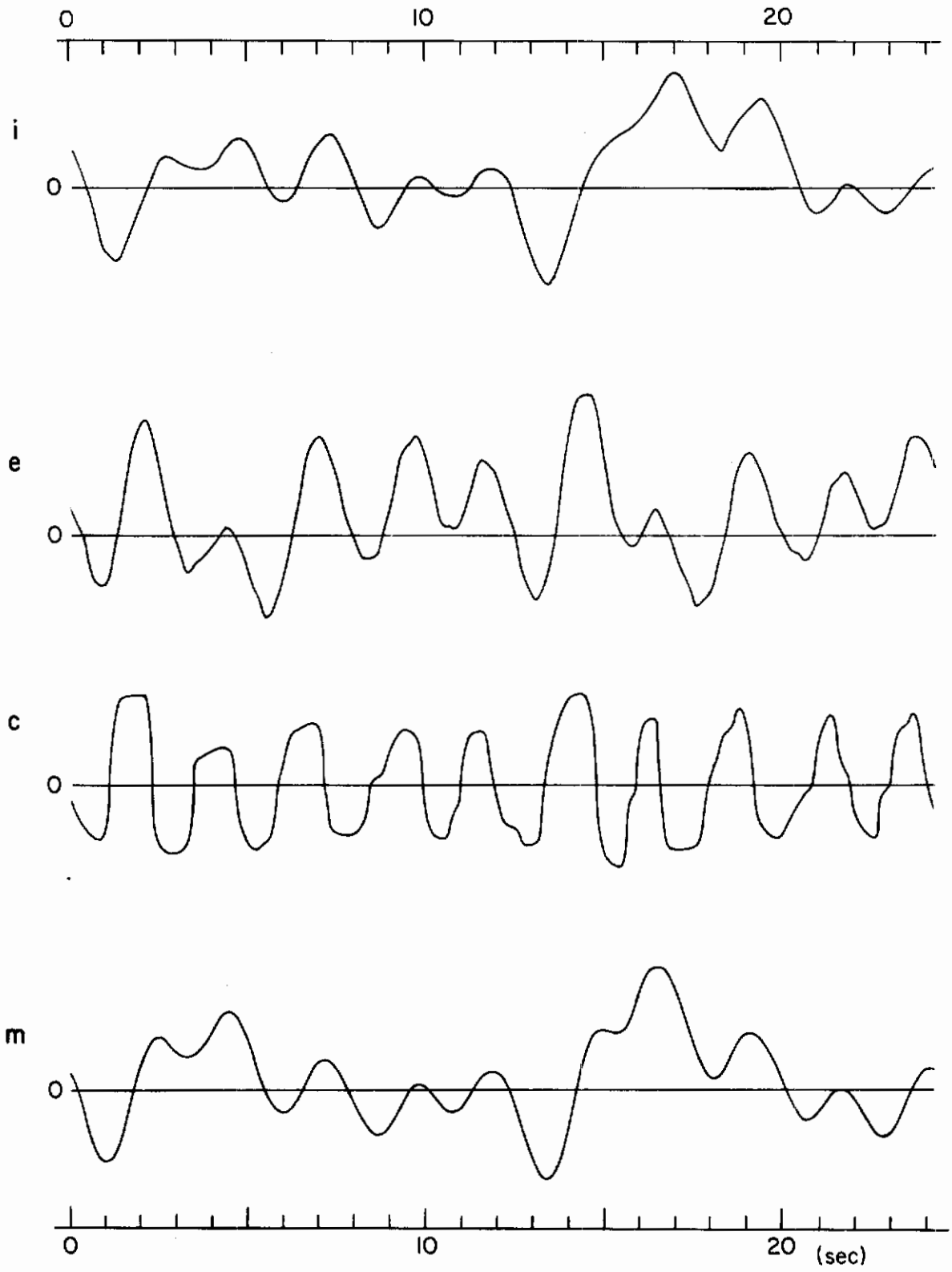

Figure 15. Example of Bimodal Amplitude Distribution Time History
($Y_c = K_c/s^2$, ω_1 = 1.5 rad/sec)

Approved for Public Release

Contrails

B. VELOCITY-SENSING MODEL

1. The Model as a Whole

For the velocity input model of low frequency lead generation, the stimulus velocity is considered to be a fundamental sensory modality. At the initial stage of the visual process neither the rods nor the cones have velocity as a specific stimulus, but several stages farther along at the optic nerve output of the eye itself there are ganglion cells with discharges which are functions of stimulus velocity. Between the basic sensors and the optic nerve there are both bipolar and horizontal cells which serve as summation loci for the discharges from many rods. The enormous sensing and computing capacity available (10^8 rods and 6×10^6 cones converging via bipolar and horizontal cells on about 10^6 ganglion cells feeding the optic nerve fibers) certainly provides adequate capacity for the computation of velocity within the retina itself. The velocities so attained will, however, incur a penalty in delay. As will be shown in the next article, the delay, T_d, will depend on the variance of the input velocity. For complex stationary signals the average delay will depend on the spatial characteristics of the signal as projected on the retinal field. For the very simple model proposed here a signal proportional to velocity is not required; instead, only an indication of the sign of the velocity, albeit delayed, is needed. This is consistent with the approximately constant amplitude output pulses of Fig. 15 (although not with other operator "styles"). The first or velocity-sensing stage of the model then has input and output characteristics, depicted in Fig. 16 in the first and third lines.

In the remainder of the process the additional time delays due to conduction and coding delays in signal transmission and to lags in the neuromuscular actuation system will all be represented by a pure time delay, $e^{-j\omega T_A}$, as the low frequency approximation. The neuromuscular system portion of this is replaced with higher order approximations. Finally, connecting the sensed velocity signal, sgn $\dot{e}(t - T_d)$, with pilot output, we shall use a simple gain proportional to the rms velocity input. The idealized pilot's output will then

Approved for Public Release

Contrails

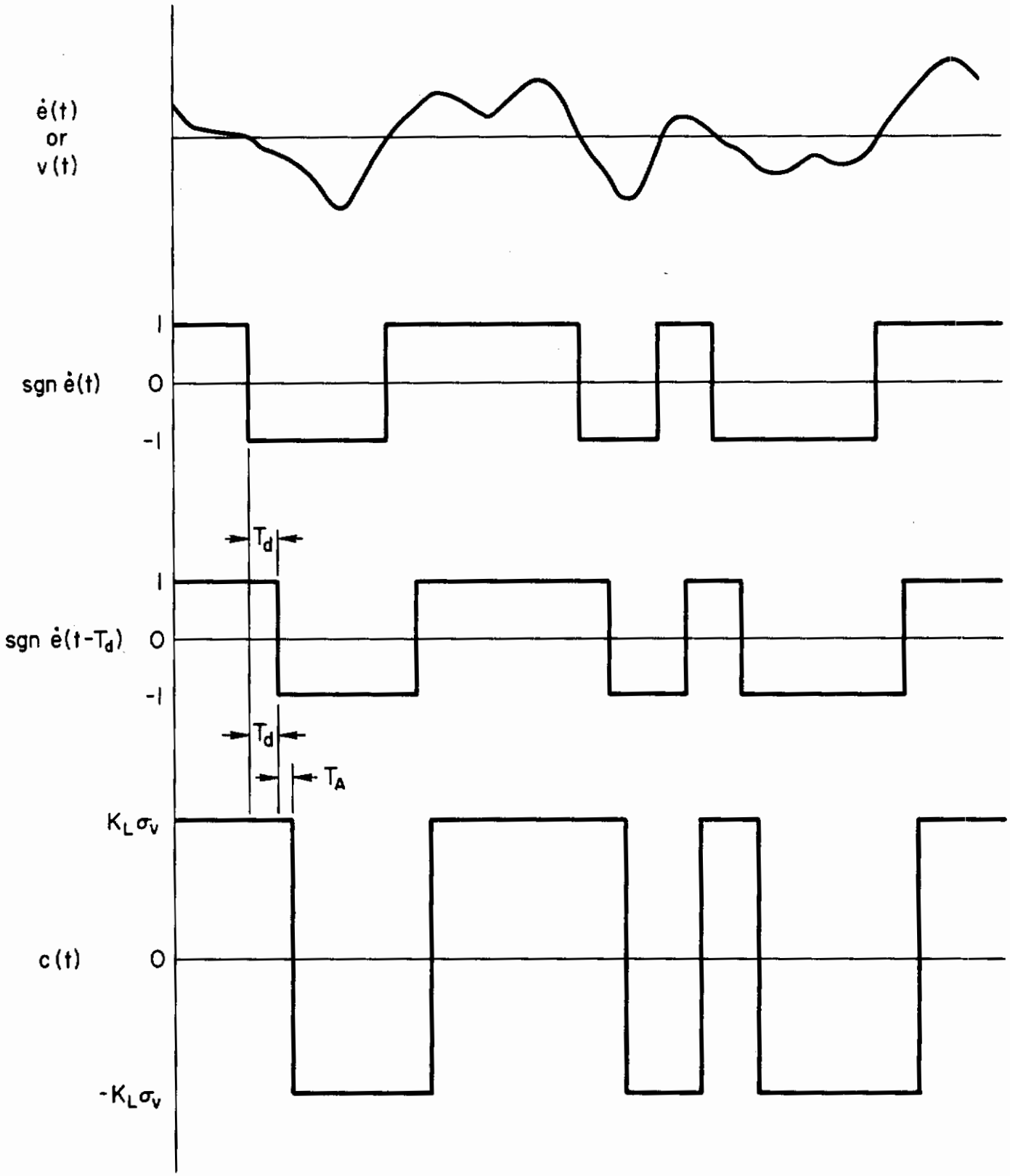

Figure 16. Signals in the Velocity-Sensing Lead Generation Model

Approved for Public Release

Contrails

be boxcarlike in nature with a magnitude proportional to the rms input velocity and axis crossings which coincide with the sign changes of the detected velocity. The pilot output is shown in line 4 of Fig. 16; if higher order approximations are used for the neuromuscular system, the output velocity changes would be accomplished with finite accelerations and velocities, and the sharp corners would be rounded. A block diagram showing the idealized system is given in Fig. 17.

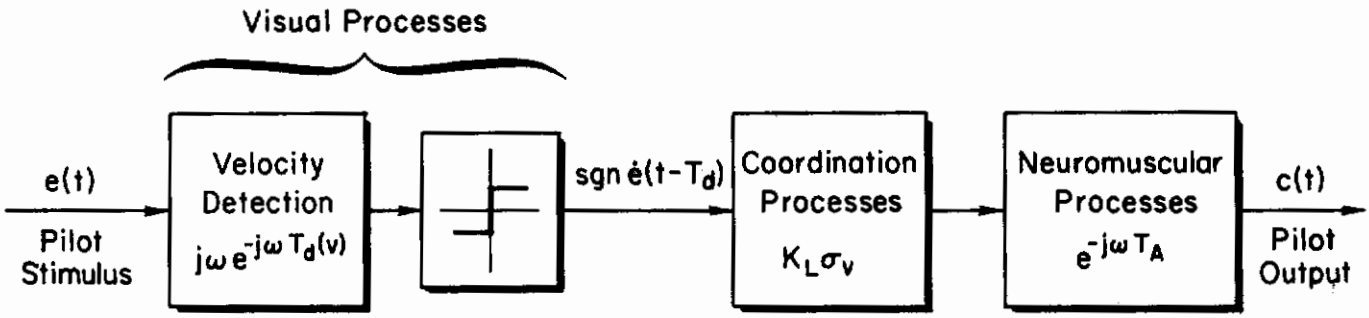

Figure 17. Block Diagram for Velocity-Sensing Lead Generation Model

The pilot output as a function of time is given by

$$c(t + T_A) = K_L\sigma_v \operatorname{sgn} v\left[t - T_d(v)\right] \tag{17}$$

where $\dot{e} = v$ is used for convenience. If the stimulus, e(t), is presumed to have a Gaussian amplitude distribution and if, further, the velocity detection delay time, T_d, is taken as an average value which will be a function of the variance, σ_v^2, of the input velocity, then the output can be written as

$$c(t + T_A) = K_L\sigma_v \operatorname{sgn} v\left[t - T_d(\sigma_v)\right] \tag{18}$$

The Gaussian input describing function between the pilot stimulus, e(t), and pilot output, c(t), will then be

$$Y_p(j\omega, \sigma_v) = \underbrace{\left[j\omega e^{-j\omega T_d(\sigma_v)}\right]}_{\text{Velocity distribution}}\underbrace{\left[\sqrt{\frac{2}{\pi}}\frac{1}{\sigma_v}\right]}_{\text{Sgn function}}\underbrace{K_L\sigma_v e^{-j\omega T_A}}_{\substack{\text{Coordination, conduction,} \\ \text{and neuromuscular processes}}} \tag{19}$$

$$= \sqrt{\frac{2}{\pi}}K_L(j\omega)e^{-j\omega\left[T_A + T_d(\sigma_v)\right]}$$

product, 43
not function!

Approved for Public Release

Contrails

This describing function has the appropriate form for low frequency lead generation, and also exhibits a time delay increase, i.e., T_d, over that (T_A) which would be present in a proportional channel. Thus, the characteristic time difference between situations with and without low frequency lead is accounted for qualitatively.

The constant-amplitude output pulses provided in this model result in sharply peaked bimodal amplitude distributions. These are compatible with the outputs generated by some subjects, but by no means all, e.g., compare Figs. 13 and 15. The model as it stands will not, accordingly, be suitable for those subjects whose output amplitude distributions are flatter or more Gaussianly distributed. To account for these we can use the constant-amplitude output model as an average characteristic and add a random fluctuation about this average. For example, an increment, $\Delta c(t)$, which is constant for each pulse, independent of all other increments, normally distributed, and for which the expected value, $E|\overline{\Delta c^2}|$, is proportional to σ_v^2 would provide a simple process which could be tailored to account for less clear-cut and sharp bimodal characteristics. More complex schemes are also possible.

2. Velocity Detection

The means available within the retina to detect stimulus velocity has been hinted at above. In this article we shall make the mechanism conceptually more concrete by proposing a very simple model which is made plausible by comparison with existing data.

The simplified model has two basic levels, as shown in Fig. 18. At the stimulus end is an ensemble of basic "receptive field sensors," all impinging on a single ganglion cell. The axon of the ganglion cell is one of the fibers in the optic nerve. Each "receptive field sensor" is made up of a variety of rod (and/or cone) cells connected to a single bipolar cell. This view is similar to that advanced in Ref. 48.

In the simplified model the pilot stimulus is assumed to be moving across the retina with a constant velocity, v. The illumination from the stimulus is presumed to be large enough to activate each receptive field in turn as it passes through that field of influence. If but one action

Approved for Public Release

Contrails

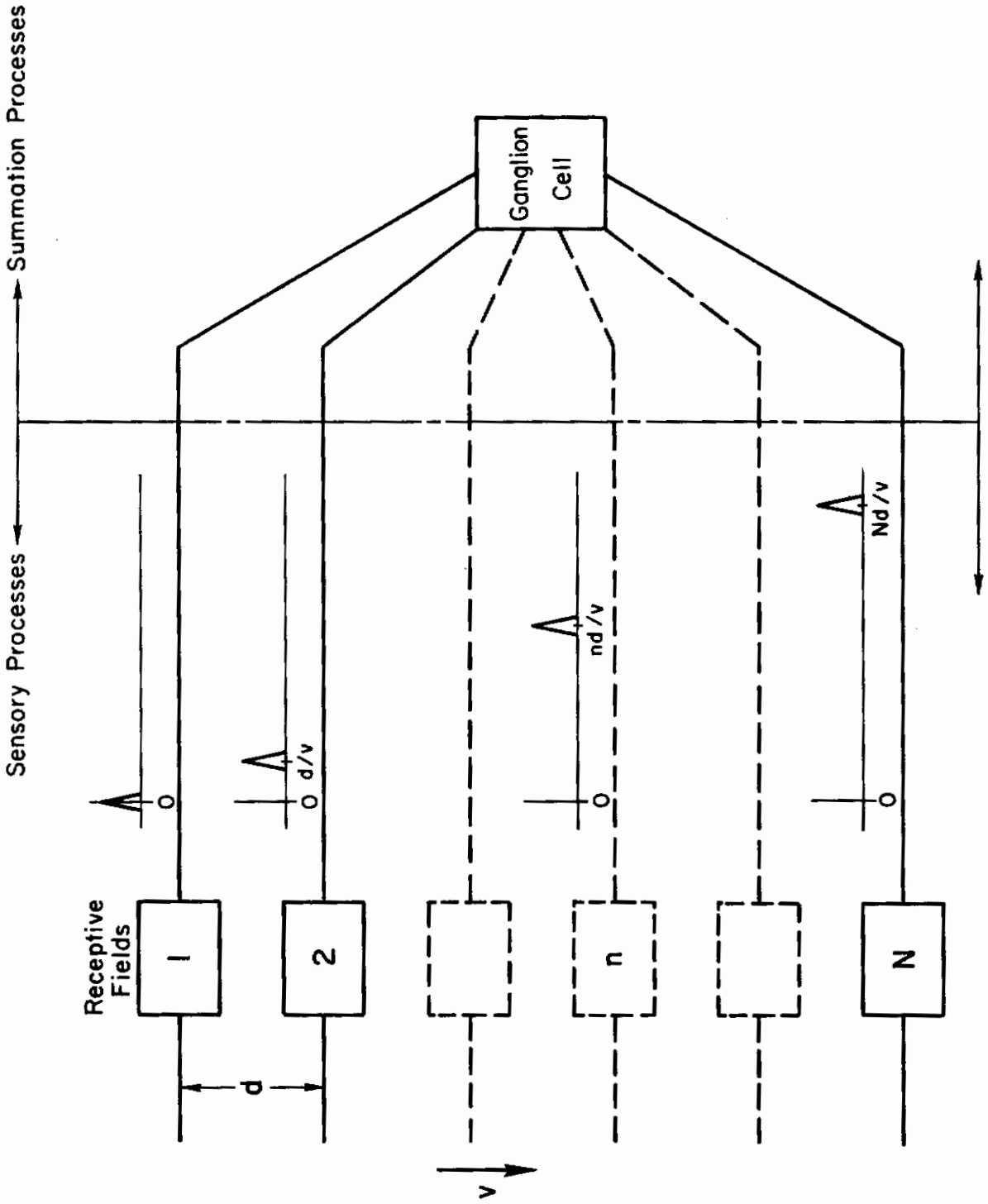

Figure 18. Conceptual Mechanization of Velocity-Sensing Mechanism

Approved for Public Release

Contrails

potential is generated in a bipolar cell by the encounter of the visual stimulus with each receptive field, and if the fields served by these bipolar cells are separated on the average by a distance d, then the net input to the ganglion cell will be approximately

$$x_r(t) = \delta(t) + \delta\left(t-\frac{d}{v}\right) + \cdots + \delta\left(t-\frac{nd}{v}\right) + \cdots$$

$$= \sum_{n=0}^{N} \delta\left(t-\frac{nd}{v}\right) \qquad (20)$$

Here each action potential is represented by a delta function and the voltage scales are normalized on a per unit action potential basis. If all the action potentials are assumed to have equal weights, and if, further, the effective weighting function of the ganglion cell to an individual action potential input is $w_g(t)$, then the subthreshold electric potential in the ganglion cell due to the activity of its associated sensory and bipolar cells will be

$$x_g(t) = \int_0^t w_g(\tau)x_r(t-\tau)\, d\tau$$

$$= \sum_{n=0}^{N} \int_0^t w_g(\tau)\delta\left[t-\frac{nd}{v}-\tau\right] d\tau \qquad (21)$$

$$= \sum_{n=0}^{N} w_g\left(t-\frac{nd}{v}\right)u\left(t-\frac{nd}{v}\right)$$

The general appearance of the subthreshold potentials will look like those shown in Fig. 19, where T_g is a representative time constant of the ganglion cell's weighting function. In Fig. 19a the time interval between the stimulus exciting receptive field ① and that exciting receptive field ② is large relative to the time constant of the ganglion cell. The resulting ganglion cell potential is then a sequence of well-separated weighting function responses to each of the sensory action potentials in sequence. Because the maximum value of the weighting function is subthreshold, the ganglion cell will not discharge and the visual event is recorded only in the local potential and in the underlying action potentials of the rods (cones) and the bipolar cells, and nowhere farther downstream. On the other hand, when the time between receptive field discharges is of the same order or smaller than the ganglion cell time constant, as in Fig. 19b,

Approved for Public Release

Contrails

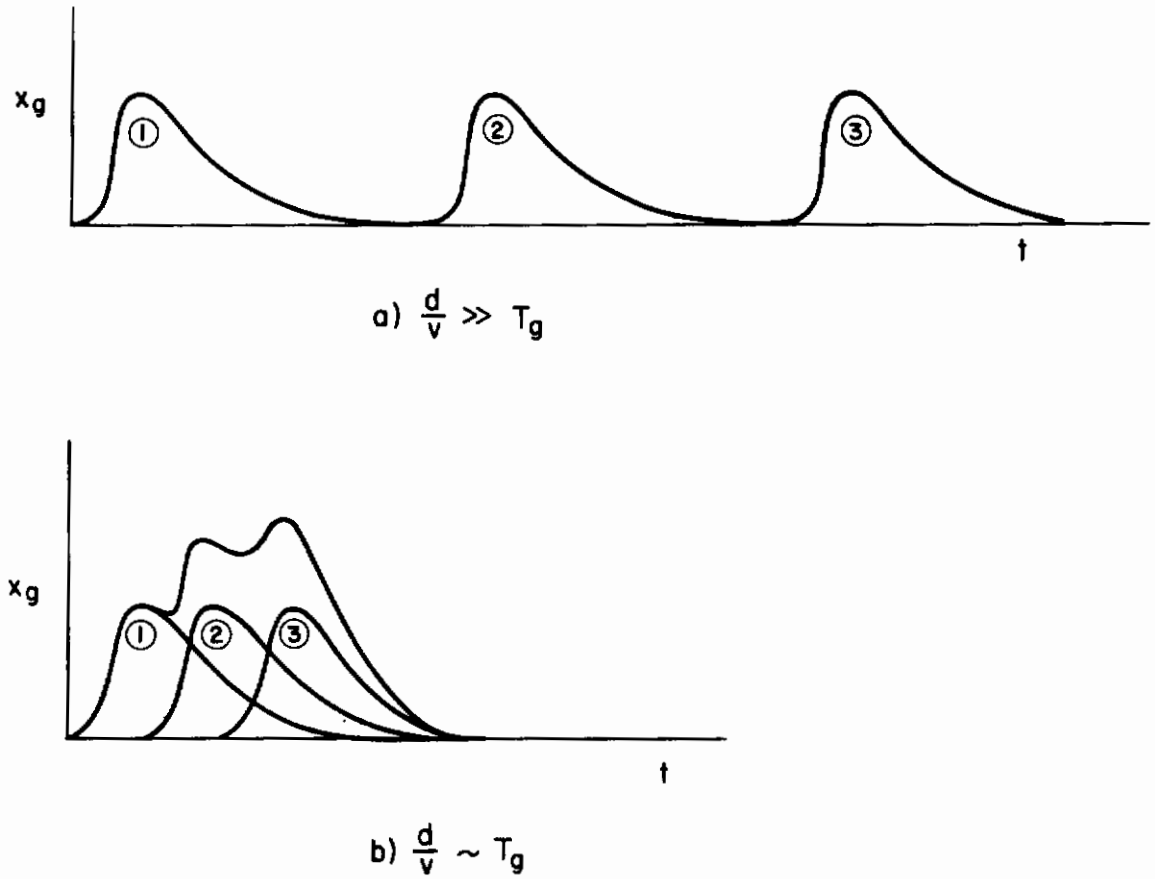

Figure 19. Bipolar Cell Subthreshold Potentials

part of the activity of fields ① and ② are summed with that of field ③, etc., to create a ganglion cell potential greater than the weighting function maximum. When this summation potential is equal to the threshold of the ganglion cell, the cell will fire. This passes on to higher centers the information that an object with velocity above a certain value has appeared in the field of view served by the ganglion cell and its associated lower level sensory and bipolar cells. Above the threshold the ganglion cell pulse rate will presumably be proportional to the rate of arrival of bipolar cell action potentials, thereby providing some indication of the magnitude as well as the presence of the input stimulus.

To obtain a mathematical description of this process we shall derive below an approximate expression for ganglion cell potential due to the input stimulus. Then for the condition where the cell potential just

Approved for Public Release

Contrails

barely exceeds its threshold we can connect the input velocity with detection time. The first step in this process is to approximate the ganglion cell weighting function, $w_g(t)$, as a first-order exponential response such as that shown in Fig. 20, and then further approximate

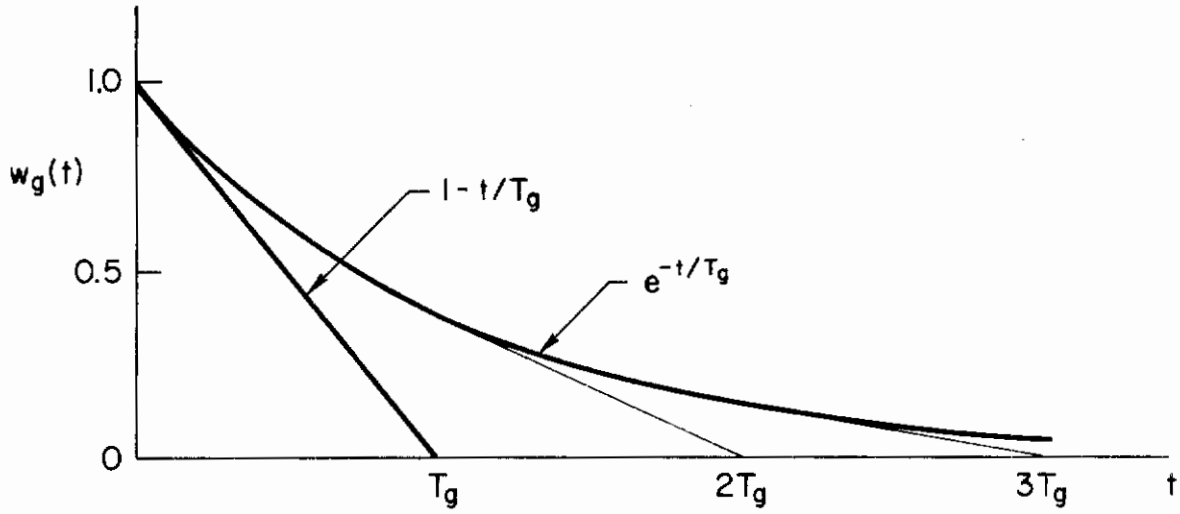

Figure 20. Approximate Bipolar Cell Weighting Function

this by the simple triangle, i.e.,

$$\begin{aligned} w_g(t) &= e^{-t/T_g} \\ &\doteq 1 - \frac{t}{T_g} \quad , \quad 0 \le t < T_g \\ &\doteq 0 \qquad\qquad \text{elsewhere} \end{aligned} \tag{22}$$

When the triangular approximation is used, only the N pulses in an interval, T_g, need to be considered in the summation. Then over an interval, T_g, the cell potential will be approximately

$$\begin{aligned} x_g(t) &= w_g\left(t - \frac{nd}{v}\right) u\left(t - \frac{nd}{v}\right) \\ &\doteq \left(1 - \frac{t}{T_g}\right) u(t) + \left[1 - \frac{\left(t - \frac{d}{v}\right)}{T_g}\right] u\left(t - \frac{d}{v}\right) + \left[1 - \frac{\left(t - \frac{2d}{v}\right)}{T_g}\right] u\left(t - \frac{2d}{v}\right) \\ &\quad + \cdots + \left[1 - \frac{\left(t - \frac{Nd}{v}\right)}{T_g}\right] u\left(t - \frac{Nd}{v}\right) \\ &\doteq \sum_{n=0}^{N} \left[1 - \frac{\left(t - \frac{nd}{v}\right)}{T_g}\right] u\left(t - \frac{nd}{v}\right) \end{aligned} \tag{23}$$

Approved for Public Release

Contrails

where N is the largest integer in the $T_g(v/d)$. In a somewhat different form the ganglion cell potential will be

$$x_g(t) = \begin{cases} 1 - \dfrac{t}{T_g} & , \quad 0 \le t < \dfrac{d}{v} \\ 2 - \dfrac{2t}{T_g} + \dfrac{d/v}{T_g} & , \quad \dfrac{d}{v} \le t < \dfrac{2d}{v} \\ 3 - \dfrac{3t}{T_g} + \dfrac{3d/v}{T_g} & , \quad \dfrac{2d}{v} \le t < \dfrac{3d}{v} \\ 4 - \dfrac{4t}{T_g} + \dfrac{6d/v}{T_g} & , \quad \dfrac{3d}{v} \le t < \dfrac{4d}{v} \\ \vdots & \\ (N+1) - \dfrac{(N+1)t}{T_g} + \dfrac{d/v}{T_g}\dfrac{N(N+1)}{2} & , \quad \dfrac{Nd}{v} \le t \le T_g \end{cases} \tag{24}$$

The waveform is a complex sawtoothlike shape as illustrated in Fig. 21.

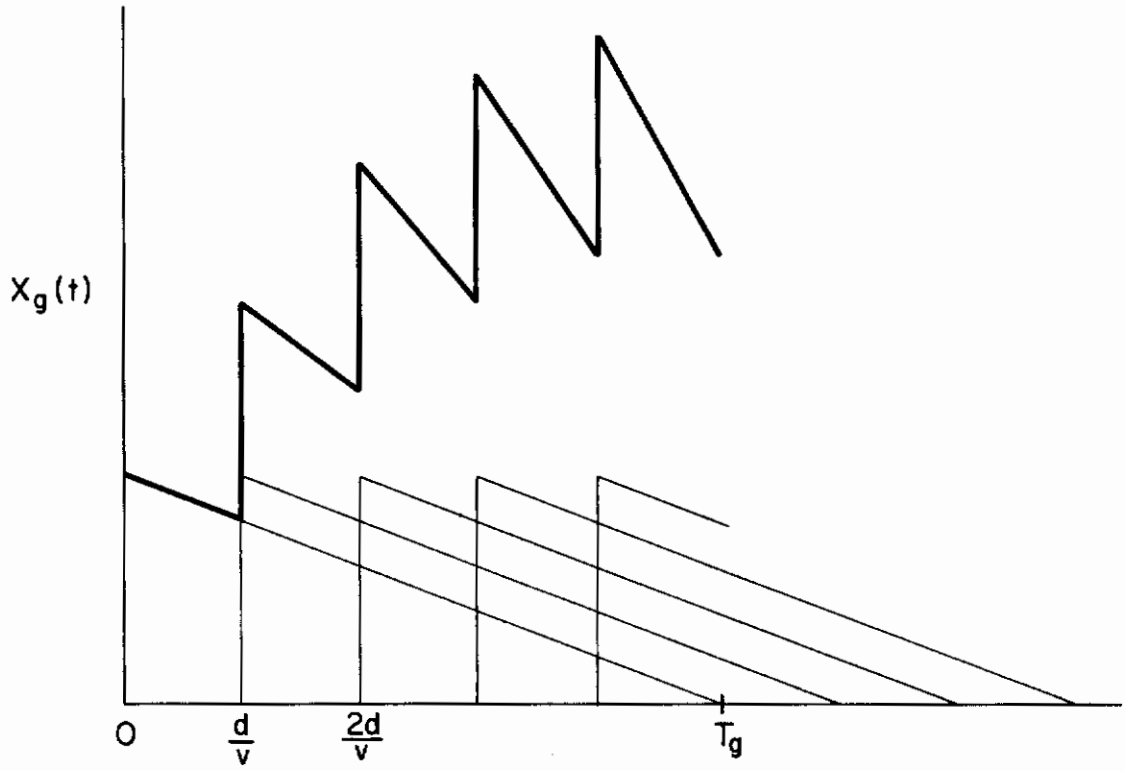

Figure 21. Illustrative Summation of Bipolar Cell Triangular Weighting Functions

Approved for Public Release

Contrails

The various local maxima corresponding to the tooth tips are given by

$$x_g(t)\Big]_{max} = \left(1 + n\right)\left(1 - \frac{1nd/v}{2T_g}\right)\Bigg]_{n = \frac{v}{d}t}$$

$$= \left[1 + \left(T_g \frac{v}{d}\right)\frac{t}{T_g}\right]\left[1 - \frac{1}{2}\frac{t}{T_g}\right] \qquad (25)$$

or, changing the variable to $t' = t/T_g$ and letting $\alpha = T_g(v/d)$,

$$x_g(t')\Big]_{max} = \left(1 + \alpha t'\right)\left(1 - \frac{1}{2}t'\right) \qquad (26)$$

If $\alpha \leq 1/2$, $x_g(t')\Big]_{max}$ is a monotonically decreasing function, so the velocity cannot be detected if more than one spike needs to be summed in the ganglion cell to trigger it.

If the threshold of the ganglion cell is equal to a, then the normalized detection time, T_d', will be such that $x_g(T_d') \geq a$. The minimum detection time will occur when this inequality is an actual equality, and then

$$x_g(T_d') = a = \left(1 + \alpha T_d'\right)\left(1 - \frac{1}{2}T_d'\right) \qquad (27)$$

The solution for normalized detection time is

$$T_d' = \frac{\alpha - 1/2}{1\alpha}\left[1 \pm \sqrt{1 - \frac{2(a-1)\alpha}{(\alpha - 1/2)^2}}\right] \qquad (28)$$

If the roots of the quadratic are real and widely separated, they are approximately

$$T_{d_1}' \doteq \frac{2(a-1)}{(\alpha - 1/2)} \quad ; \quad T_{d_2}' \doteq \frac{2(\alpha - 1/2)}{1\alpha} \qquad (29)$$

Only the first answer depends on the threshold, which is an obvious requirement for a solution, so it is the one accepted. Converting, now, to an angular velocity, Ω, by introducing the lens-to-retina distance, m, and

Approved for Public Release

Contrails

converting back to real time, the detection time becomes

$$T_d = T'_{d_1} T_g = \frac{2T_g(a-1)}{(T_g v/d - 1/2)}$$
$$= \frac{T_g(a-1)}{T_g m\Omega/d - 1/2} \qquad (30)$$

or, if α is considered to be much larger than 1/2,

$$T_d \doteq \frac{2(a-1)d/m}{\Omega} \qquad (31)$$

or

$$T_d\Omega \doteq 2(a-1)\frac{d}{m} = \text{Constant} \qquad (32)$$

This implies a hyperbolic relationship of detection time with input velocity for constant-velocity inputs.

Experimental data which support the hyperbolic detection time velocity variation can be drawn from Ref. 49. In tests reported there the subjects were required to identify the direction and time of recognition of the motion of a target light relative to a reference light. The experiments were conducted in a planetarium environment with a star background; the reference was one such star and the object a similar light spot with a known initial position relative to the reference. The test chamber was dark except for the objects projected on the inside wall of the planetarium. These consisted of 106 simulated stars of approximately fifth magnitude plus the moving object which was slightly brighter than the background stars. The subjects were all dark-adapted, and each subject used a stopwatch to measure the time he required to detect object motion. The experimental variables included different object separations and directions. Figure 22 shows the results of one series where simple left/right motion was used. The angular velocity is plotted against the average recognition time, T_r, for the six subjects. The initial separation distance for these data was about 2° (34 mrad) and the difference between motion to the right or left was insignificant. Other experiments with different initial separations and/or directions showed that in general both separation and motion

Approved for Public Release

Contrails

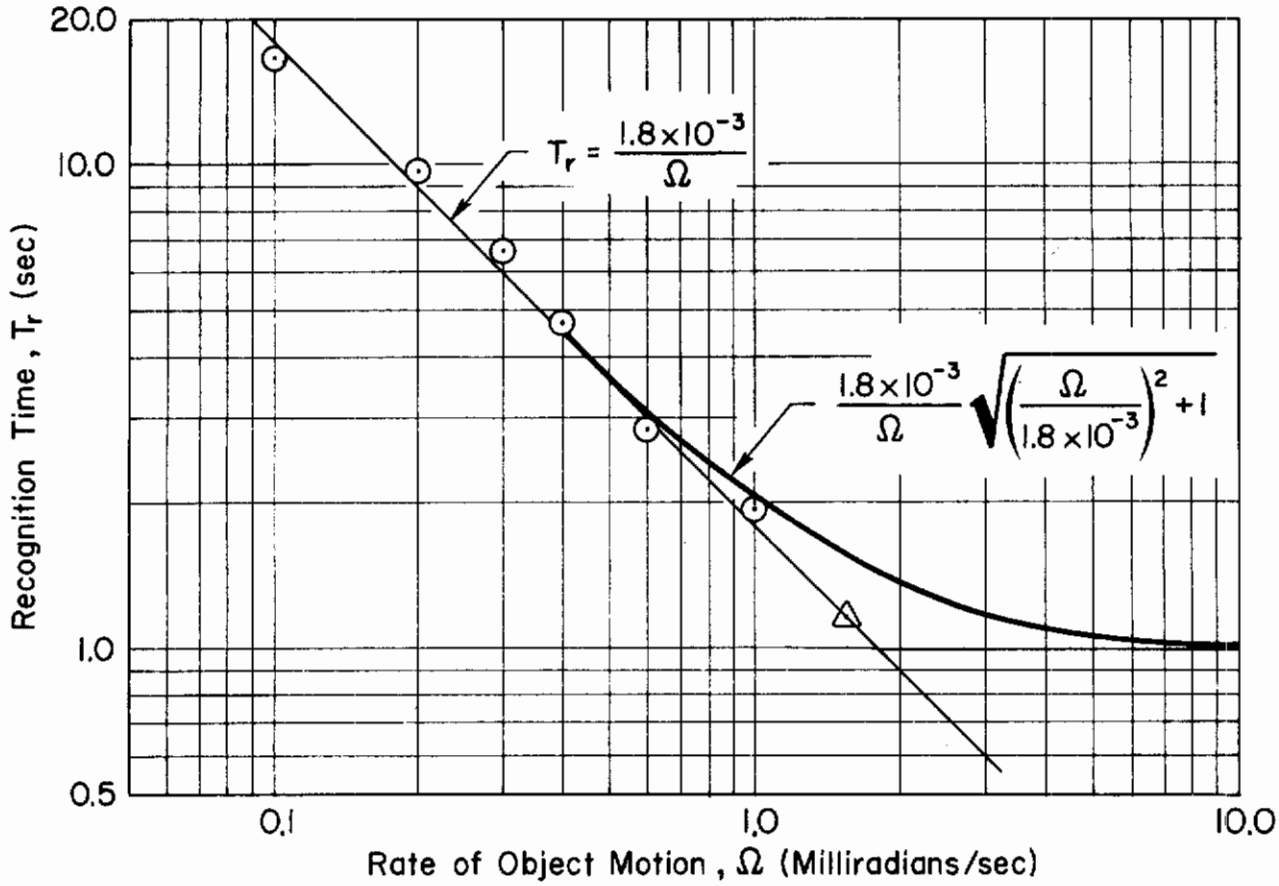

Figure 22. Velocity Detection Threshold as Function of Object Motion

direction effect the results, but the same general trend of angular velocity versus recognition time was present.

A linear fit is appropriate to the data of Fig. 22, which on these coordinates indicates a hyperbolic variation. A second curve is also fitted to take into account the experimental observation that recognition time did not change for speeds greater than 1.6 mrad/sec. The exact location of this asymptote and the variation and form of transition between constant recognition time and the inverse variation of recognition time with angular velocity is not too well defined, so an elementary form is used for simplicity. The empirical data are then summarized by

$$T_r\Omega \doteq 1.8 \times 10^{-3} \quad , \quad \Omega \leq 1.6 \times 10^{-3} \text{ rad/sec} \qquad (33)$$

or

$$T_r \doteq \frac{1.8 \times 10^{-3}}{\Omega}\sqrt{\left(\frac{\Omega}{1.8 \times 10^{-3}}\right)^2 + 1} \qquad (34)$$

Approved for Public Release

Contrails

To the extent that recognition time is proportional to detection time, the $T_d\Omega \doteq$ constant consequence of the simplified velocity detection model is justified.

One of the important deficiencies in the existing data is that only constant velocities have been considered. If the stimulus movement is sinusoidal or random, the effective time delay for detection will be quite different from that developed. If, however, the simple model presented is used as the basis, a sinusoidal motion, for example, can be applied at the input and the output of the bipolar cell estimated. This output can then be resolved into a Fourier series and an average detection time defined on the basis of the phase shift between the fundamental and the stimulus sinusoid. The calculation is quite involved and also requires an estimate for T_g, the typical time constant of the ganglion cells. To avoid this an approximate scheme in which the constant-velocity data can be used directly is indicated. What we shall do is to replace the sinusoid by an equivalent square wave for which the sinusoid is the fundamental. On this basis the equivalent velocity will be

$$\Omega_{eq} = \frac{\pi}{4} \omega A \qquad (35)$$

An average recognition time for the sinusoidal input would then be computed using this Ω_{eq} for Ω in Eq. 33 or 34.

C. DIFFERENTIAL DISPLACEMENT MODEL

In the differential stimulus displacement model for low frequency lead generation, the stimulus displacement, e, is considered to be the fundamental sensed entity. The bases for lead generation are computations using present and a store of past stimulus values to create a differential signal. The differential displacement signal then triggers an output pulse which has an area proportional to the differential stimulus increment.

Examination of Fig. 13 makes plausible the statement that the pilot output pulses are composites of one or more elementary pulses, each having a width of about 1/3 sec. In the simplest idealization of the

Approved for Public Release

Contrails

pilot output style typified by Fig. 13, the elementary pulse widths are assumed constant, thereby requiring pulse amplitude variations to achieve a pulse output area proportional to the stimulus increment.

A zero-order hold sampled-data system offers an appropriate starting point to account for the flat-topped discrete pulselike sections in the output. Ideally, for simplicity this model would involve constant-rate sampling. Similar considerations to these led to earlier versions of constant-rate sampled-data models for human operators (Refs. 50 – 52.) From the look of Figs. 11 – 13, this could be made a reasonable approximation for a few seconds, at least for this subject and manipulator. The remnant for a constant-rate sampled-data system excited by a sum of sinusoids should exhibit periodicities at other than the forcing function frequencies. Since this is not observed on run lengths of 20 sec or greater, some variation in sampling rate is necessary if a sampled-data model is to be compatible with existing remnant data. A random variation in sampling rate begets effects similar to a randomly varying time delay (Ref. 53), which is, in turn, a major likely source of remnant (Ref. 12). As shown in Ref. 54, only a small random fluctuation in an otherwise constant-rate sampling is needed to modify sharply peaked output spectra to smooth and continuous power spectral densities. So, although we shall use a constant-rate zero-order hold sampling system as the basis for the differential displacement model, it must be understood that this is an oversimplified idealization and that a random variation in sampling rate is actually present. Besides the time-varying sampling rate, the main remnant source for this model is, again, implicit in the pulselike nature of the output.

Based on these introductory comments, the block diagram of Fig. 23 illustrates a constant-rate sampled-data system suitable for approximate generation of first-order low frequency lead. Just as with the velocity-sensing model, the neuromuscular and coordination processes are oversimplified to a pure gain and time delay. The transfer function of this

Approved for Public Release

Contrails

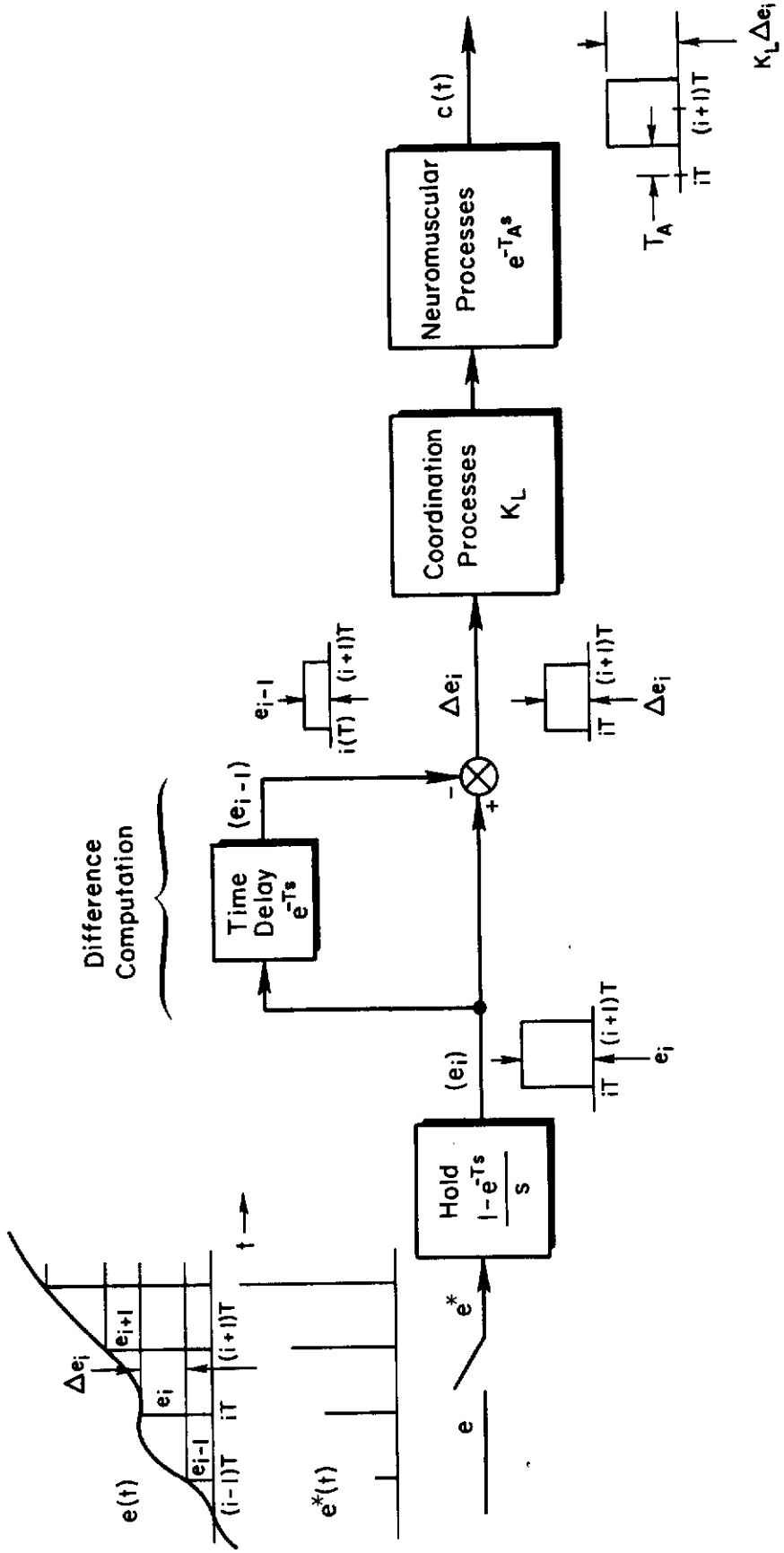

Figure 23. Block Diagram of Incremental Stimulus Displacement Lead-Generation Model

Approved for Public Release

Contrails

system is

$$\frac{C(s)}{E(s)} = \underbrace{\left(\frac{1-e^{-Ts}}{s}\right)}_{\text{First-order hold}} \underbrace{\left(1-e^{-Ts}\right)}_{\text{First-difference computation}} \underbrace{K_L e^{-T_A s}}_{\text{Coordination and neuro-muscular processes}} \tag{36}$$

$$= \frac{4K_L e^{-(T_A+T)s}}{s} \sinh^2 \frac{Ts}{2}$$

In the frequency domain this becomes

$$\frac{C(j\omega)}{E(j\omega)} = \frac{4K_L e^{-j\omega(T_A+T)}}{j\omega} \sinh^2 \frac{j\omega T}{2} \tag{37}$$

For frequencies less than about $1/T$, the describing function is approximately [using $\sinh^2 x = (x + x^3/3! + x^5/5! + \dots)^2 \doteq x^2$, for $x < 1/2$].

$$\frac{C(j\omega)}{E(j\omega)} \doteq K_L T^2 (j\omega) e^{-j\omega(T_A+T)}, \quad \omega T < 1 \tag{38}$$

This system generates low frequency lead at the expense of an additional increment in time delay. Thus it exhibits behavior qualitatively compatible with that required for low frequency lead generation.

To compute the appropriate incremental time delay for $Y_c = K_c/s^2$ over and above that for the $Y_c = K_c/s$ situation (for which $\tau_o \doteq 1/3$ sec), we must first recognize that the analog pilot for $Y_c = K_c/s$ will be that shown in Fig. 23 <u>without</u> the difference computation element. The analog pilot transfer function for the $Y_c = K_c/s$ case is then

$$\frac{C(s)}{E(s)}\Bigg] = K_L e^{-T_A s} \left(\frac{1-e^{-Ts}}{s}\right)$$

$$= \frac{2K_L}{s} e^{-(T_A+T/2)s} \sinh \frac{Ts}{2} \tag{39}$$

Approved for Public Release

Contrails

or, as a frequency domain describing function for $\omega T < 1$,

$$\frac{C(j\omega)}{E(j\omega)} \doteq K_L T e^{-j\omega(T_A + T/2)} , \quad \omega T < 1 \qquad (40)$$

Comparison of Eqs. 38 and 40 indicates that the difference in effective time delay between the $Y_c = K_c/s$ and $Y_c = K_c/s^2$ analog pilots is just $T/2$ sec. As already observed from the traces in Figs. 11 – 13, the minimum increment of the flat horizontal discrete portions of the output traces is approximately 1/3 sec. Using this as the estimate for the sampling period, T, then the incremental time delay associated with the generation of low frequency lead will be approximately 1/6 sec. This compares extremely well with the difference previously noted in Subsection A on data to be explained.

A major possible deficiency with this model is its generation of Gaussian output amplitude distributions when the input is Gaussian. Thus the output amplitude distributions will not be of the bimodal form typified by Fig. 14. On the other hand, the amplitude distributions of the output time responses for the Fig. 13 subject are probably not bimodal. There are gross variations in style from subject to subject, as exemplified by comparison of Figs. 13 and 15, which will be reflected in the amplitude distributions.

Approved for Public Release

Contrails

SECTION V

MODELS FOR TRANSIENT INPUTS

A. INTRODUCTION

The simplest nonstationary control situation is one in which a highly trained, but nonalerted, subject operating a constant-coefficient linear controlled element in a compensatory system is confronted with a randomly occurring step input. In spite of the simple circumstances, the over-all behavior is complicated when a variety of controlled elements is considered. The skilled operator's output is peculiar to each controlled element form. The system response is, however, less variant in that it tends to duplicate, after a time delay, the forcing function. Thus, the system output to a unit step forcing function shown in Fig. 24 is typical. This operator response can be analyzed by considering the three phases separately. When described in terms of a block diagram which relates stimulus to response, each temporal phase can be conceived of as having a different system organization. The block diagram structure indicates the dynamics of the association between the pilot's response and the actual or effective inputs which he is operating on to generate that response.

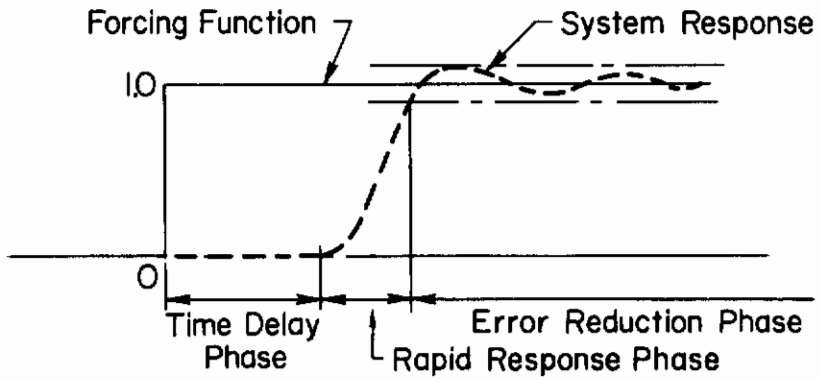

Figure 24. Typical System Step Response

For tracking random inputs with occasional step inputs, a dual-mode model of the operator is appropriate. The basic structure of the model is given in Fig. 25. The quasi-linear steady-state path is the one used for tracking random inputs, while the feedforward element operates on the

Approved for Public Release

Contrails

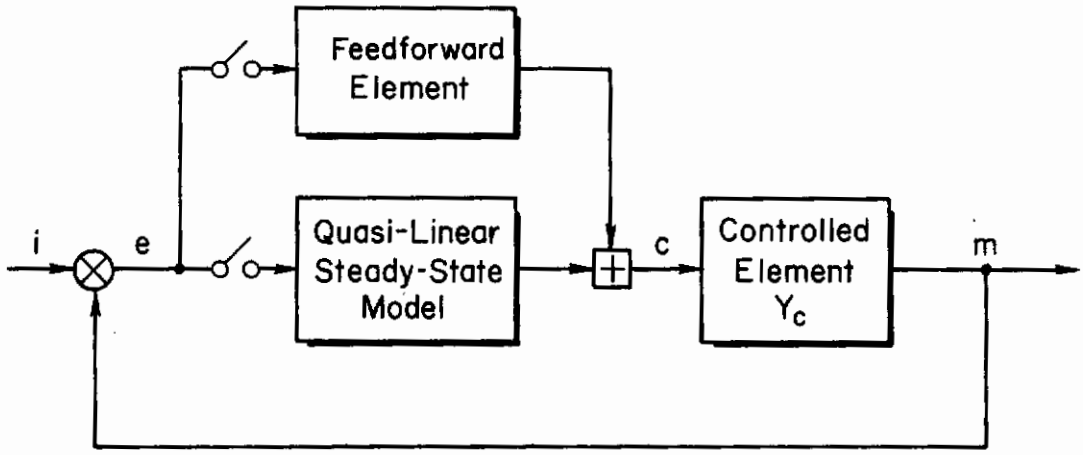

Figure 25. Structure of the Dual-Mode Model

random-occurring step inputs. The basic structure also incorporates mode switches for the two pathways. In terms of the three temporal phases the successive action structures of the dual-mode model are:

- Transition from quasi-linear mode to feedforward mode, corresponding to the time delay phase
- Patterned feedforward response, corresponding to the rapid response phase
- Quasi-linear mode, corresponding to the error reduction phase

The duration of the time delay phase has some minimum value, and its unimodal distribution is skewed to the right. The time delay, τ_s, is generally longer than the steady-state effective time delay, τ_e, in tracking. In particular,

$$\tau_s = \tau_e + \tau_d \qquad (41)$$

where τ_s is the time delay phase duration, τ_e is the effective time delay in steady-state tracking, and τ_d is the decision time. During the decision time the operator makes the pertinent decisions regarding the shape and magnitudes of the feedforward response. At the end of the time delay phase the feedforward element generates the proper response to the step input command, giving the rapid response phase. At the end of this period, the error is small and the operator switches to a quasi-linear tracking mode in the error reduction phase.

Approved for Public Release

Contrails

Much is known about the quasi-linear controller; therefore, attention in the following is confined to the parallel feedforward path utilized in response to step inputs. As a starting point, an existing model for step response behavior is reviewed.

B. EXTANT SAMPLED-DATA STEP FUNCTION RESPONSE MODEL

Several attempts have been made to model operator step response behavior The most modern and complete model is presented in Ref. 42. This model proposed a sampled-data element for the feedforward. An adaptation, for step behavior only, is shown in Fig. 26 and the sampled-data portion alone is given in Fig. 27. Note that the model is a hybrid of Young's eye-movement model (Ref. 55) and a hand-tracking model by LeMay and Westcott (Ref. 56). It borrows the two-channel pursuit/saccadic control logic of the eye-movement model and the velocity triangle force program of the hand-movement model. The model also incorporates a dual-rate sampler that provides a high sampling rate while waiting, to account for reaction time delays, then slows down after the input is sensed to permit the system to complete its response before the next sample is taken. Finally, the model is extended to account for higher order controlled elements via the equalization block shown at the end of a long train.

The sampler is an impulse modulator which has a sampling period of 0.15 sec while waiting, and switches to a sampling period of 0.3 sec when the step is detected. The sampled pulse is delayed 0.15 sec, and then goes into the force programmer. The force program has an s-domain representation obtained by letting $z = e^{Ts}$, i.e.,

$$\frac{\alpha_c^*}{e^*} = 1 - 2e^{-(T/4)s} + e^{-(T/2)s} \quad ; \quad T = 0.3 \text{ sec} \qquad (42)$$

Notice that at the start $i = e$ since initially $m = 0$. This produces the series of pulses, α_c^*, shown in Fig. 28, when the first pulse in e^* arrives. The force program pulses produced by subsequent samples of the error are shown dashed. The total feedforward output, α_c, is determined by the hold and the equalization, which are in turn a function of the closed-loop effective neuromuscular system dynamics and the controlled element order. The

Approved for Public Release

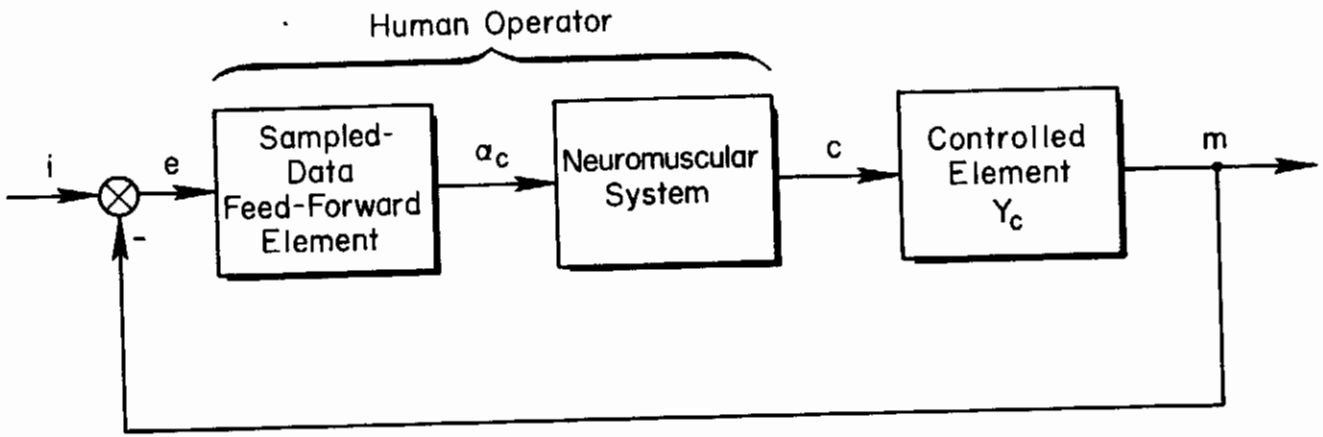

Figure 26. Sampled-Data Model for Step Inputs

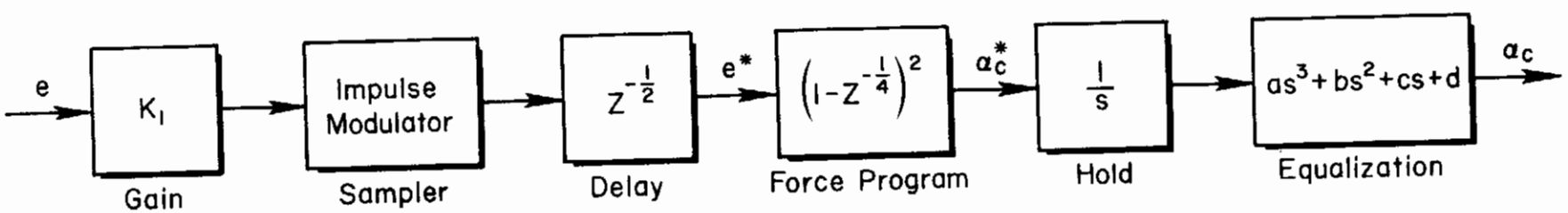

Figure 27. Sampled-Data Feedforward Element for Step Inputs (Ref. 42)

Approved for Public Release

Contrails

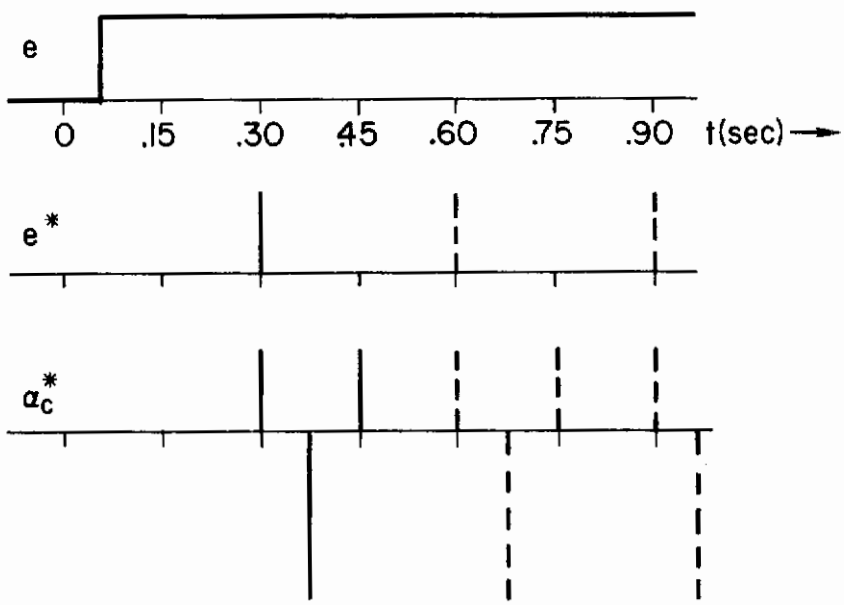

Figure 28. Force Program Response to Step Error

equalization contains high frequency lags that are not shown for simplicity. It is shown earlier in the report that the pilot output-to-α_c transfer function (i.e., the neuromuscular system dynamics) is approximately given by

$$\frac{c}{\alpha_c} \doteq \frac{Ke^{-\tau_\alpha s}}{\left(T'_{M_1} s + 1\right)\left(T'_{M_2} s + 1\right)} \qquad (43)$$

For a sampling period of 0.3 sec in the sampler, the effective neuromuscular system dynamics have a transfer function of the form K/s^2 to a first approximation; that is,

$$\frac{c}{\alpha_c} \doteq \frac{K_\alpha}{s^2} \quad \text{where} \quad K_\alpha \doteq \frac{K}{T'_{M_1} T'_{M_2}} \qquad (44)$$

The Ref. 56 force programmer model is adequate only for pure gain controlled elements and works best for step inputs only. Elkind, Kelly, and Payne in attempting to incorporate the force program concept of LeMay and Westcott into the Ref. 42 model make the further assumption that the time to complete the force program remains the same for various controlled element dynamics in addition to $Y_c = K_c$. To satisfy this assumption, we allow, as they do, for an equalization of the form $(as^3 + bs^2 + cs + d)$, as shown in Fig. 27, whose coefficients are then adjusted to give an effective (m/α_c^*)

Approved for Public Release

Contrails

transfer function:

$$\frac{m}{\alpha_c^*}(s) = \frac{1}{s}\left(as^3 + bs^2 + cs + d\right)\left(\frac{K_\alpha}{s^2}\right)\left[Y_c(s)\right] = \frac{K}{s^3} \tag{45}$$

This will produce a series of control actions by operating on α_c^* which will accomplish the rise time phase stick deflection in one sampling interval. The actual signals predicted by the model of Figs. 26 and 27 are summarized in Fig. 29 for various controlled elements. The required equalization coefficients to arrive at Eq. 45 are summarized in Table VII.

TABLE VII

REQUIRED EQUALIZATION

CONTROLLED ELEMENT, Y_c	EQUALIZATION COEFFICIENTS
K_c	$d \neq 0$, $a = b = c = 0$
K_c/s	$c \neq 0$, $a = b = d = 0$
K_c/s^2	$b \neq 0$, $a = c = d = 0$
K_c/s^3	$a \neq 0$, $b = c = d = 0$

It is clear from Fig. 29 that the step response is completed by $t = 0.45$ sec, when the next sample of the error is taken by the impulse modulator. Thus, the error is zero and the sampled-data feedforward returns to a waiting status. Note that the stick deflection curves (c) of Fig. 29 bring forth the principal assumption of this model that the time to complete the force program is the same for all Y_c, resulting in the various peculiar shapes for the stick deflections. However, when $Y_c = K_c$ this model produces a bang-bang α_c signal to the neuromuscular system which correlates with the successive firing of the agonist and antagonist muscles to accomplish a rapid ballistic-like hand motion. The above relationship does not hold for controlled elements of a higher order, and hence the merit of the analogy is rather limited.

Approved for Public Release

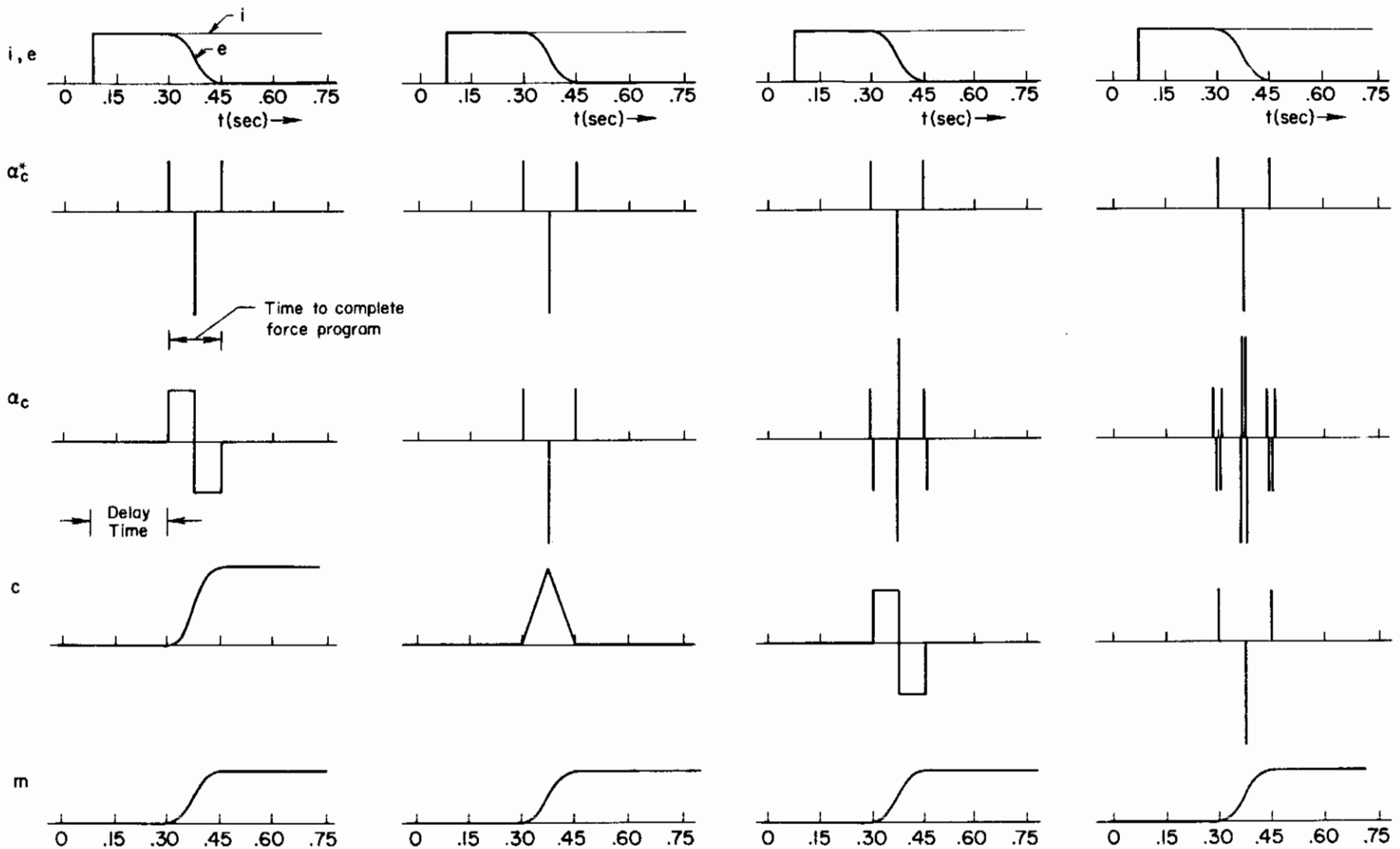

Figure 24. Feedforward Command Signals for Step Inputs

Approved for Public Release

Contrails

Having explained the existing sampled-data model, its salient features are summarized in Table VIII. Note that the delay time distribution of the proposed sampled-data model is rectangular and uniformly distributed between 0.15 and 0.30 sec, in contrast with past data which indicate a near-Gaussian distribution of the inverse time delay. This is the major piece of existing evidence that the model presented above did not explain at the time of its genesis.

TABLE VIII

SUMMARY OF MODEL PREDICTIONS

CONTROLLED ELEMENT Y_c	TIME TO COMPLETE FORCE PROGRAM (STICK)	SHAPE OF STICK DEFLECTION RESPONSE
K_c	0.15 sec	 : Second-order response to step
K_c/s	0.15 sec	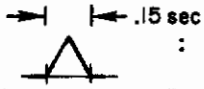 : Triangle
K_c/s^2	0.15 sec	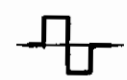 : Double pulse
K_c/s^3	0.15 sec	 : Impulse train

C. NEW EXPERIMENTAL DATA AND CONCLUSIONS

With the intent to confirm or modify the hypothesized sampled-data model of Figs. 26 and 27, step response data for various controlled elements and differing magnitude step inputs were obtained. Sample step responses for $Y_c = K_c$, K_c/s, K_c/s^2, and K_c/s^3 are presented in Fig. 30a, b, c, and d, respectively. For each controlled element the value of the gain, K_c, was picked on the basis of best pilot opinion rating for the overall system.

The important step response parameters are obtained by averaging data extracted from several runs; these are tabulated in Table IX. The comments regarding shape and nature of the control are given in the last

Approved for Public Release

Contrails

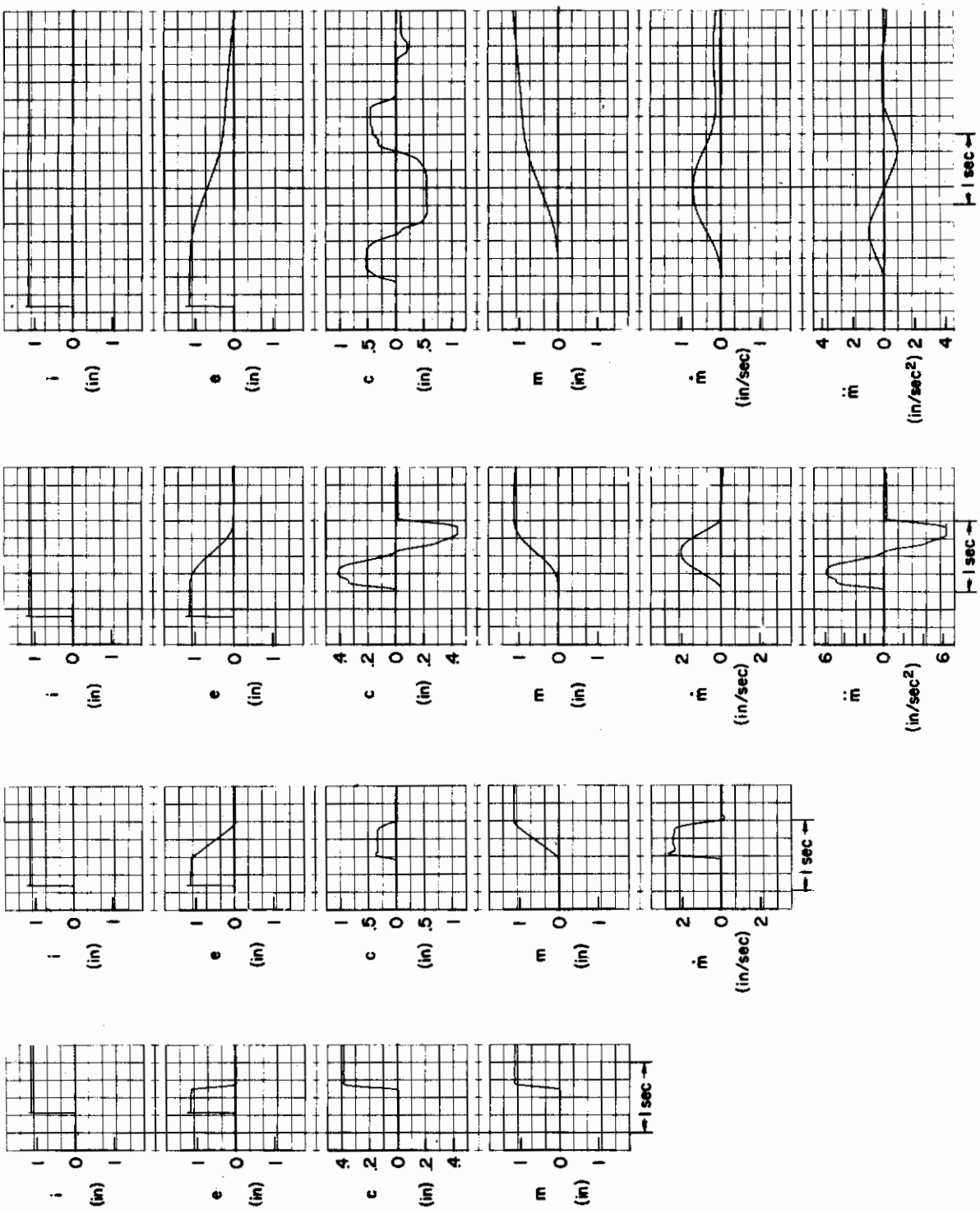

Figure 30. Sample Step Response Data

Approved for Public Release

TABLE IX

STEP RESPONSE PARAMETERS FROM DATA (STI)

(Note: Magnitude in inches, time in seconds. Mean at top, standard deviation at bottom.)

CONTROLLED ELEMENT Y_c	INPUT HEIGHT	SYSTEM RISE TIME	DELAY TIME	FIRST PULSE c(t)		SECOND PULSE c(t)		THIRD PULSE c(t)		TIME TO COMPLETE FORCE PROGRAM	COMMENTS
				Height	Width	Height	Width	Height	Width		
2.86	$\frac{8}{7}$	0.072 0.013	0.347 0.035	0.360 0.014	—	—	—	—	—	0.134 0.020	Step deflection of stick
2.86	$\frac{10}{7}$	0.055 0.010	0.310 0.041	0.405 0.041	—	—	—	—	—	0.132 0.015	
$\frac{7.1}{s}$	$\frac{6}{7}$	0.420 0.063	0.320 0.032	0.250 0.036	0.518 0.061	—	—	—	—	0.518 0.061	Single-pulse deflection of stick
$\frac{7.1}{s}$	$\frac{8}{7}$	0.432 0.048	0.352 0.029	0.283 0.031	0.523 0.045	—	—	—	—	0.523 0.045	
$\frac{7.1}{s}$	$\frac{10}{7}$	0.545 0.148	0.355 0.073	0.303 0.046	0.590 0.060	—	—	—	—	0.590 0.060	
$\frac{14.3}{s^2}$	$\frac{6}{7}$	0.905 0.100	0.347 0.063	0.201 0.032	0.513 0.059	0.157 0.034	0.640 0.069	—	—	1.153 0.059	Double-pulse deflection of stick (±). Approximately equal amplitude bangs and equal pulse width.
$\frac{14.3}{s^2}$	$\frac{8}{7}$	0.830 0.063	0.367 0.063	0.297 0.029	0.524 0.046	0.267 0.052	0.540 0.068	—	—	1.063 0.060	
$\frac{14.3}{s^2}$	$\frac{10}{7}$	0.675 0.065	0.323 0.057	0.452 0.122	0.510 0.054	0.422 0.125	0.561 0.107	—	—	1.071 0.155	
$\frac{3.6}{s^3}$	$\frac{8}{7}$	2.542 0.448	0.378 0.045	0.420 0.094	0.755 0.112	0.443 0.150	1.212 0.216	0.320 0.139	0.825 0.195	2.792 0.330	Triple-pulse deflection of stick
$\frac{3.6}{s^3}$	$\frac{10}{7}$	2.145 0.868	0.403 0.076	0.620 0.116	0.710 0.053	0.753 0.166	1.132 0.140	0.517 0.166	0.965 0.386	2.807 0.385	

Approved for Public Release

Confidential

Contrails

column of Table IX and are discussed later in the section. However, certain basic differences between the hypothesized sampled-data model and experimental results become apparent on inspecting Tables VIII and IX and the sample step responses of Fig. 30. These differences are presented in Table X for ease of comparison.

In the light of the new data, the principal error in the hypothesized model is seen to be the assumption that the time to complete the force program is a constant for all Y_c. Unfortunately, this is a key assumption, and its discard implies that the hypothesized sampled-data model is inappropriate for controlled elements other than pure gain.

D. A NEW DUAL-MODE CONTROLLER MODEL

An important aspect obvious from the step response data is the bang-bang nature of the stick deflection control movements. This property leads us to the pertinent problem of optimality of the operator and his related performance indices. One explanation is that the operator is optimal or suboptimal relative to the minimum time criterion. Consider an nth order single input-single output control system with $|c(t)| \leq M$, where the scalar M may represent either a physical limit on the stick deflection or more likely an implicit restraint imposed by the operator for the given situation. In any case, it represents a magnitude constant on the control input. For i(t) = constant, the time optimal control has the following properties:

- The control c(t) is bang-bang, i.e., c(t) = +M or −M.
- There are at most (n−1) switchings (i.e., +M to −M or vice versa) for systems with n real eigenvalues.
- The switching logic is dependent on the order of the controlled element. In general, the switching surface is a nonlinear function of the state variables.
- For a given initial condition of the state variables, there is one unique control c(t).

For the problem at hand, there is a specific type of initial condition of the system state vector, namely:

$$\begin{aligned} e(0) &= \text{input height} \\ \dot{e}(0) &= 0 \\ \ddot{e}(0) &= 0 \\ &\vdots \end{aligned}$$

The terminal state is the origin.

Approved for Public Release

Contrails

TABLE X

HYPOTHESIZED MODEL PREDICTIONS VERSUS EXPERIMENTAL RESULTS

MODEL PREDICTIONS	EXPERIMENTAL RESULTS
1. Delay Time	
Model predicts a uniform distribution for the delay time between 0.15 sec and 0.30 sec for all Y_c.	Data indicate a different mean delay time, for each Y_c, with low variance.
2. Time to Complete Force Program	
Model predicts a constant time of 0.15 sec, for all Y_c, to complete the force program.	Data show that the time to complete the force program increases monotonically with the order of Y_c.
3. Shape of Stick Deflection	
a. Step change for $Y_c = K_c$. b. Triangular pulse for $Y_c = K_c/s$. c. Double rectangular pulse (plus-minus) of equal amplitude and pulse width for $Y_c = K_c/s^2$. d. Train of three impulses (plus-minus-plus) for $Y_c = K_c/s^3$. Etc.	The stick deflection is pulsatile: a. Step change for $Y_c = K_c$. b. Rectangular pulse for $Y_c = K_c/s$. c. Same as for model. d. Three pulses of alternating signs. The width of the middle pulse is approximately twice that of the first and third pulses. Pulse amplitude is approximately constant for three pulses.

Approved for Public Release

Contrails

In order to measure the degree to which the available step response with $c(t) = \pm M$ data is time-optimal, certain invariance conditions, one for each controlled element, are obtained by solving a two-point boundary value problem. These are stated and described in Table XI without presenting their derivation; thus, let

T_c = time to complete the force response (i.e., duration of the stick response correction for step inputs)

M = average absolute amplitude (for each Y_c) of the stick response assuming it to be bang-bang with equal positive and negative amplitudes

A = input height

K_c = controlled element gain

$(\cdot)_o$ = time optimal value of the parameter in parenthesis

The conditions are:

TABLE XI

INVARIANCE CONDITIONS FOR TIME OPTIMALITY

CONTROLLED ELEMENT, Y_c	INVARIANCE CONDITION FOR TIME OPTIMALITY
K_c	$= A/K_c$
K_c/s	$(T_c M)_o = A/K_c$
K_c/s^2	$(T_c M^{1/2})_o = 2(A/K_c)^{1/2}$
K_c/s^3	$(T_c M^{1/3})_o = (32A/K_c)^{1/3}$

Assuming a wide band neuromuscular system response, the ideal time-optimal step response character for differing controlled elements is shown in Fig. 31. Note that the smoothing effect of the neuromuscular system would round off the corners in the Fig. 31 responses yielding results similar to that in Fig. 30. Note further that the control movement starts after the end of the delay time phase, and time optimality pertains to that period of control only. Finally, in Table XII we present a comparison of the actual data to the optimal.

On the basis of the comparisons in Table XII, it may be safely concluded that the step response behavior of operators is nearly

Approved for Public Release

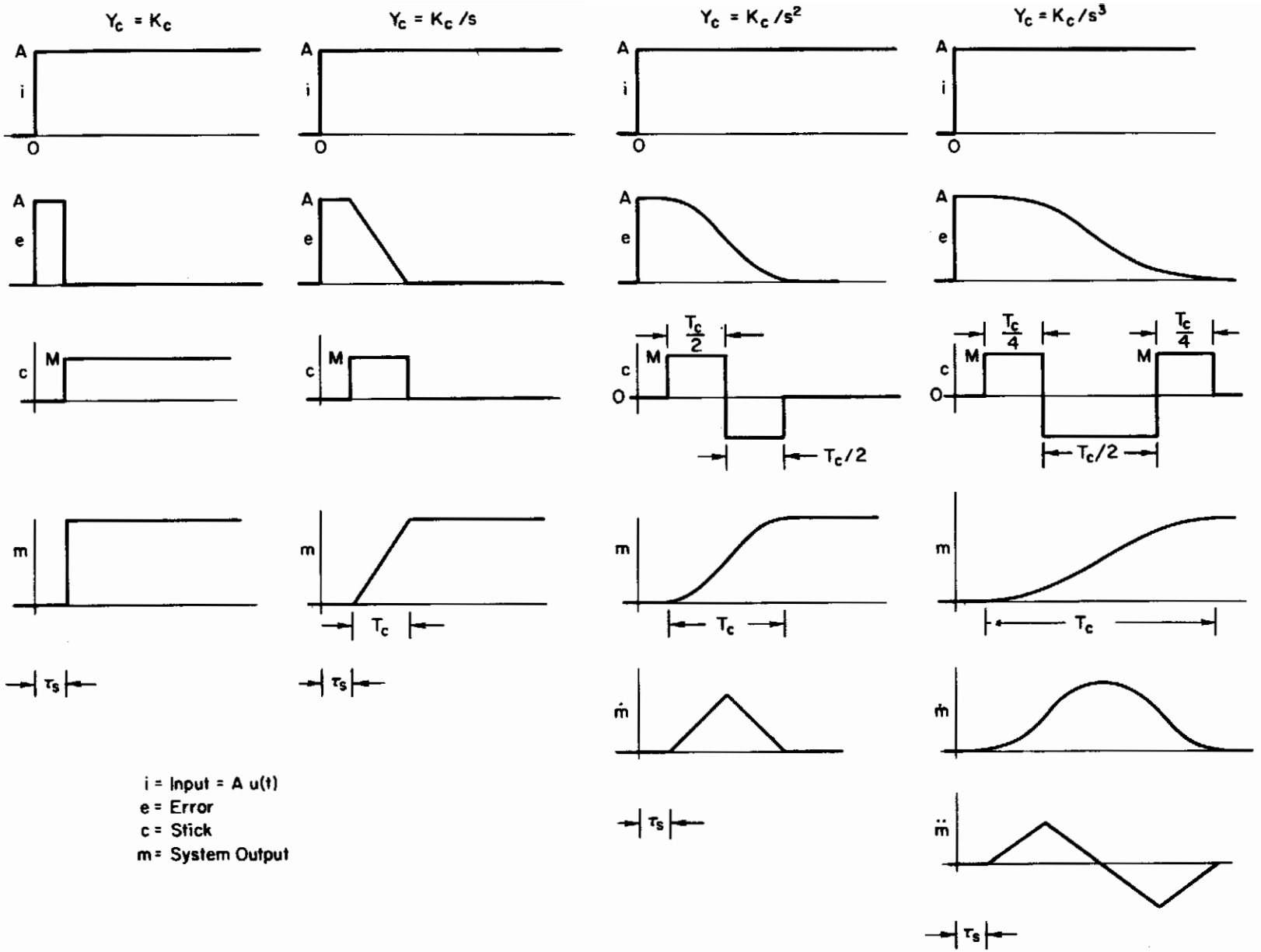

Figure 31. Ideal Time-Optimal Response Characteristics
(T_c = Time to Complete Force Program)

Approved for Public Release

Contrails

TABLE XII

TIME-OPTIMAL CONTROL CHARACTERISTICS FOR STEP INPUTS;
COMPARISON WITH EXPERIMENTAL RESULTS

CONTROLLED ELEMENT Y_c	INDEX FOR TIME OPTIMALITY: Invariance Condition	Optimal		Expt.	DEGREE OF TIME OPTIMALITY*
K_c	$(M)_o = \frac{A}{K_c}$, $(T_c)_o = 0$	$K_c = 2.86$			
		A	$(M)_o$	$(M)_e$	
		8/7	0.4	0.36	10
		10/7	0.5	0.40	20
K_c/s	$(T_cM)_o = \frac{A}{K_c}$	$K_c = 7.1$			
		A	$(T_cM)_o$	$(T_cM)_e$	
		6/7	0.120	0.130	8.34
		8/7	0.161	0.148	8.10
		10/7	0.201	0.178	11.45
K_c/s^2	$(T_cM^{1/2})_o = 2\left(\frac{A}{K_c}\right)^{1/2}$	$K_c = 14.3$			
		A	$(T_cM^{1/2})_o$	$(T_cM^{1/2})_e$	
		6/7	0.490	0.488	0.41
		8/7	0.564	0.568	0.71
		10/7	0.632	0.707	11.8
K_c/s^3	$(T_cM^{1/3})_o = \left(\frac{32A}{K_c}\right)^{1/3}$	$K_c = 3.6$			
		A	$(T_cM^{1/3})_o$	$(T_cM^{1/3})_e$	
		8/7	2.17	2.04	6
		10/7	2.33	2.40	3

*Percent error $= \left|\frac{\text{Optimal} - \text{experimental}}{\text{Optimal}}\right| \times 100$

**$(\cdot)_e$ = value of the parameter in parenthesis from experimental data

Approved for Public Release

Contrails

time-optimal. Variations in the switching logic appearing in actual data do not affect the terminal zero error condition substantially, but do affect terminal error rate and acceleration. Perhaps the operator strategy is to reduce e, $\dot{e}$, ..., $e^{(n-1)}$ to small values rather than to try and make these exactly zero. The operator resorts to quasi-linear steady-state control behavior once the error phase trajectory enters the region near the zero state. Another explanation for the suboptimal control may be that the operator trades off time optimality to minimize some other secondary performance index. It is also worth noting from Table IX that the stick amplitudes and pulse durations for different controlled elements seem to be roughly the same. This may be the reason for selecting the particular controlled element gains on a "best" pilot opinion rating basis.

E. SUMMARY

In conclusion, a time-optimal control model is one possible idealization for the feedforward step response path of the dual-mode, mode-switching model for the operator. The complete model is presented in Fig. 32, as one explanation of available data. The quasi-linear path is the usual operator describing function for compensatory steady-state tracking of random inputs. The feedforward parallel path represents the control plus decision model of the operator in response to step inputs. The nonlinear error sensing blocks in Fig. 32 automatically route the error signal through the appropriate channel based upon whether $e \gtrless e_T$ (e_T is some threshold magnitude of error).

The control logic for each different controlled element and as a function of the error state $\underline{e}$ $\left[e = \text{col}\ (e, \dot{e}, \ldots)\right]$ is given in Table XIII for time-optimal response. Note that M, the constraint on the control input, is some function of the step input height, controlled element gain, and its order.

The decision logic model behaves like a function switch (FSW) and accounts for the initial increase in the time delay (beyond that due to quasi-linear tracking) in response to a step input. The neuromuscular command used by the operator seems to be γ_c input rather than α_c.

Approved for Public Release

Contrails

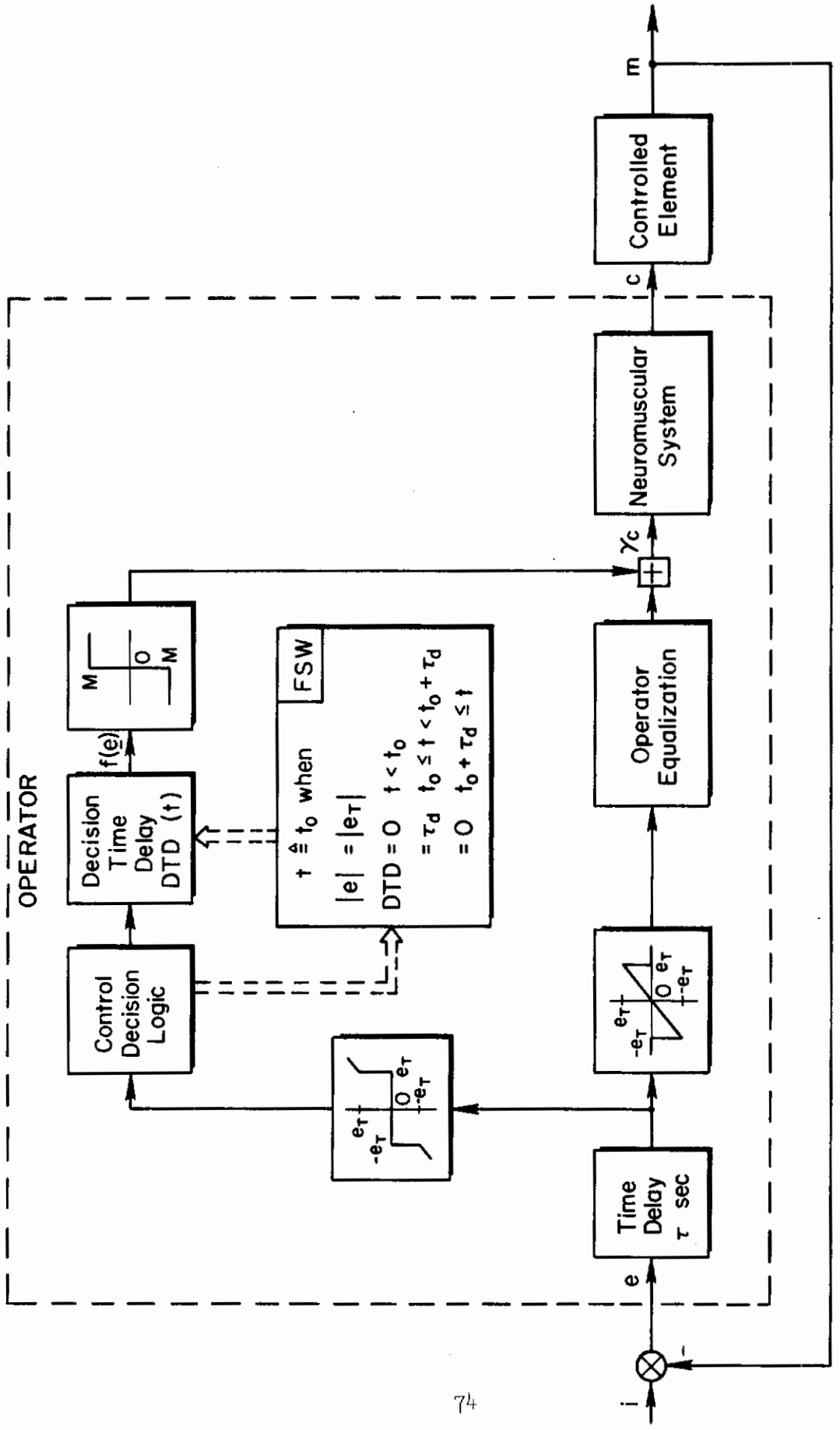

Figure 32. Dual-Mode Controller Model

Approved for Public Release

Contrails

TABLE XIII

CONTROL LOGIC FOR VARIOUS CONTROLLED ELEMENTS

CONTROLLED ELEMENT Y_c	CONTROL LOGIC $f(\underline{e})$
K_c	$(A/MK_c)e(t)$
K_c/s	$e(t)$
K_c/s^2	$\left[\dot{e} + \sqrt{2MK_c\lvert e\rvert}\ \operatorname{sgn} e\right]$
K_c/s^3	$\left\{e + (1/3)\dddot{e}^3 + W\dot{e}\ddot{e} + W\left[(1/2)\ddot{e}^2 + W\dot{e}\right]^{3/2}\right\}$
	$W = +1$ for $\left[\dot{e} + (1/2)\ddot{e}\lvert\ddot{e}\rvert\right] > 0$
	$= -1$ for $\left[\dot{e} + (1/2)\ddot{e}\lvert\ddot{e}\rvert\right] < 0$
	(Ref. 57)

The model of Fig. 32 should thus serve as one possible explanation of operator behavior in response to random plus step inputs.

F. CONCLUSIONS

The proposed model is a first step towards evolving composite operator models, good for both random and transient inputs. Indeed, it is an idealization; so with this in mind, future experiments must be directed to verifying its optimality and sensitivity. Other performance indices may be tried to see if the given system is relatively optimal with regard to them. This way, one may be able to show that operator control is perhaps not so sensitive to variations in performance criteria.

Approved for Public Release

Contrails

SECTION VI

IMITATING THE SUCCESSIVE ORGANIZATION OF PERCEPTION OF HUMAN OPERATORS

A. THE SUCCESSIVE ORGANIZATION OF PERCEPTION THEORY

The human attributes of multimodal sensory perception, multimode output behavior, and judgment and adaptability to the received inputs, outputs, and error lead to an enormous number of possible control loop structures for any given situation. Through higher order processes, such as judgment and memory, the pilot can evolve and modify his performance criteria, select relevant inputs, decide between competing control loop structures, and optimize his fine-grained behavior with respect to several criteria. To cope with this kaleidoscope of possibilities, the theory of Successive Organization of Perception (SOP) was evolved (Ref. 58). This theory postulates possible interpretations and organizations of the input data, and the establishment of the appropriate internal system organizations so that the information may be exploited for effective control.

On the one hand, SOP theory can be viewed as explaining the various modes of human pilot behavior observed in particular situations. On the other, this theory can serve as a tool for the pilot/vehicle system analyst by providing the set of rules for selecting the mathematical pilot model appropriate to a particular situation. This latter use of the theory is that which concerns us here.

The necessity for SOP theory in the model selection sense is only now beginning to develop. However, as human pilot behavior becomes better understood, and hence more behavioral modes become amenable to mathematical modeling, rules for model selection will assume much greater importance than they do at present. Current rules for model selection are almost entirely qualitative. Because the over-all family of pilot models may be expected to grow substantially in both numbers and complexity, the eventual necessity of an orderly quantitative model selection scheme would seem to be necessary for routine application of these pilot models.

Approved for Public Release

Contrails

It appears, however, that an all-out effort to develop such a quantitative model selection scheme would be premature at this time. What does, at present, seem warranted is a summary of the techniques which might be used to formulate the selection scheme, and the development of some exemplary application of the technique. The purpose would be to provide a framework to encourage development of quantitative criteria for model selection. A very limited number of existing quantitative criteria (for the most part pertaining to the quasi-linear pilot describing function for use in the visual modality, single-loop compensatory tracking of a narrow band random input situation) could be fitted to this framework now. To approach the ultimate goal of an "automatic" selection scheme more closely than indicated above, for example, by constructing a detailed decision process algorithm, is just not consistent with the present state-of-the-art in either human pilot modeling or SOP theory.

The question thus arises, "Should we attempt to construct an interim set of model selection rules which will be only partly quantitative?" The answer seems to be "yes" for at least two reasons. First, an interim effo: will provide a well-organized procedure which will assure that a reasonabl; complete, albeit largely subjective, set of criteria is considered in selecting appropriate pilot models for pilot/vehicle analysis. This organ ized procedure would eliminate some of the artistic flavor presently assoc: ated with the model selection process in the mind of the working engineer. The second reason recommending an interim effort arises from the detailed complexities that will accompany the programming of the ultimate "automati selection scheme. The complexities are precisely those of exposing the logical decision processes used by the knowledgeable human analyst in selecting a model. The success of the programming depends on being able tc "ask the right questions." That is, to formulate a set of hypotheses as tc how the analyst selects the model. It does not matter that some hypothesis may be incorrect, since there are techniques of varying sophistication for eliminating incorrect hypotheses (see, for example, Ref. 59). What is important is that the set of hypotheses includes as a subset the "correct" hypothesis. It appears that the only way hypotheses may be introduced is by external statement. Here the experience of the human analyst plays an important role. It is important that the stated hypotheses be the result

Approved for Public Release

Contrails

of informed judgment and not pure guesses for efficiency in hypothesis testing.

In the following we shall review the highlights of SOP theory, and then proceed to speculate on models which imitate the SOP process itself. These models will be suggestive of a sequential decision process.

The essential stages in the SOP learning sequence are shown in Fig. 33, and are described below (after Ref. 58):

> **Compensatory** (Fig. 33a). The pilot is given, or pays attention, only to the error (input minus output) characteristics represented by Y_{p_e}.
>
> **Pursuit** (Fig. 33b). The pilot perceives both the input and output (and, hence, error). He uses any predictable aspects of the input (represented by Y_{p_i}), as well as the learned characteristics of his proprioceptive sense of control motions, Y_{p_p}, and the controlled element, Y_{p_m}, to operate in some "optimum" manner on the input with a compensatory vernier correction operation on the residual errors, Y_{p_e}.
>
> **Precognitive** (Fig. 33c). The pilot perceives the input and recognizes (or chooses) a perfectly predictable pattern. His selected response is subsequently preprogrammed or open-loop for large intervals of time.

The block diagrams of Fig. 33 are suitable to represent not only the pilot's progression to, or regression from, higher levels of internal system organization in a given situation, but also grossly represent the possible loop structures when different levels of display information are provided.

For example, in early stages of training a pilot will operate mainly on the perceived error (i.e., in a dominantly compensatory manner) even if the output and input are both displayed, as in a pursuit-type instrument. Conversely, even with a compensatory display (error only), if the input has a definite pattern, leading to a corresponding pattern in his required control actions which he can perceive, perhaps only subconsciously, then he can structure a loop based on this proprioceptively sensed control action to provide a self-generated "input," i_p, to generate most of the required control movement. This progression to an internally organized pursuit mode, given a pure compensatory display, is represented in Fig. 33b by switching to i_p via the Y_{p_p} loop. After much training, the

Approved for Public Release

Contrails

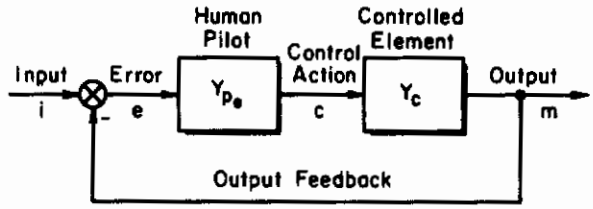

a) Initial Phase : COMPENSATORY (Single Loop)

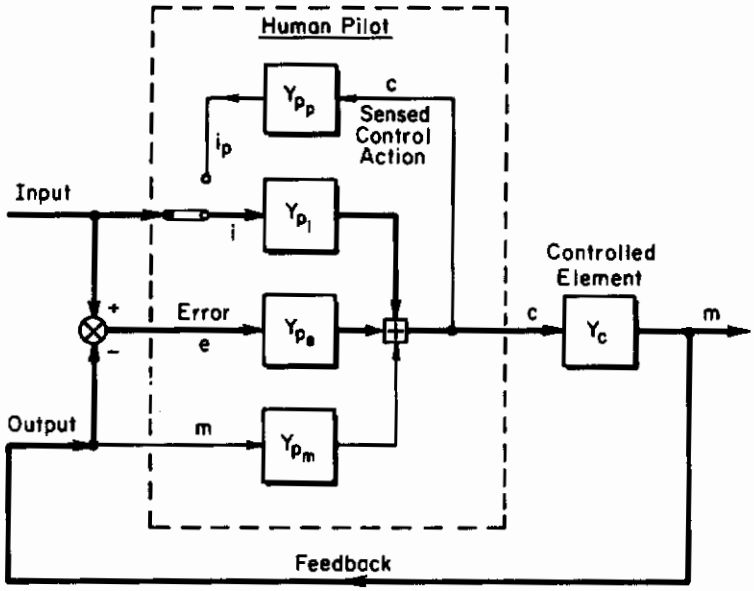

b) Second Phase: PURSUIT (Multiloop)

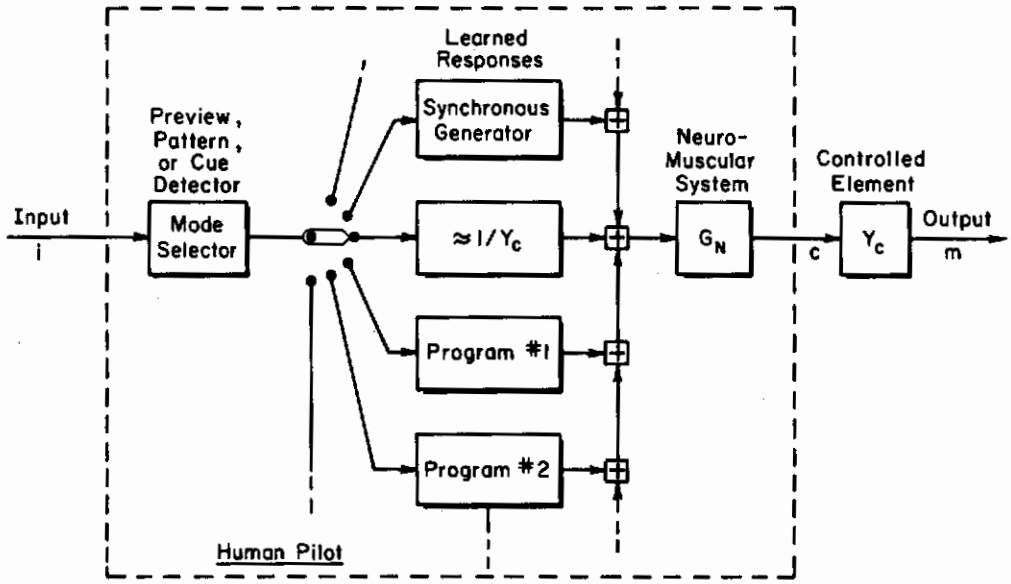

c) Final Phase : PRECOGNITIVE (Open-Loop)

Figure 33. The Three Main Phases in the Successive Organization of Perception (SOP)

Approved for Public Release

Contrails

pilot can even close his eyes, thus opening the Y_{pe} loop and operating solely on his learned response pattern. Thus, given some pattern, or "coherence," to the input, he can actually progress to the precognitive mode for short intervals with only a compensatory display! This will be illustrated later, but the key point is that the Successive Organization of Perception theory describes the human pilot's construction, via internal organizational changes, of a succession of perceptual inputs which

- Are equivalent to more elaborate displays than those from which the stimuli were obtained
- Induce background or references not physically present
- Make highly efficient use of any coherence in the presented stimuli

The SOP theory leads to an understanding of both the progressive and the regressive control behavior during training, transfer, stress, equipment failures, etc., and it offers a unifying approach to the display problem.

Before proceeding it is appropriate to expand upon the modeling process. First, there are two general types of mathematical modeling activity which can be described as:

Data descriptor models. These models need have no direct structural analog in the process, but are intended to codify measured data more efficiently and to permit prediction within the explored ranges of variables. Models of this type include input/output catalogs, statistical regression models, statistical detection and decision models, closed-loop describing function measurements and data fits. They have the advantage of simplicity, analytical utility and efficiency, and known confidence limits.

Structural or analog models. These models attempt to describe the mechanization or internal cause/effect events which lead to the observed input/output data. In some important cases these can be partially derived from the data descriptor models (e.g., determining, or measuring, human operator open-loop describing functions in single-loop compensatory tracking of random inputs), but in most cases they are derived from heuristic reasoning in the face of an array of facts to be "explained." Analog models, or "mimics," are often too complex or nonlinear to measure efficiently and seldom achieve the statistical confidence possible with data descriptor models. Nevertheless they are ultimately desirable to rationalize the observed over-all behavior or to simulate the fine-grained behavior.

Approved for Public Release

Contrails

A blending of these types of models is usually achieved in human process modeling when a theory is fitted to a large body of codified data and the variations are accounted for by recognizable features in the operator's physiology.

B. MODELS IMITATING THE SOP PROCESS

The Successive Organization of Perception process has been described as a progression through three main phases of loop organization, each containing a number of subsets of behavior appropriate to the task. Assume that identifiable limits and conditions can be found (e.g., experimentally) for each subset mode of observed behavior. Then one model for the SOP process would be an active off-line monitor which identifies the conditions, selects some most likely mode, monitors the result, reselects a new mode when necessary or when further information is brought out by the first operations, and so forth. This model is not intended to be an analog of the mental processes involved, but is merely an efficient way of coding and selecting the most likely mode of behavior from those which have been distinctly identified and modeled. This model is, among other things, a description of an analysis procedure in which estimates of behavior mode are the key outputs desired.

An appropriate form for this model is a flow or decision process algorithm. Such models have been described in Refs. 60 and 61, and applied to a specified task involving a given sequence of subtasks in Refs. 59 and 62–64. For example, Seigel and Wolf (Ref. 62) use a sequential state model with probabilistic state transitions (estimated by direct inquiry of squadron commanders) and a Monte-Carlo computer analysis to investigate the pile-up of sequential tasks required to effect the downwind approach, turns, flap and landing gear preparation, and flight path line-up for landing on an aircraft carrier. Thomas and Tou in Refs. 59 and 64 set up the selection of an optimal path from point-to-point by dynamic programming. Braunsten, et al (Ref. 63), give computer algorithms for the car-following driver task, interpreted as an on-going sequential process, and they attempt some statistical measurements of one subroutine parameter required by highway tests. Thus, this approach is by no means novel, and there are several current programs which should

Approved for Public Release

Contrails

yield material useful to the present problem. Most of these attempts have had limited success because of the inordinate complexity and repetitive cycling required to represent continuous tasks.

The suggestion here is that algorithm models may be much more appropriate and successful when applied to the SOP sequence itself than to describe any particular mode of tracking. This is because most of the observed manual control behavior falls into relatively few categories from which logical criteria can select the most suitable, e.g., the three phases of SOP in Fig. 33. Within these phases of SOP various submodes are required, but many of these already have well-modeled characteristics. The rather heterogeneous forms and degree of approximation described here and elsewhere are ideally called up by mode-selection algorithms. Thus, the algorithmic models are used where they are best suited (logical functions), while the continuous servo models of human behavior are used where they are most efficient (well-defined tracking or stimulus response situations).

Some preliminary work on an algorithmic-type model for the SOP process is shown in Figs. 34, 35, and 36. The process of constructing a flow diagram to simulate a decision-making or learning process is instructive in itself because one is forced to formally define and examine the logical structure behind decisions which are often made in a casual manner. The formalism also focuses attention on categorizing and finding efficient hierarchies of decision-making criteria. For example, the difficulty of constructing Figs. 34 and 35 illustrates why some investigators have had a hard time using and adapting the well-established quasi-linear pilot models to real-world problems. Even for these models it is hard to specify written criteria or instructions for selection.

Part of the problem lies in the heterogeneity of the types of models evolved, and part lies in the diverse concepts and words which might form suitable categories or descriptors. These problems are common to library search routines, and some library document retrieval procedures were adapted to simplify the concepts.

Figure 34 shows a flow diagram for some key steps which must precede the selection of a particular human pilot mode of behavior and thence the appropriate model and adjustment rules. The "situation" selection

Approved for Public Release

Contrails

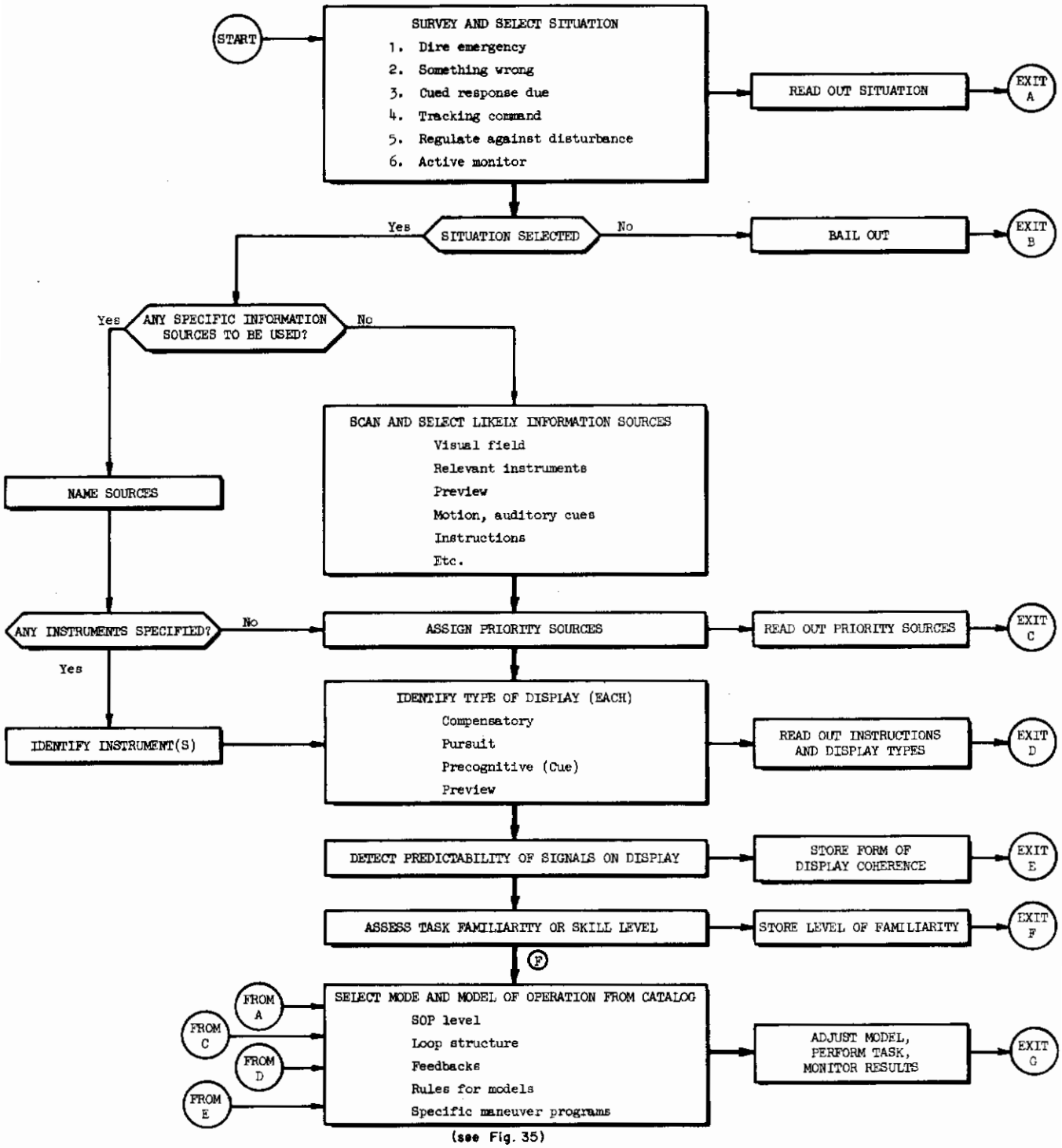

Figure 34. Flow Diagram for Mode Selection Via SOP

Approved for Public Release

FROM A SITUATION	FROM C PRIORITY FEEDBACKS	FROM D DISPLAY TYPE	FROM E DISPLAY COHERENCE	FROM F FAMILIARITY	APPROPRIATE LOOP STRUCTURE AND MODEL	CONFI-DENCE LEVEL	POSSIBLE ALTERNATE
Tracking	IFR (specific)	Compensatory (e only)	Random	Some	1. Compensatory, quasi-linear	High	—
Rough air (regulation)	VFR (roll)	Outside horizon	Random	Some	$Y_{OL} = Y_{p_e} Y_c \rightarrow \frac{\omega_c}{j\omega} e^{-\tau_e j\omega}$; etc.	High	No. 2
New situation	Attitude errors	Pursuit or compensatory	Random	Nil		Med.	No. 2, 4
Tracking	IFR (specific)	Pursuit	Random	Much	2. Pursuit, quasi-linear	Med.	No. 1, 4
Aerial refueling	VFR (relative positions)	Pursuit	Random (gusts)	Much	$Y_{p_i} \rightarrow 1/Y_c$, etc. $Y_{p_e} \rightarrow$ quasi-linear compensatory form of pilot describing function; etc.	High	No. 1, 3
Formation maneuvers	VFR (relative positions)	Pursuit; preview	Programmed maneuvers	Much	3. Pursuit, hybrid	Med.	No. 2, 1
Landing flare	VFR; h, $\dot{h}$, y_e	Preview; pursuit	Programmed + random gusts	Some	$Y_{p_i} \rightarrow$ cued program(s) $Y_{p_e} \rightarrow$ quasi-linear compensatory form of pilot describing function; etc.	Med.	No. 5, 2
Tracking	IFR (specific)	Compensatory	Periodic, 1< period < 10s	Much	4. Pursuit, internal	Med.	No. 3
Precision aerobatics	VFR (?) (specific)	Pursuit	Prescribed output and control	Some	$Y_{p_i} \rightarrow$ from i_p $Y_{p_e} \rightarrow$ quasi-linear compensatory form of pilot describing function; etc.	Low	No. 3, 5
Tracking, divert attention	Cue only	Compensatory	Periodic and simple	Extreme	5. Precognitive, programmed (open-loop)	Low	No. 4, 2
Imminent collision	VFR	Preview	Discrete	Some	Cued program(s)	High	No. 3
Bank and stop	Cue	Preview	Discrete step	Much	6. Precognitive, quasi-optimal (open-loop)	Med.	No. 5, 4, 2
Sideslip	VFR or IFR (attitude cues)	Preview or cue	Discrete step	Much	Precomputed before execution	Low	No. 5, 3
Etc.	Etc.	Etc.	Etc.	Etc.		Etc.	Etc.

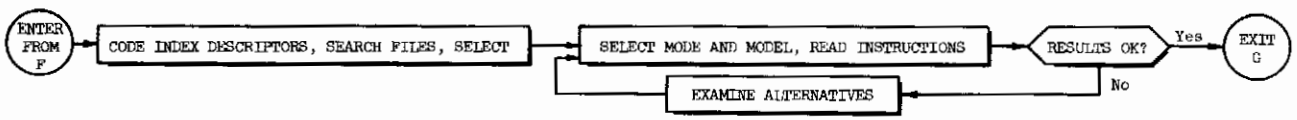

Figure 35. Typical Mode/Model Catalog and Selection Process

Approved for Public Release

Contrails

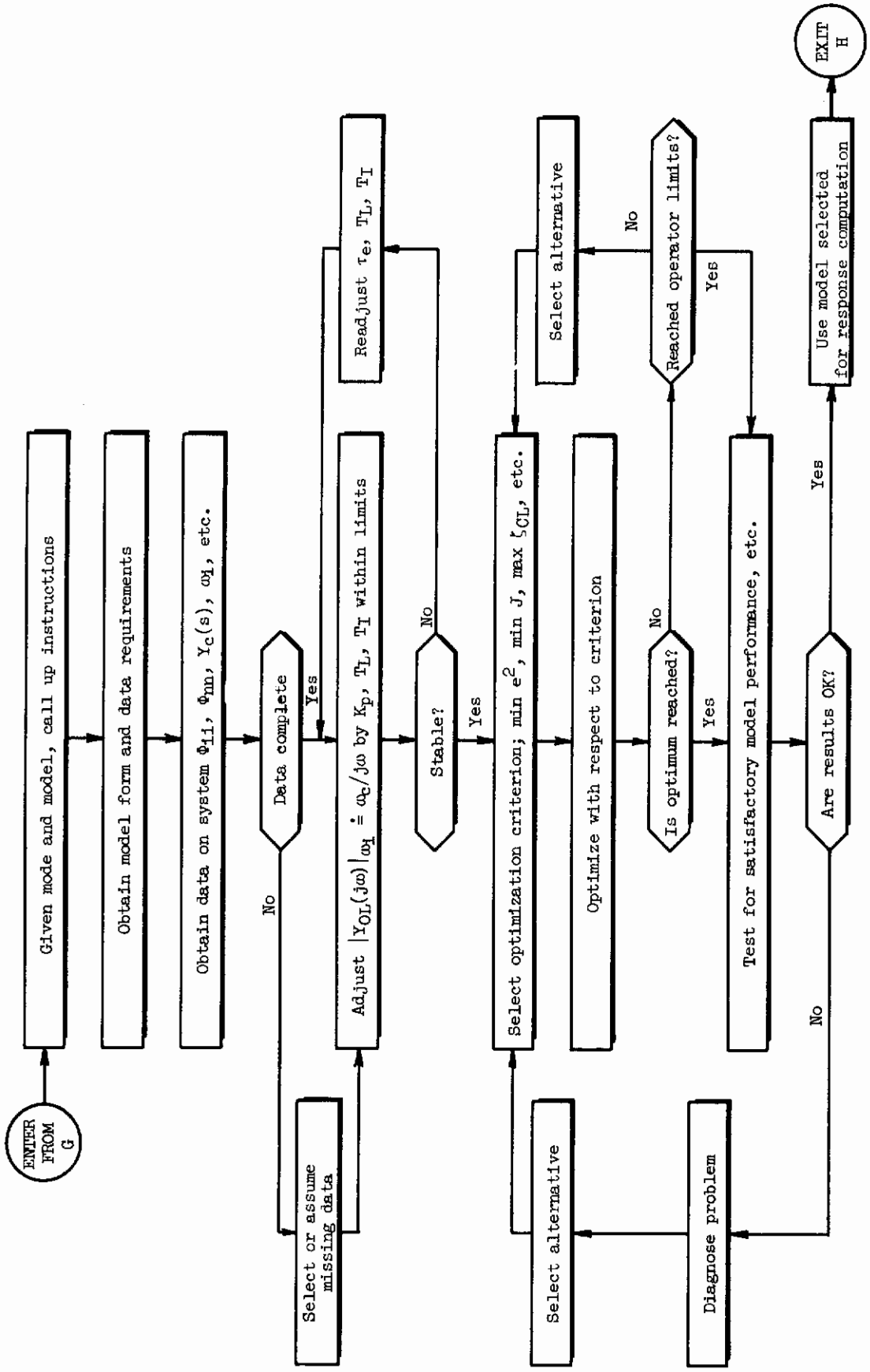

Figure 36. Typical Subroutine for Compensatory Mode

Approved for Public Release

Contrails

is the most vaguely defined at present. It is easy to describe any given situation verbally, but not to categorize it in compact form. Probably something like ten to twenty suitably different descriptors would cover any reasonable case here, and only five to ten would be required for the majority of cases. As few descriptors as possible are desired to avoid the problem of dimensionality. Once the situation is selected, one can go directly to specific instruments if these are specified (or if the pilot is already in a given loop, in a transition or failure mode situation). Otherwise, possible information channels assigned to a given situation must be scanned, and the most likely or priority items then selected. Subroutines for this step are more apparent, but the details for their implementation are difficult to describe in a quantitative manner. For example, the multiloop hypothesis can be used, and heuristics and empirical experience might be used to evolve a rational selection procedure.

Identification of the type of display is straightforward if it is an instrument (single or integrated), but may be more difficult for the visual field situation.

Determining the predictability, or coherence, of the information available will be very difficult in many cases. Strong discrete cues or random inputs are no problem, since subjective criteria for unpredictability are not too hard to define. But to recognize subtle cues, complex periodic waveforms, etc., will require both analytical and experimental data not yet available.

Assessment of the operator's familiarity with the task and instruments (i.e., skill level) is an important factor in selecting his mode of operation. This criterion must be externally prescribed, and will not be tested for directly.

Finally, all these preliminary criteria have been selected, and a set of descriptors will be available at Exits A, C, D, E, and F of Fig. 34.

The mode and model can then be selected. Two general approaches are possible here:

1. A logical selection tree, from which the correct mode is picked by climbing along a sequence of branches, guided at each branch node by one of the (say, n) descriptors previ-

Approved for Public Release

Contrails

ously evolved. The main advantage is speed in going directly to the desired branch in n steps. The disadvantage is that there is an enormous number of terminal branches, but only a relatively few modes and models to select from. Hence, the same item appears on many branches, and the storage and logic coding process is cumbersome.

2. A cross-filed catalog of each mode, as it becomes available, from which the appropriate model is selected by the conjunction of a set of n entry descriptors with those labeling the model. The advantage is ease of coding and storing the relatively few (say, m; $m > n$) modes and descriptors, and the disadvantages are the slightly longer search required (if a simple sequential search is used) and the fact that a mode can be retrieved only for sets of descriptors assigned to storage.

Much more work needs to be done on this, including use of combined logical trees and descriptor conjunctions. At present, the best scheme appears to be No. 2 above, which is illustrated in Fig. 35. Note that each model in Fig. 35 has a large number of descriptor sets associated with it, of which only a couple samples of each are shown. Another descriptor set may be added at any time as the range of validity of a model is extended, and a given group of descriptors and models may be taken out, refined, and given separate identity without changing the remaining items. A great deal of work needs to be done in simplifying and rationally indexing the descriptor sets to facilitate the search. Also shown on the right of Fig. 35 are descriptors for the confidence level and alternative items to search in case the likely mode does not work out.

Once an appropriate mode of operation and model have been selected, the adaptation rules and criteria are called up and the human pilot's behavior is suitably simulated. This adjustment and optimalization process is shown in Fig. 36. Details of this process have been discussed in previous sections.

The problem has been fairly well structured at this point, although refinements will continue to be required. The next most pertinent task is to make the theory operational for a few simple cases. This will demonstrate the feasibility of the approach, and the interactions with other topics (such as optimal control patterns) discussed in this report.

Approved for Public Release

Contrails

SECTION VII

PHYSIOLOGICAL BASES FOR TRACKING BEHAVIOR

This section will consider the physiological problems and mechanisms involved in human pilot tracking behavior, especially those concerned with more complex functions which are not simply accounted for at the peripheral neuromuscular level. The recent surge of research devoted to neuromuscular mechanisms has gone a long way toward clarifying the properties of the peripheral neuromuscular command and control apparatus, and gives us helpful and suggestive insights into the mechanisms at higher levels of the nervous system which play upon the peripheral system. Although physiological research methods are still limited to the investigation of quite restricted kinds of activity in restricted situations, and usually involve experimental animals rather than humans, there are, fortunately, enough examples from which some general principles of system organization can be derived; by appealing to these through analogy and inference we will attempt here to provide a suitably sound basis for the models of human pilot behavior discussed elsewhere in this report.

This section is subdivided into four parts. First, a review of the basic peripheral neuromuscular control apparatus will be presented, in which the mass of new research data relevant to the present discussion will be summarized. This review provides some of the physiological background for the neuromuscular system model summarized in Section II, and serves as a point of departure for the discussion of higher centers involved in control. Second, a summary will be made of the functional properties of some higher neuronal centers of the brain, especially in relation to their modification of, and interaction with, the peripheral neuromuscular system described in the first part. Third, we describe the operation of two subcortical compensatory motor control systems whose organization and function are sufficiently important to consider their implications for models of skilled motor performance. These systems have possible direct parallels to the more "automatic" aspects of compensatory tracking during stationary conditions after extensive training. The

Approved for Public Release

Contrails

fourth section brings in the cerebral centers needed for logical, learning, permissive, etc., operations required before any skilled "automatic" behavior is possible.

A. PERIPHERAL NEUROMUSCULAR CONTROL ELEMENTS

Ultimately, all the complex decision-making and command-generating centers of the brain must make use of the basic neuronal circuits operating at the spinal level together with the special sensory organs associated with them at the periphery. As a result of an enormous research effort over the past ten years we have come to know relatively a great deal about them and their mode of action, at least in isolation. The behavior of pure spinal systems is a powerful determinant of the way supraspinal centers interact with them, and their behavior suggests ways in which we interpret the activity we are able to observe at higher levels.

It is not the purpose of this report to give a detailed summary of the peripheral neuromuscular control elements and systems; for this the reader is referred to several recent symposia and reviews (Refs. 65 – 71) and our own model of this system (Ref. 28) which is summarized in part in Section II. In what follows we shall merely give a very brief account of some of the more important elements and their properties so that the reader may be better able to follow later discussions.

Much of the control of neuromuscular behavior in the periphery is dependent on a complex organ located in the muscles of the body, the muscle spindle. It is in itself a complex neuromuscular integrative system receiving a continuous set of motor control and command signals from the central nervous system, and sending a constant stream of sensory information signals via several paths back to the central nervous system.

A typical muscle may have 50 to 80 of these organs, embedded at various points among the tension-producing ("extrafusal") muscle fibers of the main muscle mass. A typical spindle is elongated in shape, may be several millimeters in length, and has an orientation parallel to that of the extrafusal muscle fibers. They may be arranged in isolation, in tandem with each other, or be found in conjunction with other specialized receptor structures of the muscle. Each spindle has a central axis which consists

Approved for Public Release

Contrails

of a globular nuclear bag region (Fig. 37) connected to either pole of the spindle by means of a pair of nuclear bag fibers, which are themselves typical striated muscle fibers (~25μm in diameter). In addition to this there are from one to five subsidiary muscle fibers, the chain fibers (10–15μm in diameter), which may or may not extend the entire length of the spindle. Thus, although the two fiber systems are distinct, they may interact by virtue of their mechanical coupling. The nuclear bag and chain fibers are known collectively as "intrafusal fibers," and are never observed to contribute directly to the development of tension in the muscle. Rather, they appear to be motor fibers related solely to control within the spindle itself. From their microscopic appearance the bag fibers appear to be normal striated muscle fibers and hence would be expected to have dynamic and mechanical properties similar to those of the extrafusal fibers.

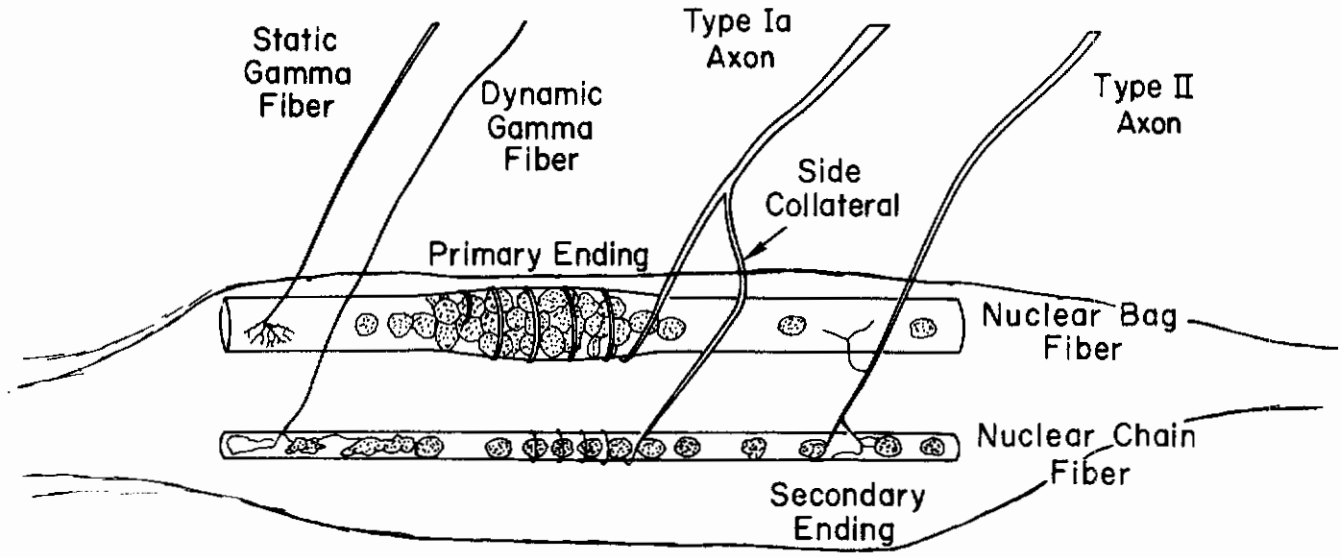

Figure 37. Diagram of Muscle Spindle

Both types of intrafusal fibers are innervated by special motor axons arising from cells in the spinal cord. The axons have a diameter range of 5–12μm and signal conduction velocities of 30–70 m/sec. They are known as gamma fibers and the cells they arise from are referred to as gamma motor neurons (or sometimes as fusimotor neurons). There is now good evidence that there are at least two independent types of gamma fibers, whose properties will be discussed below.

Approved for Public Release

Contrails

In a typical spindle, there will usually arise one large axon whose principal termination winds around the nuclear bag region (a region of the spindle without muscle or contractile elements) and additionally may terminate also on one or more of the chain fibers. These are the primary or annulospiral endings. The Type Ia axons serving these have large diameters (12-20μm) and do not have terminations on other spindles. An additional sensory terminal is the flower-spray or secondary ending, associated primarily, but not exclusively, with the chain fibers. Each axon can terminate in several such endings, and these Type II axons are about half the diameter of the Type Ia axons. Endings may have terminations on more than one spindle.

Mechanical deformation of these sensory endings leads to the development of electrical potential fields at the terminals which are directly proportional to the strength of the deformation. These generator potentials are accurate mappings of the forces operating on the terminals and can follow rather high frequencies of change in the deforming stimulus. The fields are utilized by the sensory axon in the production of nerve impulses at specialized triggering regions near the receptor endings. Nerve impulses are generated at a rate directly proportional to the magnitude of the generator potential, hence there is a continual transmission of impulses at a frequency which is a linear function of that potential and thus of the strength of the deformation. The sensory endings exhibit a high degree of sensitivity to length changes — a significant shift in firing frequency can result from length changes of only a few microns. This relationship can be used to reconstruct the time course of tension changes at the nuclear bag region from observed trains of nerve impulses.

The primary ending of a spindle usually shows some discharge even when the extrafusal muscle fibers are at their normal resting body length. This is presumably due to a small amount of residual tension in the spindle. Even in the absence of any motor signals from the spinal cord, the firing rate in the spindle will increase monotonically as a function of increasing muscle length (from a few pulses per second to a hundred or more pulses per second). This results from the disposition of the spindle within the muscle which serves to transmit length changes in the muscle to the bag

Approved for Public Release

Contrails

region where the change is reflected as an increase in bag tension. Conversely, shortening of the muscle (either passively or in response to an alpha motor command signal) will reduce the tension on the bag and hence reduce the spindle Ia sensory fiber firing frequency.

Figure 38 shows some typical plots of spindle sensory receptor firing frequency as a function of muscle length. Over a considerable range this relation is linear.

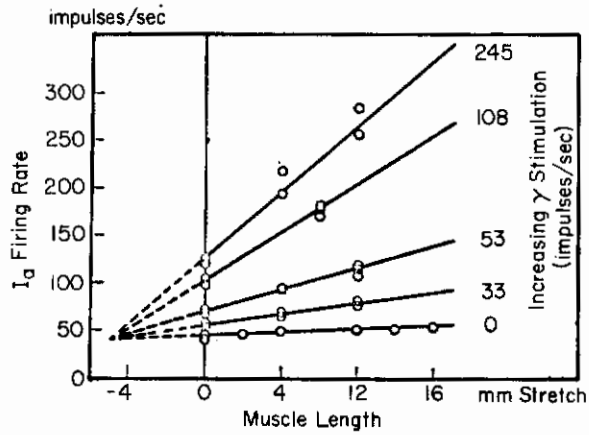

Figure 38. Steady-State Length Versus Ia Firing Rate Relations for Various Gamma Fiber Stimulation Rates (Adapted from Ref. 72)

Recent studies of single gamma fibers ending on spindles whose primary endings were being monitored have shown that repetitive stimulation of certain gamma fibers will produce a response which consists of a general increase in the firing rate of the primary ending (relative to its control rate) as a function of muscle length. This may result in (1) a family of curves of increasing slope whose relations are essentially linear (Fig. 38), or, (2) a simple translation of the length/frequency curve upward, or (3) in a combination of both. Each family of curves is a function of the stimulation frequency of the gamma fiber.

The shift in length/frequency relation for these gamma fibers is usually unaccompanied by any significant increase in the velocity sensitivity of the fiber (see below), i.e., the gamma fiber has influenced only

Approved for Public Release

Contrails

the static gain of the primary ending; such a gamma fiber is designated as a static fusimotor fiber.

In addition to this static length/firing-frequency relation, the primary ending also shows a strong sensitivity to stretch or release velocities. Its firing frequency, with rapid lengthening, can increase to several hundred pulses per second, regardless of length, and characteristically drops abruptly to zero when the muscle is allowed to shorten. This velocity-sensitive property can also be influenced by gamma stimulation, but the population of gamma fibers with this capacity is distinctly different from that which influences the static relation. Gamma fibers which increase the velocity-sensitive or dynamic part of the response to changes in muscle length with only a small effect on the static gain are called dynamic fusimotor fibers. The effect of stimulating these is also dependent on the stimulating frequency, and thus the primary ending exhibits an inherent relation between firing rate, length, and velocity. The static gamma fiber increases Ia discharge for a given length (but may in fact decrease its relative sensitivity to stretch); conversely, the dynamic fiber greatly increases the firing frequency of the primary ending during stretch, but leaves its steady-state frequencies essentially unchanged.

In terms of the block diagram of Fig. 4 and the neuromuscular system model discussion of Section II, the actions of both the static and dynamic fusimotor fibers combine to adjust, and to maintain, the levels of the lead time constant, T_K. On the other hand, only the static fibers are needed to provide a bias signal which, in conjunction with the stretch (alpha) reflex loop, results in the average tension, P_o.

Thus (Fig. 39) even at the spinal level, each muscle has associated with it a pool of thousands of alpha motor neurons, at least two systems of sense-organ-controlling motor cells, the static and dynamic gamma neurons, three classes of receptors involving several hundred channels of input information to the cord, and associated clusters of interneurons*

*Neurons of the spinal cord are generally classified as either sensory, motor, or interneurons. To this latter class, therefore, belong all cells not carrying information directly from receptor structures ("afferent fibers") nor transmitting impulses to muscle fibers ("efferent fibers"). They are by far the largest population of cells in the cord and are essential to the internal information processing and integration within and between divisions of that structure.

Approved for Public Release

Contrails

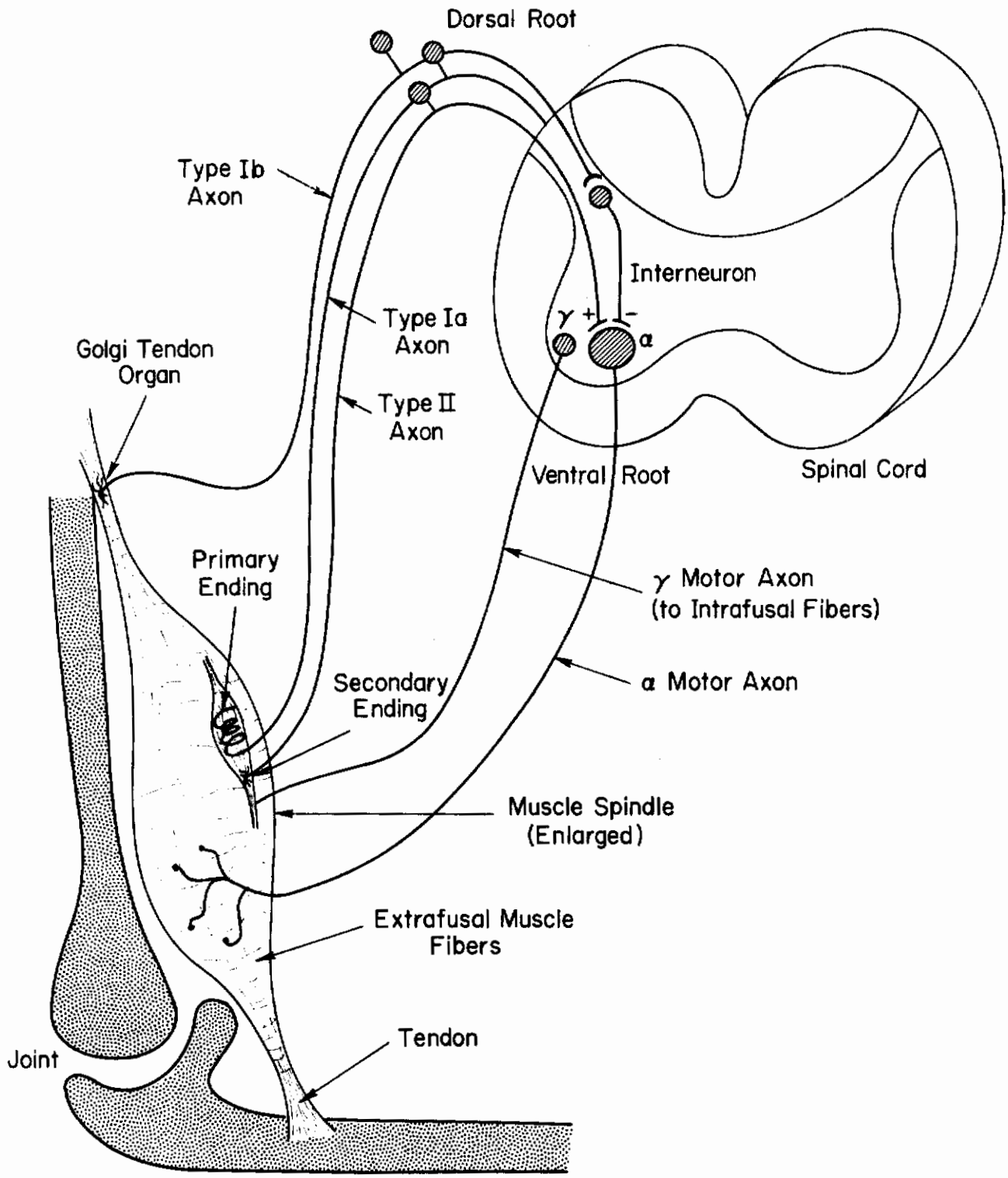

Figure 39. Motor and Sensory Supply for a Muscle

Approved for Public Release

Contrails

which serve to integrate, distribute, and modify the activity within the cord and the control loops by which communication with the muscle is effected.

Much of this activity, furthermore, is transmitted to higher levels of the nervous system, where a multiplicity of other sensory systems also converge. And while patterns of motor activity can be formulated and executed at a local spinal level, we shall henceforth be concerned primarily with patterns which are generated at higher centers. These are discussed in the next sections.

Both alpha and gamma motor neurons are subjected to a variety of inputs from centers within the brain and from other segments of the spinal cord. One of the chief differences, however, may be seen in their response to events taking place in the muscle to which their axons are directed. In this respect it has now been clearly demonstrated that the gamma cell is relatively unaffected by the peripheral events occurring in the muscle its spindles are embedded in. There are, apparently, no return pathways from the spindles or other muscle receptors which influence its immediate behavior.

The alpha motor neuron, on the other hand, is subject to several kinds of signals returning from its muscle. Most important is the activity generated by the Type Ia axons from the muscle spindles. These axons make direct ("monosynaptic") excitatory connections with alpha cells innervating extrafusal fibers in the muscle in which they are embedded, and if sufficient activity is arriving along Ia axons, output pulses will be generated in the alpha motor neurons. One way this can arise is when the muscle is being lengthened, either passively by some external force or by an antagonist muscle. The resulting increase in spindle tension causes an increase in Ia firing rates and thereby an increase in alpha firing rates which, by causing contraction of extrafusal fibers, opposes the lengthening process. Any shortening tendency of the muscle, conversely, reduces alpha activity, tending to reverse the shortening effect. Thus we have in the alpha/gamma/spindle complex the essential components of a negative feedback constant-length regulator (the differential element shown in Fig. 4), known to the physiologist as the "stretch reflex."

Approved for Public Release

Contrails

An alternative route for generating alpha motor neuron activity lies in the active production of spindle afferent activity by means of gamma command signals which will result in a gamma/spindle-controlled bombardment of the alpha motor cell (this is represented by the γ_c pathway in Fig. 4). This is a possibility of immense significance, since it opens the possibility of indirect activation of the alpha cells, and hence the possibility of generating direct and indirect command signals to the muscles. Both pathways are shown in Fig. 4.

The secondary endings from the spindle are also length- and rate-sensitive, but have somewhat different response properties from the primary endings; their central connections are more complex and involve inhibition of alpha motor neurons.

In addition to the spindle receptors there are a large number of receptors embedded in the tendons of the muscle, the Golgi tendon organs. These also are sensitive to stretch and from their placement in the muscle appear to supply tension information to the central nervous system. They appear to inhibit alpha motor neurons innervating the same muscle.

B. COMMAND AND MONITORING CENTERS IN THE BRAIN

Operating on, and interacting with, the peripheral neuromuscular units and associated spinal circuits is a hierarchy of centers in the brain itself. In general these can be expected to:

- Process information received from the peripheral neuromuscular, limb position, and skin sensors; integrate this peripheral somatic sensory input with other interoceptive (internal state monitoring sensors) and exteroceptive (external state monitoring and detecting sensors, such as the visual, auditory, and vestibular systems) information.
- Supply complex patterns of alpha and gamma command signals of appropriate timing, amplitude, and pattern to the respective alpha and gamma motor cells in the spinal cord and brain stem on the basis of the available sensory information and stored programs, according to changeable criteria of performance.
- Make short-term and long-term modifications in the actual organization of the peripheral neuromuscular system at the spinal cord and brain stem levels, and provide for storage of complex, patterned, skilled motor performance "templates."

Approved for Public Release

Contrails

All of the supraspinal centers with which we are concerned here have comparatively obscure functions relative to our state of knowledge of the peripheral and spinal motor systems. This results from the fact that our knowledge of these areas is derived largely from anatomical study of the fiber connections between them, and gross observations of the behavior of animals in which these centers or the connections between them are stimulated or destroyed. We know little or nothing about the signals that enter them or leave them under any but the most artificial or unnatural circumstances. As a result there is even very little qualitative agreement on what the functions of such centers are, and it is probably fortunate that there is agreement even on the symptoms which characterize malfunctioning or pathological states.

Consequently a large portion of the available data simply cannot be incorporated into any model of supraspinal motor control. The remarkable ability of animals with experimental trauma to retain a large degree of control further complicates the analyst's attempts and suggests that in the course of evolution equivalent systems have developed in parallel with subtle differences distinguishing them.

1. Sensory Monitoring Centers in the Brain

a. Organs monitoring the peripheral neuromuscular system. In addition to supplying input to the immediate spinal apparatus controlling neuromuscular activity, information from the peripheral sense organs of muscle, the spindle afferents and the Golgi organs, is transmitted to adjacent regions of the cord, and axons from these receptors travel up the spinal cord, establishing two important terminations in the brain (see Fig. 40). The first, and probably most important, terminus is in the cerebellum, a structure which overlies the brain stem and receives input from receptors in every muscle of the body. Moreover, this input, containing presumably length, tension, and rate information (Ref. 73) is apparently laid out in an extremely orderly fashion, forming what is sometimes referred to as a somatotopic mapping of the body musculature on parts of the cerebellar surface or cortex. The cortical surface of the cerebellum is itself an exquisite three-dimensional orthogonal matrix of cells and axons (Ref. 74), and it is upon this orderly arrangement of cellular elements that the muscle systems of the body are, in some way, mapped.

Approved for Public Release

Contrails

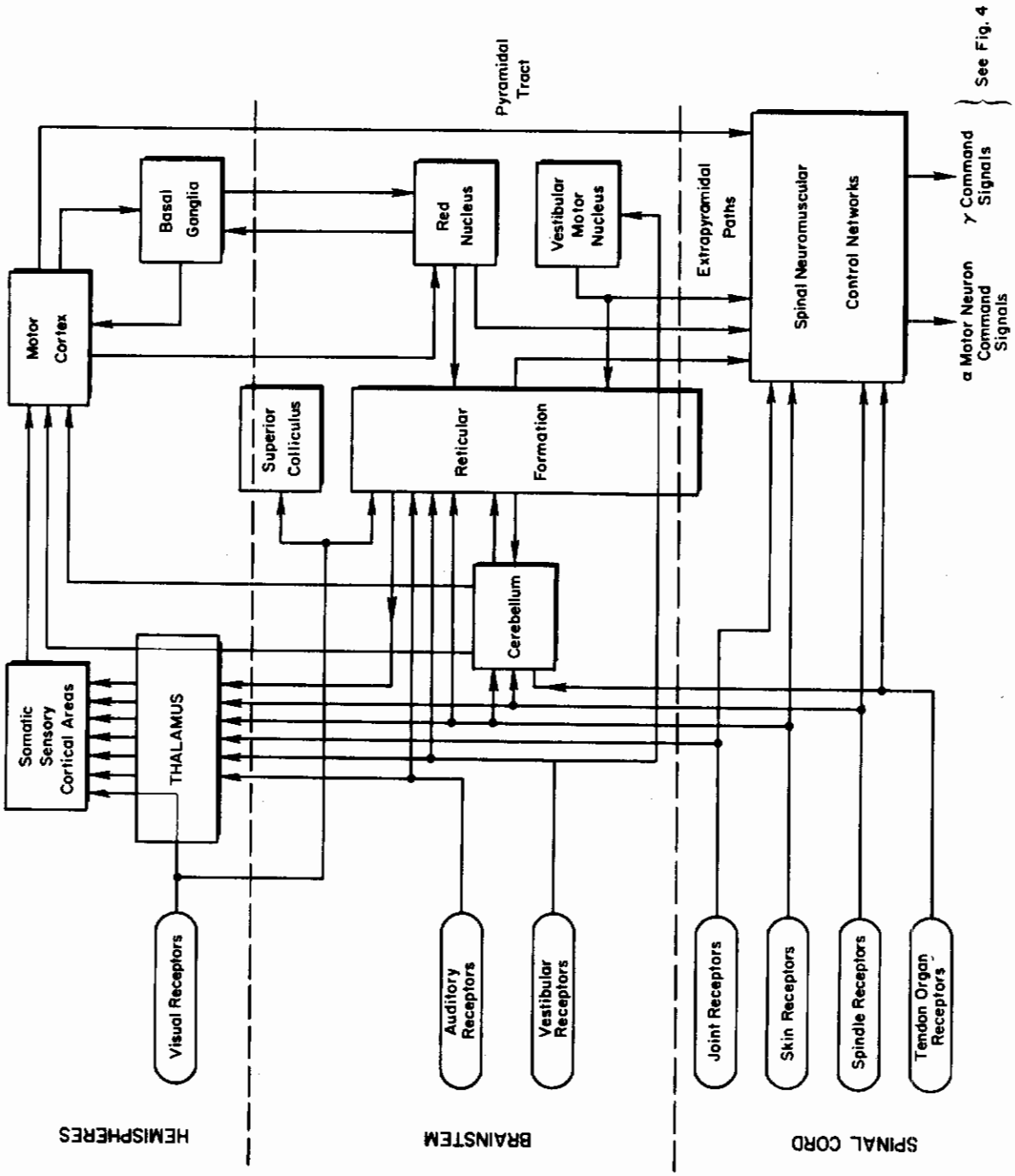

Figure 40. Major Supraspinal Centers Related to Motor Control

Approved for Public Release

Contrails

In addition, the cerebellar matrix also receives, from other pathways, (1) a continuous flow of impulses from skin receptors from all limbs, providing some proprioceptive information about the position of the body parts and (2) information from the vestibular apparatus, providing information about the relative position and acceleration of the body in space. The cerebellum does not, however, receive input from joint receptors (Ref. 75). Additional input has been described, arising from the auditory and visual systems (Ref. 76).

The other terminus for muscle and proprioceptive information is the somatic sensory cortex of the cerebral hemispheres (Ref. 77), which also receives inputs from other somatic sensory pathways involving touch, pressure, pain, and temperature (Fig. 40). Another cortical area receives vestibular input. Structural integrity of the cerebral cortex seems to be indispensible to the conscious perception of sensory input, whereas damage to the cerebellum, which does not seem to be involved at all with conscious perception of sensory input, leads to disorders in control characterized by inadequate muscle "gain," inadequate timing (Ref. 78) or phasing of individual muscles (Ref. 79) and groups of muscles, and a well-known oscillation of a limb involved in voluntary tracking behavior.

All of the major exteroceptive sensory systems, with the exception of the olfactory system, occupy distinct multisynaptic axonal tracts or pathways which terminate in the sensory portions of the thalamus (a deeply situated internal region of the brain) from whence their signals are relayed to distinct modality-specific projection areas on the cerebral cortex. This cortical representation includes special areas for visual, auditory, vestibular, and somatic sensory input, but other cortical areas appear to involve overlap in sensory input and for this reason are termed "association areas" of the cortex.

In addition to these major sensory pathways to the cortex, each exteroceptive sensory system or modality appears to involve additional collateral pathways which carry information to other brain areas such as the cerebellum, and, of prime importance for the discussion of motor mechanisms, a central core region of the brain stem called the reticular formation (Fig. 40). This area runs nearly the entire length of the brain stem and

Approved for Public Release

Contrails

indeed extends well into the spinal cord grey matter. The cells in this structure are characterized by the highly nonspecific or integrative character of the sensory input they receive, often being activated by combinations of auditory, visual, vestibular, and somatic sensory stimuli.

Furthermore the reticular formation is the apparent recipient of much of the interoceptive input of the body, i.e., input from blood pressure receptors, chemoreceptors of various sorts, temperature receptors, etc., and is itself highly sensitive to the circulating levels of blood sugar, blood CO_2, and many other substances.

It might be argued that almost any area of the brain could be called sensory since activity in that area could be modified by sensory input. But what characterizes all the areas described so far in this section is that, with the exception of the cerebellum, destruction of these centers leads to a loss in sensory perception or discriminative function. The cerebellum, on the other hand, has been included here because it receives direct input from sensory cell axons ascending from the spinal cord and from the vestibular system.

2. Command Signal Pathways from the Brain

Before considering the problem of where specific command signals from the brain are generated, we consider the principal pathways by which these commands are transmitted to effector cells or networks in the spinal cord. For convenience, and because it conforms to the present terminology in neurology, we will distinguish two classes of pathways from higher centers to the spinal cord. They are (a) the pyramidal tract,* whose fibers arise, in part, from the motor cortex of the cerebral hemispheres, and form a well-defined pathway along the medullary region of the brain stem and then, for the most part, cross to the other side of the spinal cord to terminate on or in association with cells innervating muscles on the opposite side of the body from where the pyramidal fibers originate; and (b) a group of pathways arising from the brain stem and other regions, collectively known as the "extrapyramidal" pathways (Ref. 80).

*Sometimes referred to as the "corticospinal tract."

Approved for Public Release

Contrails

Historically, it has been assumed that the pyramidal tract is the route of voluntary and skilled command signals and that these common signals go directly to alpha motor neurons. It was felt this was due to several reasons: the pyramidal tract arises partly from the cerebral cortex, the cortex is associated with the most complex forms of behavior, and electrical stimulation of the surface of the cortex produces movement. None of these assumptions appears to be entirely valid, however, for the following reasons:

- It is only in primates, particularly humans, that significant numbers of pyramidal tract fibers even terminate on motor (as opposed to interneuron) cells in the spinal cord (Refs. 81, 82).
- It appears (Refs. 76, 83) that the motor cortex exerts control on both alpha and gamma cells, so that it is unlikely that the pyramidal tract is a "private line" from motor cortex to alpha cells.
- It is apparent that skilled voluntary movement is possible in experimental animals when the pyramidal tract is interrupted in the brain stem (Ref. 81), so that, if voluntary movement is initiated cortically, alternate descending routes must be available for the signals.
- Many of the fibers constituting the pyramidal tract are not, in fact, of cortical origin.

In experiments on monkeys where the pyramidal paths are cut on both sides of the brain, the animals are able to recover normal movement to a large extent, but with some reduction in the speed or rapidity of movement and a greater tendency toward fatigue. Moreover, fine dissociative control, for example the ability to move a single finger, is lost and thereafter finger movements involve all five digits at once (Ref. 81).

There appears to be some differentiation of fiber types of pyramidal tract cells. The larger, faster conducting fibers show intermittent activity and tend to terminate on motor neurons which innervate distal phasic muscles (such as the digits), while the smaller, slower fibers probably tend to end more on interneurons related to alpha and gamma fibers of proximal tonically active muscles (Refs. 84, 85). Fibers of the fast conducting system probably establish a direct excitatory connection with alpha motor neurons.

In recent studies of single neurons in the primate motor cortex, cells sending axons to the pyramidal tract have been observed which undergo marked changes in discharge pattern in associated contralateral arm movements (Ref. 86). Moreover, on the basis of conduction velocity measurements,

Approved for Public Release

Contrails

there appear to be at least two classes of pyramidal tract cells — the faster conducting cells apparently fire only in association with discrete peripheral movements without a background discharge; the slower cells, on the other hand, have a more or less continuous background discharge even in the absence of movement which may either increase or decrease during spontaneous voluntary movements (Ref. 86).

In addition to its contribution to the pyramidal tract, the motor cortex has extensive connections with a number of subcortical areas, including the basal ganglia, reticular formation, and cerebellum. Hence damage to the motor cortex leads to far more severe and irreparable loss of motor control than does pyramidal tract section.

The extrapyramidal system consists of a number of distinct pathways arising from centers in the brain stem and terminating on interneurons in the spinal cord from which they all appear to exert control on the gamma pathways. The main centers of origin we shall be concerned with are the reticular formation, already mentioned, from whence the reticulospinal tract emerges; the red nucleus, giving rise to the rubrospinal tract; and the nucleus of the vestibular system, giving rise to the vestibulospinal tract. While we do not know in any precise detail how these pathways contribute to the over-all coordination of precise movement, we can give a rough characterization of their peripheral effect. The vestibulospinal tract appears to be concerned primarily with postural readjustments to changes in body orientation with respect to gravity. This has been demonstrated by testing the effect of labyrinthine stimulation on feedback loops at the neuromuscular level (Refs. 87-89). From such experiments we can say, for example, that in standing-man the effect of an increased gravitational force would be to increase the intensity of the muscle spindle response to increased gravitational stress by means of combined alpha and gamma control signals. When the body is tilted in space, appropriate readjustments in the position of the supporting limbs are made, tending to restore the original orientation of the body.

The rubrospinal tract appears to have a major influence on the gamma motor system and indeed there appear to be subdivisions in the red nucleus for selective control of dynamic or static gamma fibers (Refs. 90, 91),

Approved for Public Release

Contrails

and therefore one would be tempted to guess that overall ratios of static-gamma/dynamic-gamma activity are regulated here. While it is not clear whether specific muscles can be controlled selectively by this pathway, it is fairly certain that muscle groupings are differentially activated, e.g., the extensors or flexors of a given limb (Ref. 91).

In addition to its involvement in the motor control of autonomic functions, the reticulospinal tract has been shown to exert powerful excitatory or inhibitory effects on interneurons in the cord and on gamma activity (Refs. 92-94). Moreover, the reticular system seems to be able in some sense to set the levels of sensory input over different sensory pathways arising in the spinal cord.

For the formulation of command signals to be effective in a given situation, there must be a continuous inflow of information from sensory input channels to motor command centers. The reticular formation is an example of a self-integrated sensory-motor system, but a number of other critically important sensory motor loops also exist in the brain.

As previously pointed out, the cerebellum receives what is perhaps the most complex array of information concerning body and limb position and muscle tension, and it is essential to the orderly execution of voluntary activity. Toward this function, the cerebellum directs its output to higher centers in the brain, principally to the motor cortex of the cerebral hemispheres. The loop, moreover, is a closed one, for fibers from the motor cortex* provide a return path through the red nucleus and reticular formation back onto the cerebellar cortex. Other loops involving the cerebellum consist of fiber connections to and from the red nucleus and the reticular formation directly. Stimulation or destruction of any of the centers involved in this loop will result in marked changes in gamma and spindle activity observed peripherally (Refs. 75, 79, 93, 94).

Another area of interest in motor functions is a cluster of subcortical nuclei in the cerebral hemispheres which make complex connections with the

---

*The motor cortex, moreover, has additional sensory inputs via its connections with the sensory, visual, and auditory cortices, both directly and through cortical association areas.

Approved for Public Release

Contrails

motor cortex and with the brain stem. They are the so-called basal ganglia, and these centers are frequently implicated as the site at which complex "stored-program" motor activities may be initiated. There are now on record (see, for example, Refs. 95 and 96) sufficient observations of long-term chains or sequences of motor and other behavioral activity, such as those observed in mating, food gathering and consumption, etc., which can be repeatedly triggered by electrical or chemical stimulation of precisely localized areas of the brain, to suggest that in such cases the entire sequence of behavior is not generated at the locus of stimulation, but is merely triggered from that locus. This has led to the hypothesis that the full sequential program is stored in some fashion at some area of the brain, and the basal ganglia are favored by a number of observers as a possible site for program storage. Unfortunately, like much of the evidence relevant to motor behavior, the evidence is highly indirect and must be regarded at present as speculative. Nevertheless, trauma to the basal ganglia leads to more or less profound interference with normal motor function.

C. MODELS OF SUPRASPINAL CONTROL OF MOTOR ACTIVITY

In this section we will consider some data resulting from a number of recent investigations of the detailed mechanisms of motor control systems of the brain. The first example will examine how a system functioning as a regulator of the internal environment interacts with the basic neuromuscular spinal cord networks previously considered, and how this system is organized to minimize the error in the regulator and to minimize the effect of fluctuations in load. The second example illustrates a very simple situation in which information-processing centers can enable an external stimulus to be "tracked." A third section considers some important timing relations involved in complex pattern recognition/response situations involving the cerebral cortex.

1. Subcortical Interoceptive-Tracking Compensatory Control

First we consider a continuously active regulatory motor system whose physiological parameters and mechanisms have been studied far more extensively than any other. From it we can derive a number of hypotheses about how compensatory systems are organized. Indeed, no better example of the

Approved for Public Release

Contrails

detailed workings of the nervous system can be found than the action of the respiratory motor system which results in the periodic inflation and deflation of the lungs (Fig. 41). Many muscles are involved in this activity, but we consider here only the intercostal muscles which cause an increase or decrease in the volume of the chest by moving the ribs.

The function of the respiratory control centers in the brain stem reticular formation is to regulate the level of oxygen and carbon dioxide in the blood, and this is achieved by changing the ventilation rate of the lungs by varying the rate and/or the depth of respiration. In quiet respiration only the muscles of inspiration are used, and expiration occurs passively from elastic recoil once the action of the inspiratory muscles has ceased. In heavier respiration, the muscles of expiration become active.

One of the most potent stimuli to increase respiration is an elevated level of carbon dioxide, which apparently stimulates chemosensitive neuronal elements in the brain stem directly, and also stimulates a network of chemosensitive cells located in the walls of several major blood vessels, whose output also reaches the brain stem. These are connected to brain stem networks intrinsically organized to produce alternating bursts of impulses which are transmitted to motor neurons in the spinal cord. The organizational details of these brain stem networks are not well understood, but experiments suggest the existence of two mutually inhibitory pools of neurons which are active primarily during inspiration and expiration, respectively.

The control of respiratory volume is effected by several different means. First, an increase in blood CO_2 can cause an increase in frequency of firing of an individual cell during the inspiratory cycle. Second, the respiratory rate may be increased by altering the duration of the burst and the interburst period. Third, the antagonistic action of expiratory cells may be reduced during the inspiratory phase, but be accelerated during the expiratory phase. Fourth, there are apparently a large number of normally inactive neurons in the brain stem which can be recruited into an increased respiratory effort, thereby increasing the total drive to the spinal cord.

From a number of studies we find that to every state of blood/gas level there will correspond a specific output pattern from the brain stem which

Approved for Public Release

Contrails

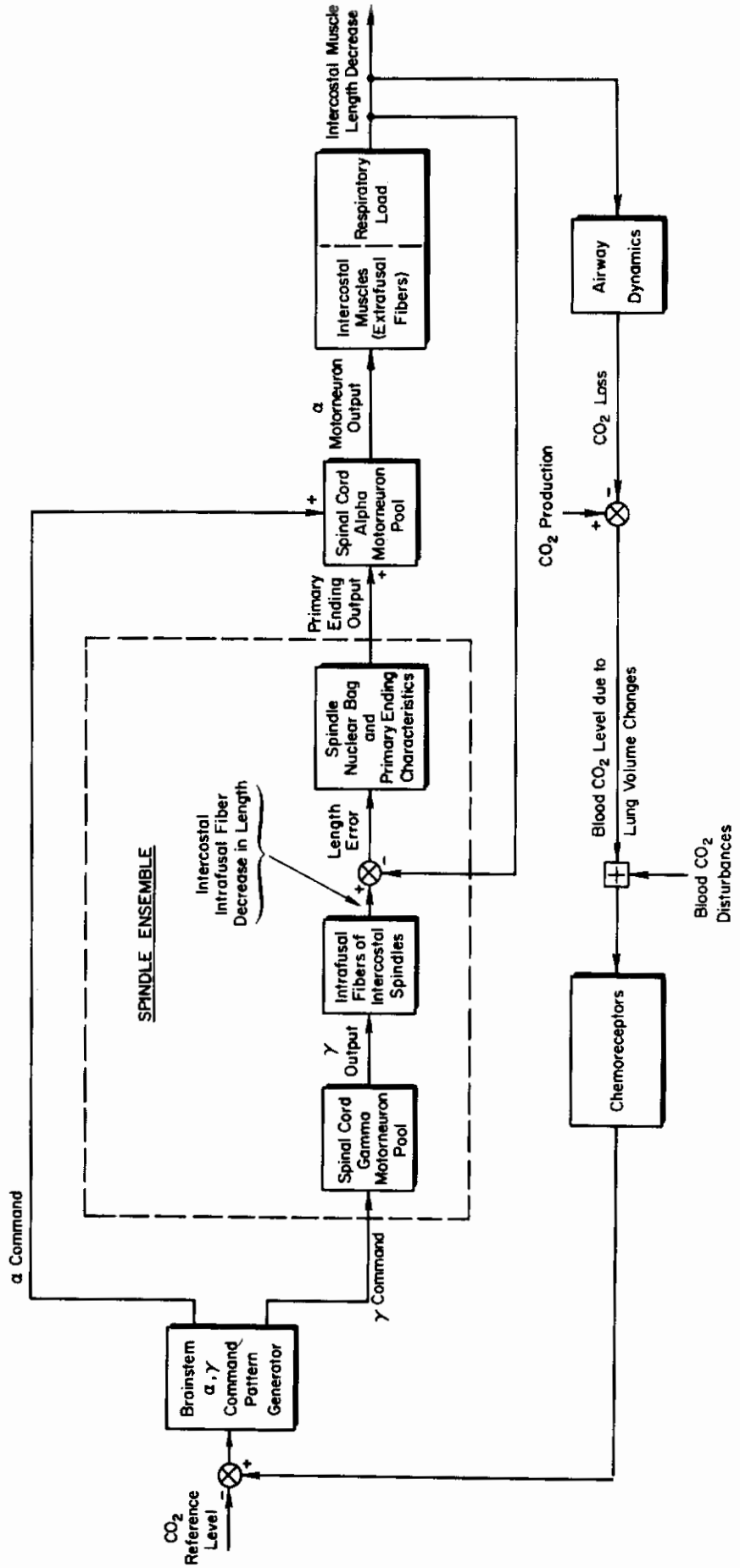

Figure 41. Blood CO_2 Control System Block Diagram

Approved for Public Release

Contrails

effectively commands the spinal neuromuscular apparatus to effect a maneuver adequate for maintaining a desired blood/gas level or for offsetting any deviations from the optimum level. These commands are equivalent to a volume of air to be moved in and out of the lungs. But even though the parameters of the output are variable, the output is always patterned in a stereotyped way, with periods of approximately constant frequency nerve impulse bursts alternating with silence.

The firing patterns of motor neurons in the spinal cord are similar in many respects to those in the brain stem, and electrical recordings from individual motor neurons supplying the external intercostal muscles (which are inspiratory) and the internal intercostal muscles (expiratory) show again the alternating burst/silence pattern of activity. Indeed, the phasing of firing of these two groups of motor cells with inspiratory and expiratory activity extends also to the gamma motor neurons in these pools. In fact, it has been shown that the pattern of firing of the gamma cells is closely related to the carbon dioxide level of the blood, suggesting that the command signals from the brain are relayed in parallel to both the alpha and the gamma systems (Ref. 97), see Fig. 41.

There is now considerable evidence that gamma activity slightly leads alpha activity in respiratory neurons. The evidence for this comes from direct simultaneous observation of several neurons, but is further strengthened by the finding that when the dorsal roots are cut (thereby interrupting the spindle flow to the alpha motor cells) the alpha cells may actually fail to fire during the normal phase of respiration,* while the gamma cells continue to fire. This suggests that alpha discharge may actually be dependent on a considerable amount of gamma-produced spindle support. In addition, observation of spindle discharge during contraction of respiratory muscles shows that, in contrast to what might be expected during respiration, spindle discharge increases; we conclude, therefore, that increased gamma bias has offset the unloading effect of contraction. These observations apply to both inspiratory and expiratory intercostal muscles (Refs. 97, 99–103).

*In humans, dorsal root section here leads to a paralysis of these respiratory muscles of which the subject is unaware (Ref. 98).

Approved for Public Release

Contrails

This parallel transmission of a command signal from the brain stem insures that adequate ventilation will occur in spite of changes in muscle power, airway resistance, or driving pressures, for during the execution of the command signal any mismatch between the required contraction (signaled via the gamma system) and the actual contraction will be signaled by the spindle afferent (which measures the difference between "required" muscle length and actual muscle length). If the shortening of the muscle is too small, for example as a result of increased airway resistance, this will immediately cause a burst of impulses from the spindle to increase the level of excitation to the corresponding alpha motor neuron. This hypothesis has, in fact, been tested in experiments in which the airway resistance was suddenly altered just prior to a respiratory cycle (Ref. 102). The effect on alpha motor neuron discharge is immediate (i.e., much too fast to have arisen by CO_2 stimulation of the brain stem), which supports the hypothesis that the gamma/spindle loop can be used to drive the neuromuscular system as a "follow-up servo."

Further investigation of the gamma fiber input to the intercostal muscles has revealed, in addition to the intermittent discharge phase-locked with respiration, a "tonic" (continuous) gamma component. This latter activity can be influenced by cerebellar stimulation and tilting the head (Ref. 100). In the case of the intercostal muscles, this is correlated with the fact that these muscles have a dual function — that of respiration on the one hand and postural control on the other. Thus, two independent routes of gamma command signals impinge on common spindles; one from the respiratory system and, simultaneously, one from the tonic postural or position-determining system. As a result, the tension of intercostal muscles periodically fluctuates at an amplitude determined by the phasic gamma system. The fluctuation occurs about an average tension determined by postural demands via the tonic gamma system.* Since both the tonic and phasic gamma input can activate the same spindle, it is concluded that several distinctly different gamma pathways can reflexly command the same pool of alpha motor neurons (Ref. 100).

*It is possible that some of the tonic gamma activity is also related to respiration and determines the mid-thoracic position around which the respiratory excursions are superimposed.

Approved for Public Release

Contrails

We have introduced this example in order to consider a situation of minimum complexity, namely, that of a neural regulatory system "tracking" a constant internally generated reference signal. Two loops in the controller are involved: (1) a conventional outer feedback loop carrying information concerning the state of the controlled variable (blood CO_2 level), and (2) a peripheral/spinal feedback loop which enables the system to remain relatively insensitive to changes in muscle dynamics (for example, in the presence of fatigue) or load changes (as in changes in airway resistance). Indeed, we have considered this example primarily in order to introduce some of the peripheral physiological mechanisms in skilled tracking behavior, regulated at a subcortical level. In terms of Fig. 40, this subcortical command system amounts only to that shown in Fig. 42.

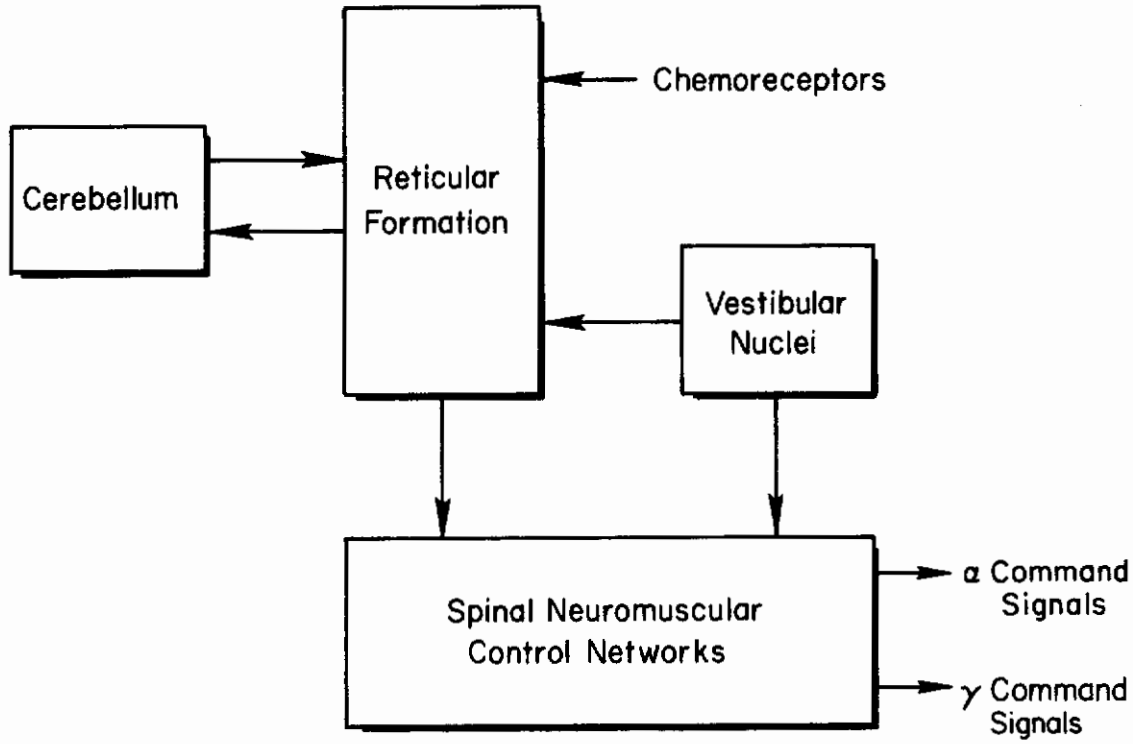

Figure 42. Command Subsystem of Fig. 40 Related to Respiratory Control

2. Exteroceptive Tracking System

We now wish to extend the complexity of the situation by considering how externally generated time-varying signals can be tracked; i.e., we wish to examine the servo properties of a neurophysiological exteroceptive tracking system.

Approved for Public Release

Contrails

An interesting example of such a system is afforded by the visual tracking mechanisms of the brain which enable an animal to center a visual target on the optical axis of the eye where visual acuity is greatest. A complete neural system adequate for such activity appears to exist in the brain stem and, indeed, there is evidence from recent experiments on monkeys that simple tracking behavior does not necessarily involve sensory and motor cortical areas, and that even manual tracking of a simple food-reward stimulus can be performed when only subcortical areas are available for the effort (Ref. 104). This correlates with the fact, pointed out previously (Fig. 40), that a number of subcortical centers have access to visual, auditory, and proprioceptive information, and that complex (if not all) motor patterns can be generated in the absence of a pyramidal tract, at least in primates.* A scheme for such behavior using subcortical centers can be postulated by appealing to a synthesis of prototype modes of behavior that have been demonstrated in a variety of animal experiments. In principle, such a system requires target position and velocity information to be processed into command signals available to the motor nuclei of the eight extraocular muscles of the eyes, whose concerted action enables the eyes to move to a position appropriate for target-centering.

Target information is fed into this system in several different ways. First, owing to the optical properties of the eye itself, there is a point-to-point mapping of the visual field onto the retina of each eye. The mapping follows the normal inversion seen in any lens system with points in the visual field to the right of the vertical meridian being projected onto the left side of each retina, etc. Thus the spatial ordering of the target field is preserved by the anatomical ordering of receptor cells on the surface of the retina. This spatial arrangement is preserved at higher levels of the nervous system, and in particular it is preserved by a point-to-point mapping onto the surface of structures in the mid-brain known as the superior colliculi (Ref. 105). These are paired structures overlying the brain stem, and on each colliculus is mapped one-half of the opposite visual field, with each retina overlapping in its projection. That is,

*Of course, nonpyramidal cortical motor paths to the spinal cord also exist.

Approved for Public Release

Contrails

the right-hand visual field projected on the left side of both retinas is mapped onto the entire surface of the left superior colliculus (Fig. 43).

Recent studies have shown that in addition to this position information, activity in optic nerve fibers coming from the retina carries information concerning target velocity and direction of travel (Refs. 106 and 107) and probably also information about target shape, boundary, and contrast with surroundings (Ref. 106).

From the available sensory information we assume that command signals appropriate to the tracking of a target are generated from the colliculus itself, for when a point on the surface of the colliculus, corresponding to a specific point in the visual field, is stimulated, a conjugate movement of both eyes occurs, whose magnitude and direction are such as to tend to center the target, i.e., move the target projection point on the surface toward the zero/zero horizontal and vertical meridian points (Refs. 108 and 109).

Thus, the colliculus converts the sensory projection mapping into a command signal vector which nulls the mapping of a point on the surface.

The command signals generated by the colliculus are transmitted by direct pathways to the clusters of motor cells (motor nuclei) in the brain stem whose axons control the muscles of the eye (see Figs. 44 and 45). It is at this level also that additional compensatory information from the vestibular system concerned with head position and angular velocity is integrated into the final motor command. In addition, pathways from the colliculus to the cerebellum and from the vestibular nuclei to the cerebellum enable the cerebellum to participate in the coordinated and smooth execution of target-centering actions. Furthermore, output pathways from the superior colliculus to the reticular formation and spinal cord can generate head and neck movements associated with the tracking of targets, and these we will presume to depend on spinal regulatory mechanisms already described.

Detailed studies of eye movement in tracking situations also show that, as in the case of the respiratory system motor output, the over-all response is not arbitrary, but appears to be synthesized from patterned or stereotyped subcomponents. In the visual/motor system, two principal modes are available, one a quick step change in muscle length (the saccadic movement)

Approved for Public Release

Contrails

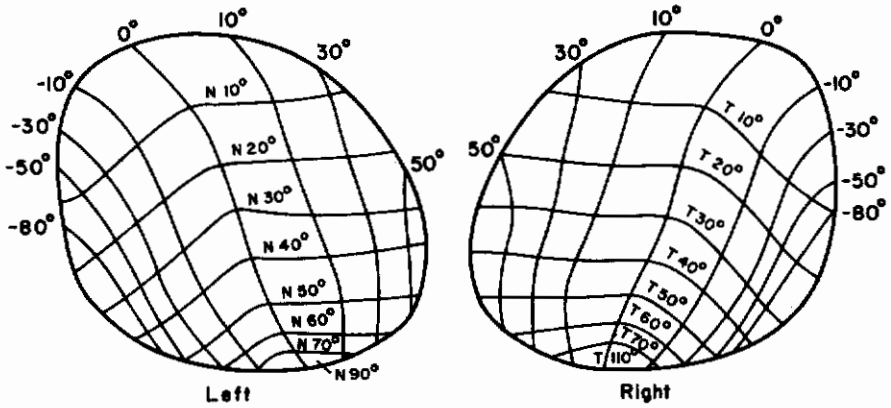

a) Projection of visual field onto surface of colliculus. T, N refer to nasal and temporal coordinates of powers relative to vertical meridian + and − refer to coordinates relative to horizontal meridian. (from 105)

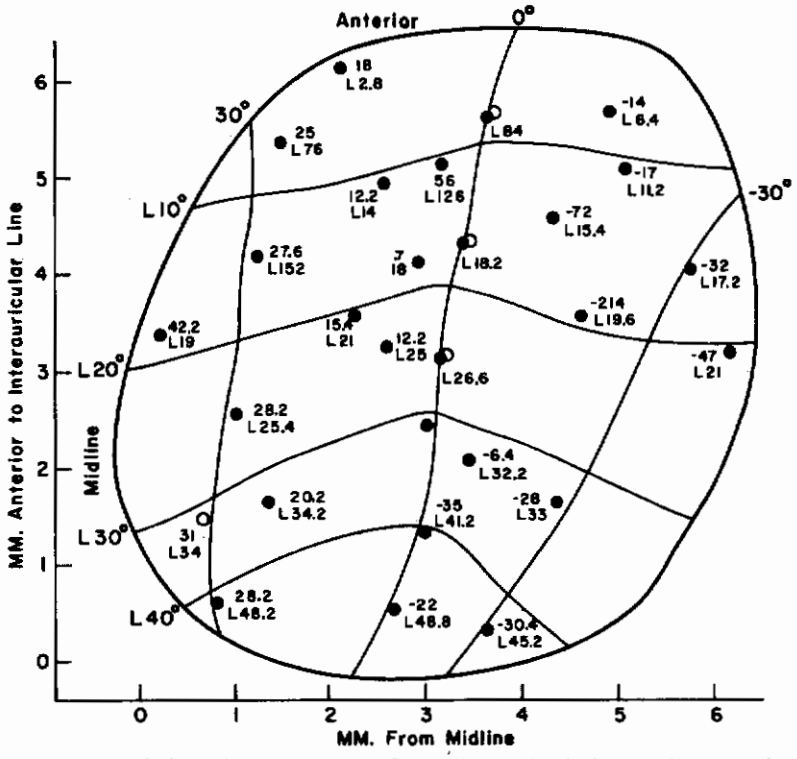

b) Points on R Superior colliculus surface whose stimulation produces motion shown. L = degrees deviation to the left; ± refers to motions above or below horizontal meridian. (from 108)

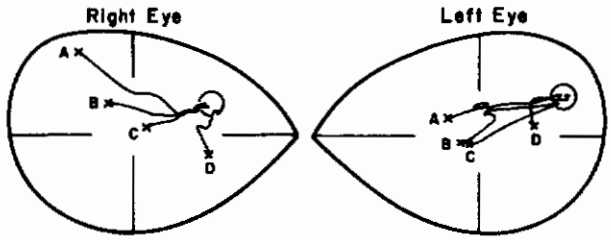

c) Motion of R and L eye in response to repeated stimulation of single point on colliculus. In each case eye starts from different direction of gaze. (from 109)

Figure 43. Sensory Mapping Patterns of the Superior Colliculus

Approved for Public Release

Contrails

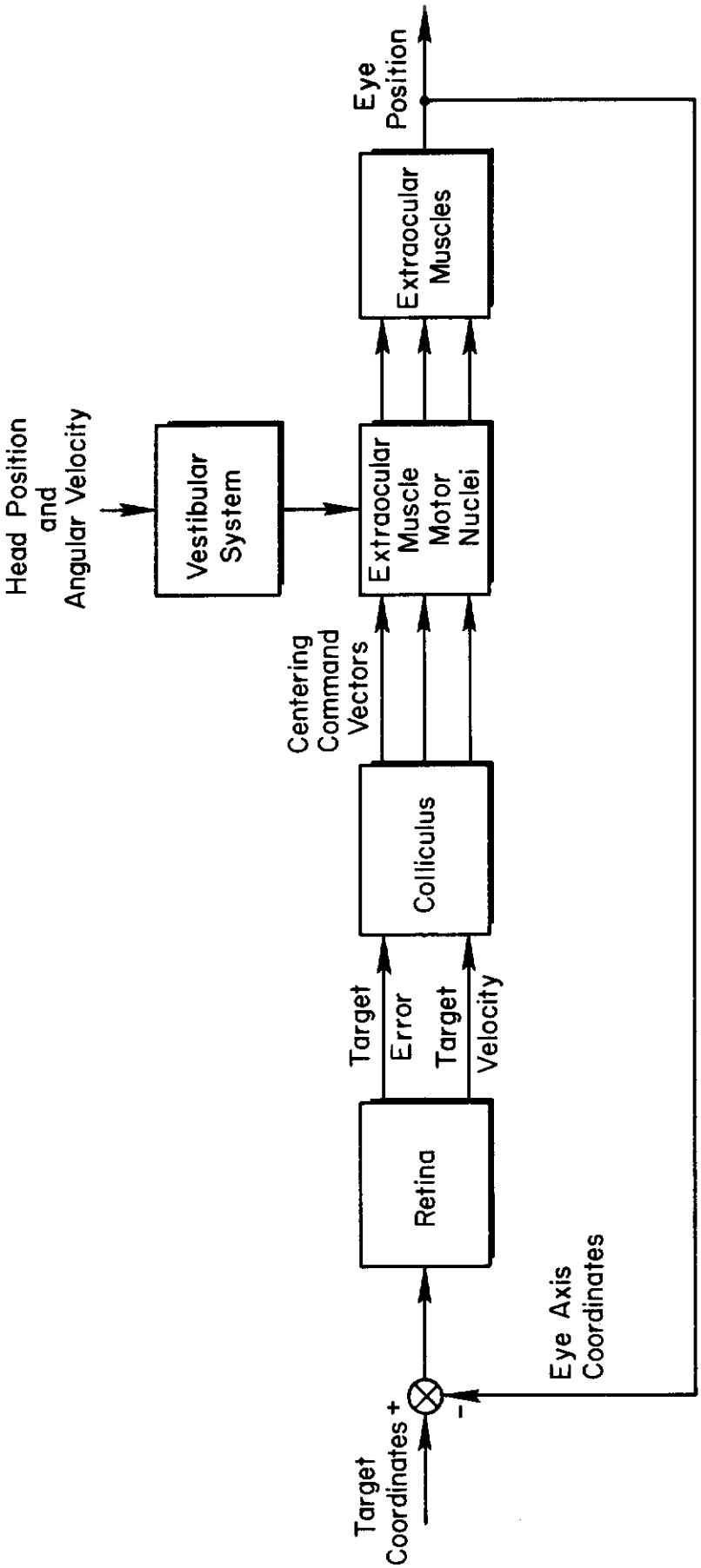

Figure 44. Block Diagram of Eye Tracking System

Approved for Public Release

Contrails

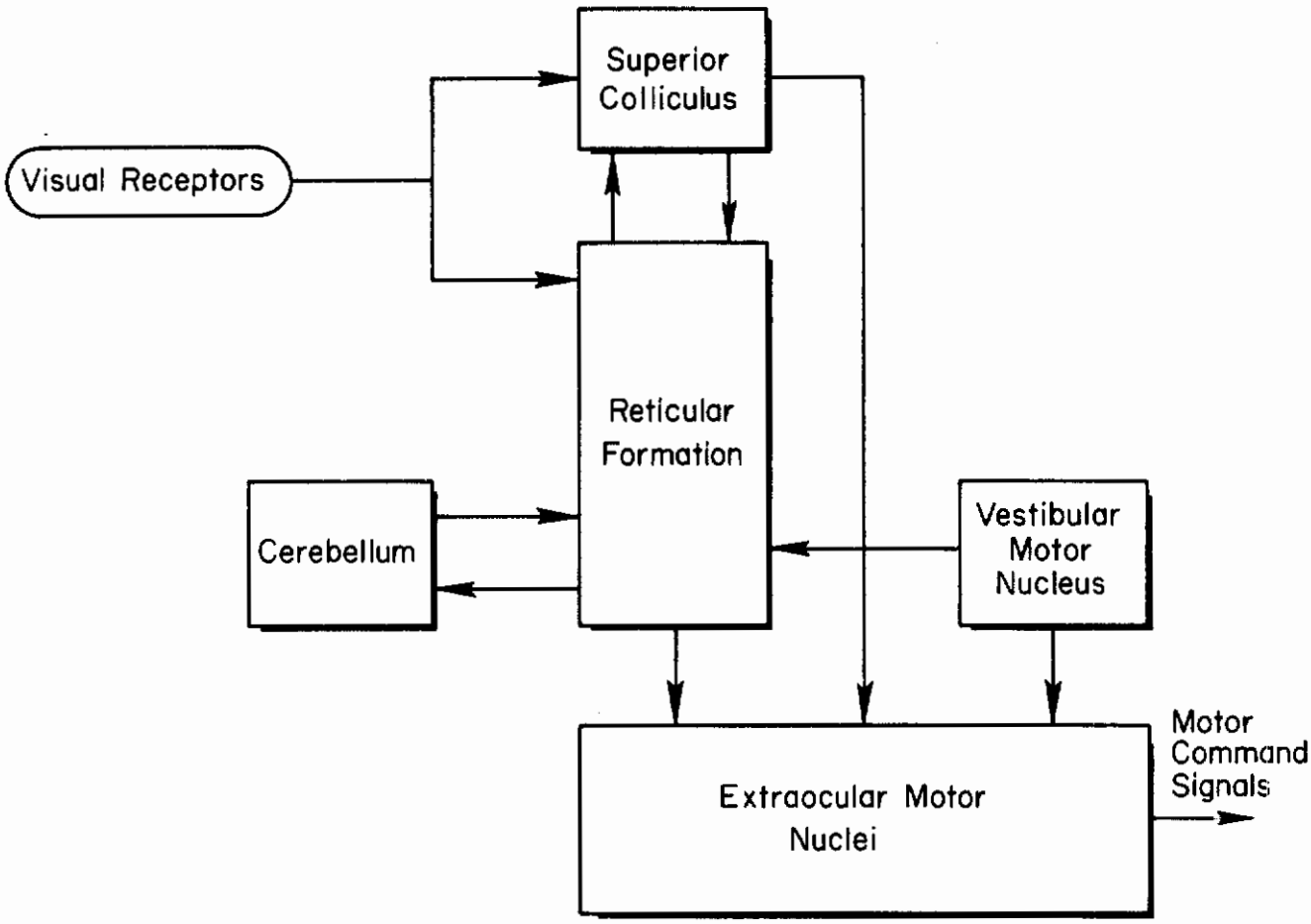

Figure 45. Subsystem of Fig. 40 Related to Eye Movement Control

Approved for Public Release

Contrails

which centers the target and the other a constant angular velocity rotation of the eye (pursuit movement) which permits following of the target once it is centered; in most situations complex eye motions are superpositions or successions of these basic modes.

A number of additional generalizations of importance emerge from the study of the two subcortical systems which have been described, and these are valid in their application to motor control systems generally.

- Motor systems are organized around reciprocally acting (and usually reciprocally inhibitory) antagonist components.
- Precision command-following in the presence of motor and load variations is provided by low delay feedback loops at the motor unit level. Thus a patterned motor command results in a nearly duplicate response with shorter delays and more precision than would be possible in an open-loop system.
- For this reason, patterned coordinated command signals generally involve coactivation of the alpha and gamma motor cells.
- Independent motor command signals can play simultaneously and in parallel in effector networks.

D. CORTICAL CONTROL FUNCTIONS

1. The Nature of Cortical Control

The systems discussed so far are apparently capable of operating autonomously at a subcortical level in the execution of certain control or tracking tasks. At the subcortical level they operate on a more or less continuous stream of sensory input and sensory feedback information. In their processing of this information, and in the synthesis of their output from subcortically available motor patterns, generated on a proportional or rate control basis with appropriate mechanisms for equalization of body position or load changes, they appear to operate essentially as quasi-linear pure gain controllers. This is probably typical of the capabilities of subcortical motor control systems, but in the presentation of these systems, in order to illustrate some intrinsic mechanisms within them, we have been forced to ignore the influence that higher centers can, and normally do, have on them.

Approved for Public Release

Contrails

In what follows, we would like to consider some of the "metacontroller" problems that are inherent to the function of higher or cortical areas of the brain.

Even in the case of visual tracking there are several logical or decisional functions involved, for example,

- Is the stimulus "interesting" or important? Are its parameters of movement and conformation matched to certain "filters" in the brain which monitor the available information?
- Should the stimulus, even if interesting, be tracked at all, given the constellation of other factors concerning the internal and external state of the body?
- If the decision is made to track, by what mode and with what precision should the action be undertaken?

We know, in answer to the first question, that several areas of the brain receiving polysensory input receive highly specific kinds of sensory information. Indeed, specific neurons in the reticular formation, superior colliculus, and cerebral cortex appear capable of responding only to highly specialized kinds of stimuli (Refs. 106, 110–112) which are of great natural importance to survival; for example, in the detection of prey or predators. Their ability to react selectively to certain kinds of stimuli ("property filtering") provides the physiological basis for the detection of, and the focusing of attention on, such stimuli in preference to unimportant or neutral events, and for the alerting of appropriate areas for response initiation.

It is also obvious that a process such as visual tracking, unlike respiratory or cardiovascular control, is not entirely obligatory or involuntary, but involves logical start and stop decisions. In humans this is apparently a cortical function, and with damage to certain cortical areas neurological patients are unable to track a stimulus unless commanded to do so or are unable to "let go" of the object, i.e., they cannot stop the tracking operation (Ref. 113).*

*Behavior analogous to this has also been observed in hand-grasping of objects by monkeys with pyramidal tract lesions (Ref. 81).

Approved for Public Release

Contrails

Finally, if the decision is made to track, what mode should be used? The colliculus is capable of generating signals which cause the eyes to turn appropriately, but there are alternate pathways available to it which can initiate head-turning or body-turning (Refs. 114, 115). In some cases the mode of output is even dependent on the detection and recognition process. For example, humans generally cannot voluntarily generate a smooth constant-velocity eye movement unless they are tracking a target moving with that velocity. Moreover, it may be necessary to transfer the tracking operation in whole or in part to other effector systems, and in the case of manual control, for example, the process of visual tracking is essentially deferred to muscles of the arm and hand which are not intrinsically related to eye movement at all. But this again requires a prior logical decision; hence it is important to bear in mind the vast difference between compensatory tracking of a visual stimulus with the oculomotor apparatus and compensatory tracking with some manually controlled device. We now know that this latter task can be performed by primates (Ref. 116), but there is no evidence that lower animals can do this.

Thus, while the mechanisms for accurate pure-gain types of tracking behavior exist at subcortical levels, they are subject to an increasingly complex hierarchy of logical decision-making structures and it is likely that the cerebral cortex is increasingly involved, in an evolutionary sense, in precisely those metacontroller functions.

Moreover, in contrast to the situations considered above in which tracking behavior occurs in response to time-varying or random sensory signals, there is a decisive need for the nervous system to be able to initiate motor commands from internal sources and to predict the future behavior of the external world so that appropriate motor action can be initiated in advance of, instead of in response to, certain stimuli. It seems likely that the cerebral cortex is indispensable for such precognitive or predictive control of movement in which, in effect, complex trackable stimuli are internally generated.

As a basis for such a process, we assume that the cortex, in conjunction with other brain centers, has considerable ability to learn or store

Approved for Public Release

Contrails

complex sensory patterns, to synthesize complex patterns out of simpler patterns, and finally to transfer stored sensory patterns to motor centers where they can be "tracked."

There is now good evidence, based on studies of the ability of the nervous system to transfer learned information from one half of the brain to the other, that some complex sensory and motor patterns are indeed stored at cortical levels. Transfer of visual pattern recognition activity, for example, is dependent on an intact visual receptive cortex. Manual skills, on the other hand, are very poorly learned from purely visual experience, and acquisition of skill seems rather to depend on somatic sensory input from the limbs and cannot be transferred from one hemisphere to the other without both somatic sensory and motor cortices (Ref. 104).

Thus, we see a functional requirement for the cortex in the execution of complex pattern generation. In view of this we may conceive of predictive tracking as involving neuromuscular following, not of the immediate sensory input, but rather of a cortically generated signal which is perhaps only intermittently compared with the direct sensory input.

While conceivably the ability of the cortex to generate signals may be unlimited, it is clearly capable of generating linear and sinusoidal signals. On the other hand, certainly in humans the nature of the cortex is revealed in terms of its ability to generate symbolic patterns, e.g., those associated with speech production. This might be considered a special case of neuromuscular tracking of an internally generated "auditory" signal. The number of basic motor pattern elements available for this task is not clear, but apparently it is finite and a function of the particular language. There is now some evidence that the continuous "predictive mode" output involved in speech involves sequential synthesis of blocks of output of syllable length, i.e., in blocks of output requiring about 200 ms of activity (Ref. 117). This is also approximately the period required, in certain eye movement studies, before additional visual information is processed (Ref. 24); and also correlates with the minimum period for attention-switching from one modality to another, and appears to be the minimum period required for a reaction time task and for alternation of repetitive motor activity. One model has been proposed in which these blocks are called up

Approved for Public Release

Contrails

and sequenced by the cortex, and then transferred to subcortical centers prior to execution while the next block is being assembled cortically (Ref. 117).

In short, what is being suggested here is that, while a considerable number of skilled or stereotyped movement patterns and even the capacity to track may be potentially available at a subcortical level, the more complex patterns may be generated in the cortex. The subcortical patterns may be triggered or suppressed by the cortex, in which case the function of the cortex might be the execution of complex data-processing operations and operations of a logical character. These would include, among others, the following kinds of functions which are presently recognized by neurophysiologists as involving higher neuronal centers:

- Pattern recognition involving space and time
- Attention,* input channel selection and switching, arousal
- Detection
- Output mode selection, including rapid modification of subcortical and spinal circuits
- Symbolic referencing
- Prediction
- Time estimation

These functions, in man, actually occupy the sphere of activity called "consciousness." They are not at all well developed in other animals.**

2. Timing Relations in Supraspinal Control

When the cortex is involved in the elaboration of a motor response, we have only scanty amounts of information about the way it participates. Most of this, in fact, only gives us some clues as to the timing sequence involved.

---

*There is some evidence that "attention-switching" may require intact loops to the cerebellum.

**For example, in the monkey there is no evidence of any predictive ability in eye movement control when tracking a periodically moving target (Ref. 118).

Approved for Public Release

Contrails

In a recently reported series of experiments, monkeys were conditioned by standard operant techniques to perform some simple manual responses such as lever-pushing for a food-reward when presented with a particular visual stimulus (Ref. 86). Single neurons in the motor cortex with axons in the pyramidal tract were observed before and during the presentation of the stimulus and the subsequent motor response. It was found that those units which showed a change in firing pattern prior to the hand movement showed it only in response to a visual stimulus when the hand movement followed, i.e., cells responded if and only if the stimulus succeeded in eliciting the conditioned response. Apparently the decision process occurs not later than this stage and very likely occurs earlier.

For these neurons there was a high correlation between the latency of the cell response and the latency of the motor response as measured by the EMG or total reaction time. The minimum latency of these cells to a light flash was 100 ms, corresponding to a total reaction time of 180 ms, which is quite short for a monkey (whose usual response time is between 275 ms and 400 ms). Thus an observed minimum response latency of a cortical cell, in response to a light flash, might be 120 ms; the EMG latency (of the contralateral hand) might be 170 ms, and the reaction time 220 ms.

Similar reaction time experiments have been performed with humans in which the latency (response delay) of the visual cortex to the visual stimulus was measured (by means of the characteristic wave which appears in the EEG recorded over the visual areas). Also measured was the total time from the stimulus onset to the beginning of the peripheral EMG response. Corresponding to the time of onset of activity in pyramidal tract cells of the motor cortex, there appears in the motor area EEG a recognizable wave which has been termed the "motor potential" (Refs. 119, 120). This appears only when a voluntary motor response is actually made. It appears 50–150 ms prior to first sign of motor activity in the limbs, and reaches a peak during maximum muscle activity. From the evidence presented, we can construct a rough timing diagram of the sequence of events following a conditional stimulus and leading to a motor response (see Fig. 46).*

*There is considerable evidence also that the total reaction time may vary by 5–10 ms, depending on the phase of the alpha rhythm of the EEG at which the stimulus is presented (Ref. 121).

Approved for Public Release

Approved for Public Release

*Note: The movement latency which is the time derived to take up the slack in muscle and tendon depends on the initial tension and slacking angle of the limbs (Ref.122)

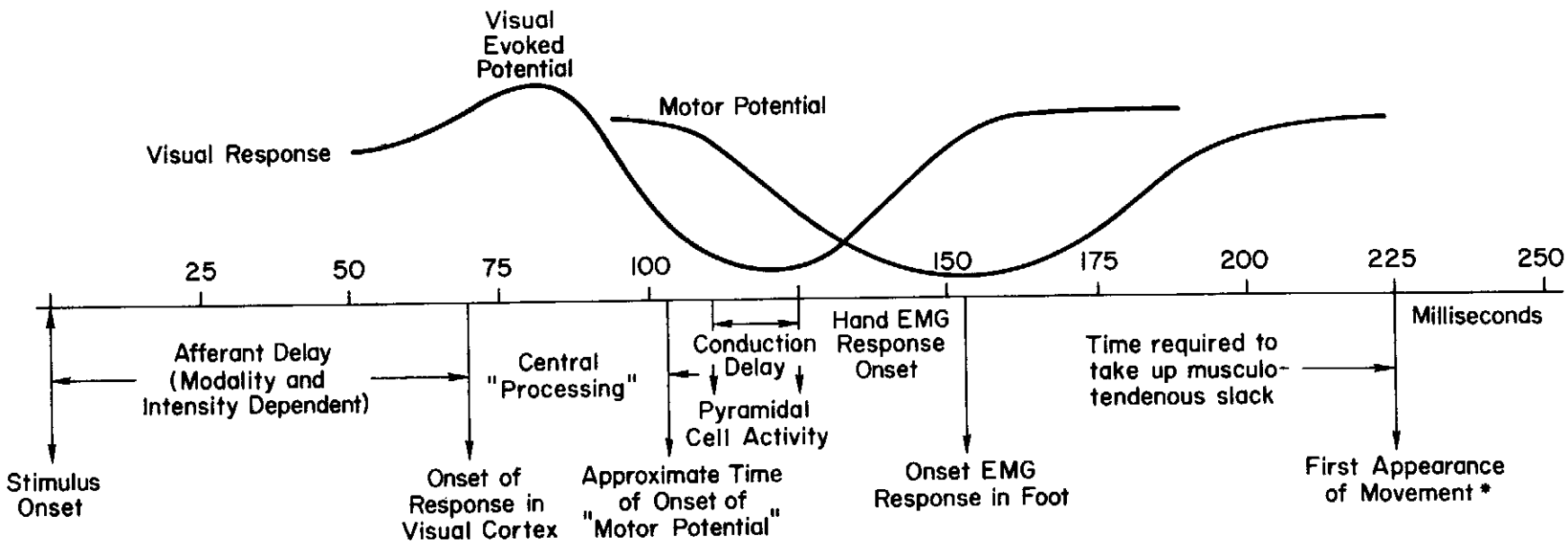

Figure 46. Timing Diagram of Events Related to Cortical Decision and Motor Response Task

Contrails

In this section we have summarized experimental results from several areas of neurophysiology which may be helpful in suggesting prototypes of brain organization that underly adaptive behavior in the human. While the examples chosen may indicate the limited and tentative character of even the most sophisticated conclusions available from the physiological laboratory, they have been offered in the conviction that as models they are indispensable to the further thinking and experimentation of the engineer who wishes to understand and interpret overall behavior in terms of the unitary elements of the neurcmuscular system and the brain. In this respect, the necessity of the engineer to study the models of the physiologist mirrors the growing awareness on the part of the physiologist that systems engineering concepts and models and studies of adaptive motor performance in humans can provide key insights into the often intractable complexities of brain structures and components. The present chapter clearly reflects the mutual influence of these two disciplines and, we believe, offers a real basis for the optimistic view that the world of macroscopic observation of human performance and the microscopic world of the neurophysiologist can be unified. The connecting link is the constraint that appropriate ensembles of microscopic elements must yield behavior that can explain macroscopic performance.

Approved for Public Release

Contrails

SECTION VIII

A SIMPLE TEST FOR OPTIMALITY

A. INTRODUCTION

This section and Section IX describe methods for determining the quantities which may be minimized by the human operator in tracking tasks, i.e., his criteria for optimality. Only quadratic criteria are considered. As explained in Ref. 123, optimality with respect to such criteria implies optimality with respect to many other criteria for systems forced by stationary random-appearing Gaussian inputs. The present section describes a simple test for optimality which requires only information about the mean-squared values of input signal, controller response, system response, and system error, where "error" is defined as the difference between the actual system response and a "desired" response. The desired response is identical to the input signal in the tracking tasks considered here. The test yields a quadratic criterion for which the describing function is optimal; but it does not give the describing function of the optimum system in literal or numerical terms.

Section IX uses a more complicated procedure to identify not only the criterion, but also the optimal describing function. The criterion is further generalized to include cross-product terms.

These sections represent two different (but by no means mutually exclusive) ways of solving essentially the same problem. Future progress in the quest for human operator optimization criteria may well involve a combination of both approaches. It is therefore important that projected measurement programs take into account the data requirements for the application of each technique.

B. THE TEST FOR OPTIMALITY

This subsection describes a simple test for optimality, applicable to systems forced by stationary random inputs, e.g., the human operator in some tracking tasks. The test has the advantage that it does not require calculation of the describing function of the system.

Approved for Public Release

Contrails

If the system satisfies the criterion

$$\text{Minimum } \left(\widetilde{\widetilde{\epsilon^2}} + k\widetilde{\widetilde{c^2}}\right)$$

where k is a constant, ϵ is the difference between the desired response, m_d, and the actual system response, m, and c is the controller output as in Fig. 47, with the wavy bars denoting averaged values, then the following relationship is satisfied:

$$\widetilde{\widetilde{\epsilon^2}} = \widetilde{\widetilde{m_d^2}} - \widetilde{\widetilde{m^2}} - 2k\widetilde{\widetilde{c^2}} \qquad (46)$$

A proof is given in the appendix. For k = 0 (the Wiener system), proofs have been given by Lee (Ref. 124) and others.

1. Application of the Test

We shall illustrate the application of Eq. 46 to human pilot behavior in both pursuit and compensatory tracking tasks with a stationary random forcing function. In tracking tasks the desired response, m_d, is equal to the input signal i, hence in Fig. 47, $F_1 = 1$.* Because Eq. 46 does not require any information regarding the system structure other than the transfer function of the controlled element, it is not necessary to specify the feedbacks used by the pilot. Thus in Fig. 47, $H\bar{J}$ represents

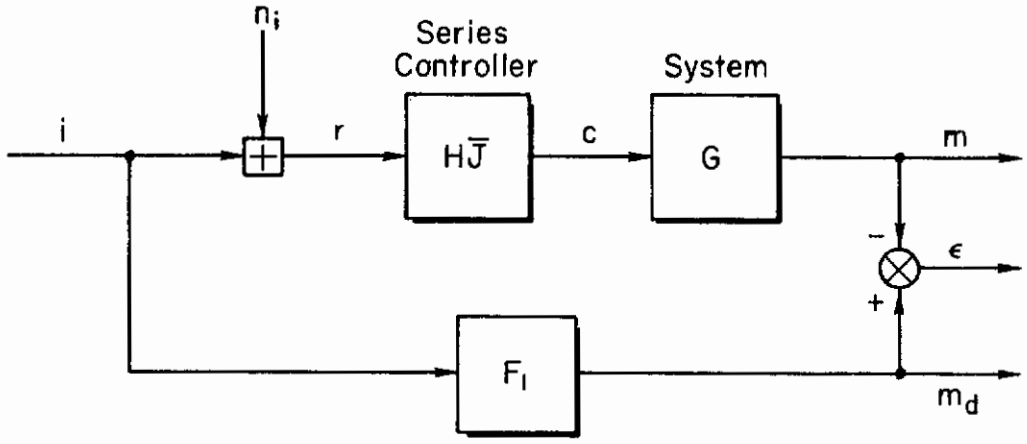

Figure 47. General Formulation of System

*The notation of Fig. 47 is explained in the appendix.

Approved for Public Release

Contrails

the transfer function of an equivalent series controller which produces the same Φ_{ic} cross spectrum as the human pilot, given the same input signal, i, and uncorrelated noise, n_i, the latter representing the remnant. Figure 47 therefore can represent either pursuit or compensatory tracking.

In Fig. 47 the remnant, n_i, has been referred to the input. This is purely for convenience; Eq. 46 is not affected by the choice of injection point for the remnant.

The derivation of Eq. 46 assumes that both i and n_i are stationary. This condition may be only approximately satisfied in actual tracking tests. The proportion of the remnant that is stationary depends on the controlled element. For pure gain controlled elements (as in the tests described below) Ref. 18 concludes that the remnant is mainly composed of stationary noise.

The data graphed in Fig. 48 are taken from tests (Ref. 18) on a human operator tracking a series of inputs generated by randomly phased sine waves to approximate a stationary random Gaussian signal with an augmented rectangular spectrum. One set of inputs was identical to those of Ref. 12 with ten component frequencies. The amplitudes of the lowest six, seven, or eight frequencies were set equal, for cutoff frequencies designated as ω_i = 1.5, 2.5, and 4.0 rad/sec, respectively, in Fig. 48. The amplitudes of the frequencies greater than ω_i were set to one-tenth of that of the low frequencies. The input designated R14 comprised ten equal-amplitude sine waves with frequencies ranging from 0.314 to 14.03 rad/sec. The B5 input was similar, except that the four highest frequencies (starting at 4.29 rad/sec) were attenuated 10 db. The rms value of each input was 1 in. deflection on the CRT display. For the tracking task these inputs were equal to the "desired response," m_d.

The data given in Ref. 18 include mean-squared values of ϵ in display inches and c in degrees of stick deflection, but not m. However, for the case when the controlled element was a pure gain it is easy to obtain m, using $m = K_c c$, where K_c = 1 in. display per 6° stick.

Approved for Public Release

Contrails

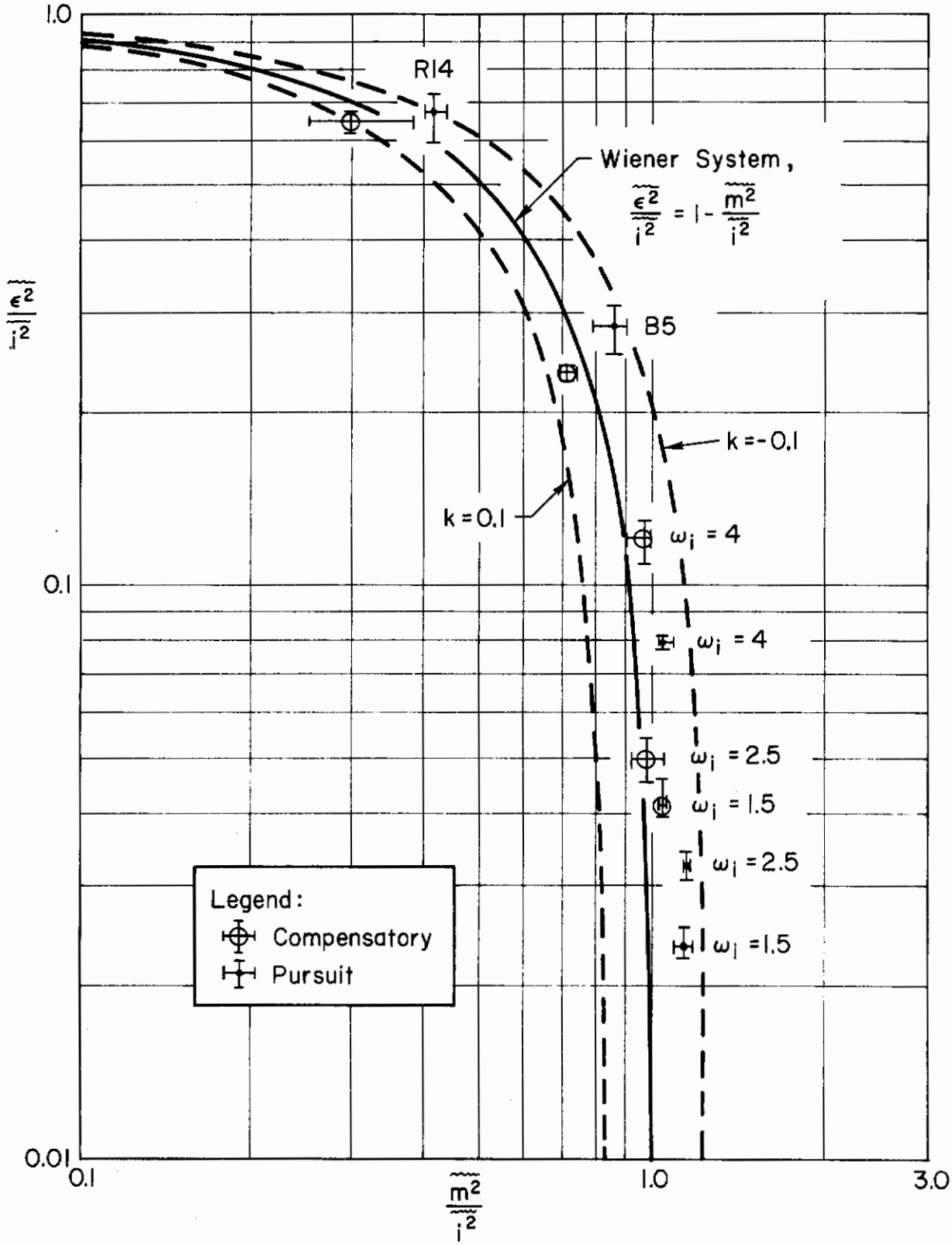

Figure 48. Normalized Mean-Squared Error Versus Normalized Mean-Squared Response ($Y_c = K_c =$ [illegible])

Approved for Public Release

Contrails

Figure 48 illustrates $\widetilde{\epsilon^2}/\widetilde{i^2}$ graphed against $\widetilde{m^2}/\widetilde{i^2}$. It is seen that the measured performance is close to optimum in the Wiener sense, i.e., k = 0. (The term "close" is defined more precisely below.)

The most significant and interesting region of Fig. 48 from the standpoint of criteria is the "knee" of the graph where $\widetilde{\epsilon^2}/\widetilde{i^2}$ is relatively large, e.g., greater than 0.10. As we shall show shortly, in this region the Wiener system is quite critically defined (as opposed to the region where $\widetilde{\epsilon^2}/\widetilde{i^2}$ is small, where almost any reasonable system can closely approach the Wiener performance). Figure 48 also illustrates Eq. 46 graphed for k = 0.1 and −0.1. To achieve the most compact presentation, k has been made dimensionless by normalizing c such that for the pure gain controlled element considered here, $Y_c = K_c = 1$. That is, the units of c have been referred to the displacement of m observed at the display. To make this clear, consider the criterion

$$\text{Minimum } \left(\widetilde{\epsilon^2} + \widetilde{kc^2}\right)$$

k = 1 implies that equal weight is attached to mean-squared values of ϵ of 1 in.^2 (1 in. difference between i and m on the display) and to mean-squared values of c equal to the square of the steady-state value of c that would produce a steady deflection of 1 in. at the m display.

The foregoing discussion will be extended later when we consider controlled elements having dimensions which involve time, e.g., K/s and K/s^2. With k normalized as indicated above, $Y_c = 1$ for the data of Fig. 48, c = m, and hence k can be found (see Table XIV) from Eq. 47 modified for c = m as follows:

$$\frac{\widetilde{\epsilon^2}}{\widetilde{i^2}} = 1 - (1 + 2k)\,\frac{\widetilde{m^2}}{\widetilde{i^2}} \qquad (47)$$

Because of the limited accuracy of the data measurement and reduction, the calculation of k to an accuracy closer than about ±0.04 is not meaningful. Within this restriction, it appears that for compensatory displays the human operator is essentially optimal in the Wiener sense for the pure gain controlled element $K_c = 1$. The pursuit data show a small but definite tendency for negative k.

Approved for Public Release

Contrails

TABLE XIV

COMPUTATION OF k FOR PURE GAIN CONTROLLED ELEMENT, $Y_c = 1$
(Data graphed in Fig. 48)

INDIVIDUAL RUNS					
Input	Display	$\widetilde{\epsilon^2}/\widetilde{i^2}$	$1-\widetilde{\epsilon^2}/\widetilde{i^2}$	$\widetilde{m^2}/\widetilde{i^2}$	k
R14	c	0.65	0.35	0.293	+0.097
R14	p	0.675	0.325	0.415	−0.11
B5	c	0.24	0.76	0.71	+0.035
B5	p	0.285	0.715	0.86	−0.085
$\omega_i = 4.0$	c	0.08	0.92	1.04	−0.0575
$\omega_i = 4.0$	p	0.122	0.878	0.97	−0.0475
$\omega_i = 2.5$	c	0.05	0.95	0.97	−0.01
$\omega_i = 2.5$	p	0.0322	0.9668	1.14	−0.075
$\omega_i = 1.5$	c	0.0415	0.9585	1.02	−0.03
$\omega = 1.5$	p	0.0235	0.9765	1.14	−0.07

AVERAGED RESULTS			
Display	Mean k	RMS Deviation	Mean Absolute Deviation
Pursuit	−0.0775	0.021	0.016
Compensatory	+0.0069	0.054	0.0471

2. The Use and Interpretation of the Test Results

The formula for the optimum transfer function is derived assuming that the signal and remnant are unaffected by small variations from the optimum transfer function. This assumption is supported by the experimental data of Refs. 18 and 125 which show that for pure gain controlled elements the remnant referred to the pilot's input varies very little with signal bandwidth and amplitude. (The test equation, Eq. 46, holds provided the remnant is constant, irrespective of whether it is referred to i, c, or m.)

The results can therefore be used to estimate the human pilot describing function by calculating the minimum $(\widetilde{\epsilon^2} + k\widetilde{c^2})$ system, the transfer function of which is given at the beginning of the Appendix (Eq. A-1). The data required are:

Approved for Public Release

Contrails

- An expression for the nonminimum phase part of the human operator describing function, associated with his time delay, τ, assumed to be invariant with the remainder of his describing function, and usually represented by a Padé approximation.
- The spectrum of the tracking signal expressed as (or approximated by) an algebraic function of $(j\omega)$ which is factorable in the Wiener-Hopf sense.
- The spectrum of the remnant, similarly expressed. (To use Eq. A-1 directly the remnant should be referred to the signal, i, but Eq. A-1 can be reformulated if it is more convenient to refer the remnant to c or m.)

The interpretation of the value of k requires care. For $k = 0$ the part of the pilot's output linearly correlated with i certainly minimizes $\tilde{\tilde{\epsilon^2}}$. But we cannot conclude that the pilot as a whole is minimizing $\tilde{\tilde{\epsilon^2}}$ because a smaller value of $\tilde{\tilde{\epsilon^2}}$ would certainly be attained if he retained the same describing function but eliminated his remnant. Only if we regard Φ_{nn_i} as fixed (an assumption which, as noted above, is realistic for the $Y_c = K_c$ data of Refs. 12 and 18, where $\Phi_{nn_i} = \Phi_{nn_e}$ because of the compensatory display) can we claim that the pilot as a whole is minimizing $\tilde{\tilde{\epsilon^2}}$. Note that the instructions given to the pilot state that he is to "move the stick to keep the error small." Since for Gaussian inputs this is equivalent to demanding minimum $\tilde{\tilde{\epsilon^2}}$ (see p. 27 of Ref. 123), we should expect experimental results to indicate a value of k close to zero. Reference 126 describes experiments in which a pilot was instructed to minimize $\tilde{\tilde{\epsilon^2}} + k\tilde{\tilde{c^2}}$. His behavior varied with the value of k. Unfortunately, $\tilde{\tilde{m^2}}$ data are not obtainable for the tests of Ref. 126, and Eq. 46 therefore cannot be applied to check the actual value of k against that used in the instructions.

For $k > 0$ the argument of the preceding paragraph can be repeated, replacing $\tilde{\tilde{\epsilon^2}}$ by $\tilde{\tilde{\epsilon^2}} + k\tilde{\tilde{c^2}}$. Similar considerations apply for $k < 0$, but it must be noted that large negative values of k are inadmissible because of stability limitations on the optimum system transfer function. These restrict $|k|$ for $k < 0$ to the value that would cause the optimum system transfer function (Eq. A-1) to be unstable.

Approved for Public Release

Contrails

3. Sensitivity of the Test

The sensitivity of the test formula has been investigated by applying it to two series of systems, one optimal in the Wiener Sense ($k = 0$) and the other deliberately constructed to be nonoptimal for $k = 0$.

The input signal spectrum assumed is $\Phi_{ii} = 1/(1 + \omega^2)$, the noise (remnant) spectrum is $\Phi_{nn_i} = \alpha^2/(1 + \omega^2/100)$, and the desired response, m_d, is equal to the signal. Both signal and noise enter at the same point, as in Fig. 47. The parameter α is the ratio of the dc levels of noise to signal. The nonoptimal systems were produced by modifying the Wiener system transfer function, which is calculated in Ref. 127 as

$$H(j\omega) = \frac{\frac{11}{10}}{1 + \alpha^2 + \sqrt{\left(1+\alpha^2\right)\left(\alpha^2 + \frac{1}{100}\right)}} \times \frac{1 + \frac{j\omega}{10}}{\left(1 + j\omega\sqrt{\frac{\alpha^2 + (1/100)}{\alpha^2 + 1}}\right)} \qquad (48)$$

The nonoptimal systems have the same gain, but no equalization, i.e., the transfer function is

$$H(j\omega)_{\text{nonopt}} = \frac{\frac{11}{10}}{1 + \alpha^2 + \sqrt{\left(1+\alpha^2\right)\left(\alpha^2 + \frac{1}{100}\right)}} \qquad (49)$$

Figure 49 compares the Wiener and nonoptimal systems. For the test to be of practical value, the graph of $\tilde{\tilde{\epsilon}}^2/\tilde{\tilde{i}}^2$ versus $\tilde{\tilde{m}}^2/\tilde{\tilde{i}}^2$ of the nonoptimal system should depart appreciably from the graph of the test formula. As shown in Figure 49, for $\tilde{\tilde{\epsilon}}^2/\tilde{\tilde{i}}^2 > 0.1$ the graphs become quite dissimilar, and there is a wide spread in the location of points on each graph corresponding to a given noise/signal ratio. Of course only one range of nonoptimal systems has been tested here, and there is no limit to the number that could be examined. However, Fig. 49 does provide at least a preliminary indication that the test formula is of adequate sensitivity in the interesting region where even for the optimum system $\tilde{\tilde{\epsilon}}^2/\tilde{\tilde{i}}^2 > 1$.

Approved for Public Release

Contrails

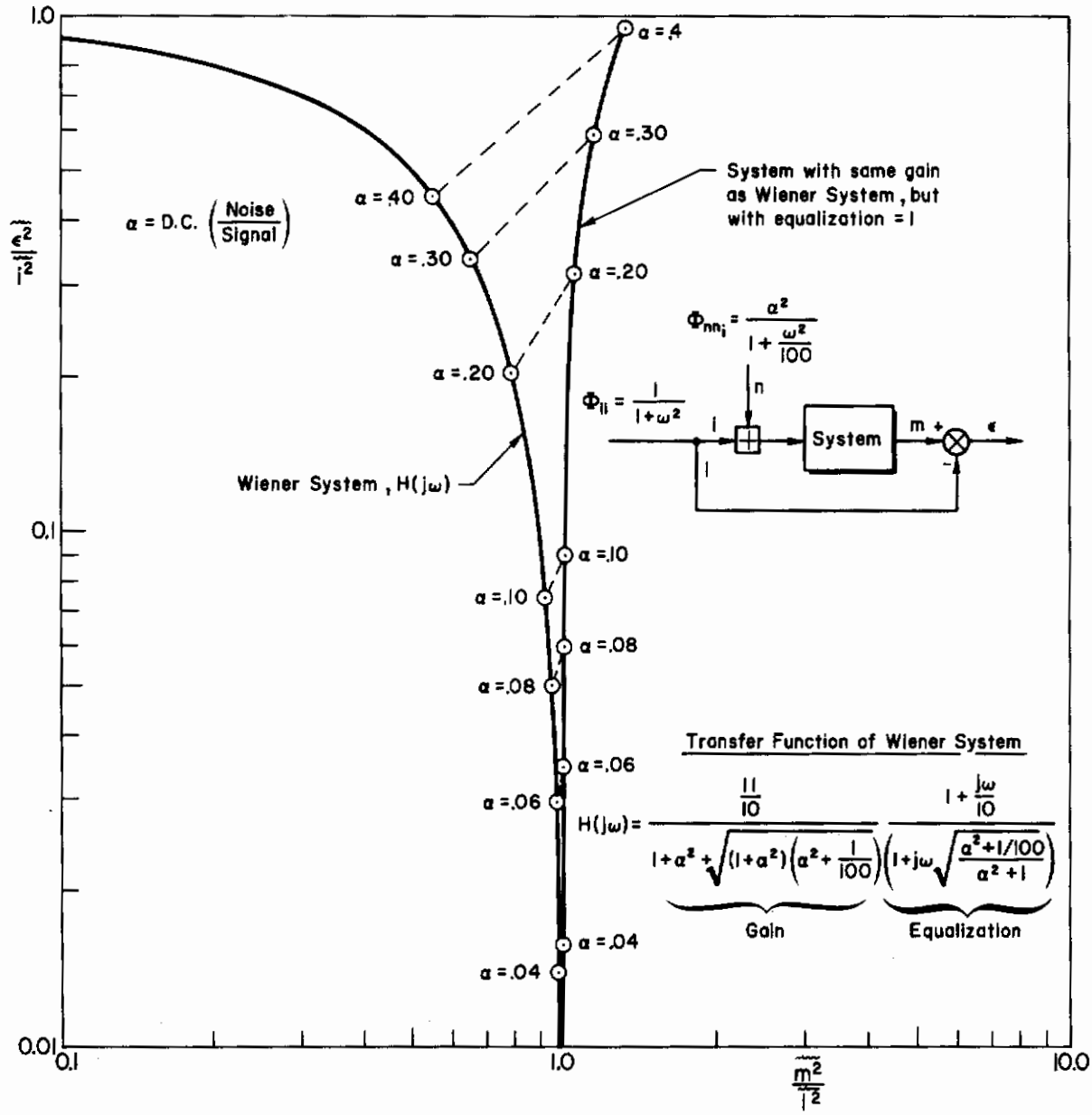

Figure 49. Example of Sensitivity of Optimality Test $\tilde{\epsilon}^2 = \tilde{i}^2 - \tilde{m}^2$

Approved for Public Release

Contrails

C. APPLICATION OF THE TEST TO K_c/s AND K_c/s^2 CONTROLLED ELEMENTS

In this subsection we describe the application of Eq. 46 to tracking tasks using controlled elements of the following forms:

$$Y_c = K_c/s$$
$$Y_c = K_c/s^2$$

These data were taken from Ref. 18. The operator was the same as that for the $Y_c = K_c$ data, a pilot with lightplane experience only. As with the previously examined tests on $Y_c = K_c$, values of $\tilde{\tilde{m}}^2$ were not recorded. Because of the more complicated nature of the controlled elements, there is no way to deduce $\tilde{\tilde{m}}^2$ knowing only $\tilde{\tilde{c}}^2$, $\tilde{\tilde{\epsilon}}^2$, and $\tilde{\tilde{i}}^2$. It was therefore necessary to rerun the tapes of i, ϵ, c, and m which were taken during the tests of Ref. 18. Some discrepancies were noted between the rerun and original data, and the results on K_c/s and K_c/s^2 controlled elements must therefore be regarded as provisional.

1. Results

The reduced data are listed in Table XV. Appropriate experimentally obtained values of $\tilde{\tilde{\epsilon}}^2/\tilde{\tilde{i}}^2$ are graphed versus $\tilde{\tilde{m}}^2/\tilde{\tilde{i}}^2$ in Fig. 50. Note that due to difficulties with the tape readout equipment, $\tilde{\tilde{c}}^2$ was not available on all runs. Consequently, k could not be calculated via Eq. 46 for all runs.

2. Interpretation of Results

Figure 50 shows that the data points do <u>not</u>, in general, satisfy the relationship $\tilde{\tilde{\epsilon}}^2 = \tilde{\tilde{i}}^2 - \tilde{\tilde{m}}^2$. Thus the system is not tending towards the Wiener optimum. The values of k required to fit the more general equation $\tilde{\tilde{\epsilon}}^2 = \tilde{\tilde{i}}^2 - \tilde{\tilde{m}}^2 - 2k\tilde{\tilde{c}}^2$ have been calculated where possible, and are listed in the right column of Table XV. For $Y_c = 5/s^2$, the k's for compensatory tracking were −0.107, and −0.102, −0.108, and −0.0932 (mean k = −0.1027); for pursuit, −0.0748 and −0.0685 (mean k = −0.717). The overall mean is k = −0.0907.

Figure 51 is a "carpet" illustrating the deviation of the experimental results from the formula $\tilde{\tilde{\epsilon}}^2 = \tilde{\tilde{i}}^2 - \tilde{\tilde{m}}^2 - 2k\tilde{\tilde{c}}^2$ with k = −0.09 sec^4 for $Y_c = 5/s^2$.

Approved for Public Release

Contrails

TABLE XV

$\widetilde{i^2}$, $\widetilde{\epsilon^2}$, $\widetilde{m^2}$, AND $\widetilde{c^2}$ DATA

SYMBOL	RUN NO.	Y_c	DISPLAY	$\widetilde{i^2}$	$\widetilde{\epsilon^2}$	$\widetilde{m^2}$	$\widetilde{c^2}$	$\widetilde{\epsilon^2}/\widetilde{i^2}$	$\widetilde{m^2}/\widetilde{i^2}$	$\widetilde{c^2}/\widetilde{i^2}$	k
1	042864-1	$\frac{5}{s^2}$	c	0.258	0.059	0.346	0.745	0.229	1.34	2.89	$-0.0932\ sec^4$
2	042864-2	$\frac{5}{s^2}$	c	0.264	0.0425	0.345	0.57	0.161	1.31	2.16	$-0.108\ sec^4$
3	042764-15	$\frac{7}{s}$	c	0.259	0.0745	0.288	N.A.	0.288	1.11	N.A.	N.A.
4	042764-16	$\frac{7}{s}$	p	0.253	0.0592	0.240	N.A.	0.235	0.95	N.A.	N.A.
5	042764-17	$\frac{7}{s}$	p	0.2465	0.0586	0.210	N.A.	0.239	0.85	N.A.	N.A.
6	042764-18	$\frac{7}{s}$	p	0.2415	0.0638	0.232	N.A.	0.265	0.96	N.A.	N.A.
7	043063-5	$\frac{1}{s}$	c	0.2415	0.049	0.314	0.46	0.202	1.3	1.91	$-0.131\ sec^2$
8	042964-2	$\frac{5}{s^2}$	c	0.25	0.206	0.51	2.2	0.824	2.04	8.7	$-0.107\ sec^4$
9	042964-3	$\frac{5}{s^2}$	c	0.25	0.194	0.49	2.12	0.775	1.96	8.49	$-0.102\ sec^4$
10	042964-4	$\frac{5}{s^2}$	p	0.25	0.154	0.364	1.79	0.615	1.46	7.16	$-0.0748\ sec^4$
11	042964-5	$\frac{5}{s^2}$	p	0.25	0.132	0.28	1.18	0.528	1.12	4.71	$-0.0685\ sec^4$

The dimensions of i, ϵ, and m are inches of deflection on the scope. The scale of c is adjusted to be the same as the scale of m for $Y_c = 1$. Note that the dimensions of k equal the dimensions of $|Y_c|^2$.

Approved for Public Release

Contrails

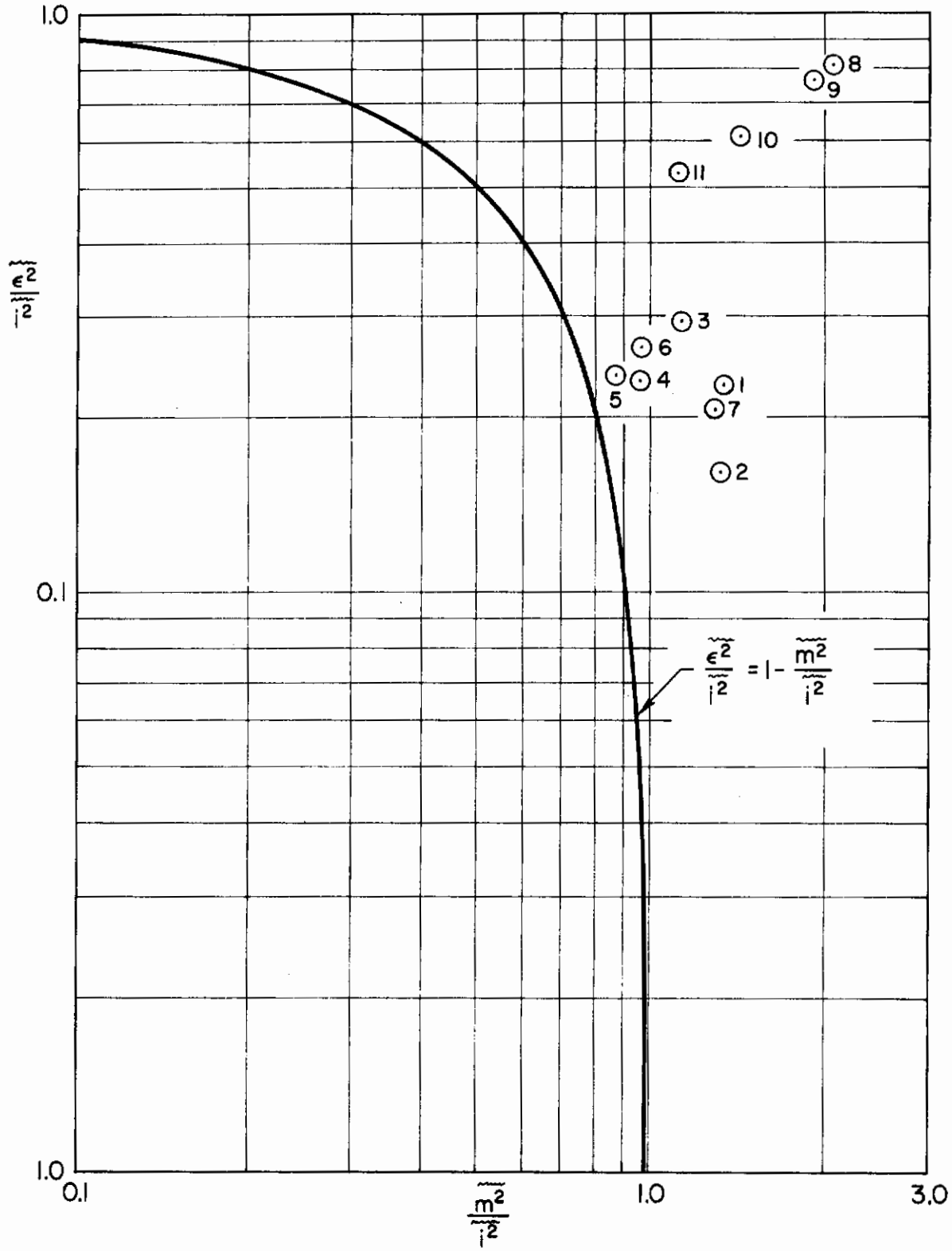

Figure 50. Normalized Mean-Squared Error Versus Normalized Mean-Squared Output

Approved for Public Release

Contrails

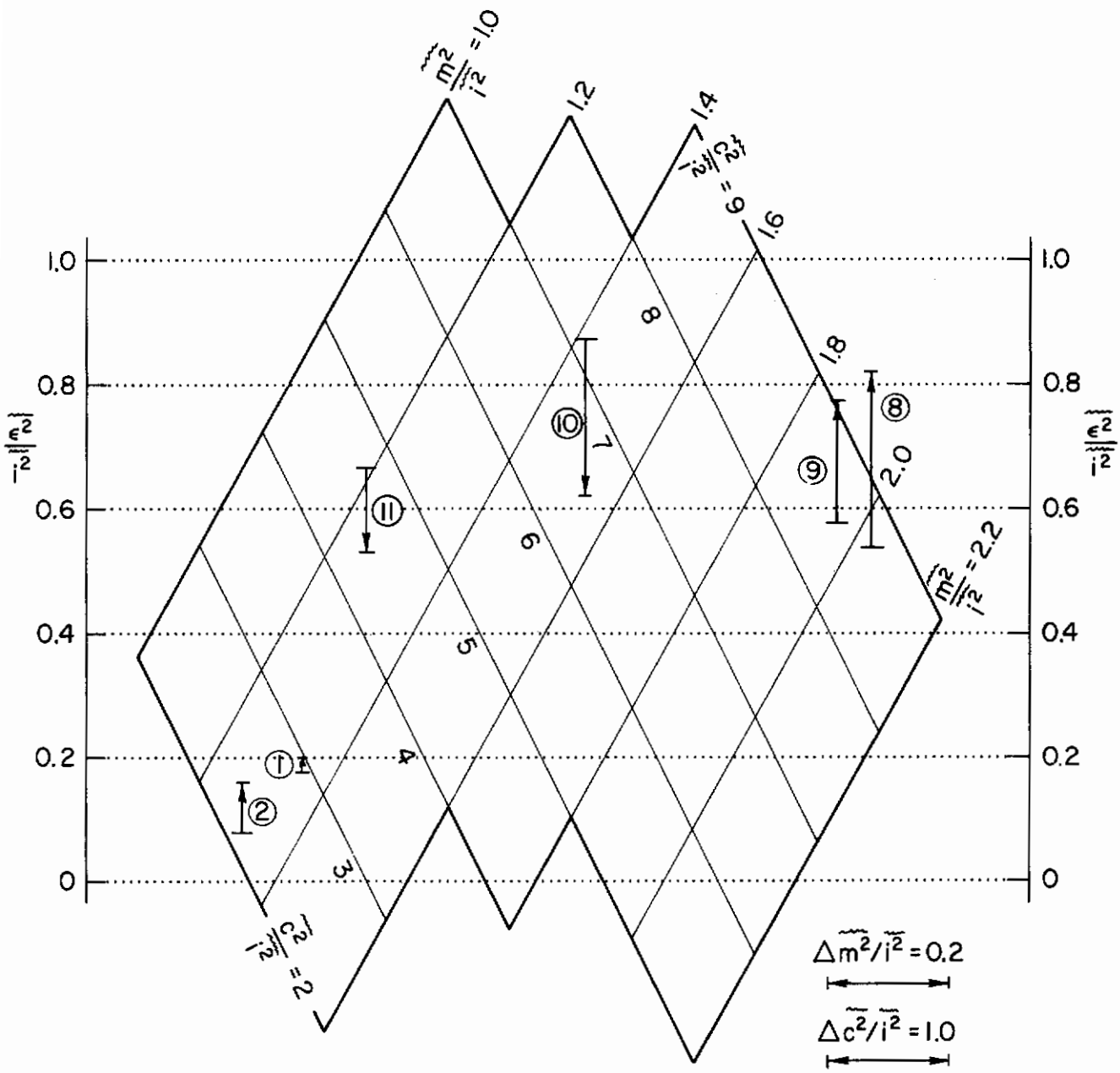

Figure 51. Carpet of $\widetilde{\epsilon^2}/\widetilde{i^2} = 1 - (\widetilde{m^2}/\widetilde{i^2}) - 2k(\widetilde{c^2}/\widetilde{i^2})$ for $k = -0.09$ sec^4 $Y_c = 5/s^2$ Throughout

Approved for Public Release

Contrails

(This k represents a rounded-off value of the above mean k; with these data, accuracy of more than one significant figure in the determination of k should not be expected.) The "carpet" may be regarded as a projection of the three-dimensional graph of $\tilde{\tilde{\epsilon}}^2/\tilde{\tilde{i}}^2 = 1 - (\tilde{\tilde{m}}^2/\tilde{\tilde{i}}^2) + 0.18(\tilde{\tilde{c}}^2/\tilde{\tilde{i}}^2)$ with the $\tilde{\tilde{m}}^2/\tilde{\tilde{i}}^2$ and $\tilde{\tilde{c}}^2/\tilde{\tilde{i}}^2$ axes projected to match the horizontal scales shown, and the $\tilde{\tilde{\epsilon}}^2/\tilde{\tilde{i}}^2$ vertical scale. The advantage of this form of presentation is that it permits linear interpolation between the lines of constant $\tilde{\tilde{m}}^2/\tilde{\tilde{i}}^2$ and constant $\tilde{\tilde{c}}^2/\tilde{\tilde{i}}^2$. For the $\tilde{\tilde{m}}^2/\tilde{\tilde{i}}^2$ and $\tilde{\tilde{c}}^2/\tilde{\tilde{i}}^2$ scales to be applicable, such interpolation must be made horizontally.

The length of each arrow on Fig. 51 indicates the divergence of the appropriate experimental data point from the formula

$$\tilde{\tilde{\epsilon}}^2/\tilde{\tilde{i}}^2 = 1 - (\tilde{\tilde{m}}^2/\tilde{\tilde{i}}^2) + 0.18(\tilde{\tilde{c}}^2/\tilde{\tilde{i}}^2)$$

for the controlled element $Y_c = 5/s^2$. It is logical to inquire how the previously obtained data for $Y_c = 1$ would fit this formula. For this simple controlled element, c = m and the fit could be demonstrated by drawing an additional line in Fig. 48 corresponding to k = −0.09. However, to obtain a more direct comparison with the K_c/s^2 data, Fig. 52 has been prepared. This is an extension of Fig. 51 showing the points graphed on Fig. 48 that correspond to the higher bandwidth inputs R14, B5, and $\omega_1 = 4$. Note that the deviation from the formula is of the same order as the deviation in $\tilde{\tilde{\epsilon}}^2/\tilde{\tilde{i}}^2$ due to uncertainties in the measurement of this quantity, and $\tilde{\tilde{m}}^2/\tilde{\tilde{i}}^2$. For example, in Fig. 48, for the R14 compensatory case, $\tilde{\tilde{m}}^2/\tilde{\tilde{i}}^2$ lies between 0.25 and 0.38. Thus, in Fig. 52, $\tilde{\tilde{m}}^2/\tilde{\tilde{i}}^2$ and hence $\tilde{\tilde{c}}^2/\tilde{\tilde{i}}^2$ lies within an "ellipse of uncertainty" on the $\tilde{\tilde{m}}^2/\tilde{\tilde{i}}^2$, $\tilde{\tilde{c}}^2/\tilde{\tilde{i}}^2$ plane, as shown. From Fig. 48, $\tilde{\tilde{\epsilon}}^2/\tilde{\tilde{i}}^2$ for this point is between 0.62 and 0.67. The area between these two levels is shaded in Fig. 52. Note that this area almost intersects the ellipse of uncertainty. This indicates that the deviation of the experimental data point from the formula only slightly exceeds the deviation that would be expected due to the uncertainties in data measurement.

As with the $Y_c = K_c$ data, it is necessary to assume that the spectrum of the remnant referred to the input is constant for the test to be a valid

Approved for Public Release

Contrails

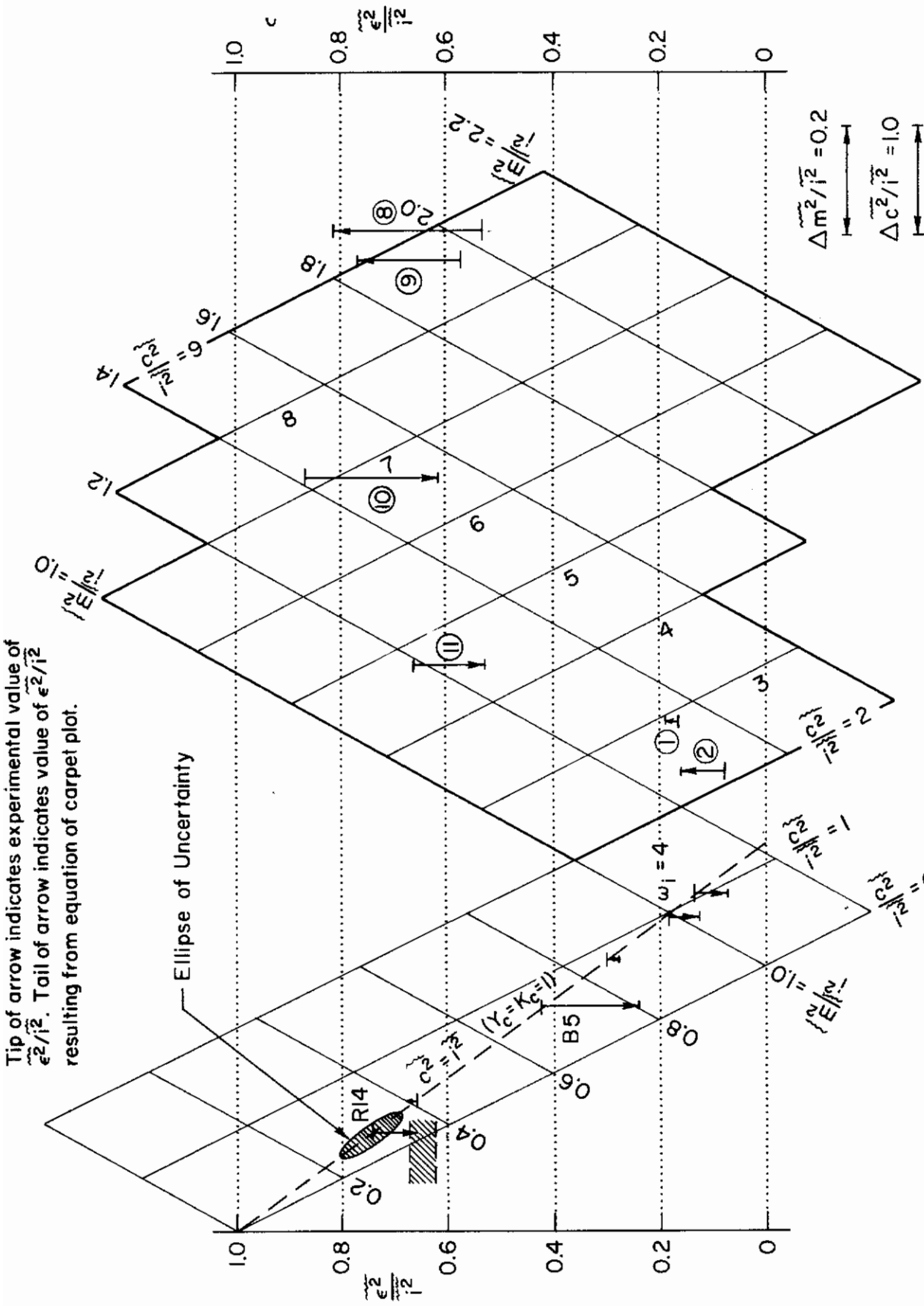

Figure 52. Carpet of $\tilde{\epsilon}^2/\tilde{i}^2 = 1 - (\tilde{m}^2/\tilde{i}^2) - 2k(\tilde{c}^2/\tilde{i}^2)$ for $k = -0.09$ sec^4

Approved for Public Release

Contrails

indication that the pilot is minimizing $\widetilde{\widetilde{\epsilon^2}} + k\widetilde{\widetilde{c^2}}$. The experimental remnant data of Fig. 61 of Ref. 12 indicate that the variation of Φ_{nn_e} with ω_i is slight. Quoting Ref. 12, "...the spread present is probably as indicative of run-to-run variability as it is of any Φ_{nn_e} dependence on forcing function bandwidth." Figure 64 of Ref. 12 shows a similarly small variation of Φ_{nn_e} with large changes in controlled elements. Reference 12 concludes, "...the major effect of (controlled element) variation on the remnant is as much intersubject as inter-controlled-element." Thus it is concluded that with controlled elements of the form K_c/s^2 the human operator acts in such a fashion that $\widetilde{\widetilde{\epsilon^2}} + k\widetilde{\widetilde{c^2}}$ is minimized, where k is about -0.09 sec^4.

D. APPLICATION OF THE TEST TO LONGITUDINAL SHORT-PERIOD CONTROL

Reference 128 describes fixed-base simulator compensatory tracking tests in which the pilot was required to track a commanded random-appearing pitch angle. This was the sole input and was intended to represent target motion. The input was generated by sums of randomly phased sine waves such that the spectrum was essentially flat, extending from $\omega = 0.157$ to $\omega = 1$ rad/sec, with a high frequency shelf from $\omega = 1$ to $\omega = 11$ rad/sec. The run length was 4 min. The transfer function of the controlled element was

$$\left(\frac{\theta}{\delta}\right)_{sp} = \frac{M_\delta(s + 0.585)}{s\left[s^2 + 2(0.397)(0.764)s + (0.764)^2\right]}$$

The data required for the test formula,

$$\frac{\widetilde{\widetilde{\epsilon^2}}}{\widetilde{\widetilde{i^2}}} = 1 - \frac{\widetilde{\widetilde{m^2}}}{\widetilde{\widetilde{i^2}}} - 2k\,\frac{\widetilde{\widetilde{c^2}}}{\widetilde{\widetilde{i^2}}}$$

are tabulated in Table XVI.

Approved for Public Release

Contrails

TABLE XVI

VALUES OF k FOR LONGITUDINAL SHORT-PERIOD CONTROL

PILOT	RUN NO.	$\widetilde{i^2}$	$\widetilde{\epsilon^2}$	$\widetilde{m^2}$	$\widetilde{c^2}$	k
		$\widetilde{(\theta_c)^2}$ deg^2	$\widetilde{(\theta_c-\theta)^2}$ deg^2	$\widetilde{\theta^2}$ deg^2	$\widetilde{(\delta M_\delta)^2}$ (deg/sec)^2	(sec^4)
A	670127-15	4.64	0.80	6.00	39.1	−0.0279
	670127-16	4.61	0.96	6.14	25.2	−0.0495
	670127-17	4.81	0.98	6.40	38.7	−0.0332
B	670202-16	4.15	0.714	5.29	18.7	−0.0495
	670202-17	4.19	0.789	5.31	18.0	−0.0530
	670202-18	4.27	0.717	5.56	21.3	−0.0469

Both operators were highly experienced commercial pilots. It is noteworthy that Pilot B obtained the lower $\widetilde{\epsilon^2}$, despite the fact that his $|k|$ was farther removed from zero. This implies that his remnant power referred to his output, $\widetilde{m_n^2}$, must be lower. This is confirmed by examination of the Φ_{nn_e} spectra which show very little variation from run to run, but indicate a difference between the pilots' Φ_{nn_e}, which is about 6 db lower for Pilot B at frequencies above about 25 rad/sec. The Φ_{nn_e} spectra for both pilots were closely similar at lower frequencies.

E. SUMMARY OF RESULTS FOR ALL CONTROLLED ELEMENTS

The mean values for the constant in the performance criterion are summarized in Table XVII.

Approved for Public Release

Contrails

TABLE XVII

MEAN EXPERIMENTAL VALUES OF k

CONTROLLED ELEMENT Y_c	PURSUIT			COMPENSATORY		
	Mean	Average Deviation		Mean	Average Deviation	
		rms	Absolute		rms	Absolute
1	−0.0775	0.021	0.016	+0.0069	0.054	0.0471
$5/s^2$	−0.0717 sec^4	0.0032	0.0031	−0.1027 sec^4	0.00586	0.00496
$1/s$	−0.131 sec^2	One run only		——	——	——
Pilot A $(\theta/\delta)_{sp}$				−0.0369 sec^4	0.00917	0.00843
Pilot B $(\theta/\delta)_{sp}$				−0.0498 sec^4	0.00238	0.00203

F. CONCLUSIONS

Systems forced by stationary random inputs may be tested for optimality with respect to the criterion of minimum $(\widetilde{\epsilon^2} + k\widetilde{c^2})$ by applying the following formula (Eq. 46):

$$\widetilde{\epsilon^2} = \widetilde{m_d^2} - \widetilde{m^2} - 2k\widetilde{c^2}$$

where m_d = the desired system response

m = the actual system response

c = the controller output

$\epsilon = m - m_d$

The derivation of Eq. 46 assumes that the system is forced by a signal and noise, both of which (1) have no first-order dependence on the input, and

Approved for Public Release

Contrails

(2) are stationary and random. The application of Eq. 46 to tracking tests involving human operators requires these conditions to be satisfied to the accuracy compatible with the inevitable run-to-run variations. In this regard the critical input component is the remnant, because the forcing function is controlled to be random-appearing and stationary (within the limits imposed by finite run length). For pure gain controlled elements the principal component of the remnant, Φ_{nn_e}, is stationary noise, which shows only slight variation with controlled element gain. For other controlled elements, nonstationary transfer effects appear to be more significant, and the remnant is strongly dependent on the controlled element. Reviewing the available data in the light of the above considerations, it is concluded that Eq. 46 should be used with caution unless the remnant is small or the mean-squared error due to nonstationary effects is small compared to that due to the stationary remnant component and the fixed delays of the human operator.

For most controlled elements small negative values of k were obtained (Table XVII). The k values deduced from the K_c/s and K_c/s^2 controlled elements are provisional because of discrepancies noted in the experimental data, resulting in some uncertainty about the values of $\tilde{\tilde{m^2}}$.

The consistent trend toward negative k, and the invariance of the remnant spectrum, Φ_{nn_e}, implies that the pilot could achieve a smaller mean-squared tracking error, $\tilde{\tilde{\epsilon^2}}$, if he was less eager to move the stick. It may therefore be worthwhile conducting further investigations to see if this can be achieved by a change in instructions and/or display. The numerical values of k measured in units of seconds vary remarkably little with changes in controlled element. However, because of the dimensionality of k, it must not be interpreted as a "universal constant" valid for all controlled elements.

Approved for Public Release

Contrails

SECTION IX

THE INVERSE OPTIMAL CONTROL APPROACH

Currently the quasi-linear human pilot describing function is adapted to a given controlled element by using verbal adjustment rules. These require a certain engineering artistry to apply effectively. Interest in the inverse optimal control problem stems from a desire to alleviate this difficulty by obtaining a more concise mathematical statement of these rules. Identification of a performance index which represents the essential criterion for pilot adaptation would provide such a statement of rules. The derived performance index would be most useful if it had some invariant properties for a broad spectrum of controlled elements, but even if this were not the case the indices would be an interesting alternate means for considering human operation.

A. COMMENTS ON THE INVERSE OPTIMAL CONTROL PROBLEM

Briefly, the inverse optimal control problem is that of finding the conditions (or performance index) under which a given system is optimal. Kalman considered this problem at length in Ref. 129. In development of the solution, Kalman uses constraints such that any system synthesized using the performance index found from the inverse problem will produce a stable system. Stability is assured via Lyapunov's Second Method, so the constraints are sufficient rather than necessary; in fact, the restrictions are usually overly conservative. In that case, the class of allowable optimal systems is restricted to those for which no element of the cost is allowed to assume negative values. This restriction affects the ability to find the performance index for many stable systems which are otherwise optimal. In particular, negative values of some terms in the performance index can exist for some stable linear constant-coefficient regulator systems yielding good performance. Furthermore, these systems have a minimum performance measure and can thus be considered to be optimal as long as the cost is a real number.

Obermayer and Muckler (Ref. 130) have considered applying the theory of the inverse optimal control problem to identify that performance index

Approved for Public Release

Contrails

which a pilot "must" be satisfying in a given continuous compensatory control task. They were dissatisfied with their results largely because negative values of the cost were a distinct possibility in a large number of instances. Reference 129 shows that second-order optimal control systems with positive costs of the form $\overline{x^2} + \lambda\overline{u^2}$ (where x is a state variable and u the control variable) tend to have damping ratios, ζ, greater than $1/\sqrt{2}$. Smaller damping ratios can result from performance indices like $\overline{x^2} + \alpha\overline{\dot{x}^2} + \lambda\overline{u^2}$, where $\alpha < 0$, thereby contributing a negative cost increment. Now, the human pilot in a compensatory tracking system behaves such that the dominant closed-loop poles of the closed-loop describing function for the system have damping ratios on the order of 0.2. Thus, those factors which discouraged Obermayer and Muckler really seem to indicate that the overrestrictive Lyapunov sufficiency condition should be replaced by a necessary and sufficient condition on the performance index for stability of the optimal system. The question of stability as implied by the performance index will not be a prime concern here, since the stability of optimal linear constant-coefficient systems is clearly evident upon solution of the direct problem. Negative cost components will be allowed in the following analysis without immediate regard for stability.

Obermayer and Muckler also assumed that off-diagonal terms in the performance index matrix are zero. This assumption was apparently made so that numerical solutions for the remaining coefficients of the performance index could be obtained for each controlled element. This approach can be made more general if the off-diagonal terms in the performance index are not arbitrarily set to zero. Then a single performance index can be found that is invariant for several different controlled elements. If the "different controlled elements" are chosen to span the spectrum of controlled elements controllable by the pilot, then it seems plausible that this criterion would apply for intermediate controlled elements in the spectrum also.

The foregoing possibilities are explored in greater detail in the following discussion. Considered in turn are the use of time domain techniques, the use of frequency domain techniques for "discovering" the human pilot's performance index, and a current estimate of results that may be obtained through these techniques.

Approved for Public Release

Contrails

B. TIME DOMAIN TECHNIQUES

Time domain techniques appear to be useful in the current context mainly for the purpose of demonstrating that the approach which retains off-diagonal terms in the performance index matrix is feasible. Actual solution via this technique appears impractical except when numerical evaluations of performance index coefficients are desired. Algebraic expressions for performance index coefficients are much preferred because of the additional insights which can be gleaned. Thus, the time domain is ultimately abandoned for the frequency domain.

1. Development

The time domain approach to the inverse optimal problem is developed by Kalman in Ref. 129. The essential relationships are summarized below for the general problem.

Plant (nth order): $$\dot{\underline{x}} = A\underline{x} + \underline{b}u \tag{50}$$

Performance index: $$2J = \int_0^\infty (\underline{x}'Q\underline{x} + 2\underline{r}'\underline{x}u + u^2)\,dt \tag{51}$$

Optimal control law: $$u_o = -\underline{k}'\underline{x} \tag{52}$$

u = the scalar control variable
$\underline{x}$ = the state vector of plant ($n \times 1$)
$\underline{r}$ = a vector of performance index coefficients ($n \times 1$)
$\underline{k}$ = the optimal vector of feedback gains ($n \times 1$)
$\underline{b}$ = an $n \times 1$ vector
A = an $n \times n$ matrix
Q = an $n \times n$ symmetric matrix of performance index coefficients
$( )'$ = transpose of matrix

The inverse optimal control problem is:

Given Eqs. 50 and 52, find Q and $\underline{r}$ for which J is minimum

Solution: Q and $\underline{r}$ satisfy the equations

$$\underline{r} + P\underline{b} = \underline{k} \tag{53}$$

$$Q + PA + A'P = \underline{k}\,\underline{k}' \tag{54}$$

P = an unknown $n \times n$ symmetric matrix called the "payoff matrix"

Approved for Public Release

Contrails

2. Example for First-Order Plants (n = 1)

To illustrate the general approach, presume that we have data for two first-order systems, each of which is considered to be an optimal system derived by minimizing the performance index, 2J. In this case we know the plants, A_1 and A_2 (b may be set equal to unity without loss of significant generality), and the controller gains, k_1 and k_2. (Because the systems are first-order, all quantities are scalars.) The problem is to find the performance index coefficients Q and r for which the two systems are optimal.

In this scalar case P may be easily eliminated from Eqs. 53 and 54, giving

$$Q = k_1^2 - 2A_1(k_1 - r) = k_2^2 - 2A_2(k_2 - r) \tag{55}$$

Solving for r,

$$r = \frac{k_2^2 - k_1^2 + 2(A_1 k_1 - A_2 k_2)}{2(A_1 - A_2)} \tag{56}$$

Using this result in Eq. 55 gives

$$Q = \frac{(A_1 k_2^2 - A_2 k_1^2) + 2A_1 A_2 (k_1 - k_2)}{A_1 - A_2} \tag{57}$$

Values for Q and r given by Eqs. 56 and 57 define the performance index of the form Eq. 51, which is a minimum for the <u>two</u> first-order systems characterized A_1, k_1 and A_2, k_2. This demonstrates that the approach works in principle.

The characteristics of first-order optimal control systems which minimize the criterion function

$$2J = \int_0^\infty (Qx^2 + 2rxu + u^2)\, dt \tag{58}$$

are summarized below and in Fig. 53:

Optimal control law:

$$u_o = -kx \quad \text{where} \quad k = A - \sqrt{(A-r)^2 + (Q - r^2)} \tag{59}$$

Equivalent open-loop transfer function:

$$G(s) = k/(s - A) \tag{60}$$

Closed-loop inverse time constant:

$$\alpha = \sqrt{(A-r)^2 + (Q - r^2)} = A - k \tag{61}$$

Approved for Public Release

Contrails

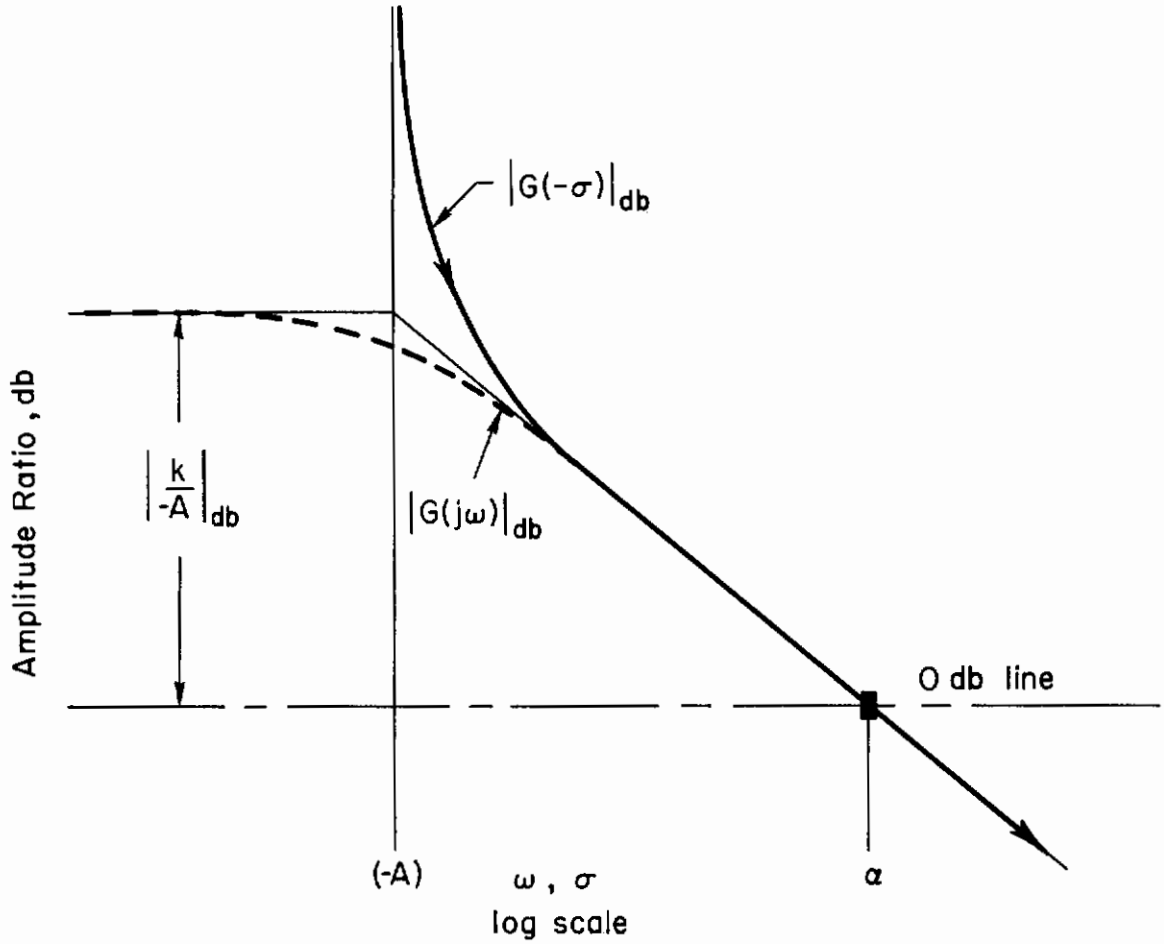

Figure 53. σ- and jω-Bode Diagram for First-Order Optimal Control System

Let us now apply these results to idealizations of the elementary manual control systems, $Y_c = K_c/s$ and $Y_c = K_c$. The approximate human operator describing function forms appropriate to these controlled elements are $Y_p = K_p e^{-\tau_e s}$ and $K_p e^{-\tau_e s}/(T_I s + 1)$, respectively. If, now, the pure time delay terms are neglected, and the low frequency first-order lag for the $Y_c = K_c$ case is presumed to be fixed and is transferred to the controlled element, then the systems so idealized fit our first-order optimal control format.

Consider first $Y_c = K_c/s$, which corresponds to A = 0. The optimal controller gain, k, which includes the controlled element gain, K_c, is

$$k = K_p K_c = -\sqrt{Q} = -\alpha \qquad (62)$$

The basic experimental data from which Q is to be derived will be

Approved for Public Release

Contrails

values k_1 and k_2 taken from experiments with two different values of K_c. By virtue of the ω_c invariance property of ω_c-K_c independence (see p. 11), $k_1 \doteq k_2 \doteq \omega_c$. Consequently $Q = \omega_c^2$, $r = 0$, and the performance measure underlying systems of this type is

$$2J = \int_0^\infty (\omega_c^2 x^2 + u^2)dt \tag{63}$$

For the second example, $A_1 = (-1/T_I)_1$ and $A_2 = (-1/T_I)_2$. The experimental data for the ω_c-K_c independence property still apply, so the crossover frequency is invariant with K_c changes. As a second category of experimental data, we appeal to those data from which the equalization selection and adjustment property, (c), on p. 8 is derived, i.e., "$|Y_p Y_c| \gg 1$ at low frequencies to provide good low frequency closed-loop response to system forcing functions." On this basis the low frequency breakpoints, $1/T_{I_1}$ and $1/T_{I_2}$, are much less than the crossover frequency, so that

$$k_1 = \frac{K_{p_1} K_{c_1}}{(1/T_{I_1})} \doteq \omega_c \tag{64}$$

and

$$k_2 = \frac{K_{p_2} K_{c_2}}{(1/T_{I_2})} \doteq \omega_c \tag{65}$$

Using these relationships in Eqs. 56 and 57, the performance indices are seen to be

$$Q \doteq \omega_c^2 \quad , \quad r \doteq \omega_c \tag{66}$$

and the performance measure is

$$2J = \int_0^\infty (\omega_c^2 x^2 + 2\omega_c xu + u^2)dt \tag{67}$$

Although these examples are trivially simple, they illustrate the use of inverse optimal control theory for the evolution of performance indices which can then be used to establish estimates for other systems without recourse to the adjustment rules. The two examples also make clear that the performance criterion to yield an optimal controller which matches human operator data is different for each type of plant. For practical purposes this may not be too awkward, as it seems likely that performance criteria can be developed for classes of plants which lead to reasonably

Approved for Public Release

Contrails

good, albeit approximate, estimates for the human controller. For example one criterion function could be used for those plants which approximate $Y_c = K_c$ in the frequency region about crossover, another criterion for plants which are nearly $Y_c = K_c/s$ in the same region, etc.

3. Problems in Application

One problem in extending the ideas outlined above is that of dealing with the large number of algebraic equations implicit in Eqs. 53 and 54.

A system of $n + \frac{n(n+1)}{2}$ scalar linear algebraic equations results for each plant/controller combination (i.e., A, $\underline{b}$, and $\underline{k}$ combination) considered. We seek values of Q and $\underline{r}$ which will be invariant for these different plant/controller combinations. Thus, $\frac{n(n+1)}{2} + n$ unknowns arise from Q and $\underline{r}$, and $\frac{n(n+1)}{2}$ unknowns arise from the P matrix (corresponding to each plant/controller combination). If m is the number of plant/controller combinations considered, then the number of equations and unknowns for an nth-order plant are given in Table XVIII. Notice that m' is an integer in the last column for odd n. When n is odd, $m' = m$. Because m must be an integer, when n is even, m is the next lowest integer to m'. The above says nothing about the existence of a solution of the equations. For a solution to exist, the determinant of the coefficients of Eqs. 53 and 54 considered together must be nonzero. This condition has been met for the very limited number of cases considered so far in the literature.

TABLE XVIII

REQUIRED EQUATIONS AND UNKNOWNS FOR nTH-ORDER PLANT

	NUMBER OF UNKNOWNS	m' FOR NUMBER OF EQ. TO EQUAL NUMBER OF UNKNOWNS
General case of Eq. 56	$\frac{n(n+3)}{2} + m\frac{n(n+1)}{2}$	$\frac{n+3}{2}$
With $r \triangleq 0$	$\frac{n(n+1)}{2} + m\frac{n(n+1)}{2}$	$\frac{n+1}{2}$
With $q_{ij} \triangleq 0$, $i \neq j$	$2n + m\frac{n(n+1)}{2}$	2
With $r \triangleq 0$ and $q_{ij} \triangleq 0$, $i \neq j$ (Case treated in Ref. 134)	$n + m\frac{n(n+1)}{2}$	1
Number of equations (all cases)	$m\frac{n(n+3)}{2}$	

Approved for Public Release

Contrails

Clearly, a large number of equations can be involved even for moderately small values of n. For $n = 1$ then $m = 2$, and there are four equations, for $n = 2$ then $m' = 2.5$ and $m = 2$, so there are ten equations. If we take $n = 3$ (which provides a minimal representation of the human pilot situation), $m = 3$ for the general case (the only one applicable for our purpose) and the number of equations (and unknowns) is 27. The matter has progressed beyond the realm of practical analytical solution, although numerical solution remains a distinct and practical possibility.

Another difficulty in the application of straightforward and conventional optimal control theory to the generation of estimates for pilot control behavior is the occasional presence of lags in the pilot model. Thus, for a fairly general controlled element transfer function,

$$\frac{m}{c} = \frac{K_c}{d_2 s^2 + d_1 s + d_0} \tag{68}$$

the pilot describing function may have the approximate form

$$\frac{c}{e} = \frac{-K_p(-\tau s + 1)(T_L s + 1)}{(T_{I,N} s + 1)} \tag{69}$$

where we have approximated pilot time delay by a lead term $(-\tau s + 1)$ instead of a Padé. Here c is the actual output of the human operator presuming **his** remnant is zero. Because the optimal regulator problem results in a control law consisting of linear feedbacks of the plant output variable and its first $(n-1)$ time derivatives, it is more appropriate for the application of conventional optimal control theory to redefine the plant and controller as

$$\frac{m}{u_o} = \frac{K_c}{(T_{I,N} s + 1)(d_2 s^2 + d_1 s + d_0)} \tag{70}$$

$$\frac{u_o}{e} = -K_p(-\tau s + 1)(T_L s + 1) \; ; \; e = -m \tag{71}$$

K_c, d_0, d_1, and d_2 are controlled element parameters, while K_p, τ, T_L, and $T_{I,N}$ are parameters of the pilot describing function. This was the procedure adopted previously in the first-order system example for $Y_c = K_c$.

Approved for Public Release

Contrails

Recently, Rynaski and Whitbeck (Ref. 131) have shown that the inclusion of cost-of-control rates in the performance index results in optimal controllers containing lags. Since formulation in terms of Eqs. 70 and 71 amounts to assuming that $T_{I,N}$ is known or can be found by other means, inclusion of control rates or their equivalent in the performance index and use of Eq. 68 for definition of the plant seems most appropriate. However, this does not lead to a reduction in the number of equations that must be solved simultaneously, and the really fundamental difficulty of dimensionality remains. For this reason, the time domain approach is set aside in favor of frequency domain techniques. The latter offer some promise for reducing the number of equations which must be solved simultaneously.

C. FREQUENCY DOMAIN TECHNIQUES

The frequency domain formulation for the single-input, single-output controlled element is the case of interest here. The effect of a random input generated by shaping white noise with a first-order lag is included for a small expenditure of effort by taking advantage of the transient analog concept (see Ref. 123). The development follows the approach used by Rynaski and Whitbeck in Ref. 131. It differs from that presented in Ref. 131 in that frequency-weighted error is used in the performance index, and cross-products between the frequency-weighted error and the control are included in the performance index (see Ref. 123). The former refinement admits lags into the optimal controller in much the same manner as cost-of-control rate terms do in Ref. 131. The advantage of this alternate method is that existence of the first variation of the performance index on the control is not crucially dependent on the choice of the random input shaping filter. The problem is defined according to Fig. 54.

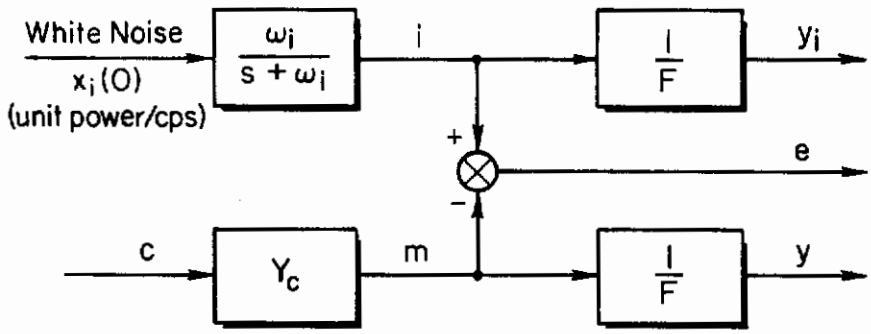

Figure 54. Block Diagram for Frequency Domain Formulation

Approved for Public Release

Contrails

where Y_c = the controlled element transfer function

i = the transient analog of the random input with power spectral density given by $\Phi_{ii}(\omega) = \omega_i^2/(\omega_i^2 + \omega^2)$

e = the displayed error

c = the control variable, limb position

m = the controlled element output variable

F = the frequency weighting applied to m and i

The Laplace-transformed equations for the frequency-weighted variable and plant are given by

$$[Y] = \begin{bmatrix} Y_i \\ Y \end{bmatrix} = \begin{bmatrix} 0 \\ Y_c/F \end{bmatrix} c(s) + \begin{bmatrix} i(s)/F \\ 0 \end{bmatrix} = w(s)c(s) + b(s) \quad (72)$$

$$w(s) = \begin{bmatrix} 0 \\ Y_c/F \end{bmatrix} \quad , \quad b(s) = \begin{bmatrix} i(s)/F \\ 0 \end{bmatrix}$$

and

$$m(s) = Y_c c(s) \quad (73)$$

Using Parseval's theorem, the performance index, Eq. 51, is converted to its frequency domain equivalent, where the state vector of interest is now [Y] above.

$$2J = \frac{1}{2\pi j} \int_{-j\infty}^{j\infty} (\bar{Y}'QY + \bar{Y}'rc + r'Y\bar{c} + c\bar{c})ds \quad (74)$$

where $\bar{Y} = Y(-s)$, etc, Q and r are weighting coefficients as follows:

$$Q = \begin{bmatrix} q_{11} & q_{12} \\ q_{12} & q_{22} \end{bmatrix} \quad , \quad r = \begin{bmatrix} r_1 \\ r_2 \end{bmatrix}$$

Substitute from Eq. 72 to eliminate Y, getting

$$2J = \frac{1}{2\pi j} \int_{-j\infty}^{j\infty} \Big\{ (\bar{c}\bar{w}' + \bar{b})Q(wc + b) + (\bar{c}\bar{w}' + \bar{b}')rc + \bar{c}r'(wc + b) + \bar{c}c \Big\} ds \quad (75)$$

Approved for Public Release

Contrails

Now, take a variation on c, letting

$$c = c_0 + \lambda c_1 \tag{76}$$

where c_0 is the optimal control and c_1 is any arbitrary variation on the control. Then, that component of 2J, J_c (see for example Ref. 131), containing the first variation is

$$J_c = \frac{1}{2\pi j} \int_{-j\infty}^{+j\infty} \bar{c}_1 \left\{ (\bar{w}'Qw + r'w + \bar{w}'r + 1)c_0 + (\bar{w}'Q + r')b \right\} ds \tag{77}$$

$$\triangleq \frac{1}{2\pi j} \int_{-j\infty}^{+j\infty} \bar{c}_1 z(s) ds \tag{78}$$

Letting $Y_c(s) = N(s)/D(s)$, $z(s)$ becomes

$$z(s) = \left[\frac{q_{22}\bar{N}\bar{N} + r_2(\bar{N}DF + N\bar{D}\bar{F}) + \bar{D}\bar{F}DF}{\bar{D}\bar{F}DF} \right] c_0 + \left[\frac{q_{12}\bar{N} + r_1\bar{D}\bar{F}}{\bar{D}\bar{F}} \right] b_1 \tag{79}$$

The q's and r's and the coefficients in F are the (unknown) coefficients in the performance index

The numerator of the coefficient of c_0 in Eq. 79 is the root-squared locus expression (Ref. 131). Note that if the order of N(s) is the same or less than that of D(s), J_c will exist as long as the random input shaping filter has more poles than zeros.

Solution for the optimal control, c_0, is obtained by setting Eq. 78 to zero by the following method. Set z(s) equal to

$$z(s) = \bar{Y}Yc_0 + J_1 \tag{80}$$

where the zeros of Y are the left half plane zeros of the c_0 coefficient in Eq. 79 and the poles of Y are the factors of DF. (As pointed out in Ref. 131, there is no need for the roots of DF to be in the LHP.) The optimal control is then given by

$$c_0 = \frac{-1}{Y}\left[\frac{1}{\bar{Y}} J_1 \right]_+ \tag{81}$$

where $[\ ]_+$ denotes the sum of those terms in the partial fraction expansion of the enclosed expression having left half plane roots. Solution

Approved for Public Release

Contrails

of the direct optimal control problem per se is not the immediate concern here. However, it enables a solution of the inverse problem to be obtained wherein c_0 and the parameters of the open- and closed-loop systems are known. The objective is then to solve for q's and r's and the coefficients in F.

We would like the optimal control procedure to provide control law transfer functions of the (observed) form

$$Y_p = \frac{-K_p\left(\frac{\tau}{2}s - 1\right)\left(T_L s + 1\right)}{\left(\frac{\tau}{2}s + 1\right)\left(T_{I,N}s + 1\right)} \tag{82}$$

This contains a Padé approximation to a time delay,

$$e^{-\tau s} = \frac{\left(\frac{-\tau}{2}s + 1\right)}{\left(\frac{\tau}{2}s + 1\right)} = \frac{-\left(\frac{\tau}{2}s - 1\right)}{\left(\frac{\tau}{2}s + 1\right)} \tag{83}$$

a lead time constant, T_L, and a lag compensation or neuromuscular system time constant, $T_{I,N}$. All these are needed for a reasonably general optimal controller which is to approximate the pilot describing function, Y_p. Thus, the optimal controller must contain a maximum of two lags. This requirement in turn requires that the frequency weighting, F, be of the form

$$F = f_2 s^2 + f_1 s + f_0 \tag{84}$$

This forces the root-squared locus expression to have two poles in addition to those from the controlled element.

Consider the case for $Y_c = K_c/s$. Then the simplifying assumption that $T_{I,N} = T_N = T_L$ is valid, and for a compensatory tracking loop, we desire a c_0 of the form

$$c_0 = \frac{-\omega_i x_i(0) K_p s\left(s - \frac{2}{\tau}\right)}{\left[s^2 + \left(\frac{2}{\tau} - K_p K_c\right)s + \frac{2K_p K_c}{\tau}\right]\left(s + \omega_i\right)} \tag{85}$$

Because of the above assumption, f_2 in Eq. 84 can be zero since only a

Approved for Public Release

Contrails

single lag is needed in the optimal controller. Furthermore, one of the q's, r's, or f's may be arbitrarily set equal to unity without loss of generality. We shall set $f_1 = 1$ and choose $f_0 = 2/\tau$ so that the frequency weighting will be part of the system open-loop transfer function.

Enough relations are now available to solve for the unknown coefficients of the performance index. The closed-loop roots of the system multiplied by their right half plane images must equal the (normalized) root-squared locus expression, i.e.:

$$\overbrace{s^4 + \left(\frac{8K_pK_c}{\tau} - \frac{4}{\tau^2} - K_p^2K_c^2\right)s^2 + \frac{4K_p^2K_c^2}{\tau^2}}^{\text{CL Characteristic}} = \overbrace{s^4 + \left(2K_cr_2 - f_0^2\right)s^2 + q_{22}K_c^2}^{\text{Root Square Locus}} \qquad (86)$$

The left side of Eq. 86 comes from the denominator of Eq. 85, our postulated c_0, while the right side comes from the numerator of the c_0 coefficient in Eq. 79, the theoretical c_0, with $F = f_1 s + f_0 = s + f_0$. Matching coefficients of like powers of s, and using $f_0 = 2/\tau$ as noted above

$$r_2 = \frac{-K_p}{2}\left(K_pK_c - \frac{8}{\tau}\right) \qquad (87)$$

$$q_{22} = \frac{4K_p^2}{\tau^2} \qquad (88)$$

Now Eq. 81, which states the optimal control law, must be satisfied. From Eqs. 79 and 80,

$$Y = \frac{s^2 + \left(\frac{2}{\tau} - K_pK_c\right)s + \frac{2K_pK_c}{\tau}}{s\left(s + \frac{2}{\tau}\right)} \qquad (89)$$

$$J_1 = \frac{\omega_i x_i(0) r_1 \left(s^2 - \frac{2}{\tau}s - \frac{q_{12}K_c}{r_1}\right)}{s\left(s - \frac{2}{\tau}\right)\left(s + \frac{2}{\tau}\right)\left(s + \omega_i\right)} \qquad (90)$$

Substituting Eqs. 85, 89, and 90 into Eq. 81,

Approved for Public Release

Contrails

$$c_0 = \frac{-\omega_i x_i(0) K_p s\left(s - \frac{2}{\tau}\right)}{\left(s + \omega_i\right)\left[s^2 + \left(\frac{2}{\tau} - K_p K_c\right)s + \frac{2K_p K_c}{\tau}\right]}$$

$$= \frac{-s\left(s + \frac{2}{\tau}\right)}{s^2 + \left(\frac{2}{\tau} - K_p K_c\right)s + \frac{2K_p K_c}{\tau}} \left[\frac{\omega_i x_i(0) r_1 \left(s^2 - \frac{2}{\tau}s - \frac{q_{12} 2K_c}{r_1}\right)}{\left[s^2 - \left(\frac{2}{\tau} - K_p K_c\right)s + \frac{2K_p K_c}{\tau}\right]\left(s + \frac{2}{\tau}\right)\left(s + \omega_i\right)}\right] + \tag{91}$$

Again matching coefficients of like powers of s, two algebraic equations linear in r_1 and q_{12} are obtained. Solving for r_1 and q_{12},

$$r_1 = \frac{K_p}{2}\left(K_p K_c g(\omega_i) - \frac{8}{\tau}\right) \tag{92}$$

$$q_{12} = \frac{4K_p^2}{\tau^2} g(\omega_i) \tag{93}$$

where

$$g(\omega_i) = \frac{\left(1 - \frac{\omega_i}{K_p K_c}\right)\left(1 + \frac{\omega_i}{2/\tau}\right)}{\left(1 + \frac{\omega_i}{4/\tau}\right)} \tag{94}$$

q_{11} is not involved in any of the above equations, and in fact q_{11} may be any arbitrary quantity. That this is true can be demonstrated by solving the direct optimal control problem as a check with the performance index coefficients given by Eqs. 87, 88, 92, 93, and 94 with q_{11} arbitrary.

At this point we have obtained a formal solution to the problem we set out to solve. (The solution is given by Eqs. 87, 88, 92, 93, and 94.) It remains for us to assess suitability of this answer. In short, the results are not very gratifying. This is so because the performance index is not a function of the difference $(y_i - y)$, but is a function of y_i and y separately. Inasmuch as only the displayed error $(i - m)$ and the pilot's output, c, are explicitly known to the pilot, we would expect that any reasonable performance index would involve quantities linearly related to

Approved for Public Release

Contrails

these explicitly known quantities, in particular $(y_i - y)$. However, it does not.

We might place an additional restriction upon the performance index so that it is a function of $(y_i - y)$. The necessary restriction is that

$$g(\omega_i) \equiv 1 \tag{95}$$

However, Eq. 94 shows that Eq. 95 holds only when

$$\omega_i = 0 \tag{96}$$

$$K_p K_c = \frac{4}{\tau} + 2\omega_i \doteq \omega_c \tag{97}$$

The condition of Eq. 96 is acceptable, but only applicable when there is no input. It is conceivably suitable as an approximation for very low input bandwidths. The condition of Eq. 97 is unacceptable because

$$0 < \omega_c < 2/\tau \tag{98}$$

must be satisfied for the closed-loop system to be stable.

For the $\omega_i = 0$ condition the performance indices are

$$\begin{aligned} r = r_1 = -r_2 &= \frac{K_p}{2}\left(K_p K_c - \frac{8}{\tau}\right) \\ q = q_{12} = q_{22} &= \frac{4K_p^2}{\tau^2} \end{aligned} \tag{99}$$

Experimental data for $Y_c = K_c/s$ systems can now be inserted in Eq. 99. Again using the ω_c, K_c independence data, and the approximation $K_p K_c \doteq \omega_c$,

$$\begin{aligned} r_1 = -r_2 &= \frac{\omega_c}{2K_c}\left(\omega_c - \frac{8}{\tau}\right) \\ q_{12} = q_{22} &= \frac{4\omega_c^2}{\tau^2 K_c^2} \end{aligned} \tag{100}$$

Data (ω_c, τ, K_c) from only one system are needed to establish these indices, after which the performance criterion function can be used to obtain at least approximate results for plants which approximate $Y_c = K/s$ in the region of crossover.

Approved for Public Release

Contrails

The complications in even this simple exercise of the inverse optimal control approach are sufficient to indicate that more complex systems will require an almost exclusively numerical treatment.

Approved for Public Release

Contrails

SECTION X

OBTAINING HUMAN PILOT DESCRIBING FUNCTIONS FROM CROSSOVER MODELS AND OPTIMAL CONTROL THEORY

The purpose of this section is to set forth a method for adapting the describing function portion of the quasi-linear human pilot model to a given controlled element. This is the same goal sought using the inverse optimal approach. Here, however, emphasis is placed more upon achieving a serviceable method than upon the niceties of its construction. Within this context we are, at last, more than modestly successful in demonstrating that optimal control theory can indeed be used effectively to develop a pilot describing function appropriate to a given controlled element.

This method assumes that all pilot/controlled-element combinations in compensatory tracking are well approximated in the crossover region by the so-called crossover model presented in detail in Ref. 12. This crossover model has a frequency response function:

$$G(j\omega) = \frac{\omega_c e^{-j\omega\tau_e}}{j\omega} \tag{101}$$

We shall represent the effective reaction time delay factor, $e^{-j\omega\tau_e}$, by a Padé approximation to avoid the mathematical difficulty of dealing with this factor in closed-loop analyses.

$$e^{-j\omega\tau_e} \doteq \frac{\tau_e/2 - j\omega}{\tau_e/2 + j\omega} \tag{102}$$

Because the above model has been found to prevail over a spectrum of controlled elements including the pure gain, single integration, and double integration or pure inertia, it seems reasonable to generalize and assume that the human pilot adapts in such a way as to cause the frequency response of the combination of his describing function and a given controlled element to "closely approximate" that of $G(j\omega)$ over the frequency range near pilot/vehicle system crossover. This is, in fact, a basis for the first adjustment

Approved for Public Release

Contrails

rule on "Equalization Selection and Adjustment" (p. 8). Our use of optimal control theory in this section will be to effect this "close approximation," that is, to adapt the human pilot describing function for control of the given controlled element.

In the following subsections we show that this approach is feasible and consistent with what is known to be good servo synthesis technique. Then we apply the method to a practical problem which can be checked against existing data.

A. FEASIBILITY OF APPROACH

The approach is most easily explained in terms of the block diagram in Fig. 55. The model in Fig. 55a depicts the situation of the crossover model in a compensatory tracking loop structure. This loop structure is often called "the unity gain feedback configuration" and the crossover model "the open-loop transfer function." For the feasibility assessment

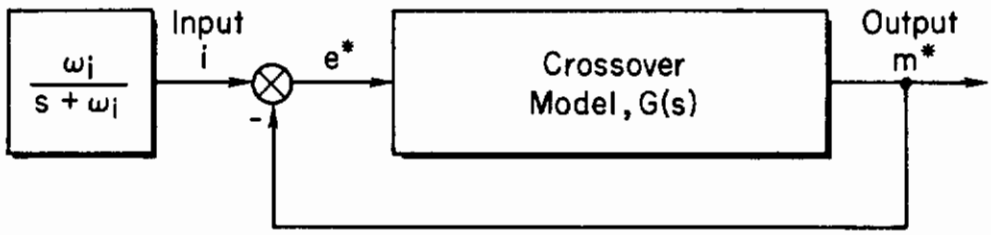

(a) Model

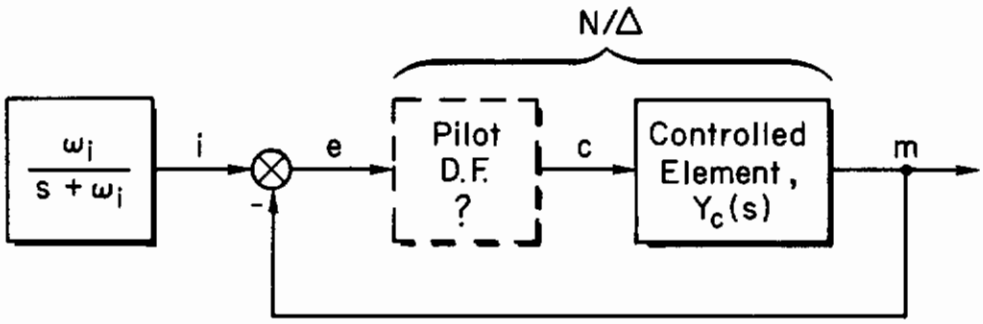

(b) System

Figure 55. Block Diagram for Model and System

Approved for Public Release

Contrails

let us temporarily use these more general terms while dealing with more general matters. The model is forced by the transient analog of R-C filtered white noise, i. (See Ref. 123 for development of the transient analog concept.) The output and error in the model are denoted by m^* and e^*, respectively.

The system in Fig. 55b has the same input and loop structure as the model. However, the open-loop transfer function, N/Δ, is separated into two elements. One is the specific controlled element, Y_c, to be controlled and the other is the pilot, or, in more general terms, the controller. The control variable is c. The output and error of the system are, respectively, m and e. At this point, the system controller is unspecified. The object is to calculate the controller transfer function that will minimize the weighted sum of the mean-squared difference between model and system outputs, plus the mean-squared control variable. Put qualitatively, we are going to trade increased response error in an optimal way for a reduction in required control activity through selection of the controller. This objective can be stated mathematically as

Minimize the performance index, J,
with respect to c, where

$$J = \int_0^\infty \left\{ q(m-m^*)^2 + c^2 \right\} dt \tag{103}$$

The constant, q, is the weight in the sum of performance index terms known as the ratio of the cost of error to the cost of control. We can define the response error as

$$\epsilon \triangleq m - m^* = e^* - e \tag{104}$$

for brevity and rewrite Eq. 103 in the frequency domain using Parseval's theorem,*

$$J = \frac{1}{2\pi j} \int_{-j\infty}^{j\infty} (q\bar{\epsilon}\epsilon + \bar{c}c)\, ds \tag{105}$$

where now $c = c(s)$, $\epsilon = \epsilon(s)$, and $\bar{\epsilon} = \epsilon(-s)$, etc. Response error can be

*We tacitly assume here that ϵ and c are such that the conditions on Parseval's theorem for equivalence of Eqs. 103 and 105 are satisfied.

Approved for Public Release

Contrails

expressed as a function of the control, c.

$$\epsilon(s) = Y_c(s)c(s) - \frac{G(s)}{1+G(s)}\left(\frac{\omega_i}{s+\omega_i}\right) \tag{106a}$$

$$= w(s)c(s) + b(s) \tag{106b}$$

At this point we have expressed the key elements needed as inputs for the optimal control procedure. The details of the derivation, which follows Ref. 131 in most respects, are sketched below, and can be bypassed if desired.

Necessary and sufficient conditions for the control to be optimal in the sense that J is minimized are:

> The first variation of J on c must vanish for $c = c_0 + \lambda c_1$, where c_0 is the optimal control and c_1 is any arbitrary stable control variation.
>
> The second variation of J on c must be greater than zero.

By substituting Eq. 106b and $c = c_0 + \lambda c_1$ into Eq. 105, we can obtain an expression for J_c, which is that component of J containing the first variation with respect to $\bar{c}_1$.

$$J_c = \frac{1}{2\pi j}\int_{-j\infty}^{+j\infty} \bar{c}_1 \left\{(1+q\bar{w}w)c_0 + q\bar{w}b\right\} ds \tag{107}$$

$$\triangleq \frac{1}{2\pi j}\int_{-j\infty}^{+j\infty} \bar{c}_1 z(s)\, ds \tag{108}$$

Since J_c must vanish and $\bar{c}_1$ corresponds to a stable function of time for $t<0$ and to zero for $t\geq 0$ ($\bar{c}_1$ is analytic in the left half plane), z(s) must correspond to a function of time which is zero for $t\geq 0$. That is, z(s) must be analytic in the left half plane.

An expression for J_d, that component of J containing the second variation with c_1, can be similarly obtained.

$$J_d = \frac{1}{2\pi j}\int_{-j\infty}^{+j\infty} \bar{c}_1 (1+q\bar{w}w)c_1\, ds \tag{109}$$

For $J_d > 0$, $(1+q\bar{w}w)_{s=j\omega} > 0$ for all ω. The quantity $(1+q\bar{w}w)$ is that involved in the so-called root-squared locus expression:

$$1 + q\bar{w}w = 0 \tag{110}$$

Approved for Public Release

Contrails

Therefore the condition $J_d > 0$ is equivalent to the condition that no zeros of Eq. 110 lie on the imaginary axis of the complex plane.

Now, if we set $$1 + q\bar{w}w = \bar{Y}Y \tag{111}$$

where Y is analytic in the right half plane and has as its poles the poles of w and let

$$J_1 = q\bar{w}b \tag{112}$$

in Eq. 107, then for the optimal control, $Y\bar{Y}c_0 + J_1 = z = 0$, and

$$c_0 = -\frac{1}{Y}\left[\frac{1}{\bar{Y}}J_1\right]_+ \tag{113}$$

$[\ ]_+$ denotes the sums of the terms in the partial fraction expansion of $[\ ]$ having left half plane poles. The poles of $[\ ]_+$ are associated with functions of time which are zero for $t \leq 0$ and are stable for $t > 0$. Hence we see that $c_0(t)$ is a stable function of time for $t > 0$ and zero for $t \leq 0$ by definition of the symbols in Eq. 113.

As stated previously, $z(s)$ must correspond to a function of time which is zero for $t \geq 0$ to satisfy the conditions for c_0 to be optimal. From Eqs. 107, 108, and 112, we can check to determine whether Eq. 113 is consistent with that requirement.

$$z(s) = Y\bar{Y}c_o + J_1 \tag{114}$$

Substituting for c_0 using Eq. 113 and noting that

$$\frac{1}{\bar{Y}}J_1 = \left[\frac{1}{\bar{Y}}J_1\right]_+ + \left[\frac{1}{\bar{Y}}J_1\right]_- \tag{115}$$

gives

$$z(s) = \bar{Y}\left[\frac{1}{\bar{Y}}J_1\right]_- \tag{116}$$

Hence $z(t)$ is zero for $t \geq 0$ by the definitions of symbols given above and the fact that the poles of $\bar{w}$ are the poles of $\bar{Y}$ and these correspond to time functions which are zero for $t \geq 0$.

Approved for Public Release

Contrails

The optimal control for the specific problem at hand is obtained by substituting for Y and J_1 in Eq. 113.

$$c_0 = -\frac{1}{(1+q\bar{Y}_c Y_c)^+}\left[\frac{-q\omega_i Y_c G/\left[(s+\omega_i)(1+G)\right]}{(1+q\bar{Y}_c Y_c)^-}\right]_+ \tag{117}$$

where $(\ ) = (\ )^+(\ )^-$ and the poles and zeros of $(\ )^+$ are in the left half plane.

Let us now proceed to determine the forms for the optimal controllers for $Y_c = K_c$, K_c/s, and K_c/s^2 when the crossover model is $G(s) = \omega_c/s$.

1. Pure Gain Controlled Element: $Y_c = K_c$

For $Y_c = K_c$ the Laplace transform of the optimal control is

$$c_0 + \frac{qK_c^2}{(1+qK_c^2)}\,\frac{\omega_c/K_c}{(s+\omega_c)}\,\frac{\omega_i}{(s+\omega_i)} = \frac{qK_c^2}{(1+qK_c^2)}\,\frac{\omega_c/K_c}{(s+\omega_c)}\,x_i \tag{118}$$

From Fig. 55b,
$$\frac{c_0}{x_i}(s)Y_c(s) = \frac{N}{\Delta+N} \tag{119}$$

and the controller transfer function is

$$Y_p(s) = \frac{1}{Y_c}\,\frac{N}{\Delta}(s) = \frac{\frac{c_0}{x_i}(s)}{1-\frac{c_0}{x_i}(s)Y_c(s)} \tag{120}$$

Substituting,

$$Y_p(s) = \frac{\frac{\omega_c}{K_c}\,\frac{qK_c^2}{1+qK_c^2}}{s+\frac{\omega_c}{1+qK_c^2}} \tag{121}$$

Several features of this optimal controller transfer function for $Y_c = K_c$ should be noted here:

- If the controller characteristics are to be independent of the controlled element gain, the product qK_c^2 should be an invariant parameter.

Approved for Public Release

Contrails

- For $qK_c^2 > 1$ the compensation in the controller is a low frequency lag, i.e., with breakpoint less than ω_c.
- As $qK_c^2 \to \infty$, $Y_p Y_c \to \omega_c/s$; that is, $Y_p \to (\omega_c/K_c)/s$ (pure integration behavior).
- The controller is independent of the input bandwidth, ω_i.

2. Single-Integrator Controlled Element: $Y_c = K_c/s$

For $Y_c = K_c/s$ the optimal control will be

$$\frac{c_0}{x_i} = \frac{\dfrac{\omega_c}{K_c}\dfrac{qK_c^2}{\left(\omega_c + \sqrt{qK_c^2}\right)\left(\omega_i + \sqrt{qK_c^2}\right)}\, s\left(s + \sqrt{qK_c^2} + \omega_c + \omega_i\right)}{\left(s + \omega_c\right)\left(s + \sqrt{qK_c^2}\right)} \qquad (122)$$

Substituting into Eq. 120 yields a controller for $Y_c = K_c/s$ of the form

$$Y_p = \frac{\dfrac{\omega_c}{K_c}\dfrac{qK_c^2}{\left(\omega_c + \sqrt{qK_c^2}\right)\left(\omega_i + \sqrt{qK_c^2}\right)}\, s\left(s + \sqrt{qK_c^2} + \omega_c + \omega_i\right)}{\left(s + \omega_1\right)\left(s + \omega_2\right)} \qquad (123)$$

where

$$\left(s + \omega_1\right)\left(s + \omega_2\right) = \left(s + \omega_c\right)\left(s + \sqrt{qK_c^2}\right) - \frac{\omega_c qK_c^2}{\left(\omega_c + \sqrt{qK_c^2}\right)\left(\omega_i + \sqrt{qK_c^2}\right)}\left(s + \sqrt{qK_c^2} + \omega_c + \omega_i\right) \qquad (124)$$

The root locus of $(c_0/x_i)Y_c$ below indicates the relative values of ω_1 and ω_2 for "small" values of ω_i and "large" values of $\sqrt{qK_c^2}$.

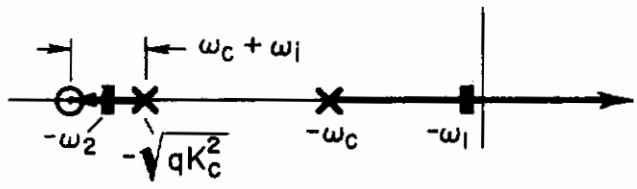

Approved for Public Release

Contrails

It can be shown that as $\omega_i \to 0$ or as $\sqrt{qK^2} \to \infty$, $\omega_1 \to 0$; and as $\omega_i \to 0$,

$$\omega_2 \to \sqrt{qK_c^2}\left[\frac{1 + \frac{\omega_c}{\sqrt{qK_c^2}} + \frac{\omega_c^2}{qK_c^2}}{1 + \frac{\omega_c}{\sqrt{qK_c^2}}}\right]$$

It can also be shown that the roots are contained in the left half plane for all ω_i when $\sqrt{qK_c^2} > 0$.

The pertinent features of this optimal controller transfer function for $Y_c = K_c/s$ are:

- If the controller characteristics are to be independent of the controlled element gain, the product $\sqrt{qK_c^2}$ should be an invariant parameter.
- For $\sqrt{qK_c^2} > \omega_c$ the compensation in the controller includes a differentiation, very low frequency lag, high frequency lag, and high frequency lead.
- As $\sqrt{qK_c^2} \to \infty$, $Y_p Y_c \to \omega_c/s$. That is, $Y_p \to \omega_c/K_c$ (pure gain behavior).

3. Double-Integrator Controlled Element: $Y_c = K_c/s^2$

The optimal control for $Y_c = K_c/s^2$ is

$$c_0 = \frac{\frac{\omega_c}{K_c} a_1 s^2 \left(s + \frac{a_0}{a_1}\right)}{\left(s + \omega_c\right)\left(s^2 + \frac{2}{\sqrt{2}} \sqrt[4]{qK_c^2}\, s + \sqrt{qK_c^2}\right)} x_i \qquad (125)$$

where

$$a_1 = \frac{\left(\sqrt{2}\sqrt[4]{qK_c^2} + \omega_c + \omega_i\right) qK_c^2}{\left(\omega_c^2 + \sqrt{2}\sqrt[4]{qK_c^2}\,\omega_c + \sqrt{qK_c^2}\right)\left(\omega_i^2 + \sqrt{2}\sqrt[4]{qK_c^2}\,\omega_i + \sqrt{qK_c^2}\right)}$$

and

$$\frac{a_0}{a_1} = \frac{\sqrt{qK_c^2} + \sqrt{2}\sqrt[4]{qK_c^2}\left(\omega_c + \omega_i\right) + \omega_c^2 + \omega_c\omega_i + \omega_i^2}{\sqrt{2}\sqrt[4]{qK_c^2} + \omega_c + \omega_i}$$

Approved for Public Release

Contrails

Substituting into Eq. 120 yields a controller for $Y_c = K_c/s^2$ of the form

$$Y_p = \frac{\frac{\omega_c}{K_c} a_1 s^2 \left(s + \frac{a_0}{a_1}\right)}{(s + \omega_1)(s + \omega_2)(s + \omega_3)} \tag{126}$$

where $$(s + \omega_1)(s + \omega_2)(s + \omega_3) = (s + \omega_c)\left(s^2 + \frac{2}{\sqrt{2}} \sqrt[4]{qK_c^2}\, s + \sqrt{qK_c^2}\right) - \omega_c a_1 \left(s + \frac{a_0}{a_1}\right) \tag{127}$$

The root locus of $(c_0/x_i)Y_c$ below indicates the relative values of ω_1, ω_2, and ω_3 for "small" values of ω_i and "large" values of $\sqrt[4]{qK_c^2}$.

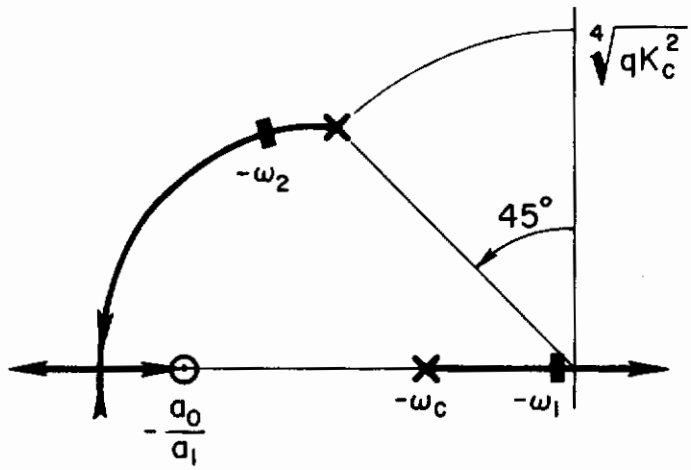

It can be shown that as $\omega_i \to 0$ or as $\sqrt[4]{qK_c^2} \to \infty$, $\omega_1 \to 0$; and as $\omega_i \to 0$,

$$(s + \omega_2)(s + \omega_3) \longrightarrow s^2 + \left[\sqrt{2}\sqrt[4]{qK_c^2} + \omega_c\right]s + \left[\frac{qK_c^2}{\omega_c^2 + \sqrt{2}\sqrt[4]{qK_c^2}\,\omega_c + \sqrt{qK_c^2}} + \sqrt{2}\sqrt[4]{qK_c^2}\,\omega_c\right]$$

It can also be shown that $\omega_1 \geq 0$ for all ω_i when $\sqrt[4]{qK_c^2} > 0$.

The pertinent features of this optimal controller transfer function for $Y_c = K_c/s^2$ are:

Approved for Public Release

Contrails

- If the controller characteristics are to be independent of the controlled element gain, $\sqrt[4]{qK_c^2}$ should be an invariant parameter.
- For $\sqrt[4]{qK_c^2} > \sqrt{2}\,\omega_c$, the compensation in the controller includes a double differentiation, very low frequency lag, high frequency lead, and high frequency lag.
- As $\sqrt[4]{qK_c^2} \rightarrow \infty$, $Y_pY_c \rightarrow \omega_c/s$. That is, $Y_p \rightarrow s\omega_c/K_c$ (pure rate behavior).

4. General Features of These Optimal Controllers

There are several features to be appreciated in connection with the entire above group of controller/controlled-element pairs:

- To obtain "good" high frequency controller cutoff characteristics in the case of $Y_c = K_c/s^2$, and qualitatively comparable "good" low frequency characteristics in the controller for $Y_c = K_c$, we see that

  $$(qK_c^2)^{1/[2n+\delta(n)]}$$

  should be "large" and approximately constant for all systems. n is the number of controlled element poles less the number of zeros, and

  $$\delta(n) = \begin{cases} 1 , & n = 0 \\ 0 , & n \neq 0 \end{cases}$$

- As $\omega_i \rightarrow 0$, we may correctly interpret the results as pertaining to systems having an optimal step response. Since many specifications in conventional control technology concern step response characteristics, these optimal controller/controlled-element pairs are summarized in Table XIX.

Clearly, the above controller/controlled-element pairs satisfy the primary rule of thumb of frequency response synthesis: "Find or create a fair stretch of −20 db/decade slope for the amplitude ratio of the open-loop frequency response function, and then make it the crossover region by putting the 0 db line through it." That is, make $|Y_pY_c(j\omega)|$ approximate $|K/j\omega|$ in the frequency region about $|Y_pY_c| = 1$. This crude prescription for acceptable stability and response is generally adequate for minimum phase systems. It can be extended directly to nonminimum phase systems by adding a prescription for a positive phase margin.

Approved for Public Release

Contrails

TABLE XIX

OPTIMAL CONTROLLER AND CONTROLLED ELEMENT PAIRS FOR STEP INPUT

CONTROLLED ELEMENT, Y_c	CONTROLLER, Y_p ($\omega_1 \doteq 0$)
K_c	$\dfrac{\dfrac{\omega_c}{K_c}\dfrac{qK_c^2}{1+qK_c^2}}{s+\dfrac{\omega_c}{1+qK_c^2}}$
$\dfrac{K_c}{s}$	$\dfrac{\dfrac{\omega_c}{K_c}\dfrac{1}{1+\bar{\omega}_c}\left[s+\sqrt{qK_c^2}\left(1+\bar{\omega}_c\right)\right]}{s+\sqrt{qK_c^2}\left(\dfrac{1+\bar{\omega}_c+\bar{\omega}_c^2}{1+\bar{\omega}_c}\right)}$ $\bar{\omega}_c = \dfrac{\omega_c}{\sqrt{qK_c^2}}$
$\dfrac{K_c}{s^2}$	$\dfrac{\dfrac{\omega_c}{K_c}\dfrac{\sqrt[4]{qK_c^2}\left(\sqrt{2}+\bar{\omega}_c\right)}{1+\sqrt{2}\,\bar{\omega}_c+\bar{\omega}_c^2}s\left(s+\sqrt[4]{qK_c^2}\dfrac{1+\sqrt{2}\,\bar{\omega}_c+\bar{\omega}_c^2}{\sqrt{2}+\bar{\omega}_c}\right)}{s^2+\sqrt[4]{qK_c^2}\left(\sqrt{2}+\bar{\omega}_c\right)s+\sqrt{qK_c^2}\left(1+\bar{\omega}_c^2\dfrac{1+\sqrt{2}\,\bar{\omega}_c}{1+\sqrt{2}\,\bar{\omega}_c+\bar{\omega}_c^2}\right)}$ $\bar{\omega}_c = \dfrac{\omega_c}{\sqrt[4]{qK_c^2}}$

What is more, certain "practical" characteristics are displayed by these controllers outside of the crossover frequency region. In the case of $Y_c = K_c$, the controller compensation takes the form of a pseudo-integration or low frequency lag. For $Y_c = K_c/s^2$, the differentiation

Approved for Public Release

Contrails

needed in the controller for the crossover frequency region is cut off at high frequencies by lag. Each of these characteristics in the respective optimal controllers is a most elementary yet crucial consideration in design practice for the physical realization of actual controllers. Hence we may regard this particular formulation of the optimal control problem as a step forward in relating conventional control technology and optimal control theory.

At this point we can claim feasibility for the approach outlined in the introductory remarks of this section merely by noting that the controllers we have been discussing can be made fairly reasonable facsimiles to the human pilot describing function in spite of the oversimplified crossover model used.

The remaining task before us is proper selection of the parameters of the crossover model, $G(j\omega)$. Fortunately an extensive distillation of a large collection of human pilot describing function data (Ref. 12, pp. 145–164, 173–176, 179–182) can supply these parameter values. This material also enables us to include the effects of variations observed in human pilot crossover data of τ_e and ω_c with ω_i and possibly controlled element type in the human pilot describing function calculation.

In the next subsection we will use this method to compute the human pilot describing function appropriate to a novel controlled element and compare the results with actual measurements.

B. COMPUTING A HUMAN PILOT DESCRIBING FUNCTION

We have chosen the following example to illustrate the method: Given the controlled element,

$$Y_c = \frac{K_c}{s(s-1.0)} \tag{128}$$

in a compensatory control system forced by R-C filtered white noise with bandwidth

$$\omega_i = 1.5 \text{ rad/sec} \tag{129}$$

find an appropriate human pilot describing function, Y_p.

Approved for Public Release

Contrails

The first step is to select an appropriate crossover model from Ref. 12. Since the controlled element is somewhat like K_c/s^2 in the probable crossover region, we can use those crossover model parameters here. Assuming equivalence of the input bandwidth parameters, ω_i, the crossover model (Table XII, Ref. 12) is

$$G(j\omega) \doteq \frac{\omega_c e^{-j\omega\tau_e}}{j\omega} = \frac{3.25e^{-j0.385\omega}}{j\omega} \tag{130}$$

Converting to the s-domain and using the Padé approximation:

$$G(s) = \frac{-3.25(s-5.2)}{s(s+5.2)} \tag{131}$$

The next matter is to select a value for $(qK_c^2)^{1/4}$. Recalling that this parameter determines the high frequency cutoff for the system, and that such an effect could be attributed to the high frequency neuromuscular system dynamics (see pp. 164–171 of Ref. 12), a reasonable number would seem to be $\sqrt[4]{qK_c^2} = 10.0$ rad/sec. Actually, we shall consider a range of values for this parameter to see just how good this guess is:

$$qK_c^2 = 10^2, 10^3, 10^4, 10^5, 10^6, \infty \ \text{rad}^4/\text{sec}^4$$

Solving for the optimal control (given by Eq. 117) enables us to solve for the optimal controller transfer function, or, as we shall call it in proper context here, the "appropriate" pilot describing function Y_p for $Y_c = K_c/s(s-1.0)$. The parameters for this describing function for the several values of qK_c^2 listed above are given in Table XX. The form of Y_p is

$$\left[s^2 + 2\zeta_N\omega_N s + \omega_N^2\right]$$

or

$$Y_p = \frac{-K_p s(s-1.0)\overbrace{(s+z_1)(s+z_2)}}{(s+p_1)(s+p_2)\left[s^2 + 2\zeta_D\omega_D s + \omega_D^2\right]} \tag{132}$$

Notice in the last column of Table XX that as the cost of error relative to control approaches infinity, Y_pY_c approaches the crossover model $G(s)$, as indeed it should.

Approved for Public Release

Contrails

TABLE XX

PARAMETERS OF Y_p

	qK_c^2					
	10^2	10^3	10^4	10^5	10^6	$\rightarrow \infty$
K_pK_c	−4.69	−2.55	16.19	52.8	117.0	3.25 (∞)
z_1			−9.53	−6.24	−5.52	−5.2
z_2			11.37	16.47	26.33	∞
ζ_N	0.547	0.796				
ω_N	5.59	14.79				
p_1	0.390	−0.149	−0.133	−0.045	−0.028	0
p_2	2.95	3.73	4.38	4.89	5.13	5.2
ζ_D	0.363	0.510	0.564	0.616	0.654	$\sqrt{2}/2$
ω_D	4.39	6.27	10.52	18.10	31.75	∞

Equation 132 shows that the computed pilot describing function contains a zero which cancels the unstable pole of Y_c. (Cancellation of the Y_c poles will always occur in the optimal solution when only one loop can be closed by the pilot.) Usually this is not a physically acceptable situation since the cancellation cannot be exact in practice. However, in the case of the pilot describing function, we are really concerned with obtaining a mathematical representation of the pilot. From this point of view, the situation is acceptable.

Approved for Public Release

Contrails

The open-loop frequency response function, Y_pY_c, is shown plotted in Fig. 56 for qK_c^2 equal to 10^4 and in Fig. 57 for other values. The results in Fig. 56 seem to best fit the measured Y_pY_c where the pilot was controlling $Y_c = K_c/s(s-1.0)$. That this is so lends support to our assumption that the high frequency neuromuscular dynamics may be identified with the cutoff characteristics of the optimal control formulation.

Notice that the calculated frequency response departs from the crossover model frequency response in the direction of the Y_pY_c frequency response measurements. Also, the calculated frequency response best fits the data in the frequency region near crossover.

The fact that the calculated frequency response does not fit the Y_pY_c measurements very well at high and low frequencies is not a cause for faulting the method. The discrepancy at high frequency stems from the use of a simple low order Padé approximation to the effective reaction time delay term in the crossover model. At low frequencies the deviations in both phase angle and amplitude ratio from the measured quantities are probably due, at least in part, to the absence of a low frequency neuromuscular phase lag representation in the crossover model. Inclusion of this effect is possible by using the so-called precision model of Ref. 12 as the crossover model. However, this amount of detail was considered to be beyond the scope of the present effort.

The results from this example indicate that optimal control theory and the crossover models presented in Ref. 12 can indeed be used effectively to develop a pilot describing function appropriate to a particular controlled element.

What is more, in the course of performing the surveys leading to the above results we have uncovered a particularly useful formulation for the problem of synthesizing optimal closed-loop controllers. This formulation produces controllers which implement the primary rule of thumb for frequency response synthesis. Moreover, these controllers tend to use "practical" compensation elements such as approximate integration in place of exact integration and lead/lag filtering in place of exact differentiation, which are important considerations when the controller is to be realized using "real" components.

Approved for Public Release

Contrails

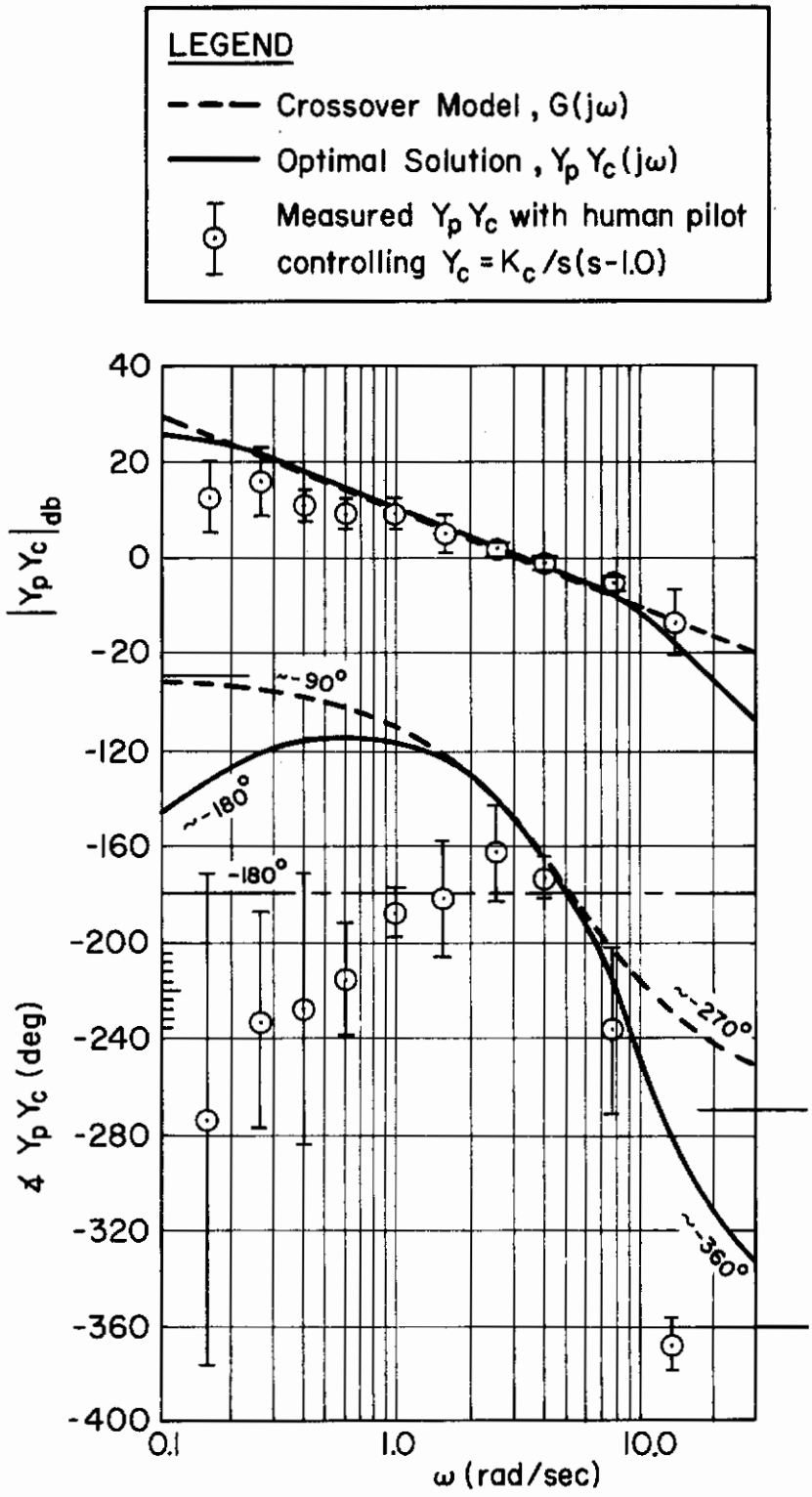

Figure 56. Comparison of Y_pY_c Calculated for $qK_c^2 = 10^4$ rad^4/sec^4 With Crossover Model and Measured Y_pY_c

Approved for Public Release

Contrails

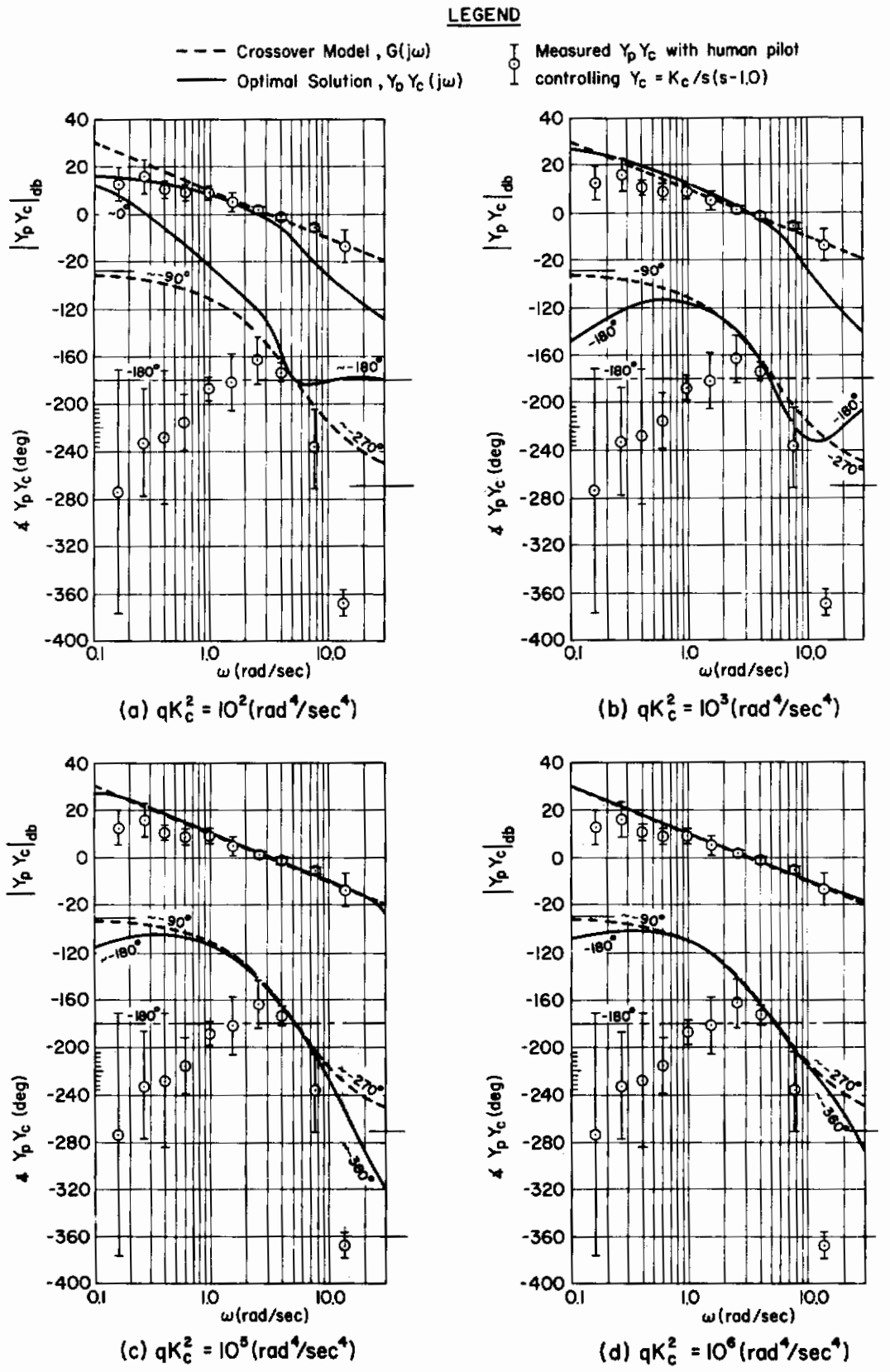

Figure 57. Comparison of Calculated Y_pY_c's for Different Values of qK_c^2

Approved for Public Release

Contrails

SECTION XI

SUMMARY

The search for new models of the human pilot in dynamic control roles has been approached in two ways. First, the status and deficiencies of existing quasi-linear pilot models have been used to specify new model requirements. Second, the large body of known analytical techniques used in the automatic control field has been reviewed in an effort to uncover new modeling methods which may be useful. In some cases, the merits of the new model/methods considered have been assessed, whereas in others only the technical basis for an assessment has been established.

Deficiencies in the existing quasi-linear models have led to an investigation of the following topics:

- Low frequency lead generation using either velocity sensing at the periphery (eye) or difference computations accomplished at a more central level.
- Mode-switching models for nonstationary or discrete inputs to the pilot/vehicle system.
- Physiological aspects of pilot dynamics in tracking tasks.
- Successive Organization of Perception (SOP) theory for levels of pilot cognition higher than compensatory.

All of these approaches are likely to prove fruitful in the future.

Analytical approaches from automatic control theory which appear to have the most promise have been investigated and summarized. These include:

- Time-optimal computing feedforward elements useful in the mode-switching models for response to nonstationary inputs.
- Optimal control theory using the crossover model in the performance criterion to estimate pilot response characteristics in compensatory tasks.
- Inverse optimal control theory using known experimental results and quasi-linear pilot response models in an effort to define the pilot's adjustment rules in terms of performance indices.

Approved for Public Release

Contrails

- Optimal control theory to provide a simple test for optimality (to an elementary quadratic criterion) using only average performance measure data.

The most promising of the analytical approaches a posteriori is the second listed, which permits a routine computational procedure to be used to estimate pilot response characteristics for novel situations.

Approved for Public Release

Contrails

REFERENCES

1. Tustin, A., "The Nature of the Operator's Response in Manual Control and Its Implications for Controller Design," J. IEE (London), Vol. 94, Pt. IIA, May 1947, pp. 190-202.

2. Russell, Lindsay, Characteristics of the Human as a Linear Servo-Element, Master's Thesis, MIT, Dept. of Electrical Engineering, May 18, 1951.

3. Human Dynamic Study, Goodyear Airc. Corp. Rept. GER-4750, Apr. 8, 1952.

4. Investigation of Control "Feel" Effects on the Dynamics of a Piloted Aircraft System, Goodyear Airc. Corp. Rept. GER-6726, Apr. 25, 1955.

5. Krendel, E. S., and G. H. Barnes, Interim Report on Human Frequency Response Studies, WADC-TR-54-370, June 1954.

6. McRuer, Duane T., and Ezra S. Krendel, Dynamic Response of Human Operators, WADC-TR-56-524, Oct. 1957.

7. Elkind, J. I., Characteristics of Simple Manual Control Systems, MIT, Lincoln Lab., Tech. Rept. 111, 6 Apr. 1956.

8. Seckel, E., I. A. M. Hall, D. T. McRuer, and D. H. Weir, Human Pilot Dynamic Response in Flight and Simulator, WADC-TR-57-520, Oct. 1957.

9. Hall, I. A. M., Effects of Controlled Element on the Human Pilot, WADC-TR-57-509, Aug. 1958.

10. Hall, I. A. M., "Study of the Human Pilot as a Servo-Element," J. Royal Aeron. Soc., Vol. 67, No. 640, June 1963, pp. 351-360.

11. McRuer, D. T., I. L. Ashkenas, and C. L. Guerre, A Systems Analysis View of Longitudinal Flying Qualities, WADD-TR-60-43, Jan. 1960.

12. McRuer, Duane, Dunstan Graham, Ezra Krendel, and William Reisener, Jr., Human Pilot Dynamics in Compensatory Systems: Theory, Models, and Experiments with Controlled Element and Forcing Function Variations, AFFDL-TR-65-15, July 1965.

13. Stapleford, R. L., D. T. McRuer, and R. Magdaleno, Pilot Describing Function Measurements in a Multiloop Task, NASA CR-542, Aug. 1966.

14. Magdaleno, R. E., and D. T. McRuer, Effects of Manipulator Restraints on Human Operator Performance, AFFDL-TR-66-72, Dec. 1966.

Approved for Public Release

Contrails

15. Smith, Harriet J., "Human Describing Functions Measured in Flight and on Simulators," Second Annual NASA-University Conference on Manual Control, Massachusetts Institute of Technology, Cambridge, Mass., February 28-March 2, 1966, NASA SP-128, 1966, pp. 279-290.

16. McRuer, D T., and E. S. Krendel, "The Human Operator as a Servo System Element," J. Franklin Inst., Vol. 267, No. 5, May 1959, pp. 381-403; No. 6, June 1959, pp. 511-536.

17. McRuer, Duane T., Dunstan Graham, and Ezra S. Krendel, "Manual Control of Single-Loop Systems," J. Franklin Inst., Vol. 238, No. 1, Jan. 1967, pp. 1-29; No. 2, Feb. 1967, pp. 145-168.

18. Wasicko, R. J., D. T. McRuer, and R. E. Magdaleno, Human Pilot Dynamic Response in Single-Loop Systems with Compensatory and Pursuit Displays, AFFDL-TR-66-137, Dec. 1966.

19. Merton, P. A., "Speculations on the Servo-Control of Movement," The Spinal Cord, A Ciba Found. Symp., ed. J. L. Malcolm and J. A. B. Gray, Little, Brown & Co., Boston, 1953, pp. 247-260.

20. Stark, L., "Neurological Organization of the Control System for Movement," Quar. Prog. Rept. No. 61, MIT, Research Lab. of Electronics, Apr. 15, 1961, pp. 234-238.

21. Stark, L., M. Iida, and P. A. Willis, "Dynamic Characteristics of Motor Coordination System in Man," Biophysics J., Vol. 1, 1961, pp. 279-300.

22. Okabe, Y., H. E. Rhodes, L. Stark, and P. A. Willis, "Simultaneous Hand and Eye Tracking Movements," Quar. Prog. Rept. No. 66, MIT, Research Lab. of Electronics, July 15, 1962, pp. 395-401.

23. Okabe, Y., H. E. Rhodes, L. Stark, and P. A. Willis, "Transient Responses of Human Motor Coordination System," Quar. Prog. Rept. No. 66, MIT, Research Lab. of Electronics, July 15, 1962, pp. 389-395.

24. Young, Laurence R., and Lawrence Stark, Biological Control Systems — A Critical Review and Evaluation: Developments in Manual Control, NASA CR-190, Mar. 1965.

25. Vossius, G., The Prediction Capabilities of the System of Voluntary Movement ["Die Vorhersageeigenschaften des Systems der Willkürbewegun," Nenere Ergebuisse der Kyberuetik (Hrsg.: K. Steinbuch n. S. W. Wagner), R. Oldenbourg, Muuchen, 1964], Systems Technology, Inc., Tech. Trans. No. 2, July 1965.

26. McRuer, D. T., and R. E. Magdaleno, Human Pilot Dynamics with Various Manipulators, AFFDL-TR-66-138, Dec. 1966.

27. McRuer, D. T., "Some Neuromuscular Subsystem Dynamics," Second Annual NASA-University Conference on Manual Control, Massachusetts Institute of Technology, Cambridge, Mass., February 28-March 2, 1966, NASA SP-128, 1966, pp. 39-43.

Approved for Public Release

Contrails

28. McRuer, D. T., R. E. Magdaleno, and G. P. Moore, "A Neuromuscular Actuation System Model," Third Annual NASA–University Conference on Manual Control, University of Southern California, Los Angeles, Calif., March 1 – 3, 1967 (forthcoming NASA SP).

29. Meiry, Jacob L., The Vestibular System and Human Dynamic Space Orientation, MIT, Man–Vehicle Control Lab., Thesis T-65-1, June 1965.

30. Jones, G. Melvill, Disorientation in Flight, Royal Air Force Institute of Aviation Medicine FPRC Memo. 96, Sept. 1958.

31. Jones, G. M., and J. H. Milsum, "Spatial and Dynamic Aspects of Visual Fixation," IEEE Trans., Vol. BME-12, No. 2, Apr. 1965, pp. 54 – 62.

32. McRuer, D. T., D. Graham, E. S. Krendel, and W. C. Reisener, Jr., "System Performance and Operator Stationarity in Manual Control Systems," Automatic and Remote Control (Proc. Third Congress of Internat. Fed. Auto. Control, London, 1966), Butterworth, Inc., Wash., D. C., 1967.

33. Miller, Duncan C., "The Effects of Performance-Scoring Criteria on Compensatory Tracking Behavior," IEEE Trans., Vol. HFE-6, No. 1, Sept. 1965, pp. 62 – 64.

34. Obermayer, R. N., R. A. Webster, and F. A. Muckler, "Study of Optimal Behavior in Manual Control Systems: The Effect of Four Performance Criteria in Compensatory Rate-Control Tracking," Second Annual NASA–University Conference on Manual Control, Massachusetts Institute of Technology, Cambridge, Mass., February 28 March 2, 1966, NASA SP-128, 1966, pp. 311 – 324.

35. Weir, David H., and Anil V. Phatak, Model of Human Operator Response to Step Transitions in Controlled Element Dynamics, NASA CR-671, Jan. 1967.

36. Sheridan, T. B., Time Variable Dynamics of Human Operator Systems, AFCRC-TN-60-169, Mar. 1960.

37. Sheridan, T. B., Studies of Adaptive Characteristics of the Human Controller, ESD-TDR-62-351, Dec. 1962.

38. Sadoff, Melvin, A Study of a Pilot's Ability to Control During Simulated Stability Augmentation System Failures, NASA TN D-1552, Nov. 1962.

39. Elkind, J. I., Human Operator Response to Changing Controlled Element Dynamics, Bolt Beranek and Newman, Inc., May 1963.

40. Young, L. R., D. M. Green, J. I. Elkind, and J. A. Kelly, The Adaptive Dynamic Response Characteristics of the Human Operator in Simple Manual Control, NASA TN D-2255, Apr. 1964.

Approved for Public Release

Contrails

41. Kelly, J. A., and J. I. Elkind, Adaptation of the Human Operator to Changes in Control Dynamics, Bolt Beranek and Newman, Inc., Rept. MR-10124-1, Mar. 15, 1964.

42. Elkind, J. I., J. A. Kelly, and R. A. Payne, "Adaptive Characteristics of the Human Controller in Systems Having Complex Dynamics," IEEE Proc. Fifth Nat. Symp. on Human Factors in Electronics, May 1964, pp. 143–159.

43. Hess, R. A., The Human Operator as an Element in a Control System with Time-Varying Dynamics, AFFDL-FDCC-TM-65-34, June 1965.

44. Hess, R. A., An Investigation of the Human Operator as an Element in Both Time Variant and Equivalent Time Invariant Systems, AFFDL-FDCC-TM-65-42, Sept. 1965.

45. Miller, D. C., A Model for the Adaptive Response of the Human Controller to Sudden Changes in Controlled Process Dynamics, B.S. and M.S. Thesis, MIT, June 1965.

46. Elkind, J. I., and D. C. Miller, "On the Process of Adaptation by the Human Controller," Proc. Third Intern. Fed. of Automatic Control Congress, London, June 1966.

47. Elkind, J. I., and D. C. Miller, Adaptive Characteristics of the Human Controller of Dynamic Systems, AFFDL-TR-66-60, July 1966.

48. Pavlidis, T., "A Modification of a Proposed Model for the Eye Tracking Movements," IEEE Trans. ("Short Communications"), Vol. BME-11, Nos. 1 and 2, Jan./Apr. 1964, p. 52.

49. Brissenden, R. F., A Study of Human Pilots' Ability to Detect Angular Motion with Application to Control of Space Rendezvous, NASA TN D-1498, Dec. 1962.

50. Ward, J. R., The Dynamics of a Human Operator in a Control System — A Study Based on the Hypothesis of Intermittency, Ph.D. dissertation, Univ. of Sydney, Australia, May 1958.

51. Bekey, G. A., An Investigation of Sampled Data Models of the Human Operator in a Control System, ASD-TDR-62-36, Feb. 1962.

52. Bekey, G. A., "The Human Operator as a Sampled-Data System," IRE Trans., Vol. HFE-3, No. 2, Sept. 1962, pp. 43–51.

53. Bergen, A. R., "On the Statistical Design of Linear Random Sampling Systems," Automatic and Remote Control (Proc. First Intern. Congress of IFAC, Moscow, 1960), Vol. 1, ed. J. F. Coales, et al, Butterworth, Inc., Wash., D.C., 1961, pp. 430–436.

Approved for Public Release

Contrails

54. Biddle, J., A. Jacobsen, and G. A. Bekey, "The Effects of Random Sampling Intervals on Sampled Data Models of the Human Operator," Third Annual NASA-University Conference on Manual Control, University of Southern California, Los Angeles, Calif., March 1-3, 1967, (forthcoming NASA SP).

55. Young, L. R., A Sampled-Data Model for Eye Movements, Sc.D. thesis, MIT, Dept. of Aeron. Engr., June 1962.

56. Lemay, L. P., and J. H. Westcott, The Simulation of Human Operator Tracking Using an Intermittent Model, paper pres. at IRE Intern. Congress on Human Factors in Electronics, Long Beach, Calif., 3-4 May 1962.

57. Flügge-Lotz, I., and H. A. Titus, Jr., "Optimum and Quasi-Optimum Control of Third- and Fourth-Order Systems," Automatic and Remote Control (Proc. Second Congress of Internat. Fed. Auto. Control, Basle, Switzerland, 1963), Vol. 2, Theory, ed. I. V. Broida, et al, Butterworth, Inc., Wash., D. C., 1964, pp. 363-370. (Also pub. as Air Force Office of Scientific Research Rept. 2928, June 1962.)

58. Krendel, E. S., and D. T. McRuer, "A Servomechanisms Approach to Skill Development," J. Franklin Inst., Vol. 269, No. 1, Jan. 1960, pp. 24-42.

59. Thomas, R. E., and J. T. Tou, "Human Decision-Making in Manual Control Systems," Second Annual NASA-University Conference on Manual Control, Massachusetts Institute of Technology, Cambridge, Mass., Feb. 28-Mar. 2, 1966, NASA SP-128, 1966, pp. 325-334.

60. Newell, A., J. C. Shaw, and H. A. Simon, "Elements of a Theory of Human Problem Solving," Psychol. Rev., Vol. 65, 1958, pp. 161-166.

61. Reitman, W. R., "Heuristic Programs, Computer Simulation and Higher Mental Processes," Behavioral Sci., Vol. 4, 1959, pp. 330-335.

62. Siegel, A. I., and J. J. Wolf, "A Technique for Evaluating Man-Machine Systems Designs," Human Factors, Vol. 3, Mar. 1961, pp. 18-28.

63. Braunstein, M. L., K. R. Laughery, and J. B. Seigfried, Computer Simulation of Driver Behavior During Car Following: A Methodological Study, Cornell Aeron. Lab. Rept. YM-1797-H-1, Oct. 1963.

64. Thomas, R. E., Developments of New Techniques for Human Controller Dynamics, Aerospace Med. Res. Labs., Rept. MRL-TDR-62-65, June 1962.

65. Matthews, P. B. C., "Muscle Spindles and Their Motor Control," Physiol. Rev., Vol. 44, No. 2, Apr. 1964, pp. 219-288.

66. Hunt, C. C. and E. R. Perl, "Spinal Reflex Mechanisms Concerned with Skeletal Muscle," Physiol. Rev., Vol. 40, No. 3, July 1960, pp. 538-579.

Approved for Public Release

Contrails

67. Granit, Ragnar, ed., Muscular Afferents and Motor Control (Proc. First Nobel Symposium, June 1965), John Wiley, New York, 1966.

68. Andrew, B. L., ed., Control and Innervation of Skeletal Muscle, (A Symposium at Queen's College, Dundee, Sept. 1965), Williams and Wilkins Co., Baltimore, 1966, p. 203.

69. Eccles, J. C., and J. P. Schadé, ed., Organization of the Spinal Cord, Vol. 11 of Progress in Brain Research, Elsevier Pub. Co., New York, 1964.

70. Eccles, J. C., and J. P. Schadé, ed., Physiology of Spinal Neurons, Vol. 12 of Progress in Brain Research, Elsevier Pub. Co., New York, 1964.

71. Eldred, Earl, and Jennifer Buchwald, "Central Nervous System: Motor Mechanisms," Ann. Rev. Physiol., Vol. 29, 1967, pp. 573-606.

72. Whitteridge, D., "The Effect of Stimulation of Intrafusal Muscle Fibers on Sensitivity to Stretch of Extraocular Muscles," Quar. J. Exp. Physiol., Vol. 44, 1959, 385-393.

73. Oscarsson, O., "Functional Organization of the Spino- and Cuneocerebellar Tracks," Physiol. Rev., Vol. 45, 1965, pp. 495-522.

74. Eccles, J. C., "Functional Organization of the Cerebellum in Relation to Its Role in Motor Control," Muscular Afferents and Motor Control (Proc. First Nobel Symposium, June 1965), ed. Ragnar Granit, John Wiley, New York, 1966, pp. 19-36.

75. Bell, Curtis C., and Robert S. Dow, "Cerebellar Circuitry," Neurosci. Res. Program Bull., Vol. 5, No. 2, Apr. 1, 1967.

76. Fadiga, E., and G. C. Pupilli, "Teleceptive Components of the Cerebellar Function," Physiol. Rev., Vol. 44, 1964, pp. 432-486.

77. Oscarsson, O., I. Rosen, and I. Sulg, "Organization of Neurones in the Cat Cerebral Cortex That are Influenced from Group I Muscle Afferents," J. Physiol., Vol. 183, 1966, pp. 189-210.

78. Braitenberg, V., "Functional Interpretation of Cerebellar Histology," Nature, Vol. 190, 1961, pp. 539-540.

79. Glaser, G. H., and D. C. Higgins, "Motor Stability, Stretch Responses and the Cerebellum," Muscular Afferents and Motor Control (Proc. First Nobel Symposium, June 1965), ed. Ragnar Granit, John Wiley, New York, 1966, pp. 121-138.

80. Brodal, A., "Some Data and Perspectives on the Anatomy of the So-Called 'Extrapyramidal System'," Acta Neurol. Scand., Vol. 39, Suppl. 14, 1963, pp. 17-38.

Approved for Public Release

Contrails

81. Lawrence, D. G., and H. G. J. M. Kuypers, "Pyramidal and Non-Pyramidal Pathways in Monkeys: Anatomical and Functional Correlation," Science, Vol. 148, 1965, pp. 973-975.

82. Hern, J. E. C., S. Landgren, C. G. Phillips, and R. Porter, "Selective Excitation of Corticofugal Neurones by Surface-Anodal Stimulation of the Baboon's Motor Cortex," J. Physiol., Vol. 161, 1962, pp. 73-90.

83. Mortimer, E. M., and K. Akert, "Cortical Control and Representation of Fusimotor Neurons," Am. J. Phys. Med., Vol. 40, 1961, pp. 228-248.

84. Evarts, E. V., "Relation of Discharge Frequency to Conduction Velocity in Pyramidal Tract Neurons," J. Neurophysiol., Vol. 28, pp. 216-228.

85. Takahashi, K., "Slow and Fast Groups of Pyramidal Tract Cells and Their Respective Membrane Properties," J. Neurophysiol., Vol. 28, pp. 908-924.

86. Evarts, E. V., "Pyramidal Tract Activity Associated with a Conditioned Hand Movement in the Monkey," J. Neurophysiol., Vol. 29, pp. 1011-1027.

87. Pompeiano, O., K. Diete-Spiff, and G. Carli, "Two Pathways Transmitting Vestibulospinal Influences from the Lateral Vestibular Nucleus of Deiters to Extensor Fusimotor Neurones," Flüg. Arch. ges Physiol., Vol. 293, 1967, pp. 272-275.

88. Diete-Spiff, K., G. Carli, and O. Pompeiano, "Spindle Responses and Extrafusal Contraction on Stimulation of the VIIIth Cranial Nerve or the Vestibular Nuclei in the Cat," Flüg. Arch. ges Physiol., Vol. 293, 1967, 276-280.

89. Timo-Iaria, C., and J. Antunes-Rodrigues, "Reticular Influences on a Spinal Reflex Arc," Acta Physiol. Latinoamer., Vol. 13, 1963, pp. 165-176.

90. Appelberg, B., "The Effect of Electrical Stimulation in Nucleus Ruber on the Response to Stretch in Primary and Secondary Muscle Spindles Afferents," Acta Physiol. Scand., Vol. 56, 1962, pp. 140-151.

91. Appelberg, B., and F. Emonet-Dénand, "Central Control of Static and Dynamic Sensitivities of Muscle Spindle Primary Endings," Acta Physiol. Scand., Vol. 63, 1965, pp. 487-494.

92. Llinas, R., "Mechanisms of Supraspinal Actions Upon Spinal Cord Activities. Differences Between Reticular and Cerebellar Inhibitory Actions Upon Alpha Extensor Motoneurons," J. Neurophysiol., Vol. 27, 1964, pp. 1117-1126.

93. Granit, R., O. Pompeiano, and B. Waltman, "Fast Supraspinal Control of Mammalian Muscle Spindles: Extra- and Intrafusal Co-activation," J. Physiol., Vol. 147, 1959, pp. 385-398.

Approved for Public Release

Contrails

94. Eldred, E., R. Granit, and P. A. Merton, "Supraspinal Control of the Muscle Spindles and Its Significance," J. Physiol., Vol. 122, 1953, pp. 498-523.

95. Delgado, J. M. R., "Sequential Behavior Induced Repeatedly by Stimulation of the Red Nucleus in Free Monkeys," Science, Vol. 148, pp. 1361-1363.

96. Wyrwicka, W., and R. W. Doty, "Feeding Induced in Cats by Electrical Stimulation of the Brain Stem," Exp. Brain Res., Vol. 1, 1966, pp. 152-160.

97. Eklund, G., C. von Euler, and S. Rutkowski, "Spontaneous and Reflex Activity of Intercostal Gamma Motoneurones," J. Physiol., Vol. 171, 1964, pp. 139-163.

98. Nathan, P. W., and T. A. Sears, "Effects of Posterior Root Section on the Activity of Some Muscles in Man," J. Neurol. Neurosurg. Psychiat., Vol. 23, 1960, pp. 10-22.

99. Von Euler, C., "Proprioceptive Control in Respiration," Muscular Afferents and Motor Control (Proc. First Nobel Symposium, June 1965), ed. Ragnar Granit, John Wiley, New York, 1966, pp. 197-207.

100. Corda, M., C. von Euler, and G. Lennerstrand, "Reflex and Cerebellar Influences on α and on 'Rhythmic' and 'Tonic' γ Activity in the Intercostal Muscle," J. Physiol., Vol. 184, 1966, pp. 898-923.

101. Critchlow, V., and C. von Euler, "Intercostal Muscle Spindle Activity and Its γ Motor Control, J. Physiol., Vol. 168, 1963, pp. 820-847.

102. Corda, M., G. Eklund, and C. von Euler, "External Intercostal and Phrenic α Motor Responses to Changes in Respiratory Load," Acta Physiol. Scand., Vol. 63, 1965, pp. 391-400.

103. Sears, T. A., "Efferent Discharges in Alpha and Fusimotor Fibres of Intercostal Nerves of the Cat," J. Physiol., Vol. 174, 1964, pp. 295-315.

104. Ettinger, E. G., ed., Functions of the Corpus Callosum, Ciba Found. Study Group, No. 20, Little, Brown and Co., Boston, 1965. (See especially contributions of Trevarthan, and Black and Myers.)

105. Apter, J. T., "Projection of the Retina on Superior Colliculus of Cats," J. Neurophysiol., Vol. 8, 1945, pp. 123-134.

106. Lettvin, J. Y., H. R. Maturana, W. H. Pitts, and W. S. McCulloch, "Two Remarks on the Visual System of the Frog," Sensory Communication (Contributions to the Symposium on Principles of Sensory Communication, July 19-August 1, 1959, MIT), ed. Walter A. Rosenblith, John Wiley, New York, 1961, pp. 757-776.

Approved for Public Release

Contrails

107. Barlow, H. B., R. M. Hill, and W. R. Levick, "Retinal Ganglion Cells Responding Selectively to Direction and Speed of Image Motion in the Rabbit," J. Physiol., Vol. 173, 1964, pp. 377-407.

108. Apter, J. T., "Eye Movements Following Strychninization of the Superior Colliculus of Cats," J. Neurophysiol., Vol. 9, 1946, pp. 73-86.

109. Hyde, J. E., "Interrelationship of Brainstem and Cortical Areas for Conjugate Ocular Movements in Cats," The Oculomotor System, ed. Morris B. Bender, Harper and Row (Hoeber Medical Div.), New York, 1964, pp. 141-150.

110. Kilmer, W. L., and W. S. McCulloch, Towards a Theory of the Reticular Formation, AFCRL-64-463, Apr. 1964.

111. Horn, G., and R. M. Hill, "Responsiveness to Sensory Stimulation of Units in the Superior Colliculus and Subjacent Tectotegmental Regions of the Rabbit," Exp. Neurol., Vol. 14, 1966, pp. 199-223.

112. Bell, C., G. Sierra, N. Buendia, and J. P. Segundo, "Sensory Properties of Neurons in the Mesencephalic Reticular Formation," J. Neurophysiol., Vol. 27, 1964, pp. 961-987.

113. Whitteridge, D., "Central Control of Eye Movements," Handbook of Physiology, Sec. 1, Neurophysiology, Vol. II, ed. J. Field, et al, Williams and Wilkins Co., Baltimore, 1960, pp. 1089-1109.

114. Jassik-Gerschenfeld, D., "Activity of Somatic Origin Evoked in the Superior Colliculus of the Cat," Exp. Neurol., Vol. 16, 1966, pp. 104-118.

115. Sprague, J. M., and T. H. Meikle, Jr., "The Roll of the Superior Colliculus in Visually Guided Behavior," Exp. Neurol., Vol. 11, 1965, pp. 115-146.

116. King, W. J., "Continuous Compensatory Tracking by a Cebus Monkey," Science, Vol. 134, 1961, pp. 947-948.

117. Kozhevnikov, V. A., and L. I. Chistovich, Speech: Articulation and Perception, Joint Pub. Res. Serv., Off. Tech. Serv., U.S. Dept. of Comm., Wash., D. C., 1965.

118. Fuchs, A. F., "Periodic Eye Tracking in the Monkey," J. Physiol., Vol. 193, 1967, pp. 161-171.

119. Vaughan, H. G., Jr., L. D. Costa, L. Gilden, and H. Schimmel, "Identification of Sensory and Motor Components of Cerebral Activity in Simple Reaction-Time Tasks," Proc. 73rd Conf. Amer. Psychological Assn., Vol. 1, 1965, pp. 179-180.

Approved for Public Release

Contrails

120. Gilden, L., H. G. Vaughan, Jr., and L. D. Costa, "Summated Human EEG Potentials with Voluntary Movement," Electroenceph. Clin. Neurophysiol., Vol. 20, 1966, pp. 433–438.

121. Dustman, R. E., and E. C. Beck, "Phase of Alpha Brain Waves, Reaction Time and Visually Evoked Potentials," Electroenceph. Clin. Neurophysiol., Vol. 18, 1965, pp. 433–440.

122. Yensen, R., "Neuromotor Latency and Take-Up of Musculotendinous Slack as Components of RT," Percept. and Motor Skills, Vol. 23, 1966, pp. 751–758.

123. Wolkovitch, J., and R. Magdaleno, Performance Criteria for Linear Constant-Coefficient Systems with Random Inputs, ASD-TDR-62-470, Jan. 1963.

124. Lee, Y. W., Statistical Theory of Communication, John Wiley, New York, 1960.

125. McDonnell, J. D., and H. R. Jex, A "Critical" Tracking Task for Man-Machine Research Related to the Operator's Effective Delay Time, Pt. II, Experimental Effects of System Input Spectra, Control Stick Stiffness, and Controlled Element Order, NASA CR-674, Jan. 1967.

126. Miller, D. C., "The Effects of Performance-Scoring Criteria on Compensatory Tracking Behavior," IEEE Trans., Vol. HFE-6, No. 1, Sept. 1965, pp. 62–65.

127. Wolkovitch, J., Optimization of Linear and Nonlinear Systems by Minimization of Auxiliary Effort, Systems Technology, Inc., Tech. Rept. 900-1, Mar. 1967.

128. Stapleford, Robert L., Samuel J. Craig, and J. A. Tennant, Measurement of Pilot Describing Functions in Single-Controller Multiloop Tasks, Systems Technology, Inc., Tech. Rept. 167-1, Aug. 1967.

129. Kalman, R. E., "When Is a Linear Control System Optimal?" Trans. ASME, Series D, J. Basic Engineering, Vol. 86, 1964. (Also pub. as RIAS Tech. Rept. 63-5, Mar. 1963.)

130. Obermayer, R. W., and F. A. Muckler, On the Inverse Optimal Control Problem in Manual Control Systems, NASA CR-208, Apr. 1965.

131. Rynaski, E. G., and R. F. Whitbeck, The Theory and Application of Linear Optimal Control, AFFDL-TR-65-28, Jan. 1966.

132. Chang, S. S. L., Synthesis of Optimal Control Systems, McGraw-Hill, New York, 1961.

Approved for Public Release

Contrails

APPENDIX

PROOF THAT EQ. 51, $\overset{\sim\sim}{\epsilon^2} = \overset{\sim\sim}{m_d^2} - \overset{\sim\sim}{m^2} - 2k\overset{\sim\sim}{c^2}$, IS A NECESSARY AND SUFFICIENT CONDITION FOR OPTIMALITY WITH RESPECT TO THE CRITERION MIN$(\epsilon^2 + kc^2)$

Employing a procedure similar to that of Chang (Ref. 132), it can be shown that the optimum system transfer function is, with the formulation of Fig. 47,

$$H\bar{J}G = \frac{\bar{J}}{J} \frac{\left[\frac{J}{\bar{J}} \frac{\Phi_{rm_d}}{(\Phi_{rr})^-(1 + k/G\bar{G})^-}\right]_+}{\left(1 + \frac{k}{G\bar{G}}\right)^+ \left(\Phi_{rr}\right)^+} \qquad \text{(A-1)}$$

where the controller transfer function $H\bar{J}$ can be factored into a product of H, containing only left half plane poles and zeros, and $\bar{J}$, containing right half plane zeros ($\bar{J} = J = 1$ for a minimum-phase controller). For the human operator, $\bar{J}$ is the nonminimum-phase factor of the Padé approximation to the time delay term, $e^{-j\omega\tau_e}$. The controlled element transfer function G is stable but may contain right half plane zeros. Φ_{rr} is the power spectrum of the total input $r = i + n_i$, hence $\Phi_{rr} = \Phi_{ii} + \Phi_{in} + \Phi_{ni} + \Phi_{nn}$; Φ_{rm_d} is the cross spectrum between the input and desired output. If the output can be generated by a linear operation with transfer function F_1 acting on i, then $\Phi_{rm_d} = (\Phi_{ii} + \Phi_{ni})F_1$. $(x)^+$ denotes the product of all factors of x with LHP poles and zeros, $(x)^-$ denotes the remaining factor, and $[x]_+$ denotes the partial fraction expansion of x, retaining only the partial fractions with LHP poles.

$$\begin{aligned}
\Phi_{\epsilon\epsilon} + k\Phi_{cc} = {} & \Phi_{ii}\left\{\left[H\bar{J}G - F_1\right]\left[\bar{H}\bar{J}\bar{G} - \bar{F}_1\right] + kH\bar{H}J\bar{J}\right\} \\
& + \Phi_{in}\left\{\left[\bar{H}\bar{J}\bar{G} - \bar{F}_1\right]H\bar{J}G + kH\bar{H}J\bar{J}\right\} \\
& + \Phi_{ni}\left\{\left[H\bar{J}G - F_1\right]\bar{H}\bar{J}\bar{G} + kH\bar{H}J\bar{J}\right\} \\
& + \Phi_{nn}\left\{H\bar{J}G\bar{H}\bar{J}\bar{G} + kH\bar{H}J\bar{J}\right\} \qquad \text{(A-2)}
\end{aligned}$$

Approved for Public Release

Contrails

Integrating and replacing the sum of the middle terms by twice the real part, $\mathcal{R}$, of either, and using $\Phi_{rr} = \Phi_{ii} + \Phi_{in} + \Phi_{ni} + \Phi_{nn}$,

$$\tilde{\epsilon}^2 + k\tilde{c}^2 = \tilde{m}^2 + \tilde{m}_d^2 - \mathcal{R}\frac{1}{2\pi j}\int_{-j\infty}^{j\infty}\left(2H\bar{J}G\Phi_{m_d r} - k\Phi_{rr}H\bar{J}\bar{H}J\right) dj\omega \qquad (A\text{-}3)$$

Substituting from Eq. A-1,

$$H\bar{J}G\Phi_{m_d r} = \left[\frac{J}{\bar{J}}\frac{1}{(\Phi_{rr})^-}\frac{\Phi_{rm_d}}{(1 + k/G\bar{G})^-}\right]_+ \frac{\bar{J}}{J}\frac{\Phi_{m_d r}}{(\Phi_{rr})^+(1 + k/G\bar{G})^+} \qquad (A\text{-}4)$$

Splitting up $(\bar{J}/J)\left[\Phi_{m_d r}/(\Phi_{rr})^+(1 + k/G\bar{G})^+\right]$ into partial fractions, only those partial fractions with RHP poles contribute to the integral, so Eq. A-3 becomes

$$\tilde{\epsilon}^2 + k\tilde{c}^2 = \tilde{m}^2 + \tilde{m}_d^2 + k\tilde{c}^2 - \frac{1}{\pi j}\int_{-j\infty}^{j\infty}\left[\frac{J}{\bar{J}}\frac{1}{(\Phi_{rr})^-}\frac{\Phi_{rm_d}}{(1 + k/G\bar{G})^-}\right]_+\left[\frac{\bar{J}}{J}\frac{1}{(\Phi_{rr})^+}\frac{\Phi_{m_d r}}{(1 + k/G\bar{G})^+}\right]_- dj\omega \qquad (A\text{-}5)$$

The $\mathcal{R}$ sign has become redundant, as the integrand is now the product of complex conjugates. The last term in Eq. A-5 can be written as

$$\cdots \frac{-2}{2\pi j}\int_{-j\infty}^{j\infty} H\bar{J}G\bar{H}J\bar{G}\Phi_{rr}(1 + k/G\bar{G})\, dj\omega = -2\tilde{m}^2 - 2k\tilde{c}^2 \qquad (A\text{-}6)$$

Substituting Eq. A-6 into Eq. A-5 yields

$$\tilde{\epsilon}^2 + k\tilde{c}^2 = \tilde{m}^2 + \tilde{m}_d^2 + k\tilde{c}^2 - 2\tilde{m}^2 - 2k\tilde{c}^2 \qquad (A\text{-}7)$$

which simplifies to the desired result, Eq. 51,

$$\tilde{\epsilon}^2 = \tilde{m}_d^2 - \tilde{m}^2 - 2k\tilde{c}^2$$

Approved for Public Release

Contrails

Unclassified
Security Classification

DOCUMENT CONTROL DATA - R & D

(Security classification of title, body of abstract and indexing annotation must be entered when the overall report is classified)

1. ORIGINATING ACTIVITY *(Corporate author)*
Systems Technology, Inc.
13766 So. Hawthorne Blvd.
Hawthorne, Calif. 90301

2a. REPORT SECURITY CLASSIFICATION
Unclassified

2b. GROUP
N/A

3. REPORT TITLE

NEW APPROACHES TO HUMAN-PILOT/VEHICLE DYNAMIC ANALYSIS

4. DESCRIPTIVE NOTES *(Type of report and inclusive dates)*
Final Report - March 1966 to June 1967

5. AUTHOR(S) *(First name, middle initial, last name)*
McRuer, D. T. Moore, G. P. Wolkovitch, J.
Hofmann, L. G. Phatak, A. V.
Jex, H. R. Weir, D. H.

6. REPORT DATE	7a. TOTAL NO. OF PAGES	7b. NO. OF REFS
February 1968	188	132

8a. CONTRACT OR GRANT NO.	9a. ORIGINATOR'S REPORT NUMBER(S)
AF 33(615)-3652	
b. PROJECT NO. 8219	TR 164-2
c. Task No. 821904	9b. OTHER REPORT NO(S) *(Any other numbers that may be assigned this report)*
d.	AFFDL-TR-67-150

10. DISTRIBUTION STATEMENT

Distribution of this report is unlimited.

11. SUPPLEMENTARY NOTES	12. SPONSORING MILITARY ACTIVITY
None	Air Force Flight Dynamics Laboratory Wright-Patterson Air Force Base, Ohio

13. ABSTRACT

New models for human pilot dynamics and new methods for pilot/vehicle dynamic analysis are investigated. The status of existing quasi-linear models is reviewed and deficiencies are noted as a basis for pinpointing areas needing the most effort. The pilot modeling topics explored include: low frequency lead generation using either velocity sensing at the periphery (eye) or difference computations accomplished at a more central level; mode-switching models for nonstationary or discrete inputs to the pilot/vehicle system; physiological aspects of pilot dynamics in tracking tasks; Successive Organization of Perception (SOP) theory for levels of pilot cognition higher than compensatory. For pilot/vehicle analysis, analytical approaches from control theory which appear to have promise are studied, including: time-optimal computing feedforward elements useful in the mode switching models for response to nonstationary inputs; optimal control theory using the crossover model in the performance criterion to estimate pilot response characteristics in compensatory tasks; inverse optimal control theory using known experimental results and quasi-linear pilot response models in an effort to define the pilot's adjustment rules in terms of performance indices; optimal control theory to provide a simple test for optimality (to an elementary quadratic criterion) using only average performance measure data.

Distribution of this Abstract is Unlimited

DD FORM 1 NOV 65 1473

Unclassified
Security Classification

Approved for Public Release

Contrails

14. KEY WORDS	LINK A		LINK B		LINK C	
	ROLE	WT	ROLE	WT	ROLE	WT
Manual Control						
Mathematical Models						
Pilot Dynamics						
Pilot/Vehicle Analysis						
Quasi-Linear Models						
Sampled-Data Pilot Models						
Transient Input Pilot Models						
Successive Organization of Perception						
Tracking Physiology						
Optimal Control Pilot Models						

Approved for Public Release